The University Of Sheffield.

Tight Junction Protein Expression in Human Astrocytes

Sarah Victoria Morgan

BSc Hons, MA Dunelm

Supervised by:

Prof. S. Wharton & Dr. J. Simpson

A thesis submitted for the degree of Doctor of Philosophy (PhD)

The University of Sheffield

Faculty of Medicine, Dentistry and Health

Department of Neuroscience

June 2016

Abstract

Tight junctions are formed from a complex of different individual proteins. These complexes are expressed by epithelial cells and form an intercellular barrier which restricts and regulates paracellular permeability. Tight junction proteins have also been shown to be expressed in non-epithelial cells which do not form tight junctions, including astrocytes. The function(s) of these proteins within non-epithelial cells, however, remains unclear. This study aims to characterise the expression of tight junction proteins in astrocytes and investigate the function(s) of these proteins in these cells.

The expression of the tight junction proteins occludin, claudin-5 and zonula occludens-1 (ZO-1) was characterised *in vitro* in both human primary astrocytes and the 1321N1 human astrocytoma cell line and *in vivo* in human autopsy brain samples. The function(s) of occludin was investigated using a pull-down protein binding assay and mass spectrometry analysis to identify putative binding partners for this protein in astrocytes.

The current study demonstrates astrocytic and nuclear expression of occludin and ZO-1 *in vitro* and *in vivo*. The expression of claudin 5 in astrocytes remains difficult to determine due to contradictory evidence in which the astrocytic expression of this protein *in vitro* is not supported *in vivo*. Putative binding partners were also identified for the N- and C-terminal domains of occludin. Many of these proteins have functions in RNA metabolic processes, consequently their identification as putative occludin binding partners implicates occludin in functions beyond the formation of the tight junction complex. Although these interactions have not yet been validated, this study's findings provide a platform upon which future research can be constructed.

Acknowledgements

First and foremost, I would like to thank ARUK who provided the scholarship and funding which made this research possible. I must also thank my supervisors, Prof. Stephen Wharton and Dr. Julie Simpson, not only for giving me an opportunity from which I have learnt so much but also for their advice and guidance for which I will never be able to thank them enough.

My heartfelt thanks go to Dr. Guillaume Hautbergue for his invaluable knowledge, guidance and support. His enthusiasm saw me through the more challenging phases of this project and, without him, I would truly have been lost. I would also like to give my sincerest thanks to Dr. Matthew Walsh and Simeon Mihaylov who provided be with brilliant laboratory instruction. I will be forever grateful to them for their help.

I would also like to thank my collaborator Dr. Mark Dickman and his research group for their expertise and assistance. I am also grateful to the Newcastle brain bank for providing me with the tissue used in this project.

My thanks also go to all my friends at SITraN. It was their company, perspective and support which saw me through the worst and the best of the last three years. A special thanks also goes to my fabulous best friend, Emily Alderton. We have seen each other through all our degrees and I could not possibly have completed this PhD without her and all the wine. Finally, I would like to thank my parents for never losing faith.

Table of Contents

List of Figures

List of Tables

List of Abbreviations

20-HETE	20-hydroxyeicosatetraenioc acid
aa	Amino acid
AA	Arachidonic Acid
ABC	Avidin-biotin Complex
ABC-AP	Avidin-biotin Complex-Alkaline Phosphatase
ABR	Actin-binding Region
AD	Alzheimer's Disease
AGS	Astrocyte Growth Supplements
AJ	Adherens Junction
AM	Astrocyte Medium
AMPA	α-amino-3-hydroxy-5-methyl-4isozole propionic acid
APP	Amyloid Precursor Protein
APS	Ammonium persulphate
ATP	Adenosine Triphosphate
BBB	Blood-Brain Barrier
BCA	Bicinchoninic Acid
BL	Biotin Ligase
bp	Base pair
BREC	Bovine Retinal Endothelial Cells

BSA	Bovine Serum Albumin
Ca^{2+}	Calcium ions
cAMP	cyclic Adenosine Monophosphate
CBP	CREB-binding protein
CDC42	Cell Division Control protein 42 homologue
CNS	Central Nervous System
COX	Cyclooxygenase
CREB	Cyclic AMP response element binding protein
CRM1	Chromosomal maintenance 1
Cx	Connexin
DAB	3, 3-diaminobenzidine
DDX3X	DEAD-box helicase 3, X-linked
DEAD-box	Asp-Glu-Ala-Asp box motif
dH_2O	Deionised water
DMEM	Dulbecco's Modified Eagle Medium
DPX	Distyrene Plasticizer Xylene
EAAT	Excitatory amino acid transporter
EC	Extracellular Cadherin
E-cad/CTF1	E-cadherin C-terminal fragment 1

E-cad/CTF2	E-cadherin C-terminal fragment 2
ECGS	Endothelial Cell Growth Supplements
ECL	Extracellular loop
ECM	Endothelial Cell Medium
EDTA	Ethylene diamine tetra-acetic acid
eEF2	Eukaryotic translation elongation factor 2
EET	Epoxyeicosatrienoic acid
EGTA	Ethylene glycol-bis(2-aminoethyl ether)-N,N,N’N’-tetra-acetic acid
eIF4F	eukaryotic Initiation Factor 4F
EJC	Exon Junction Complex
ELL	Eleven-nineteen lysine-rich leukaemia proteins
ER	Endoplasmic Reticulum
Esp15	Epidermal growth factor receptor substrate 15
FACT	Facilitates chromatin transcription
FBS	Foetal Bovine Serum
FFPE	Formalin fixed, paraffin embedded
GABA	γ-aminobutyric acid
GABA-T	GABA transaminase
GAD	Glutamic Acid Decarboxylase

GAT	GABA transporter
GECI	Genetically Encoded Calcium Indicators
GFAP	Glial Fibrillary Acidic Protein
GFP	Green Fluorescent Protein
GJC	Gap Junction Channel
GPCR	G protein-coupled receptor
GRD	Glycine-rich Domain
GUK	Guanylate Kinase Domain
HA	Human embryonic primary astrocytes
HC	Hemichannel
HCV	Hepatitis C Virus
HEK 293	Human Embryonic Kidney 293 cells
HIV-1	Human Immunodeficiency Virus-1
hnRNP	heterogeneous Nuclear Ribonucleoprotein
HRP	Horseradish Peroxidase
Hrs	Hepatocyte growth factor-regulated tyrosine kinase substrate
HUVEC	Human Umbilical Vein Endothelial Cells
ICW	Intercellular Calcium Waves
INM	Inner Nuclear Membrane

IP_3	Inositol 1,4,5-trisphosphate
IP_3R	Inositol 1,4,5-triphosphate Receptor
IPTG	Isopropyl β-D-1-thiogalactopyranoside
JAM	Junctional Adhesion Molecule
K^+	Potassium ions
kDa	kiloDalton
KH	K homology domain
Kir	Inwardly rectifying potassium channel
KO	Knockout
LB	Luria-Bertani
LPS	Lipopolysaccharide
LUHMES	Lund human mesencephalic cells
MAGUK	Membrane-Associated Guanylate Kinase like proteins
MAPK	Mitogen-activated protein kinase
MARVEL	MAL and related proteins for vesicle trafficking and membrane link domain
MCI	Mild Cognitive Impairment
MDCK	Madin-Darby Canine Kidney cells
MEMα/F-10	Minimum Essential Medium α/Ham's F-10 nutrient mix
MCI	Mild Cognitive Impairment

MLCK	Myosin Light Chain Kinase
MPP	Metalloproteinases
MRCKβ	Myotonic dystrophy kinase-related CDC42-binding kinase β
mRNA	messenger Ribonucleic Acid
mRNP	messenger Ribonucleoprotein
NaAc	Sodium Acetate
NES	Nuclear Export Signal
NaF	Sodium fluoride
$NaVO_4$	Sodium orthovanadate
NLS	Nuclear Localisation Signal
NMDA	N-methyl-D-aspartate
NO	Nitric Oxide
NPC	Nuclear Pore Complex
NVC	Neurovascular Coupling
NVU	Neurovascular Unit
ONM	Outer Nuclear Membrane
OSP	Oligodendrocyte-Specific Protein
PABP	Poly(A)-binding protein
PBMC	Human Peripheral Blood Mononuclear cells

PBS	Phosphate Buffered Saline
PDZ domain	An acronym derived from the first three proteins in which this structural domain was identified, Psd-95, Dlg and ZO-1
PFA	Paraformaldehyde
PGE_2	Prostaglandin E_2
PIC	Protease Inhibitor Cocktail
PKA	Protein Kinase A
PLA_2	Phospholipase A_2
PLC	Phospholipase C
PPA2	Protein Phosphatase A2
P/S	Penicillin/Streptomycin
PS1	Presenilin-1
RRE	Rev Response Element
RGG	arginine/glycine-rich box
RLE	Rat Lung Endothelial cells
RT	Room Temperature
RNA	Ribonucleic acid
RNP	Ribonucleoprotein
RRM	RNA Recognition Motif
SAF-B	Scaffold Attachment Factor-B

SF	Superfamily
SH3	Src homology 3
SNARE	Soluble N-ethylmaleimide-sensitive factor attachment protein receptor
SRSF1/2	Serine/arginine-rich splicing factors 1 and 2
SSRP1	Structure specific recognition protein 1
TAMP	Tight junction-associated MARVEL protein
TAP	Tip-associated protein
TB	Terrific Broth
TBS	Tris Buffered Saline
TEMED	Tetramethylethylenediamine
TER	Transepithelial Electrical Resistance
TFA	Trifluoroacetic acid
TJ	Tight Junction
TJC	Tight Junction Complex
TJP	Tight Junction Protein
TM	Transmembrane
TRPA1	Transient Receptor Potential A1
TRPC4	Transient Receptor Potential Channel-4
UIM	Ubiquitin-interacting Motif

UTR	Untranslated Region
UV	Ultra-violet
V-ATPase	Vacuolar proton ATPase
VD	Vascular Dementia
VEGF	Vascular Endothelial Growth Factor
VGLUT	Vesicular Glutamate Transporters
VSERT	Vesicular D-serine transporter
VSMC	Vascular Smooth Muscle Cells
v/v	Volume/volume
WML	White Matter Lesions
w/v	Weight/volume
x g	Relative centrifugal force
XPO1	Exportin-1
ZO	Zonula occludens
ZONAB	ZO-1 associated nucleic acid-binding protein

1. Introduction

1.1 Astrocytes

Astrocytes are highly heterogeneous, multifunctional glial cells located throughout the central nervous system (CNS) which are typically characterised by a highly branched morphology (Hu et al., 2016). Astrocytes are a functional component in synaptic transmission capable of influencing neuronal signalling and are also involved in the modulation of cerebral blood flow.

1.1.1 Astrocytes & the Tripartite Synapse

The tripartite synapse is structurally composed of neuronal pre- and post-synaptic terminals surrounded by astrocytic processes with synaptic transmission being defined by the dynamic communication which occurs between these components (Alberto and Alfonso, 2013; Allen, 2014; Araque et al., 1999). Neurotransmitters released from pre-synaptic terminals bind to receptors located at both the post-synaptic terminal and astrocytic processes. Unlike neurons, astrocytes are incapable of generating action potentials, instead astrocytic receptor activation elicits dynamic changes in the intracellular concentration of calcium (Ca^{2+}) ions within these cells, known as calcium transients (Shigetomi et al., 2016). These transients trigger the release of gliotransmitters which influence synaptic transmission and consequently neuronal signalling.

Astrocytes express ionotropic and metabotropic receptors for many neurotransmitters including glutamate and γ-aminobutyric acid (GABA), respectively the principal excitatory and inhibitory neurotransmitters within the CNS (Bradley and Challiss, 2012; Lalo et al., 2011; Lee et al., 2011; Meier et al., 2008). Ionotropic receptors are ligand-gated ion channels. Metabotropic receptors do not form ion-permeable channels and instead function through a signal transduction mechanism mediated by G-proteins, consequently these receptors are known as G protein-coupled receptors (GPCRs) (Allen, 2014).

Astrocytes also express transporters to remove neurotransmitters from the synaptic cleft. Excitatory amino acid transporters 1 and 2 (EAAT1 and EAAT2) transport glutamate into astrocytes where it is metabolised into glutamine by glutamine synthase (Lee and Pow, 2010). Glutamine is transported to neurons where it is converted back into glutamate by glutaminase (Lee and Pow, 2010).

Astrocytes also express GABA transporters 1 and 3 (GAT-1 and GAT-3) (Conti et al., 2004). GABA is formed from glutamine by glutamic acid decarboxylase (GAD)

of which two isoforms have been identified, GAD 67 and GAD 65 (Lee et al., 2011; Soghomonian and Martin, 1998). GABA is also metabolised back to glutamine by GABA transaminase (GABA-T). Immunohistochemical analysis of human tissue shows that GAD 67 and GABA-T are expressed within astrocytes throughout the brain demonstrating that these cells are capable of metabolising this neurotransmitter (Lee et al., 2011).

1.1.2 Astrocytes and Calcium Transients

Membrane-permeable fluorescent Ca^{2+} indicator dyes, examples of which include fura-2, fluo-3 and fluo-4, are used extensively in studying astrocytic intracellular calcium signalling (Gee et al., 2000; Grynkiewicz et al., 1985; Kao et al., 1989). These dyes, however, do have limitations as they fail to capture astrocytic processes beyond approximately 25 μm and also underestimate the quantity of primary astrocytic processes (Reeves et al., 2011). Consequently these dyes are able to reliably measure calcium transients located only in the astrocyte soma but are unable to reliably detect calcium transients within fine astrocytic processes (Reeves et al., 2011; Tong et al., 2013).

Genetically encoded Ca^{2+} indicators (GECIs) are also used to measure intracellular calcium transients. These probes utilise green fluorescent protein (GFP) variants which are hybridized with the calcium binding protein calmodulin and the calmodulin binding peptide M13 (Nakai et al., 2001; Pérez Koldenkova and Nagai, 2013). GECIs circumvent many of the problems presented by indicator dyes as they are transfected into cells, instead of being applied through bulk-loading like indicator dyes, and can be designed to target specific cellular compartments or subcellular regions (Reeves et al., 2011; Tong et al., 2013). Consequently GECIs are able to detect and measure calcium transients located in astrocytic processes which indicator dyes are unable to access.

1.1.2.1. Intrinsic Intracellular Calcium Fluctuations

Astrocytes express the metabotropic glutamate receptor mGlu5, the activation of which is responsible for the release of Ca^{2+} ions from the endoplasmic reticulum (ER), a subcellular organelle whose functions include the intracellular storage of Ca^{2+} ions (Biber et al., 1999). Activation of the mGlu5 receptor results in the activation of phospholipase C (PLC) and the subsequent hydrolysis of phosphoinositide phospholipids within the cell membrane to produce inositol 1,4,5-triphosphate (IP_3) (Shigetomi et al., 2016). IP_3 binds to and activates receptors

located in the ER resulting in the release of intracellular Ca^{2+} ions. Three IP_3 receptor (IP_3R) isoforms have been identified, IP_3R1, IP_3R2 and IP_3R3 (Foskett et al., 2007), of which IP_3R2 is enriched in astrocytes (Holtzclaw et al., 2002; Zhang et al., 2014).

The role of IP_3R2 receptors in calcium signalling has been investigated in hippocampal astrocytes and neurons using an IP_3R2 knockout (KO) mouse model. IP_3R2 KO mice are viable and fertile with no effect upon mortality (Li et al., 2005a). Histological analysis of the hippocampus, cortex and cerebellum shows no apparent structural differences between mutant and wildtype mice (Petravicz et al., 2008). Electrophysiological analysis of hippocampal slices taken from wildtype and mutant loaded with fluo-4 and calcium green-1 indicator dyes shows that hippocampal astrocytes in the IP_3R2 KO do not exhibit any GPCR-mediated increase in intracellular calcium and demonstrate a complete loss of calcium activity (Petravicz et al., 2008). There are, however, no significant differences in IP_3R-mediated calcium signalling in CA1 pyramidal neurons in IP_3R2 KO mice compared with the wildtype, suggesting that IP_3R2 receptors are responsible for mediating calcium transients in astrocytes but not in neurons (Petravicz et al., 2008).

Subsequent research using GECIs has, however, identified GPCR-mediated calcium transients which are preserved in the astrocytic processes of IP_3R2 KO mice (Haustein et al., 2014; Kanemaru et al., 2014; Srinivasan et al., 2015). Electrophysiological analysis of hippocampal slices taken from wildtype and IP_3R2 knockout mice utilising the GECI GCaMP6f demonstrates that calcium transients persist in the processes but are lost in the soma of KO mice. (Srinivasan et al., 2015). The GRCR agonist endothelin elicits a significant elevation in somatic calcium signalling in wildtype astrocytes which is not exhibited in the mutant, however, a comparable elevation in calcium signalling in both wildtype and mutant is present in astrocyte processes (Srinivasan et al., 2015). This demonstrates that calcium signalling in the astrocytic soma and processes is mediated by different receptors. These findings contradict those of previous studies which used indicator dyes. It appears that, due to their limitations, the indicator dyes used in these studies failed to reveal the full complexity of astrocytic calcium signalling (Petravicz et al., 2014; Petravicz et al., 2008).

1.1.2.2. Transmembrane Microdomains

Astrocytic processes also exhibit brief, spotty calcium transients located close to the membrane which were first observed in rat hippocampal astrocytes co-cultured with neurons using Lck-GCaMP2; a GECI modified to include Lck, a membrane-tethering domain (Shigetomi et al., 2010). These transients are known as microdomains and are mediated by transient receptor potential A1 (TRPA1) channels (Shigetomi et al., 2012). Not all microdomain signals in the CA3 region of the hippocampus, however, are blocked by a TRPA1-selective antagonist, suggesting the involvement of other receptors in the generation of these signals (Haustein et al., 2014).

1.1.3 Gliotransmitters

Astrocytes influence neuronal signalling through the release of chemicals known as gliotransmitters which include glutamate, adenosine triphosphate (ATP) and D-serine, as well as variety of metabolic substrates, peptides and eicosanoids (Petrelli and Bezzi, 2016). Gliotransmitter release can occur via several different mechanisms including vesicle-mediated exocytosis (Zorec et al., 2015). Vesicle-mediated exocytosis is a Ca^{2+}-dependent process which requires extensive molecular machinery involving soluble N-ethylmaleimide-sensitive factor attachment protein receptor (SNARE) proteins (Petrelli and Bezzi, 2016). Astrocytes express SNARE proteins which suggests that vesicle-mediated exocytosis is a mechanism by which these cells release gliotransmitters (Jeftinija et al., 1997; Montana et al., 2006; Wilhelm et al., 2004; Zhang et al., 2004).

Cytosolic glutamate is loaded into exocytotic vesicles by vesicular glutamate transporters (VGLUTs) which are driven by a proton gradient generated by vacuolar proton ATPase (V-ATPase). Astrocytes express all three known VGLUT isoforms (Bezzi et al., 2004; Kreft et al., 2004; Montana et al., 2004). Astrocytic glutamate release is abolished by clostridial neurotoxins, which cleave SNARE proteins, and reduced by the V-ATPase inhibitor bafilomycin A_1 demonstrating that astrocytic glutamate release occurs by vesicle-mediated exocytosis (Araque et al., 2000; Bezzi et al., 2004; Montana et al., 2004; Zhang et al., 2004). Figure 1.1 depicts the functional roles of astrocytes within a glutamatergic tripartite synapse.

The release of D-serine from cultured rat astrocytes is mediated by an elevation in intracellular Ca^{2+} which occurs in response to AMPA and mGlu receptor activation (Mothet et al., 2005). The release of D-serine from astrocytes is a Ca^{2+}-dependent process which is significantly reduced in the presence of tetanus toxin, a clostridial

neurotoxin, suggesting that astrocytic D-serine release also occurs by vesicle-mediated exocytosis (Mothet et al., 2005). This is further supported by the fact that D-serine is stored along with glutamate in vesicles bearing synaptobrevin 2, a SNARE complex protein, in rat cortical astrocytes (Martineau et al., 2013). The vesicular D-serine transporter (VSERT) has not yet been identified although the vesicular uptake of D-serine is blocked by bafilomycin A_1 and concanamycin A both of which are V-ATPase inhibitors, demonstrating that the vesicular uptake of this gliotransmitter requires a proton gradient generated by V-ATPases (Martineau et al., 2013; Mothet et al., 2005).

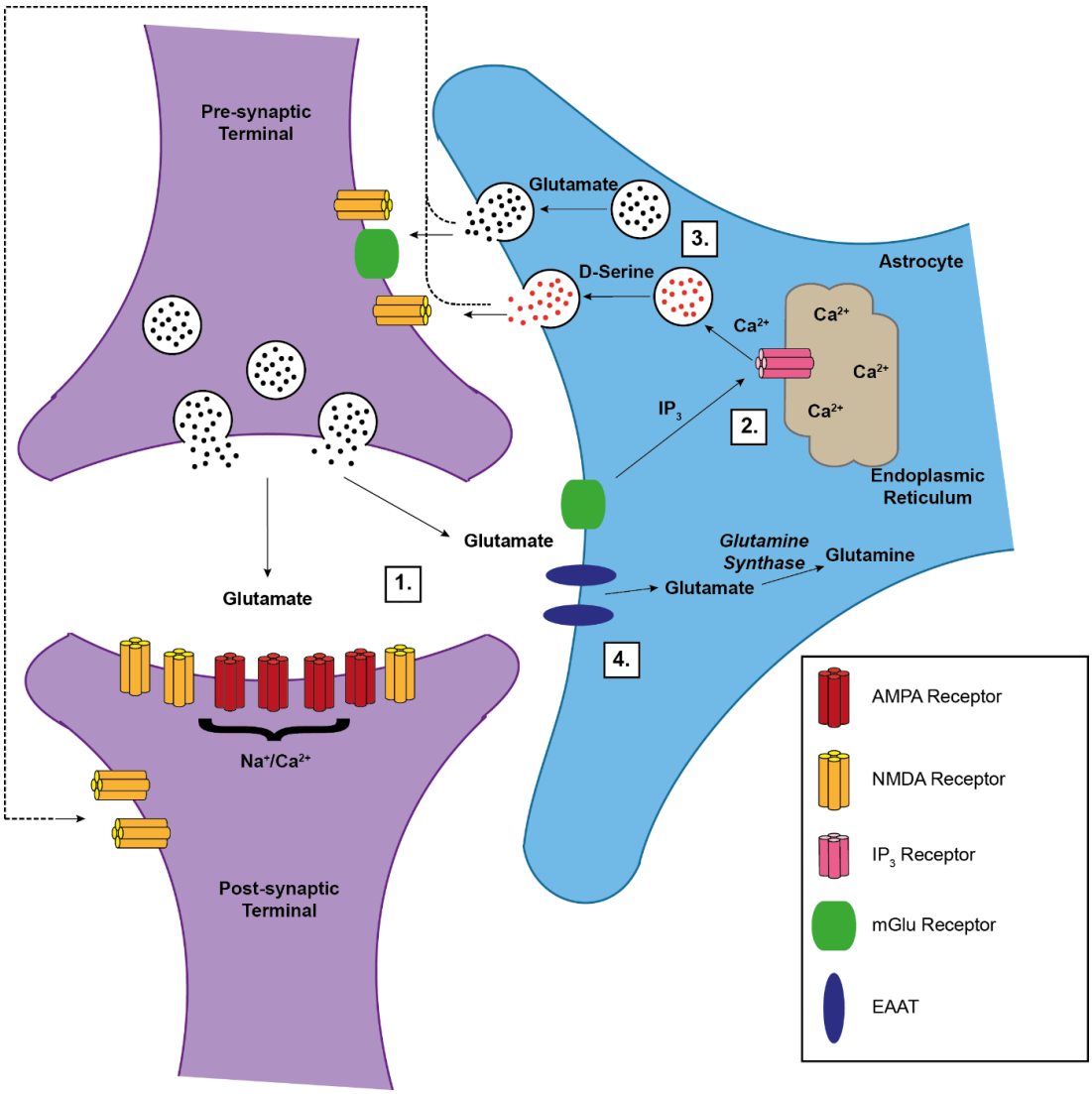

Figure 1.1: The Tripartite Synapse 1) Glutamate release from the pre-synaptic terminal activates ionotropic α-amino-3-hydroxy-5-methyl-4isozole propionic acid (AMPA) and N-methyl-D-aspartate (NMDA) glutamate receptors located at the post-synaptic terminal and metabotropic glutamate receptors located at astrocytic processes. 2) The activation of astrocytic metabotropic glutamate receptors elicits an increase in intracellular Ca^{2+} ions through IP_3-mediated release from the ER. 3) This triggers Ca^{2+}-dependent vesicle-mediated exocytosis of gliotransmitters which bind to receptors located at both the pre-and post-synaptic terminal and subsequently influence neuronal signalling. 4) Astrocytes also remove glutamate from the synaptic cleft through EAAT transporters where it is metabolised into glutamine by glutamine synthase.

1.1.4 Astrocytes and Gap Junctions

Connexins (Cx) are tetra-span transmembrane proteins with two extracellular loops, a small intracellular loop and cytoplasmic N- and C-terminal domains (Decrock et al., 2015). Six connexin proteins oligomerise to form a structure known as a connexon or connexin hemichannel (HC), which are expressed in the membrane of

adjacent cells where they bind to create an intercellular pore known as a gap junction channel (GJC), Figure 1.2 (Decrock et al., 2015). These channels exist in structures within the cell membrane known as gap junction plaques which are dense lateral clusters formed from intracellular proteins (Stout et al., 2015). The coupling of connexin hemichannels to create gap junctions produces a connectivity network enabling intercellular communication and trafficking (De Bock et al., 2014).

Pannexins are structurally similar to connexin proteins and oligomerise to create pannexin channels (Penuela et al., 2013). There are three human pannexins, Panx1, Panx2 and Panx3 and, as with connexins, six Panx1 protein subunits oligomerise to create a pannexin hemichannel (Penuela et al., 2013). Panx2 proteins do not oligomerise into hexamers but instead form heptamers or octamers (Ambrosi et al., 2010). The ability of pannexins to form intercellular channels was initially controversial, but has since been robustly established (Sahu et al., 2014).

Currently 21 human connexin proteins have been identified with differential tissue expression (De Bock et al., 2014; Söhl and Willecke, 2003). Astrocytes express Cx26, Cx30, Cx43, Cx40 and Cx45 which are responsible for creating an extensive astrocytic network within the CNS, with Cx30 and Cx43 being of particular functional importance (Dermietzel et al., 1991; Ezan et al., 2012; Giaume et al., 2013; Nagy et al., 1999). GJCs allow the intercellular movement of metabolites, signalling molecules and ions including Ca^{2+} and IP_3 both of which enable the propagation of calcium signalling between astrocytes, known as intercellular calcium waves (ICWs) (De Bock et al., 2014).

Astrocytes are also able to release gliotransmitters, including glutamate and ATP through hemichannels (Stout et al., 2002; Ye et al., 2003). Connexin 43 hemichannels are permeable to ATP in C6 rat glioma cells and in rat hippocampal astrocytes (Kang et al., 2008). Electrophysiological analysis of murine hippocampal slices shows that the release of ATP from astrocytes in response to glutamate is lost in Cx43/Cx30 knockout mice and reduced in the presence of carbenoxolone, a hemichannel blocker (Torres et al., 2012). The release of glutamate from rat astrocytes is also reduced by Gap26, a connexin 43 hemichannel inhibitor (Jiang et al., 2011).

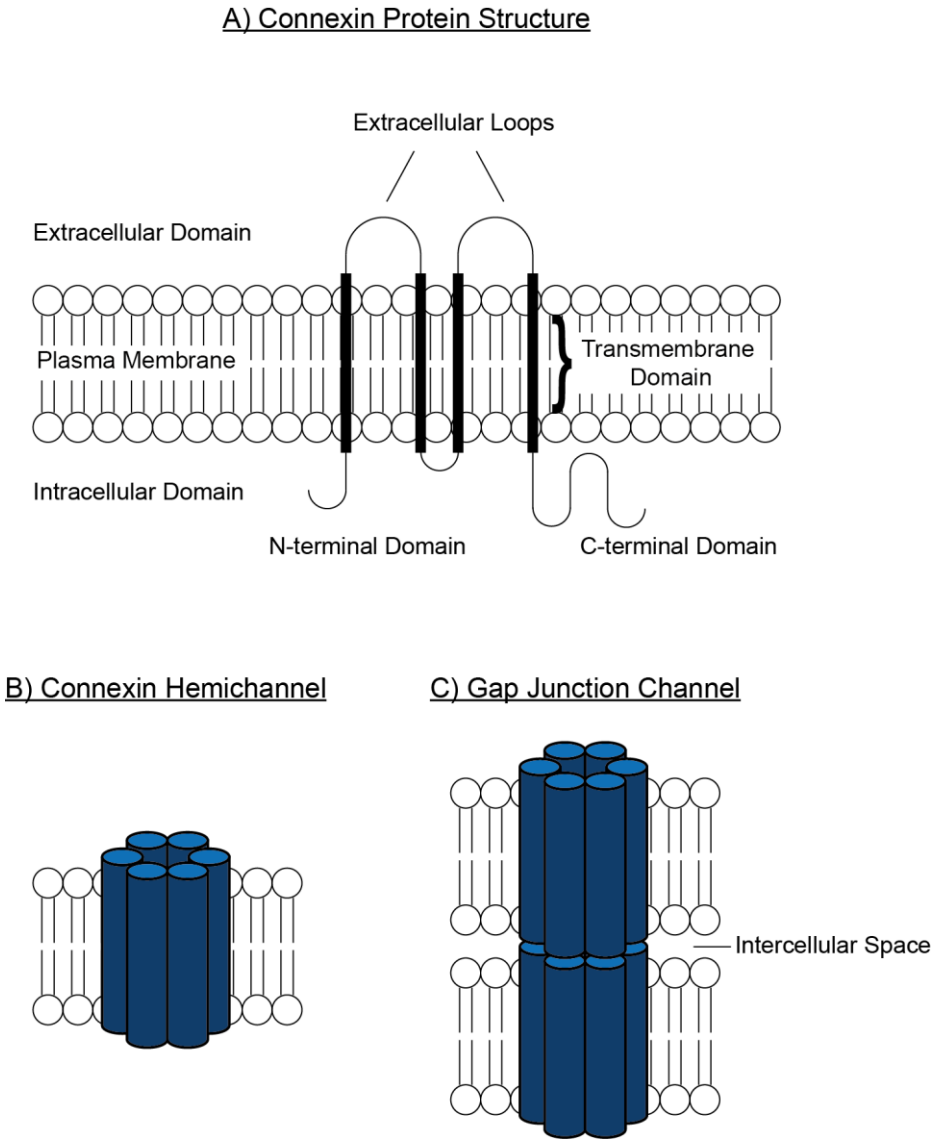

Figure 1.2: Connexin, Hemichannel and Gap Junction Structure A) Each connexin subunit is structurally composed of four transmembrane domains, two extracellular loops, a short intracellular loop and cytoplasmic N- and C-terminal domains. B) The oligomerisation of six connexin subunits forms a connexin hemichannel. C) Two connexin hemichannels expressed on adjacent cells oligomerise to generate a gap junction channel. These channels allow the intercellular movement of metabolites, molecules and ions.

1.1.5 Astrocytes and the Blood-Brain Barrier

The blood-brain barrier (BBB) is comprised of CNS endothelial cells which are connected by intercellular tight junctions (TJ) to create a continuous and non-fenestrated endothelial cellular sheet (Chow and Gu, 2015). This barrier isolates the brain from circulating blood, consequently allowing brain homeostasis to be precisely maintained and shielding the brain from potentially harmful or toxic agents, thus preserving neuronal survival (Chow and Gu, 2015). The CNS vasculature is

then sheathed in pericytes, astrocytic endfeet and neurons forming a structure known as the neurovascular unit (NVU), Figure 1.3.

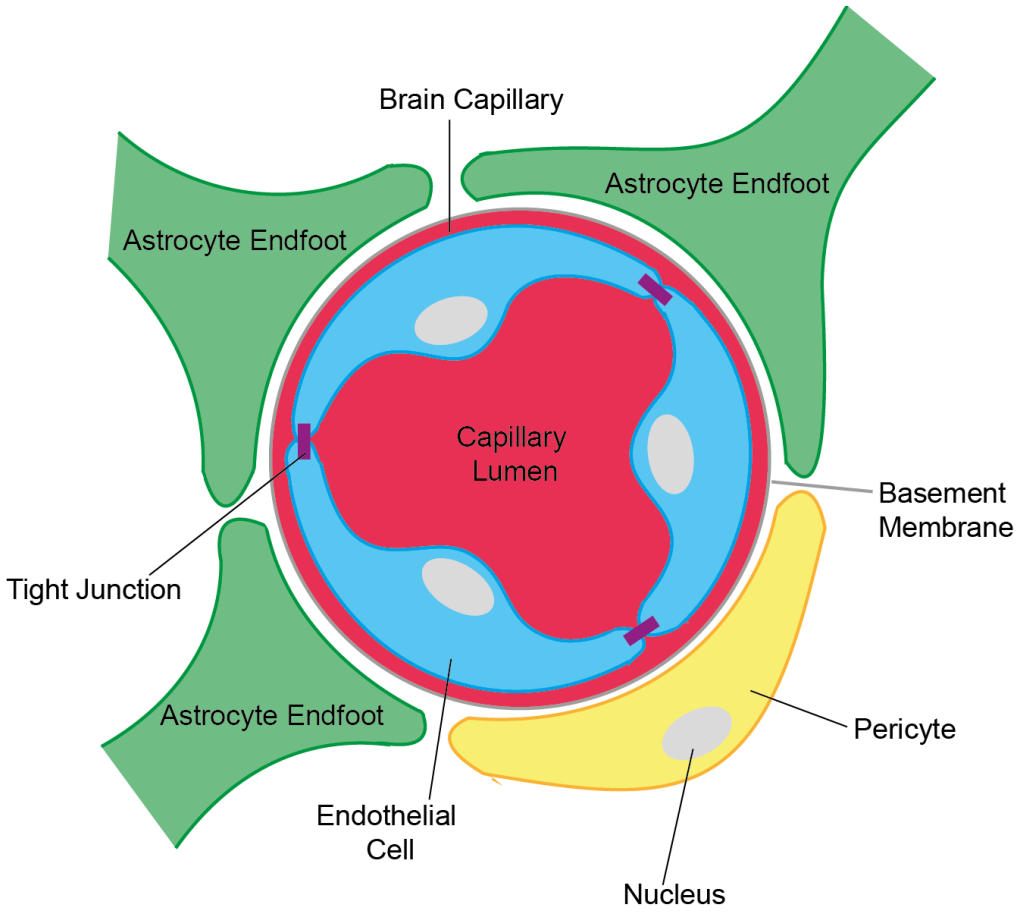

Figure 1.3: The Neurovascular Unit CNS endothelial cells are connected by tight junction complexes to create a continuous and non-fenestrated endothelial cellular sheet known as the BBB. These sheets form the CNS vascualture which is sheathed in pericytes, astrocytic endfeet and neurons to form the NVU.

Paracellular permeation and transcellular permeation are the two pathways by which molecules are able to cross epithelial/endothelial cellular sheets. Paracellular permeation occurs between cells through pores formed by intercellular tight junctions (TJs). Transcellular permeation occurs through cells and involves various different mechanisms including carrier-mediated transport and endocytosis (De Bock et al., 2016). Figure 1.4 shows a schematic depicting these two permeation pathways.

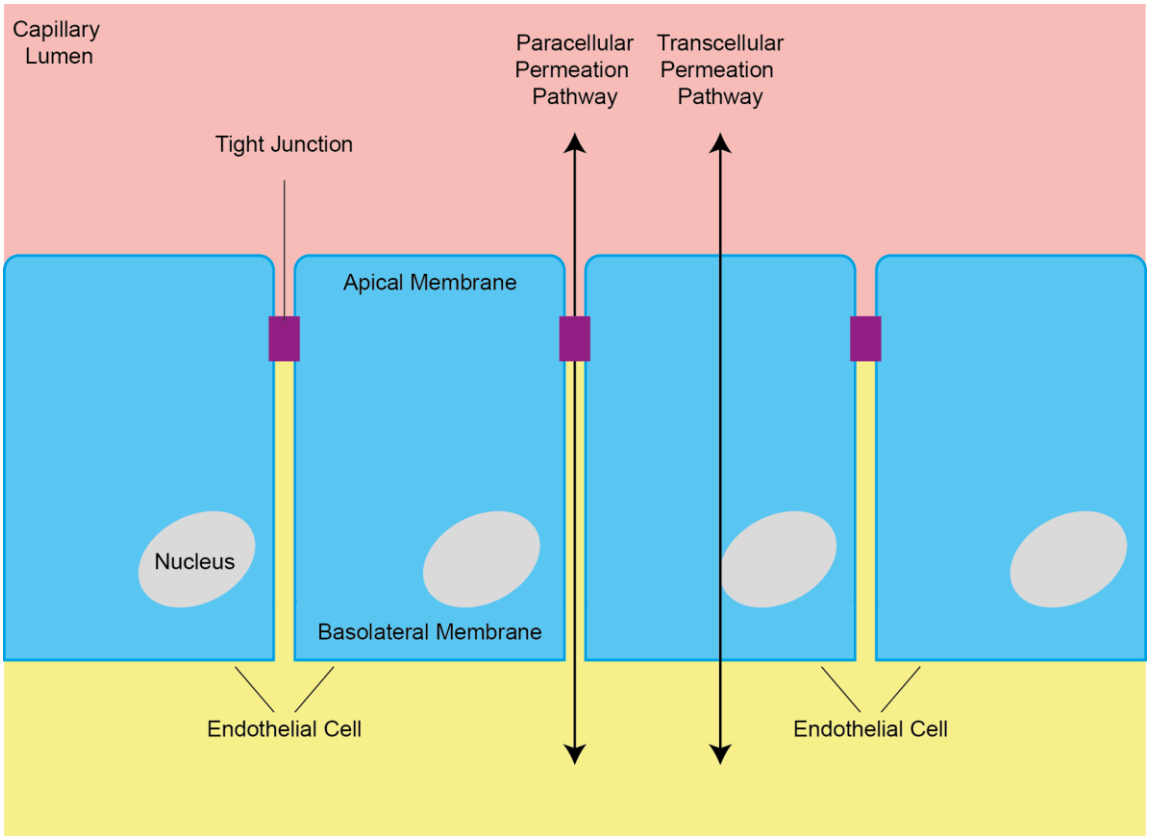

Figure 1.4: Permeation Pathways across Epithelial/Endothelial Cellular Sheets Paracellular permeation and transcellular permeation are the two pathways by which molecules cross epithelial/endothelial cellular sheets. Paracellular permeation occurs between the cells through paracellular pores formed by intercellular tight junctions. Transcellular permeation occurs through the cells and involves processes such as carrier-mediated transport and endocytosis.

Tight junctions are multiprotein complexes. The protein constituents within this complex determine the paracellular permeation properties of the tight junctions and consequently epithelial/endothelial cellular sheets (Chiba et al., 2008; Guillemot et al., 2008). Some tight junction proteins act as barriers which restrict paracellular permeation whilst others form ion-selective pores which facilitate the paracellular permeation of these molecules between epithelial/endothelial cells (Chiba et al., 2008). In the case of the BBB, paracellular permeation is highly restricted and transcellular permeation is tightly regulated (De Bock et al., 2016).

The components of the NVU engage in complex functional interactions which allow cerebral blood flow to be modulated by neuronal activity. The functional relationships between NVU components is known as neurovascular coupling (NVC) (Filosa et al., 2016). Astrocytes form an intrinsic component in NVC as they form a link between neuronal signalling and the cerebral vasculature.

1.1.6 Astrocytes and Neurovascular Coupling

In vitro experiments involving rat cortical slices demonstrate that vasodilation occurs in response to an increase in neuronal activity and is mediated by an elevation in astrocytic intracellular Ca^{2+} ions (Zonta et al., 2003). This mechanism of vasodilation involves cyclooxygenase (COX) (Zonta et al., 2003). *In vivo* experiments in mice show that an increase in astrocytic intracellular calcium activates the enzyme phospholipase A_2 (PLA_2), which releases arachidonic acid (AA) from membrane phospholipids (Takano et al., 2006). AA is then metabolised by COX-1 to produce prostaglandin E_2 (PGE_2) which mediates vasodilation (Takano et al., 2006).

Astrocytes have, however, also been shown to elicit vasoconstriction (Mulligan and MacVicar, 2004). An increase in astrocytic intracellular calcium activates PLA_2 and produces AA which diffuses to vascular smooth muscle cells where it is metabolised into 20-hydroxyeicosatetraenioc acid (20-HETE), a vasoconstrictor (Mulligan and MacVicar, 2004). The duality of astrocytic vasomotor control is illustrated in the retina as the stimulation of retinal astrocytes and Müller cells elicits both vasoconstriction and vasodilation (Metea and Newman, 2006). Vasoconstriction in the mammalian (rat) retina occurs in response to 20-HETE whilst vasodilation is mediated by other AA metabolites known as epoxyeicosatrienoic acids (EETs) (Metea and Newman, 2006).

The factors which determine and influence the duality of astrocytic vasomotor control have not yet been fully established. Nitric oxide (NO) can elicit both vasoconstriction and vasodilation and the levels of this molecule may influence astrocytic vasomotor responses (Metea and Newman, 2006). Metabolic state may also influence astrocytic vasomotor control (Gordon et al., 2008). In hippocampal and neocortical murine brain slices, an astrocytic elevation in intracellular calcium levels in response to an mGluR agonist causes arteriolar dilation in low (20%) O_2 levels whilst arterial constriction occurs in high (95%) O_2 levels. Anaerobic respiration is elevated in low O_2 causing an increase in extracellular levels of lactate which reduces the efficiency of prostaglandin transporters, thus increasing PGE_2 levels and producing vasodilation (Gordon et al., 2008). Changes in the AA pathway due to different O_2 levels have also been observed in *ex vivo* rat retina where low O_2 levels elicit vasodilation mediated by PGE_2 and EETs, whilst high O_2 levels elicit vasoconstriction mediated by 20-HETE (Mishra et al., 2011).

Potassium (K^+) ions also mediate vasomotor responses as an increase in extracellular K^+ ions in the perivascular space elicits vasodilation by increasing the conductance of inwardly rectifying K^+ (Kir) channels expressed by vascular smooth muscle cells (Filosa et al., 2006). Astrocytes were initially thought to facilitate potassium-mediated vasodilation through a mechanism known as K^+ siphoning in which neuronal activation increases the extracellular K^+ concentration generating a passive influx of these ions into astrocytic processes resulting in astrocytic depolarisation and a subsequent passive efflux of K^+ ions from astrocytic endfeet into the perivascular space (Paulson and Newman, 1987). It has since been shown, however, that this mechanism does not significantly contribute to neurovascular coupling (Metea et al., 2007). Instead, neuronal signalling elicits an elevation in astrocytic intracellular Ca^{2+} which activates Ca^{2+}-sensitive potassium (BK) channels located in perivascular astrocytic endfeet (Filosa et al., 2006; Price et al., 2002). Activated BK channels release K^+ ions into the perivascular space which activate smooth muscle Kir channels and elicit vasodilation (Filosa et al., 2006).

1.2 Tight Junctions

Tight junctions are multiprotein complexes which form intercellular barriers which can either restrict or facilitate paracellular permeation (Haseloff et al., 2015). The permeation properties of tight junctions is determined by the protein composition of the tight junction complex (TJC) (Chiba et al., 2008). Tight junctions also give epithelial/endothelial cells polarity by dividing the apical membrane from the basolateral membrane resulting in the selective distribution of membrane constituents (Haseloff et al., 2015). The proteins which form tight junctions are categorised into integral membrane proteins and cytoplasmic scaffolding proteins (Guillemot et al., 2008; Haseloff et al., 2015).

Tight junction integral membrane proteins are membrane-spanning proteins which have both extracellular and intracellular domains (Haseloff et al., 2015). Proximate integral membrane proteins in the cell membrane interact through intracellular cis-oligomerisation (Krause et al., 2008; Van Itallie and Anderson, 2014). The extracellular domains of integral membrane proteins expressed by adjacent cells also interact through intercellular trans-oligomerisation, Figure 1.5 (Krause et al., 2008; Van Itallie and Anderson, 2014). It is through these interactions that tight junction integral membrane proteins create an intercellular barrier. TJ integral membrane proteins are further categorised into three families: claudins, tight

junction-associated marvel proteins (TAMPs) and junctional adhesion molecules (JAMs) (Haseloff et al., 2015).

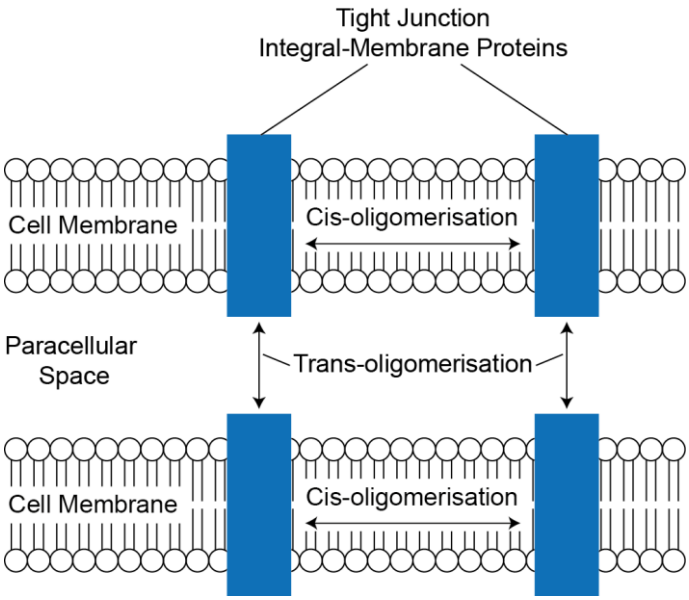

Figure 1.5: The Cis- and Trans-oligomerisation of Tight Junction Integral Membrane Proteins Tight junction integral membrane proteins create an intercellular barrier through oligomerisation. Proximate integral membrane proteins within the cell membrane interact through intracellular cis-oligomerisation. The extracellular domains of integral membrane proteins expressed on adjacent endothelial cells interact through intercellular trans-oligomerisation. Collectively these protein interactions create an intercellular barrier which can either restrict or facilitate paracellular permeation. The paracellular permeation properties of this barrier are determined by tight junction integral membrane proteins.

Tight junction cytoplasmic scaffolding proteins are structurally composed of multiple protein binding domains which enable them to link the integral membrane proteins to the actin cytoskeleton and strengthen the intercellular barrier (Guillemot et al., 2008). These proteins are also involved in cell signalling pathways (Guillemot et al., 2008). Tight junction cytoplasmic scaffolding proteins consist of numerous protein families which can be categorised into those with and without PDZ domains. PDZ is an acronym derived from the first three proteins identified with this structural domain: Psd-95, Dlg and ZO-1 (Guillemot et al., 2008).

This project focuses specifically on TAMPs and claudin proteins, consequently JAMs will not be discussed further. For a review of JAMs see (Garrido-urbani et al., 2014). This project also focuses on one cytoplasmic scaffolding protein family known as zonula occludens (ZO) proteins. For a comprehensive review of all the cytoplasmic scaffolding proteins see (Guillemot et al., 2008; Van Itallie and Anderson, 2014).

1.2.1 Tight Junction-associated Marvel Proteins

The TAMP family consists of occludin, tricellulin and MarvelD3 (Ikenouchi et al., 2005; Steed et al., 2009). TAMPs are defined by a conserved four-transmembrane (TM1-TM4) domain known as the MARVEL (MAL and related proteins for vesicle trafficking and membrane link) domain (Haseloff et al., 2015; Sánchez-Pulido et al., 2002). This project specifically focuses on occludin.

Occludin was first identified through experiments conducted on junctional fractions sourced from chicken liver tissue (Furuse et al., 1993). Human occludin is a 522 amino acid (aa), 59.144 kDa protein of which several isoforms have currently been identified, Table 1.1 (Ando-Akatsuka et al., 1996; Kohaar et al., 2010).

Occludin Isoform	No. of amino acids	Protein Size (kDa)	Uniprot Identifier
WT-OCLN	522	59.144	Q16625-1
OCLN-ex4del	468	52.706	Q16625-2
OCLN-ex7ext	479	54.124	Q16625-3
OCLN-ex3del	271	31.602	Q16625-4
OCLN-ex3-4del	200	23.324	Q16625-5
OCLN-ex3p-9pdel	69	8.033	Q16625-6
OCLN-ex3p-7pdel	70	8.175	Q16625-7

Table 1.1: Occludin Isoforms A list of all the occludin isoforms currently identified.

Beyond the MARVEL domain, the structure of occludin consists of a cytoplasmic N-terminal domain, two extracellular loops (ECL1 and ECL2), a short cytoplasmic loop and a long cytoplasmic C-terminal domain which is divided into the membrane-proximal and membrane distal domains, Figure 1.6 (Haseloff et al., 2015; Li et al., 2005b).

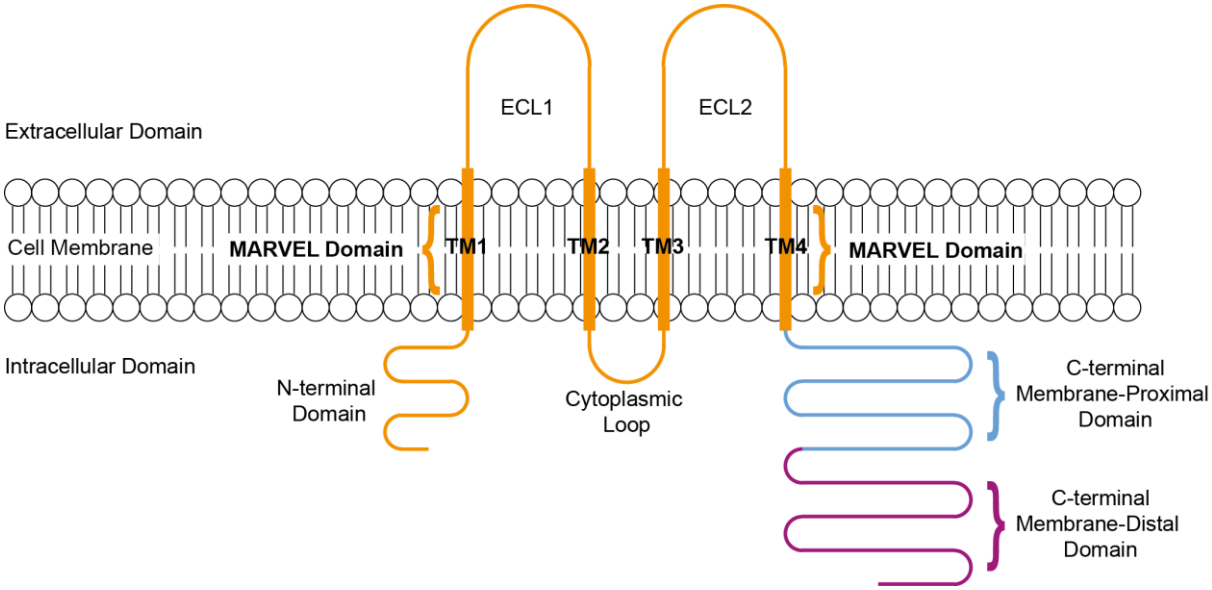

Figure 1.6: A Schematic depicting the general structure of Occludin Occludin is a tight junction integral membrane protein and a member of the TAMP family. TAMPs are structurally defined by the four-transmembrane MARVEL domain (TM1-TM4). Occludin has two extracellular loops (ECL1 and ECL2) which interact through trans-oligomerisation with the ECLs of occludin proteins expressed on adjacent endothelial cells. Occludin is also composed of a cytoplasmic N-terminal domain, a short cytoplasmic loop which links TM2 with TM3 and a long cytoplasmic C-terminal domain. The C-terminal domain is composed of the membrane-proximal domain (blue) and the membrane-distal domain (purple).

Occludin's N-terminal domain contains a PPPY motif which binds to E3 ubiquitin ligases (Raikwar et al., 2010; Traweger et al., 2002). ECL1 is rich in tyrosine and glycine residues and ECL2 contains two conserved cysteine residues which form a redox sensitive disulphide bond essential to the cis- and trans-oligomerisation of this protein (Bellmann et al., 2014). Occludin cis-oligomerisation is also mediated by the MARVEL domain (Yaffe et al., 2012). The ECL2 disulphide bond is maintained in an oxidative environment but is disrupted in a reducing environment such as in a state of hypoxia. This results in a loss of occludin trans-oligomerisation and accounts for the tight junction disruption produced in response to hypoxia (Bellmann et al., 2014; Mark and Davis, 2002).

The C-terminal membrane-distal domain is homologous to the conserved C-terminal domain present in a group of RNA polymerase II elongation factors known as the eleven-nineteen lysine-rich leukaemia (ELL) proteins (Li et al., 2005b). This domain is also the only part of occludin that has been successfully crystalized (Li et al., 2005b). Conserved lysine and arginine residues within the membrane-distal domain create a positively charged surface which facilitates the binding of occludin to ZO

proteins (Fanning et al., 1998; Li et al., 2005b). A more detailed diagram of occludin's structure is shown in Figure 1.7.

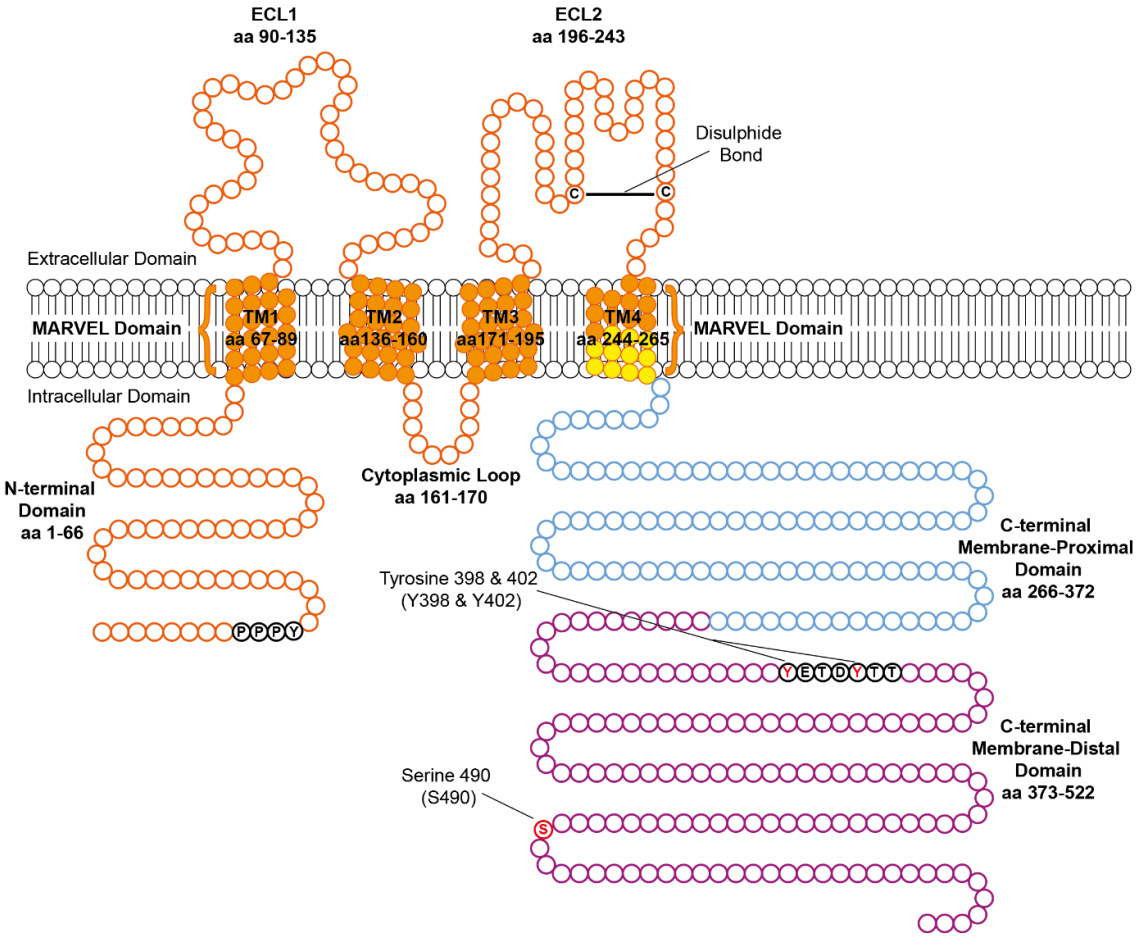

Figure 1.7: Occludin Protein Domain Structure, Motifs & Phosphorylation Sites Occludin is a 522 aa protein. The cytoplasmic N-terminal domain (aa 1-66) contains a conserved PPPY motif which mediates interactions with E3 ubiquitin ligases. ECL2 (aa 196-243) contains two conserved cysteine (C) residues which form a redox sensitive disulphide bond. This bond is required for the cis- and trans-oligomerisation of occludin. TM4 (aa 244-265) contains aa 255-265 (shown in yellow) which are involved in trafficking occludin to the cell membrane. The C-terminal membrane-distal domain is composed of aa 266-372 and the membrane-distal domain is composed of aa 373-522. The C-terminal membrane-distal domain contains conserved residues which enable occludin to bind to ZO proteins. This domain also contains a YETDYTT motif. The phosphorylation of the two tyrosine residues in this motif (shown in red) inhibits the interaction between occludin and ZO-1. Serine 490 is also located in the C-terminal membrane-distal domain and is a known phosphorylation site. Other putative post-translational modification sites have been identified throughout occludin, however, they have not yet been experimentally confirmed.

1.2.1.1. Occludin Post-translational modifications

Occludin's function is regulated by the phosphorylation of serine, threonine and tyrosine residues. Serine/threonine phosphorylation produces higher molecular

weight occludin protein bands ranging from 62-82 kDa (Sakakibara et al., 1997). Highly phosphorylated occludin is predominantly present in tight junctions suggesting that phosphorylation may influence the trafficking and inclusion of this protein into tight junctions (Sakakibara et al., 1997; Wong, 1997). Conversely, the dephosphorylation of occludin by protein phosphatase A2 (PPA2) increases paracellular permeability (Nunbhakdi-Craig et al., 2002).

The phosphorylation of occludin at serine 490 (S490) in the C-terminal membrane-distal domain reduces the interaction between occludin and ZO-1 by changing the charge distribution of the occludin binding surface (Sundstrom et al., 2009). Phosphorylation at this site increases in response to vascular endothelial growth factor (VEGF) (Sundstrom et al., 2009). The phosphorylation of tyrosine residues 398 and 402 in occludin's C-terminal YETDYTT motif by tyrosine-protein kinase Src (c-Src) also inhibits the interaction between occludin and ZO-1 (Elias et al., 2009). Mass spectrometry analysis has identified many putative phosphorylation sites in occludin with the majority of these sites located in the C-terminal domain (Butt et al., 2012a; Sundstrom et al., 2009). Phosphorylation at these sites, however, has not yet been verified experimentally.

Mass spectrometry analysis has also identified putative occludin serine and threonine residues which may be modified by O-β-glycosylation (Butt et al., 2012a). Serine residues 408 and 490 located in occludin's C-terminal membrane distal domain are also putative Yin Yang sites (Butt et al., 2012a). Yin Yang sites are serine or threonine residues which can be alternately modified by either phosphorylation or O-β-glycosylation (Haltiwanger et al., 1997; Wells et al., 2001). Residues within the C-terminal domain of RNA polymerase II are alternately subjected to either phosphorylation or O-β-glycosylation (Kelly et al., 1993). Currently, however, there is no experimental evidence confirming the presence of O-β-glycosylation or Ying Yang sites in occludin.

Ubiquitination is another post-translational modification which can affect protein function. Ubiquitin is a 76 aa protein with binds at lysine residues through an isopeptide bond (Swatek and Komander, 2016). The attachment of a single ubiquitin molecular is known as monoubiquitination, however, ubiquitin itself can be ubiquitinated in a process known as polyubiquitination to generate a polyubiquitin chain (Swatek and Komander, 2016). Monoubiquitination appears to elicits changes in protein trafficking whilst polyubiquitination generally mediates proteasome-dependent protein degradation (Pickart and Fushman, 2004).

A yeast two-hybrid screen shows that occludin interacts with Itch, an E3 ubiquitin ligase (Traweger et al., 2002). This interaction is further substantiated by the co-immunoprecipitation of endogenous Itch with endogenous occludin from homogenised embryonic mouse tissue (Traweger et al., 2002). This interaction occurs between the conserved occludin N-terminal PPPY motif and the Itch WW domain (Traweger et al., 2002).

VEGF induces occludin ubiquitination and increases the interaction between occludin and Itch which requires the phosphorylation of the occludin S490 residue (Murakami et al., 2009). Occludin is disrupted at cell borders and co-localises in intracellular puncta with lysosome-associated membrane protein 1, a marker for late endosomes and lysosomes, in bovine retinal endothelial cells (BRECs) treated with VEGF (Murakami et al., 2009). The ubiquitination of occludin induced by VEGF results in the clathrin-mediated endocytosis and endosomal trafficking of this protein leading to an increase in paracellular permeability (Murakami et al., 2009). It is during this process that occludin interacts with Epsin-1, epidermal growth factor receptor substrate 15 (Esp15) and hepatocyte growth factor-regulated tyrosine kinase substrate (Hrs). These proteins are ubiquitin receptor proteins which contain an ubiquitin-interacting motif (UIM) and mediate the endocytosis and endosomal trafficking of occludin (Murakami et al., 2009).

Occludin also interacts with Nedd4-2, another E3 ubiquitin ligase, at the N-terminal PPPY motif (Raikwar et al., 2010). The ubiquitination of occludin by Nedd4-2 also reduces the localisation of this protein to the membrane and increases paracellular permeability (Raikwar et al., 2010).

1.2.1.2. Occludin Trafficking

The intracellular trafficking of proteins to the cell membrane is a highly regulated process. The intracellular membrane trafficking of occludin appears to be functionally dependent upon aspects of this protein's molecular structure, although it remains unclear precisely which domains are required for this process. The C-terminal domain has been implicated in mediating the trafficking of occludin to the cell membrane (Furuse et al., 1994; Matter and Balda, 1998). Immunofluorescence analysis of Madin-Darby canine kidney (MDCK) cells transfected with wildtype and truncated occludin constructs, however, shows that neither the partial not complete loss of the C-terminal domain prevents the trafficking of occludin to the membrane (Subramanian et al., 2007).

Occludin splice variants in human intestinal cells which lack the fourth transmembrane domain (TM4) do not co-localise with ZO-1 at the cell membrane and instead remain in intracellular compartments, suggesting that this domain is involved in the trafficking of occludin (Mankertz et al., 2002). Mutant occludin lacking aa 260-265 in the TM4 domain localises in the cytoplasm of most MDCK cells (Subramanian et al., 2007). Further deletion of TM4 aa 255-259 results in a complete loss of membrane trafficking and the retention of occludin in the ER (Subramanian et al., 2007). A construct composed only of the TM4 and C-terminal domain (aa 244-522) is, however, also retained in the ER demonstrating that although the TM4 domain is required, it alone is unable to traffic occludin to the cell membrane (Subramanian et al., 2007).

The trafficking of vesicles containing occludin requires an intact microtubule and microfilament network. Confocal imaging of MDCK cells transfected with wildtype occludin tagged with GFP and treated with either nocodazole, a microtubule-disrupting agent, or cytochalasin D (Cyto D), an actin depolymerising agent, shows that the trafficking of occludin-carrying vesicles to the membrane is disrupted in the presence of either compound (Subramanian et al., 2007). Disruption of actin microfilaments also affects the localisation of occludin within the membrane causing this protein to disassemble from junctional complexes in a process facilitated by the activation of myosin light chain kinase (MLCK) (Subramanian et al., 2007).

1.2.1.3. The Effect of Changes in Occludin Expression

Overexpression of occludin increases the number of tight junctions and the transepithelial electrical resistance (TER) of MDCK cells (McCarthy et al., 1996). Freeze fracture analysis comparing wildtype and occludin-deficient embryoid bodies differentiated from embryonic stem cells shows no significant difference in the number or morphology of TJCs (Saitou et al., 1998). The aggregation of occludin-deficient stem cells in suspension culture demonstrates that intercellular interactions are maintained in the absence of occludin and suggests that the TJC is formed from other protein components besides occludin (Saitou et al., 1998). ZO-1 also remains capable of localising to the TJC in occludin-deficient embryoid bodies with no apparent changes in the level of protein expression suggesting that occludin is not functionally involved in junctional assembly (Saitou et al., 1998).

Occludin KO mice do not exhibit a lethal phenotype but do show a significant retardation in postnatal growth (Saitou et al., 2000). Immunofluorescence

microscopy of intestinal epithelial tissue demonstrates that there are no differences in the expression or localisation of other tight junction proteins such as claudin 3, ZO-1 and ZO-2 in either KO or wildtype mice, again suggesting that occludin is not functionally involved in the assembly of TJCs (Saitou et al., 2000). There is no significant difference in the intestinal epithelial resistance between either KO or wildtype mice, however, histological analysis shows the accumulation of granular mineral deposits, predominantly composed of calcium, located around the capillaries of the cerebellum and basal ganglia in occludin KO mice which are absent in the wildtype (Saitou et al., 2000). Occludin KO mice also exhibit significantly thinner bones compared with wildtype mice as well as abnormalities in the salivary glands, testis and gastric mucosa (Saitou et al., 2000). Although occludin does not appear to be fundamental to the formation of tight junctions, the complex phenotypes exhibited by occludin KO mice do suggest that occludin does influence the functional properties of these complexes (Saitou et al., 2000).

1.2.2 Claudin Proteins

Currently, 27 mammalian claudin genes have been identified (Mineta et al., 2011). The general structure of all claudin proteins consists of a tetra-span transmembrane domain (TM1-TM4), two extracellular loops (ECL1 is larger than ECL2), a short cytoplasmic N-terminal domain, a cytoplasmic loop and a cytoplasmic C-terminal domain, Figure 1.8 (Suzuki et al., 2014). The ECL1 of all claudin proteins contains a conserved motif, W-$[X]_{15\text{-}20}$-G($_N$)LW-$[X]_2$-C-$[X]_{8\text{-}10}$-C-$[X]_{15\text{-}16}$-R($_Q$), in which the two cysteines form a disulphide bond (Günzel and Yu, 2013). Most claudin proteins also have a PDZ-binding (YV) motif located at the end of the C-terminal domain which enables these proteins to bind to tight junction cytoplasmic scaffolding proteins (Günzel and Yu, 2013).

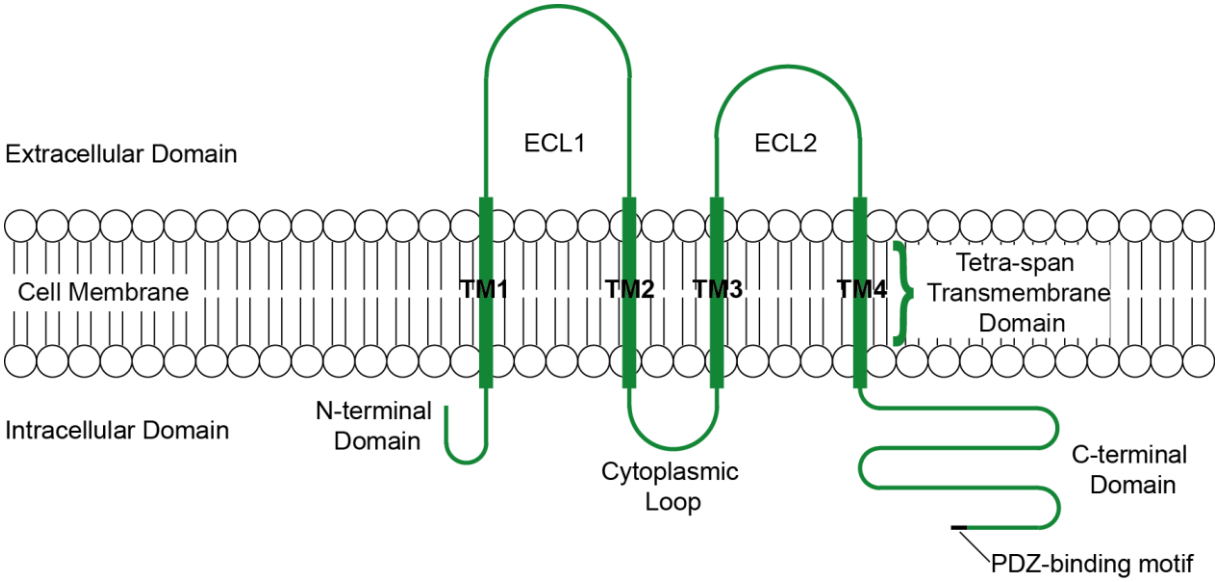

Figure 1.8: A Schematic depicting the general structure of Claudin Proteins Claudins are another family of tight junction integral membrane proteins. The general structure of claudin proteins consists of a tetra-span transmembrane domain (TM1-TM4), two extracellular loops (ECL1 is larger than ECL2), a short cytoplasmic N-terminal domain, a cytoplasmic loop and a cytoplasmic C-terminal domain. A PDZ-binding motif is located at the end of the C-terminal domain on most claudin proteins. This motif comsists of a tyrosine and a valine (YV).

ECL2 mediates the trans-oligomerisation of claudin proteins. Oligomerisation can occur between the same or different claudin proteins, known as homo- or heterophilic protein interactions respectively (Krause et al., 2015). Currently, only a few heterophilic claudin interactions have been investigated. Heterophilic trans-interactions have been identified between claudin 1/claudin 3, claudin 2/claudin 3 and claudin 3/claudin 5 (Daugherty et al., 2007; Furuse et al., 1999). Conversely, there are claudin proteins which appear unable to form heterophilic trans-interactions including claudin 1 with claudin 2, 4 and 5, claudin 3/claudin 4 and claudin 4/claudin 5 (Daugherty et al., 2007; Furuse et al., 1999).

The paracellular permeation properties of tight junctions is determined by claudin proteins. Some claudins tighten the intercellular barrier and restrict paracellular permeation whilst others form pores which facilitate the selective movement of ions between cells through the paracellular permeation pathway, Figure 1.9 (Krause et al., 2015). The charge and size-selectivity of claudin pores is determined by amino acids in ECL1 of these proteins (Krause et al., 2015).

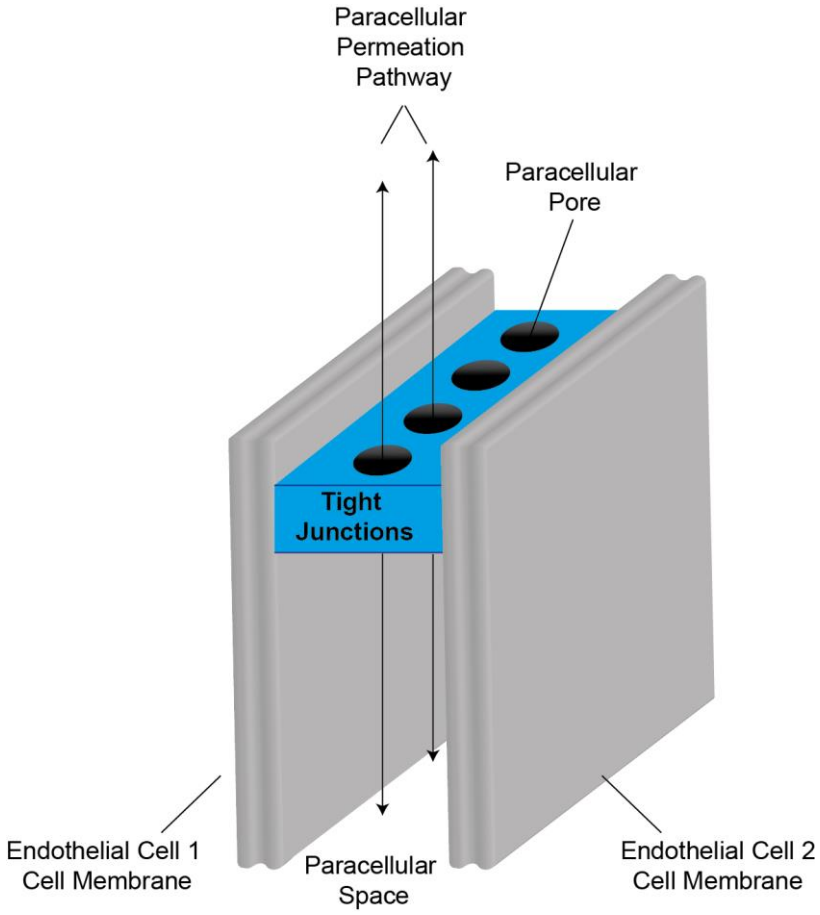

Figure 1.9: A model of Tight Junction Paracellular Pores Tight junctions create an intercellular barrier between epithelial/endothelial cells which can either restrict or facilitate paracelluar permeation. Paracellular permeation is facilitated across this barrier by intercellular pores. These pores are formed from the extracellular loops of pore-forming claudin proteins. These pores facilitate the selective movement of ions between cells via the paracellular permeation pathway.

1.2.2.1. Pore-forming Claudin Proteins

The paracellular pores formed by claudin proteins are size and charge-selective. This selectivity is determined by amino acids in ECL1 of pore-forming claudin proteins (Krause et al., 2015). Claudin 10 is a pore-forming claudin protein of which there are two splice variants, claudin 10a, which is anion-selective, and claudin 10b, cation-selective (Van Itallie and Anderson, 2006). Claudin 10a is preferentially permeable to anions due to two arginines present in the ECL1 of this protein, whilst a phenylalanine present in the ECL1 of claudin 10b contributes to the cationic selectivity of this pore (Li et al., 2013; Van Itallie et al., 2006).

Claudin 2 also forms cation-selective paracellular pores. The selectivity of these pores is conferred by an aspartic acid and a tyrosine located in ECL1 of this protein (Angelow and Yu, 2009a, b; Li et al., 2013). Cysteine-scanning mutagenesis has

also identified the amino acids which line the claudin 2 paracellular pore, Figure 1.10 (Li et al., 2014).

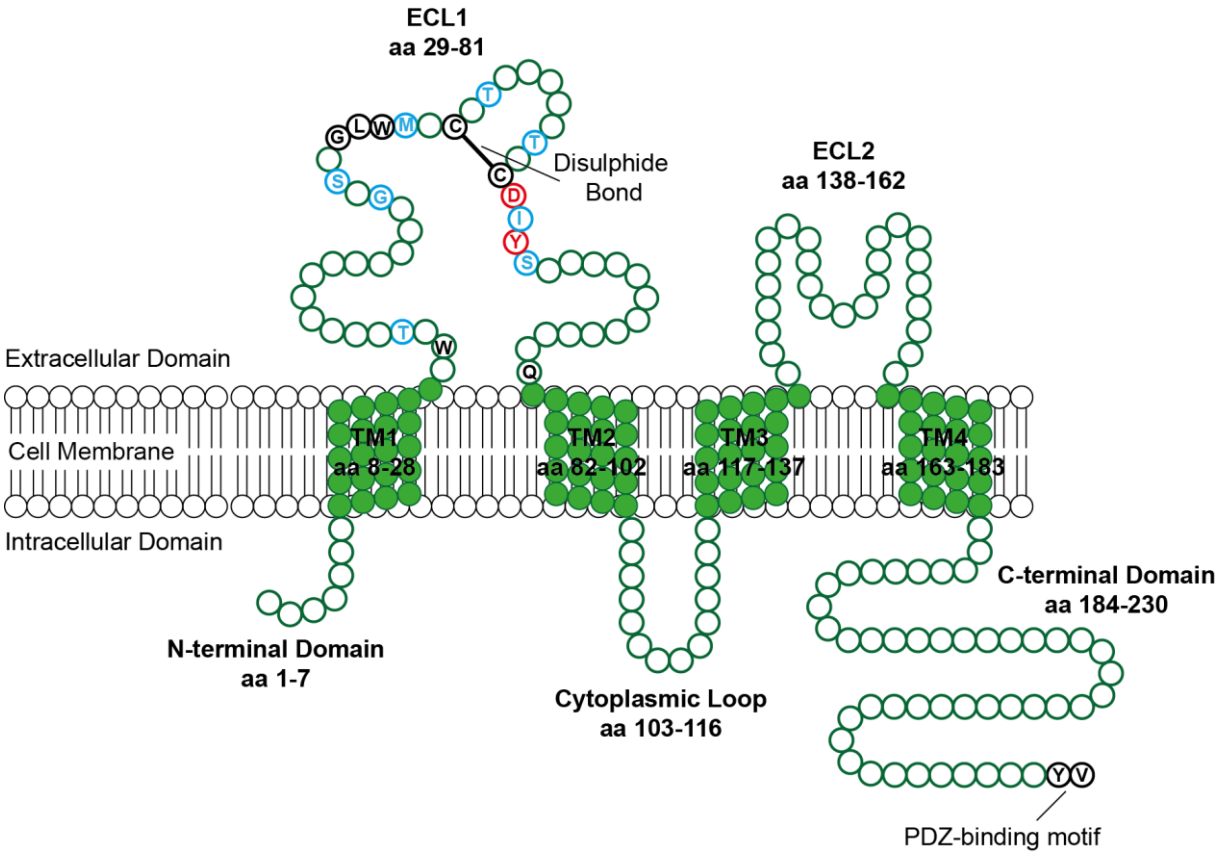

Figure 1.10: Claudin 2 Protein Domain Structure & Motifs Claudin 2 is a 230 aa protein which forms cation-selective paracellular pores. The ECL1 domain of this protein (aa 29-81) contains the conserved claudin protein W-$[X]_{15\text{-}20}$-$G_{(N)}$LW-$[X]_2$-C-$[X]_{8\text{-}10}$-C-$[X]_{15\text{-}16}$-$R_{(Q)}$ motif in which the two cysteines (C) form a disulphide bond. Aspartic acid (D65) and tyrosine (Y67) amino acids (shown in red) determine the cationic-selectivity of claudin 2 pores. The amino acids in blue also line the paracellular pore. The PDZ-binding motif (YV) is situated at the end of the C-terminal domain.

Claudin 15 creates paracellular pores which are selective for sodium ions (Na^+) while claudin 4 create pores which restrict the paracellular permeation of these ions (Colegio et al., 2002; Van Itallie et al., 2001; Van Itallie et al., 2003). The Na^+-selectivity of claudin 15 pores is reduced when acidic amino acids located in ECL1 are mutated to basic residues (Colegio et al., 2002). Similarly, the substitution of a positively charged lysine for a negatively charged aspartic acid in claudin 4 ECL1 enables the paracellular permeation of Na^+ ions through claudin 4 pores (Colegio et al., 2002). A lysine situated in ECL1 of claudin 17 has also been found to be essential to the anionic selectivity of the paracellular pores formed by this claudin protein (Krug et al., 2012).

Heterophilic claudin protein paracellular pores have also been identified. The cis-oligomerisation of claudin 4 and claudin 8 produces an anion-selective pore in mouse kidney cells (Hou et al., 2010). Claudin 16 and claudin 19 also engage in a heterophilic cis-interactions to produce cation-selective tight junctions in pig kidney epithelial cells (Hou et al., 2008).

1.2.2.2. Claudin Proteins as barriers

Some claudin proteins do not form pores and instead tighten the intercellular barrier and restrict paracellular permeation (Haseloff et al., 2015). Claudin 1, claudin 3 and claudin 5 are examples of claudin proteins which restrict paracellular permeation, consequently all three of these claudin proteins are present in the junctional complexes which form the BBB (Liebner et al., 2000; Neuhaus et al., 2008; Wolburg et al., 2003).

The barrier function of claudin 5 is determined by tyrosine 148 (Y148), tyrosine 158 (Y158) and glutamic acid 159 (E159) located in ECL2, Figure 1.11 (Piehl et al., 2010). These residues are essential to the homo- and heterophilic trans-oligomerisation interactions which enable claudin 5 to tighten the intercellular barrier and restrict paracellular permeation (Piehl et al., 2010).

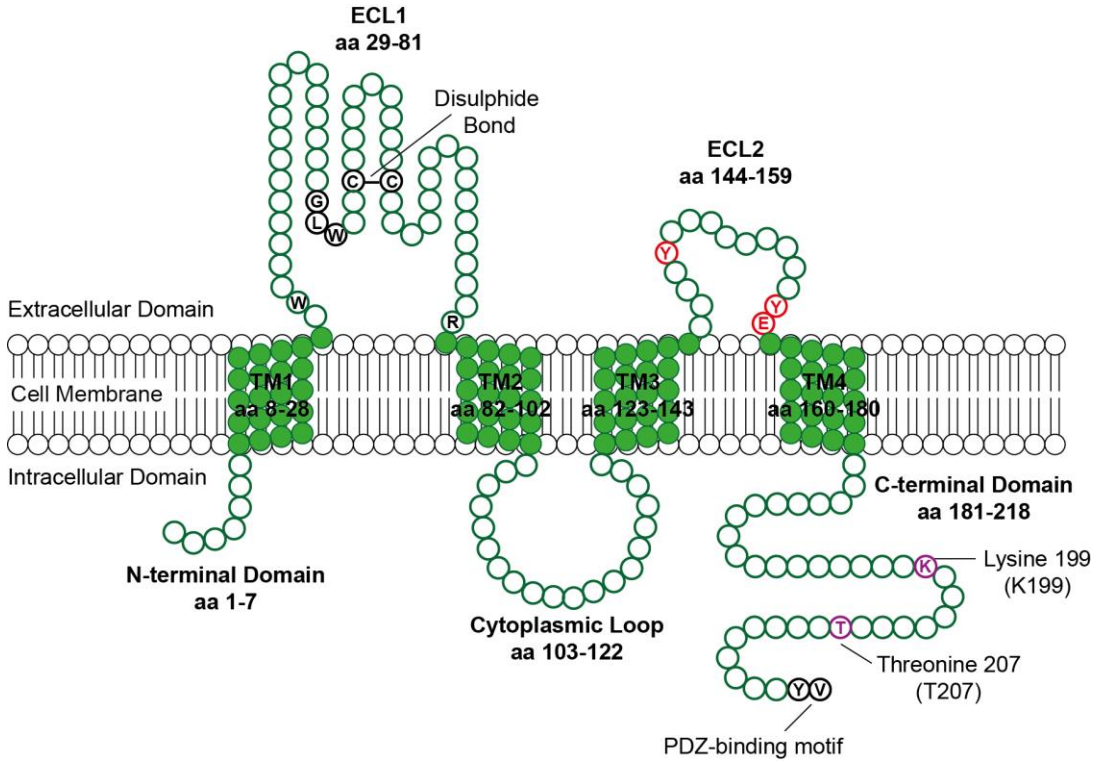

Figure 1.11: Claudin 5 Protein Domain Structure, Motifs & Post-translational Modification Sites Claudin 5 is a 218 aa protein which tightens the intercellular barrier and resticts paracellular permeation. It is due to these properties that this protein an important component in the BBB. The ECL1 domain of this protein (aa 29-81) contains the conserved claudin protein W-$[X]_{15\text{-}20}$-$G_{(N)}$LW-$[X]_2$-C-$[X]_{8\text{-}10}$-C-$[X]_{15\text{-}16}$-$R_{(Q)}$ motif in which the two cysteines (C) form a disulphide bond. The barrier function of this claudin protein is determined by three amino acids in ECL2. These are tyrosine 148 (Y148), tyrosine 158 (Y158) and glutamic acid 159 (E159) (shown in red). Claudin 5 is polyubiquitinated at lysine 199 (K199) in the C-terminal domain. Claudin 5 is also phosphorylated at threonine 207 (T207) which is located in the C-terminal domain. Both K199 and T207 are highlighted in purple. The PDZ-binding motif (YV) is situated at the end of the C-terminal domain.

Claudin 5 KO mice exhibit a lethal phenotype in which the mice do not survive more than 10 hours after birth (Nitta et al., 2003). Although brain endothelial cells remain capable of forming tight junctions in the absence of claudin 5, the integrity of the intercellular barrier is considerably compromised resulting in increased paracellular permeation and the diffusion of small molecules less than approximately 800 Da in size (Nitta et al., 2003).

1.2.2.3. Claudin Protein Regulation & Post-Translational Modifications

Post-translational modifications influence the membrane trafficking of claudin proteins and also affect the barrier function of the TJC. The phosphorylation of C-

terminal T203 in claudin 1 by mitogen-activated protein kinase (MAPK) enhances the barrier function of the junction complex (Fujibe et al., 2004). The dephosphorisation of claudin 1 by PPA2 increases paracellular permeability whilst the inhibition of this enzyme promotes claudin 1 phosphorylation and the recruitment of this protein to the TJC (Nunbhakdi-Craig et al., 2002). Similarly, the phosphorylation of claudin 2 at S208 in the C-terminal domain promotes membrane localisation of this protein (Van Itallie et al., 2012). Putative Ying Yang sites have been identified by computational analysis in claudin 1, claudin 3 and claudin 4, although there is currently no experimental evidence to confirm these predictions (Butt et al., 2012b).

Claudin 5 is phosphorylated at the C-terminal T207 by protein kinase A (PKA) (Ishizaki et al., 2003). Cyclic adenosine monophosphate (cAMP) enhances the phosphorylation of claudin 5 by PKA which promotes the membrane localisation of this protein but conversely rapidly decreases TER and increases the permeability of small molecules in porcine brain capillary endothelial cells (Soma et al., 2004). cAMP has previously been shown to increase the barrier function of the tight junction proteins in endothelial cells (Birukova et al., 2007; Rubin et al., 1991; Spindler et al., 2010). These contradictory observations suggest that other tight junction proteins may be involved in maintaining barrier integrity in response to cAMP.

Palmitoylation also promotes the membrane trafficking of some claudin proteins. Claudin proteins have four conserved cysteine residues, two of which are located in the cytoplasmic terminal of the TM2 domain and two in the cytoplasmic terminal of the TM4 domain (Van Itallie et al., 2005). The palmitoylation of these cysteine residues in claudin 14 is required for the efficient trafficking of this protein to the TJC (Van Itallie et al., 2005). Cysteine-serine claudin 14 mutants do maintain some membrane localisation, but ICC shows that the mutant protein predominantly localises to lysosomes (Van Itallie et al., 2005). Claudin 1 and claudin 2 are also palmitoylated although the effect of this modification upon the function of these proteins remains to be determined (Lynch et al., 2007). Occludin is not palmitoylated which, given the effect of this modification on claudin 14, suggests that the trafficking of occludin to the TJC does not require palmitoylation (Lynch et al., 2007). Putative palmitoylation sites have also been predicted in claudin 3 and claudin 4 (Butt et al., 2012b).

Ubiquitination mediates the endocytosis and degradation of some claudin proteins from the TJC. The ubiquitin E3 ligase LNX1p80 interacts directly with claudin 1, reduces the junctional expression of claudin 1, claudin 2 and claudin 4 in MDCK cells and promotes the ubiquitination of all three of these proteins (Takahashi et al., 2009). MDCK cells cultured in the presence of the lysosome inhibitor chloroquine contain higher levels of claudin-1 whilst the level of this protein remains unchanged in the presence of a proteasome inhibitor, suggesting that claudins are degraded by lysosomes (Takahashi et al., 2009). ICC shows LNX1p80 and claudin-2 co-localise in vesicular structures with either Rab7, a late endosome marker, or the lysosome enzyme cathepsin D. This further indicates that claudins are removed from the TJC by endocytosis and trafficked to lysosomes for degradation and suggests that this mechanism is facilitated by ubiquitination (Takahashi et al., 2009).

Claudin 5 is polyubiquitinated at lysine 199 and proteasome inhibition leads to the intracellular accumulation of polyubiquitinated claudin 5 in HeLa cells (Mandel et al., 2012). Lysosomal inhibition slightly increases the level of claudin 5 in HeLa cells, although it does not elicit an accumulation of ubiquitinated claudin 5 protein suggesting that the lysosome is involved in claudin 5 regulation through a mechanism that is not dependent upon ubiquitination (Mandel et al., 2012). It appears that the polyubiquitination of claudin 5 mediates the proteasomal degradation of this protein (Mandel et al., 2012).

1.2.3 Zonula Occludens (ZO) Proteins

Zonula occludens (ZO) proteins are a subset of a larger protein family known as membrane-associated guanylate kinase (MAGUK) like proteins (Guillemot et al., 2008). MAGUK proteins have multiple protein binding domains which are integral to their function as scaffolding proteins, as they serve to bind to and subsequently connect many different proteins to create a functional multiprotein complex (Guillemot et al., 2008). ZO-1 (195 kDa) was identified in epithelial cells and was the first tight junction protein to be identified (Stevenson et al., 1986). ZO-2 (160 kDa) and ZO-3 (130 kDa) are the two other members of the ZO protein family, both of which were discovered through co-immunoprecipitation with ZO-1 (Haskins et al., 1998; Jesaitis and Goodenough, 1994).

ZO proteins are structurally defined by the presence of three PDZ domains (PDZ-1, PDZ-2 and PDZ-3), a Src homology 3 (SH3) domain and a guanylate kinase (GUK) domain (Guillemot et al., 2008). A proline-rich region is located in the C-terminal

domain of ZO-1 and ZO-2 but is located between PDZ-2 and PDZ-3 in ZO-3 (González-Mariscal et al., 2000). These conserved domains are separated by six unique (U) domains, Figure 1.12 (Fanning et al., 2007).

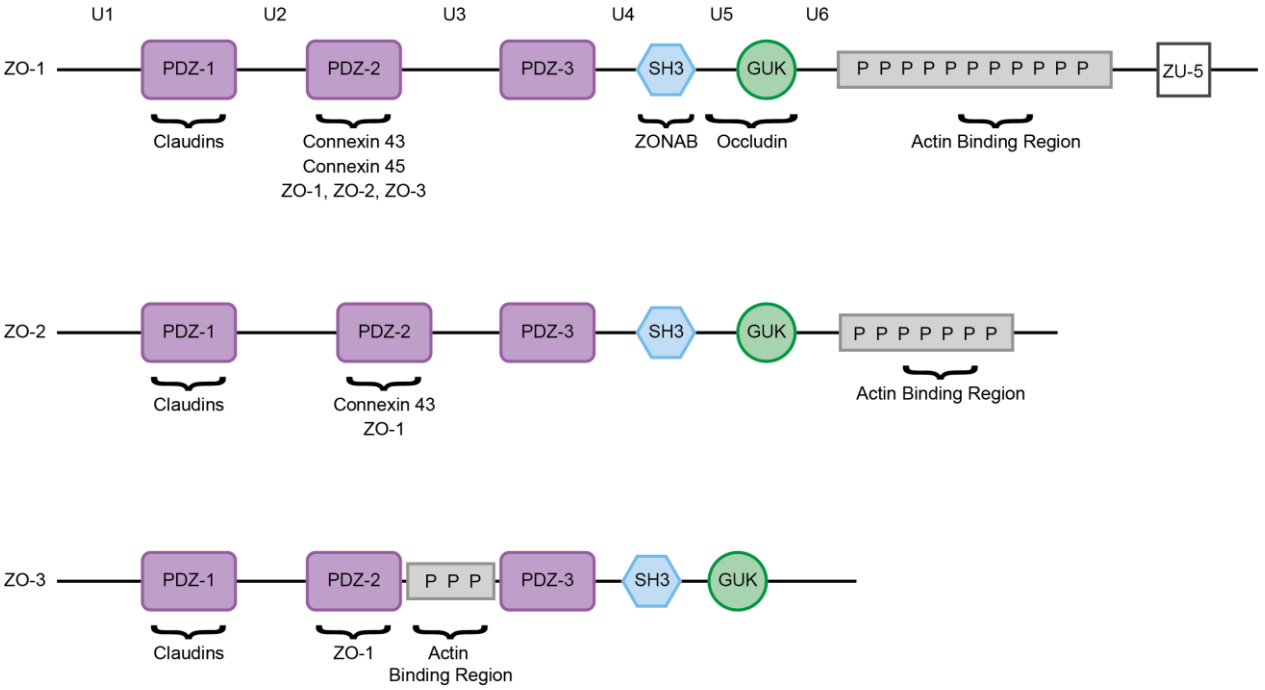

Figure 1.12: ZO Protein Structure ZO proteins are a family of cytoplasmic scaffolding proteins of which there are three members, ZO-1, ZO-2 and ZO-3. ZO proteins are structurally defined by the presence of three PDZ domains (PDZ-1, PDZ-2 and PDZ-3), a Src homology 3 (SH3) domain and a guanylate kinase (GUK) domain. These binding sites are integral to the scaffolding function of these proteins. Key protein binding partners are disclosed in this figure. The PDZ-1 domain binds to claudin proteins. The PDZ-2 domain binds to connexins and also enables ZO proteins to heterodimerise.

All three ZO proteins bind to claudins proteins at the PDZ-1 domain (Itoh et al., 1999). ZO proteins are able to heterodimerise through interactions which are mediated by PDZ-2 (Wittchen et al., 1999). ZO-1 is also able to form homodimers *in vivo* (Utepbergenov et al., 2006). The SH3 domain is approximately 60 amino acids in size and binds to proline-rich ligands initially considered to possess a PxxP binding motif, in which x denotes any amino acid (Feller et al., 1994). Further research has shown that SH3 domain peptide ligands are able to bind in two orientations. The orientation is determined by the location of a positively charged amino acid relative to the PxxP motif and gives rise to two classes of SH3 ligand, class I and class II (KAY et al., 2000). The SH3 domain present in MAGUK proteins, however, displays an atypical binding specificity as it does not bind to

proline-rich sequences but instead engages in intramolecular interactions with the GUK domain (McGee and Bredt, 1999; Shin et al., 2000).

The SH3-U5-GUK-U6 region in ZO proteins forms an intracellular hairpin which binds occludin (Fanning et al., 2007). The U5 domain within this intramolecular structure is crucial to this binding interaction and also mediates the localisation of ZO-1 to the tight junction complex whilst the U6 domain is able to negatively regulate U5 (Fanning et al., 2007). ZO proteins bind to F-actin through the actin-binding region (ABR) which is located in the proline-rich region of these proteins (Fanning et al., 1998; Fanning et al., 2002; Wittchen et al., 1999). The series of interactions between integral membrane proteins, cytoplasmic scaffolding proteins and the actin cytoskeleton which comprises the tight junction complex is illustrated in Figure 1.13.

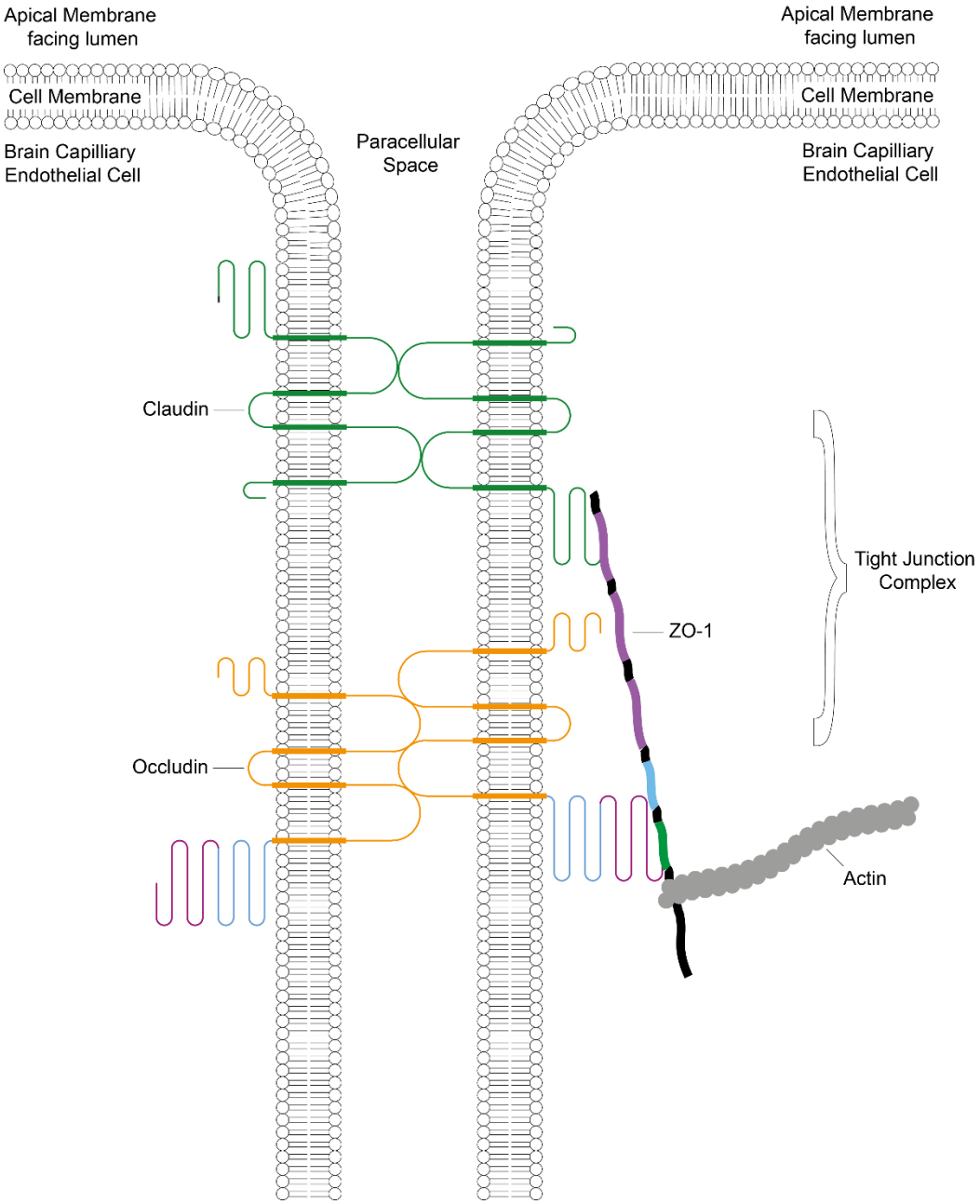

Figure 1.13: The Tight Junction Complex The barrier is generated through the intracellular cis-oligomerisation and intercellular trans-oligomerisation of integral membrane proteins. Cytoplasmic scaffolding proteins such as ZO-1 possess multiple binding domains which enable these proteins to bind to the cytoplasmic domains of integral membrane proteins and the actin cytoskeleton, consequently strengthening the integrity of the barrier.

ZO-1 also has a C-terminal ZU-5 domain which mediates the direct interaction of this protein with myotonic dystrophy kinase-related CDC42-binding kinase β (MRCKβ) (Huo et al., 2011). The interaction between ZO-1 and MRCKβ requires cell division control protein 42 homologue (CDC42) which binds to the kinase, inducing a conformational change which reveals the ZU-5 binding site (Huo et al., 2011). ZO-1 is responsible for the localisation of MRCKβ to the leading edge of

migrating cells and the complex formed from this interaction is required for cell migration (Huo et al., 2011). The ZU-5 domain implicates ZO-1 in cell migration and motility, demonstrating that the functional capacity of this protein is not restricted to the TJC.

1.2.3.1. Nuclear Localisation of ZO Proteins

The nucleus is separated from the cytoplasm by two concentric membranes known as the inner and outer nuclear membrane (INM and ONM) which are collectively known as the nuclear envelope (Webster and Lusk, 2016). Nuclear transport proteins facilitate the translocation of proteins across the nuclear envelope through nuclear pore complexes (NPCs). Proteins which possess nuclear localisation or exportation signals (NLS or NES) are able to bind to nuclear import proteins or nuclear export proteins respectively (Christie et al., 2015; Sloan et al., 2015).

ZO-1 is expressed diffusely throughout the nucleus of MDCK cells whilst ZO-2 exhibits a speckled staining pattern in these cells (González-Mariscal et al., 1999; Islas et al., 2002). Immunofluorescence shows that the localisation of ZO-2 is affected by confluency; a strong ZO-2 signal is detectable in both the nucleus and at the cell borders of sparse cultures whilst cell border staining with a weak nuclear signal is seen in confluent cultures (Islas et al., 2002). Putative nuclear localisation signals were initially identified in both ZO-1 and ZO-2 from MDCK cells using the PSORT program (González-Mariscal et al., 1999). Subsequently, the presence of nuclear localisation and export signals in all three ZO proteins has been confirmed experimentally (González-Mariscal et al., 2006).

ZO-2 partially co-localises with the pre-mRNA-splicing protein SC-35 in MDCK cells (Islas et al., 2002). ZO-2 also co-immunoprecipitates with Lamin B_1, a component of the nuclear lamina, demonstrating that this protein associates with the nuclear matrix (Jaramillo et al., 2004). ZO-2 localises with Scaffold Attachment Factor-B (SAF-B) in the nucleus of MDCK cells (Traweger et al., 2003). This interaction between these two proteins is mediated by the PDZ-1 domain of ZO-2 and the C-terminal domain of SAF-B (Traweger et al., 2003). ZO-2 also appears to be recruited to the nucleus from the cytoplasm in response to chemical stress in LLC-PK1 porcine kidney cells (Traweger et al., 2003).

The SH3 domain of ZO-1 binds to ZO-1 associated nucleic acid-binding protein (ZONAB), a Y-box transcription factor. The interaction between ZO-1 and ZONAB occurs within the tight junction complex, although ZONAB also localises to the

nucleus. (Balda and Matter, 2000). The interaction between these two proteins has been shown to regulate the expression of the erbB-2 gene, which encodes for receptor tyrosine-protein kinase-2, and is involved in epithelial differentiation and morphogenesis (Balda and Matter, 2000). The interaction between ZO-1 and ZONAB also regulates epithelial cell proliferation (Balda et al., 2003).

ZO-2 has also been shown to associate with the transcription factors Jun, Fos and C/EBP in MDCK cells (Betanzos et al., 2004) and to repress the transcription of Cyclin D1 which is involved in cell cycle progression (Huerta et al., 2007). ZO-2 forms a complex with c-Myc and HDAC1 which binds to the E-box promoter of the Cyclin D1 gene consequently repressing transcription.

1.2.3.2. ZO Proteins and Connexins

ZO-1 binds to many gap junction proteins including connexin 43 at the PDZ-2 domain (Giepmans and Moolenaar, 1998; Toyofuku et al., 1998) and with connexin 45 (Kausalya et al., 2001). ZO-1 has been shown to regulate gap junction size and also to facilitate the endocytosis and degradation of gap junction proteins (Akoyev and Takemoto, 2007; Gilleron et al., 2008; Hunter et al., 2005). Research involving cortical astrocytes isolated from mice also demonstrates *in vitro* that a dissociation between ZO-1 and connexin 43 occurs in response to intracellular acidification resulting in the persistent localisation of ZO-1 at the cell membrane whilst connexin 43 translocates into the cytoplasm (Duffy et al., 2004). *In vivo* experiments utilising mice have also observed the co-localisation of ZO-1 with Cx30 and Cx43 in astrocytes (Penes et al., 2005). Co-immunoprecipitation and *in vitro* pull-down assay experiments show that both Cx30 and Cx43 co-immunoprecipitate with ZO-1 and that Cx30 binds at the PDZ-2 domain (Penes et al., 2005). ZONAB also co-localises with ZO-1 and Cx32 in astrocytes and with ZO-1 and Cx47 oligodendrocytes (Penes et al., 2005).

1.3 Tight Junction Proteins in Astrocytes

Tight junction proteins are also expressed in non-epithelial cells including astrocytes. Rat primary cortical astrocytes and rat C6 glioma cells have been shown to express ZO-1 through ICC and immunoblotting techniques (Howarth et al., 1992). Occludin is highly expressed in undifferentiated astrocytes, astrocytes of the second to fourth passage, derived from new-born mice but is weakly expressed by both differentiated astrocytes, astrocytes of a higher passage with glial fibrillary acidic protein (GFAP) reactivity, and neurons derived from mice embryos (Bauer et

al., 1999). Human foetal cortical astrocytes have been shown to express occludin, ZO-1 and ZO-2 *in vitro* (Duffy et al., 2000). ZO-3, however, does not appear to be expressed in these cells (Duffy et al., 2000). ZO-1 also co-localises with transient receptor potential channel-4 (TRPC4), a cation channel which may be involved in astrocytic Ca^{2+}-mediated glutamate release in human foetal astrocytes *in vitro* (Song et al., 2005)

Increased expression of occludin in astrocytes and neurons has also been observed in post-mortem human brain tissue from different neurodegenerative diseases, including Alzheimer's Disease (AD) and vascular dementia (VD) (Romanitan et al., 2007). In the frontal cortex and head of the caudate nucleus occludin immunoreactivity is predominantly associated with pyramidal neurons with the ratio of neurons expressing occludin in cortex and striatum significantly higher in AD and VD cases compared with non-neurological controls. Occludin expression is also observed in both astrocytes and oligodendrocytes (Romanitan et al., 2007). A qualitative analysis of this staining determined that more astrocytes than oligodendrocytes are positive for occludin in the basal ganglia and, in the white matter of the frontal cortex, more occludin positive astrocytes and oligodendrocytes are observed in AD and VD cases compared with non-neurological controls. It also appears that, in the basal ganglia, astrocytic occludin expression is preferentially localised to the nucleus (Romanitan et al., 2007).

The same cohort was also used to investigate the expression of claudin 2, claudin 5 and claudin 11 in the frontal cortex (Romanitan et al., 2010). All three claudins are expressed in pyramidal neurons, oligodendrocytes and astrocytes, with a significant increase in the ratio of astrocytes expressing claudin 2 and claudin 11, but not claudin 5, in AD and VD cases compared with non-neurological controls (Romanitan et al., 2010).

Glial expression of occludin and ZO-1 is also observed in research investigating the effect of BBB dysfunction in the pathology of age-associated cerebral white matter lesions (WMLs) whilst claudin 5 expression is exclusively associated with endothelial cells (Simpson et al., 2010). These findings are supported by research investigating the role of BBB dysfunction in the ageing brain in relation to Alzheimer-type pathology as glia in the cerebral cortex are similarly shown to express occludin and ZO-1, but not claudin-5 (Viggars et al., 2011).

A microarray analysis investigating changes in the astrocyte transcriptome in relation to the pathogenesis of age-related neurodegenerative pathology shows that

there is a significant reduction in transcripts which encode for TJPs in association with increasing Alzheimer-type pathology (Simpson et al., 2011). The astrocytic expression of mRNA sequences encoding for TJPs determined by this microarray analysis provides further support to immunohistochemical evidence regarding the expression of TJPs in astrocytes. The pathogenesis of many neurodegenerative disorders including AD is associated with neurovascular dysfunction and BBB disintegration, the latter being partially caused by a disruption in endothelial TJP expression (Nelson et al., 2016; Zlokovic, 2011).

1.4 Hypothesis & Aims

Astrocytes both *in vitro* and *in vivo* have been shown to express tight junction proteins. Astrocytes, however, do not form tight junctions, consequently the function of these proteins within these cells is unclear and has not yet been explored. There is also evidence to suggest that the astrocytic expression of tight junction proteins changes with AD pathogenesis.

Occludin, claudin 5 and ZO-1 were selected for investigation in this project. These proteins were selected because they were all identified in the microarray study investigating changes in the astrocyte transcriptome in relation to the pathogenesis of age-related neurodegenerative pathology (Simpson et al., 2011).

This initial aim of this study was to characterise the expression of these three tight junction proteins in human primary astrocytes and 1321N1 astrocytoma cells. This study also aimed to define the cellular localisation of occludin, claudin 5 and ZO-1 in the temporal cortex and investigate whether the expression of these proteins is altered in MCI and AD cases compared with controls. This study also aimed to investigate the function of these proteins in astrocytes by identifying protein binding partners.

It is hypothesised that tight junction proteins in astrocytes display functions beyond the formation of intercellular barriers and that changes in astrocytic tight junction protein expression may contribute to AD progression.

2. Materials and Methods

2.1 Tissue Culture

2.1.1 Cells and Culture Medium

Human embryonic primary astrocytes (HA) isolated from the cerebral cortex were purchased from ScienCell Research Laboratories and were cultured in either Astrocyte Medium (AM) or MEMα/F-10 medium. AM composition: 500 ml Astrocyte Basal Medium, 2% (v/v) Foetal Bovine Serum (FBS), 1% (v/v) Astrocyte Growth Supplements (AGS) and 1% (v/v) Penicillin (10, 000 units/ml) / Streptomycin (10, 000 g/ml) solution (P/S). All reagents purchased from ScienCell Research Laboratories. MEMα/F-10 medium composition: 250 ml Minimum Essential Medium α (MEMα) (Gibco), 250 ml Ham's F-10 nutrient mix (Gibco), 10% (v/v) FBS (Sigma) and 1% (v/v) Penicillin (50 units/ml) / Streptomycin (50 g/ml) solution (P/S) (Lonza).

1321N1 human astrocytoma cell line and human embryonic kidney 293 (HEK 293) cells were cultured in Dulbecco's Modified Eagle Medium (DMEM) (Gibco), supplemented with 10% (v/v) FBS (Sigma), 1% (v/v) Penicillin (50 units/ml) / Streptomycin (50 g/ml) solution (P/S) (Lonza).

Human umbilical vein endothelial cells (HUVEC) were purchased from PromoCell and were cultured in Endothelial Cell Medium (ECM) supplemented with 5% (v/v) FBS, 1% Endothelial Cell Growth Supplements (ECGS) and 1% (v/v) Penicillin (10, 000 units/ml) / Streptomycin (10, 000 g/ml) solution (P/S). All reagents purchased from ScienCell Research Laboratories.

2.1.2 Culture Conditions

Cells were cultured in 75 or 175 cm^2 tissue culture flasks (Thermo Fisher Scientific), 10 cm tissue culture dishes and 12 or 24-well cell culture plates. Cells were grown at 37 ^oC in a humidified atmosphere of 5% CO_2/95% air. The culture medium was changed at least every third day of culture. Cells were passaged when cultures were 80% confluent and re-seeded at the required cell density. Primary cells were not cultured beyond passage 10 in accordance with company recommendations. All experiments requiring primary cells were conducted using cells cultured between passage 4 and passage 6. Experiments comparing human primary astrocytes cultured in either ScienCell Astrocyte Medium or MEMα/F-10 medium were conducted using cells of the same passage number.

2.2 Immunocytochemistry

Cells were cultured in either 12 or 24 well plates on 13 mm coverslips seeded at 5000 cells/ml. Once confluent, the cells were washed once in heated 37 ^{o}C phosphate buffered saline (PBS). The cells were then fixed with heated 37 ^{o}C 4% paraformaldehyde (PFA) (4% PFA (w/v) in PBS) for 10 minutes at 37 ^{o}C after which the cells were washed three times in PBS and permeabilised in 0.3% (v/v) Triton X-100 in PBS for 3 minutes at room temperature. The cells were again washed three times in PBS and incubated in blocking solution (3% (w/v) bovine serum albumin (BSA), 0.01% Tween 20 in PBS) for 1 hour at room temperature. The cells were then incubated in 70 µl primary antibody, Table 2.1, for 2 hours at room temperature. All primary antibodies were made up in blocking solution. A negative control (omission of the primary antibody) and an isotype control were also included to confirm antibody specificity. The isotype control consisted of a specific mouse or rabbit IgG (Vector Laboratories) used at the same concentration as the primary antibody.

Antibody	Species	Dilution	Supplier	Code
ALDH1L1	Rabbit Polyclonal	1:50	Abcam	ab79727
beta-3-Tubulin	Chicken Polyclonal	1:1000	Merck Millipore	AB9354
Claudin 5	Rabbit Polyclonal	1:50	Abcam	ab15106
DDX3X	Rabbit Polyclonal	1:50	Atlas Antibodies	HPA001648
GFAP	Rabbit Polyclonal	1:500	Abcam	ab7260
Nestin	Rabbit Polyclonal	1:250	Abcam	ab92391
Occludin	Rabbit Polyclonal	1:50	Thermo Fisher Scientific	71-1500
Vimentin	Mouse Monoclonal IgG1	1:250	Abcam	ab8978
ZO-1	Rabbit Polyclonal	1:100	Thermo Fisher Scientific	40-2200

Table 2.1: Immunocytochemistry primary antibodies

The cells were then washed three times in PBS and incubated in the dark with the appropriate fluorescent secondary antibody, Table 2.2, for 1 hour at room temperature. All secondary antibodies were made up in blocking solution.

Antibody	Dilution	Supplier	Code
Alexa Fluor® 488 goat anti-mouse	1:500	Thermo Fisher Scientific	A11001
Alexa Fluor® 488 goat anti-chicken	1:500	Thermo Fisher Scientific	A11039
Alexa Fluor® 568 donkey anti-rabbit	1:500	Thermo Fisher Scientific	A10042

Table 2.2: Immunocytochemistry secondary antibodies

The cells were again washed three times in PBS and incubated in the dark with Hoescht 33342 (10 µg/ml) diluted 1:2000 in PBS for 10 minutes at room temperature to stain the cell nuclei. Finally the coverslips were washed three times in PBS and mounted onto glass slides using fluorescent mounting medium (DAKO). Images were taken using a Nikon microscope and processed using ImageJ and Adobe Illustrator software.

2.3 Whole Cell Lysis for SDS-PAGE

The cells were cultured in 10 cm tissue culture dishes and lysed once they had reached approximately 80% confluency. The cells were washed twice in ice-cold PBS and collected using a cell scraper in 200 µl lysis buffer (100 mM Tris-HCl pH 7.5, 75 mM NaCl, 0.5% (w/v) SDS, 20 mM sodium deoxycholate, 1% (v/v) Triton X-100, 2 mM sodium orthovanadate ($NaVO_4$), 1.25 mM sodium fluoride (NaF), 10 mM ethylene diamine tetra-acetic acid (EDTA), Protease Inhibitor Cocktail (PIC) (Roche) and PhosSTOP (Roche)). The lysates were transferred into 1.5 ml Eppendorf tubes and incubated on ice for 30 minutes, after which they were sonicated for 5 seconds using a probe sonicator set to 60% amplitude. The lysates were subsequently centrifuged at 15, 500 x g for 30 minutes at 4 ^{o}C. The supernatants were transferred into fresh 1.5 ml Eppendorf tubes, flash frozen in liquid nitrogen and stored at -80 ^{o}C.

2.4 Subcellular Fractionation

Human primary astrocytes were fractionated into cytoplasmic and nuclear fractions to investigate protein localisation. Cells were cultured in 10 cm tissue culture dishes and lysed once they had reached approximately 80% confluency. The cells were washed in ice-cold PBS and collected using a cell scraper in 100 µl sterile hypotonic lysis buffer (20 mM tris-HCl, 10 mM NaCl, 3 mM $MgCl_2$, 1 mM PMSF, 1 mM DTT, pH 7.4, protease inhibitor cocktail and PhosStop). The lysates were transferred into 1.5 ml Eppendorf tubes and incubated on ice for 15 minutes. The cell lysates were then mixed with 25 µl of a 10% Nonidet P-40 solution (10% v/v Nonidet P-40 in PBS) and centrifuged at 13,000 x g for 5 minutes at 4 ^{o}C. The supernatant

(cytoplasmic fraction) was retained and the remaining pellets washed once in 50 µl hypotonic buffer before being resuspended in 50 µl cell extraction buffer (Invitrogen, supplemented with 1 mM PMSF, 1 mM DTT, protease inhibitor cocktail, PhosStop) and incubated on ice for 30 minutes. During this 30 minute incubation, the lysates were vortexed at 10 minute intervals. The lysates were then centrifuged at 17, 000 x g for 30 minutes at 4 ^{o}C. The supernatant (nuclear fraction) was retained and the pellet containing insoluble proteins and cell debris was discarded. Both cytoplasmic and nuclear fractions were flash frozen in liquid nitrogen and stored at -80 ^{o}C.

2.5 Determination of Protein Concentration

The protein concentration of whole cell lysates was determined using a bicinchoninic acid (BCA) protein assay kit (Pierce) used according to the manufacturer's instructions. This assay utilises the biuret reaction, in which peptides reduce cupric (Cu^{2+}) ions to cuprous (Cu^{1+}) in an alkaline environment (Smith et al., 1985). BCA assays were run in 96 well plates (Sigma). BSA standards (concentration range 0-2 mg/ml) diluted in PBS were included in each assay and all lysates were diluted 1:10 in PBS. Both standards and samples were plated out in duplicate. Colorimetric detection was achieved at 550 nm with a FLUOstar Omega microplate reader with Omega software (BMG Labtech).

The protein concentration for fractionated cell lysates was determined using a Bradford assay. The BCA assay could not be used to determine the protein concentration of fractionated samples due to the presence of ethylene glycol-bis(2-aminoethyl ether)-N,N,N'N'-tetraacetic acid (EGTA) in the cell extraction buffer purchased from Invitrogen to lyse cell nuclei. EGTA is not compatible with the BCA assay. A 1-5 µl sample of cell lysate was added to 1 ml of Bradford reagent mix (800 µl H_2O, 200 µl Protein Assay Dye Reagent (Bio-Rad)). Colorimetric detection was achieved at 595 nm with a spectrophotometer. A Bradford reagent mix control was also included. The protein concentration of the cell lysate was determined using the following formula:

Cell lysate protein concentration (mg/ml) =

$$\frac{Optical\ Density\ x\ 15}{Volume\ of\ lysate\ sample\ added\ to\ Bradford\ Reagent\ Mix}$$

2.6 SDS-polyacrylamide gel electrophoresis (SDS-PAGE)

Samples containing 20-30 µg of protein were used for SDS-polyacrylamide gel electrophoresis. All samples were made to contain an equal amount of protein. Samples were mixed with either 4x Laemmli buffer (200 mM Tris HCl (pH 6.8), 8% (w/v) SDS, 40% (v/v) glycerol, 0.4% bromophenol blue, 400 mM DTT) or 6x Laemmli buffer (60 mM Tris HCl (pH 6.8), 12% (w/v) SDS, 47% (v/v) glycerol, 0.06% bromophenol blue, 0.6 M DTT) and boiled at 95 ^{o}C for five minutes to denature the proteins. Claudin 5 was found to aggregate when the protein samples were boiled at 95 ^{o}C, consequently for these experiments the protein samples were heated at 70 ^{o}C for 10 minutes. The protein samples were then pulse centrifuged and loaded onto 1.5 mm gels, Table 2.3, made in disposable cassettes (Thermo Fisher Scientific). A 10% resolving gel with a 4% stacking gel was used to analyse protein samples used for the detection of occludin. An 8% resolving gel with a 4% stacking gel was used to analyse protein samples used for the detection of ZO-1 due to the high molecular weight (220 kDa) of this protein. A 15% resolving gel with a 6% stacking gel was used to analyse protein samples used for the detection of claudin 5 due to the low molecular weight (23 kDa) of this protein.

Protein samples were run with a Precision Plus Protein Dual Colour Standards ladder consisting of 10 reference bands ranging from 10-250 kDa (BioRad). The gels were electrophoresed at 120 V in 1x running buffer (25 mM Tris, 192 mM glycine, 0.1% (w/v) SDS, pH 8.3) using an Invitrogen system.

8% Resolving gel pH 8.8	**10% Resolving gel pH 8.8**
8% (w/v) acrylamide	10% (w/v) acrylamide
25% (v/v) resolving buffer	25% (v/v) resolving buffer
0.1% (w/v) ammonium persulphate (APS)	0.1% (w/v) ammonium persulphate (APS)
0.1% (v/v) TEMED	0.1% (v/v) TEMED
12% Resolving gel pH 8.8	**15% Resolving gel pH 8.8**
12% (w/v) acrylamide	15% (w/v) acrylamide
25% (v/v) resolving buffer	25% (v/v) resolving buffer
0.1% (w/v) ammonium persulphate (APS)	0.1% (w/v) ammonium persulphate (APS)
0.1% (v/v) TEMED	0.1% (v/v) TEMED
4% Stacking gel, pH 6.8	**6% Stacking gel, pH 6.8**
4% (w/v) acrylamide	6% (w/v) acrylamide
25% (v/v) stacking buffer	25% (v/v) stacking buffer
0.1% (w/v) ammonium persulphate (APS)	0.1% (w/v) ammonium persulphate (APS)
0.1% (v/v) TEMED	0.1% (v/v) TEMED

Table 2.3: Gel Compositions. Resolving buffer composition: 1.5 M Tris-HCl, 4% (w/v) SDS, pH 8.8. Stacking buffer composition: 0.5 M Tris-HCl, 4% (w/v) SDS, pH 6.8. 29:1 acrylamide/bisacrylamide, 30% solution purchased from Geneflow. Tetramethylethylenediamine (TEMED) purchased from Melford.

2.7 Western Blotting

Proteins were transferred using a BioRad system onto 0.45 µm Hybond-C extra nitrocellulose membranes (Amersham Laboratories) at a constant current of 300 mA for 2 hours in transfer buffer (25 mM Tris, 192 mM glycine, pH 8.3). The gel and nitrocellulose membrane were held between chromatography paper (Whatman) and sponges in a transfer cassette. Transfer efficiency was determined using Ponceau Red (0.1% Ponceau, 5% acetic acid in H_2O). The membranes were blocked in either 5% milk blocking buffer (5% (w/v) powdered milk (Marvel), 0.01% Tween 20 in PBS) or West-EZier blocking buffer (Novus Scientific) for 1 hour at room temperature. The membranes were subsequently probed O/N at 4 ^{o}C with primary antibody diluted in the appropriate blocking buffer, Table 2.4.

Antibody	Species	Dilution	Blocking Buffer	Supplier	Code
alpha-Tubulin	Rabbit Polyclonal	1:1000	West-EZier/Milk	Abcam	ab4074
beta-Actin	Mouse Monoclonal IgG1	1:5000	West-EZier/Milk	Abcam	ab6276
Claudin 5	Rabbit Monoclonal	1:1000	West-EZier	Abcam	ab131259
Claudin 5	Rabbit Polyclonal	1:1000	West-EZier	Abcam	ab15106
DDX3X	Rabbit Polyclonal	1:200	West-EZier	Atlas Antibodies	HPA001648
DDX3	Mouse Monoclonal IgG1	1:200	West-EZier	Abcam	ab50703
eEF2	Rabbit Polyclonal	1:10000	West-EZier	Merck Millipore	07-1382
GFAP	Rabbit Polyclonal	1:10000	Milk	Abcam	ab7260
HNRNPA2B1	Rabbit Polyclonal	1:1000	West-EZier	Proteintech	14813-1-AP
HNRPA3	Rabbit Polyclonal	1:1000	West-EZier	Abcam	ab50949
Nestin	Rabbit Polyclonal	1:50	Milk	Abcam	ab82375
Occludin	Rabbit Monoclonal	1:10000	West-EZier	Abcam	ab167161
Occludin	Rabbit Polyclonal	1:500	West-EZier	Thermo Fisher Scientific	71.1500
Occludin	Mouse Monoclonal IgG1	1:500	West-EZier	Novus Biologicals	H00004950-M01
SSRP1	Mouse Monoclonal IgG2b	1:5000	West-EZier	BioLegend	609702
Vimentin	Mouse Monoclonal IgG1	1:1000	Milk	Abcam	ab8978
ZO-1	Rabbit Polyclonal	1:500	West-EZier	Thermo Fisher Scientific	40.2200

Table 2.4: Western blotting primary antibodies.

The membranes were washed three times at ten minute intervals in 0.01% Tween 20-PBS and probed for 1 hour at room temperature with the appropriate species-specific horseradish peroxidase (HRP) conjugated secondary antibody, Table 2.5, diluted in 0.01% Tween 20-PBS. The membranes were again washed three times at ten minute intervals in 0.01% Tween 20-PBS. Protein bands were detected using

an EZ-ECL chemiluminescence detection kit (Geneflow) and visualised using a G-BOX (Syngene). Images were processed using Adobe Illustrator software.

Antibody	Dilution	Supplier	Code
Polyclonal Goat Anti-Mouse Immunoglobulins/HRP	1:10000	Dako	P0447
Polyclonal Goat Anti-Rabbit Immunoglobulins/HRP	1:5000	Dako	P0448

Table 2.5: Western blotting secondary antibodies

2.8 Histology

The tissue cohort used in this research was obtained from the Newcastle brain bank, which holds and approves the use of tissue as a Human Tissue Authority approved brain bank (ethical reference 08/H0906, Newcastle and North Tyneside REC). The cohort consisted of control, mild cognitive impairment (MCI), and AD cases, Table 2.6. Formalin fixed, paraffin embedded (FFPE) temporal cortex blocks were cut to 5 µm thickness and collected onto charged slides (Leica). All immunohistochemistry was conducted manually using a standard avidin-biotin complex (ABC) method (Vectastain Elite Kit, Vectastain Laboratories) according to the manufacturer's instructions, as detailed below.

Category	ACATU	TRQ	Case ID	Block ID - Temporal	Disease Code	Age (years)	PM	Sex	Fixation Time	Braak Stage	Initial	No. of Slides
Control	2011060	2013.13	2006_0081	I	CA	58	39	F	5w	0	LR	25
Control	2011060	2013.13	2007_0049	I	CA	72	27	F	9w	1	LR	25
Control	2011060	2013.13	2008_0005	I	CA	59	19	F	11w	0	LR	25
Control	2011060	2013.13	2009_0067	I	CA	74	67	F	14w	1	LR	25
Control	2011060	2013.13	2009_0118	AC	CA	55	41	M	14w	0	LR	25
Control	2011060	2013.13	2010_0729	I	CA	70	72	M	11w	0	LR	25
Control	2011060	2013.13	2011_0272	I	CA	78	34	F	8w	0	LR	25
Control	2011060	2013.13	2011_0524	I	PM	83	24	F	8w	1	LR	25
Control	2011060	2013.13	2011_0891	I	CA	73	25	M	9w	0	LR	25
Control	2011060	2013.13	2011_1016	I	CA	74	49	F	12w	1	LR	25
MCI	2011060	2013.13	1999_0217	W	CA	105	52	F	N/D	4	LR	25
MCI	2011060	2013.13	1999_0279	R	DS	91	17	F	N/D	4	LR	25
MCI	2011060	2013.13	2009_0065	AC	CA+	75	82	M	25w	4	LR	25
MCI	2011060	2013.13	2010_0251	I	CA	86	75	F	7w	4	LR	25
MCI	2011060	2013.13	2010_0685	I	CA	88	22	F	10w	3	LR	25
MCI	2011060	2013.13	2010_0719	I	DS	81	82	M	9w	3	LR	25
MCI	2011060	2013.13	2010_1067	I	CA	98	59	F	9w	3	LR	25
MCI	2011060	2013.13	2011_0129	I	CA	89	34	F	8w	3	LR	25
MCI	2011060	2013.13	2011_0477	I	CA	95	66	F	8w	3	LR	25
AD	2011060	2013.13	2008_0102	I	DS	84	47	F	N/D	6	LR	25
AD	2011060	2013.13	2009_0002	I	DS	77	63	F	6w	6	LR	25
AD	2011060	2013.13	2009_0016	I	DS	93	53	F	10w	6	LR	25

AD	2011060	2013.13	2009_0017	I	DS	99	71	F	17w	6	LR	25
AD	2011060	2013.13	2009_0026	I	DS	83	12	M	N/D	6	LR	25
AD	2011060	2013.13	2009_0100	I	DS	80	32	F	17w	6	LR	25
AD	2011060	2013.13	2010_0098	I	DS	86	69	F	15w	6	LR	25
AD	2011060	2013.13	2010_0320	I	DS	88	84	M	10w	6	LR	25
AD	2011060	2013.13	2010_0483	I	DS	78	37	M	14w	6	LR	25
AD	2011060	2013.13	2012_9990	I	DS	78	40	F	12w	6	LR	25

Table 2.6: Temporal Cortex Cohort Information

2.8.1 Immunohistochemistry of FFPE Tissue

The tissue sections were baked onto the slides at 65 ^{o}C for 40 mins and left to cool for 24 hrs. The sections were then dewaxed for 5 mins in two xylene solutions and rehydrated to water in a graded series of ethanol solutions (2x absolute ethanol, 95% and 70%) for 5 mins each before being submerged in running water. The sections were incubated for 20 mins in a 3% H_2O_2-methanol solution to quench endogenous peroxidase activity. Following antigen retrieval, Table 2.7, the sections were blocked for 30 minutes at room temperature in 1.5% (v/v) normal serum (Vectastain Laboratories) to prevent non-specific binding and then incubated overnight in the relevant primary antibody, Table 2.7. A negative (omission of the primary antibody) and isotype control, either an isotype specific mouse or rabbit IgG (Vector Laboratories) used at the same concentration as the primary antibody, were also included to confirm antibody specificity.

Antibody	Species	Antigen Retrieval	Dilution (time, temp.)	Supplier	Code
Claudin 5	Mouse Monoclonal IgG1	MW 15 min, EDTA pH 8.0	1:50 (O/N, 4 ^{o}C)	Thermo Fisher Scientific	35.2500
Occludin	Rabbit Polyclonal	MW 15 min, EDTA pH 8.0	1:100 (O/N, 4 ^{o}C)	Thermo Fisher Scientific	71.1500
ZO-1	Rabbit Polyclonal	MW 15 min, EDTA pH 8.0	1:50 (O/N, 4 ^{o}C)	Thermo Fisher Scientific	18.7430

Table 2.7: Immunohistochemistry Primary Antibodies This table discloses the source and conditions of use for the primary antibodies as well as the antigen retrieval method utilised for immunohistochemistry.

The sections were washed in TBS for 5 minutes and incubated for 1 hour at room temperature in 0.5% (v/v) biotinylated secondary antibody (Vectastain Laboratories) after which the sections were again washed in TBS and incubated for 30 mins at room temperature in an avidin-biotinylated horseradish peroxidase complex solution (Vectastain Laboratories) made at least 30 minutes prior to use. The sections were subsequently washed in TBS and incubated for 5 mins at room temperature in 3, 3-diaminobenzidine (DAB) solution (Vecatstain Laboratories). DAB is a chromogen which, in the presence of peroxidase, oxidises to produce a brown substrate which allows the visualisation of the location of antibody binding to the tissue section. The DAB-peroxide reaction was quenched in deionised H_2O (dH_2O). The sections were incubated for 1 minute in Harris's Haematoxylin to stain cell nuclei. The sections were then briefly submerged in acid alcohol to remove excess haematoxylin stain

from the tissue followed by Scott's tap water, an alkaline solution which neutralises the acid alcohol and blues the haematoxylin stain. The sections were dehydrated in graded ethanol solutions (75%, 95% and 2x absolute ethanol) before being cleared in xylene and permanently mounted using distyrene plasticizer xylene (DPX) mounting media (Sigma).

2.8.2 Immunohistochemistry of FFPE Tissue – Dual Immunostaining

Dual immunostaining was conducted for occludin and GFAP. Initially, single staining for occludin was conducted utilising the same protocol stated in 2.8.1 using the anti-occludin polyclonal antibody (Thermo Fisher Scientific 71.1500) at a 1:50 dilution. Subsequent to the quenching of the DAB reaction, the sections were blocked for 30 minutes at room temperature in 1.5% (v/v) normal serum (Vectastain Laboratories). This solution was removed and the sections incubated for 15 minutes at room temperature in avidin solution from an avidin-biotin blocking kit (Vectastain Laboratories) after which the sections were briefly washed in TBS and incubated for 15 minutes at room temperature in biotin solution also from the avidin-biotin blocking kit (Vectastain Laboratories). This solution was removed and the sections incubated O/N at 4 ^{o}C with anti-GFAP rabbit polyclonal antibody (DAKO, Z0334) diluted 1:500 in blocking solution. The sections were washed for 5 minutes in TBS and incubated for 1 hour at room temperature in 0.5% (v/v) biotinylated anti-rabbit IgG secondary antibody, washed again for 5 minutes in TBS and then incubated for 1 hour at room temperature in 1.5% (v/v) avidin-biotin complex-alkaline phosphatase (ABC-AP) solution (Vectastain Laboratories). This solution was made at least 30 minutes prior to use. The sections were developed for 10-15 minutes at room temperature in alkaline phosphatase red substrate (Vectastain Laboratories) and the reaction quenched in distilled H_2O. The sections were incubated for 1 minute in Harris's Haematoxylin then briefly submerged in acid alcohol followed by Scott's tap water. The sections were dehydrated in graded ethanol solutions (75%, 95% and 2x absolute ethanol) before being cleared in xylene and permanently mounted using DPX mounting media (Sigma).

2.9 Recombinant Protein Generation

2.9.1 Plasmids

pCMV-SPORT6 (4396 bp) contained occludin (OCLN) cDNA IMAGE clone. The plasmid was purchased from Source Bioscience and was hosted in the DH10B

Escherichia coli (*E. coli*) strain with ampicillin resistance and NotI/EcoRV cloning sites.

pET24b-GB1-6His (5.5 kbp) vector with kanamycin resistance containing a GB1-6His tag was used for cloning OCLN full length, N- and C-terminal sequences and recombinant protein expression in *E. coli*.

2.9.2 Primers

Primers were designed to isolate the N- and the C-terminal domains as well as the full length occludin sequence. All primers were purchased from Sigma.

Primer	Sequence
OCLN_1_Nde15	5'-GGCGGGCATATGTCATCCAGGCCTCTTGAAAG
OCLN_271_Nde15	5'-GGCGGGCATATGGACAGGTATGACAAGTCC
OCLN_522_Xho13	5'-CCCGCCCTCGAGCTATGTTTTCTGTCTATCATAG
OCLN_65_Xho14	5'-CCCGCCCTCGAGTTAAATCACTCCTGGAGGAGAGGTC

Table 2.8: Primers

2.9.3 Bacterial Strains

E. coli DH5α was used for the molecular cloning of plasmid DNA. Genotype: F-80dlacZ M15 (lacZYA-argF) U169 recA1 endA1hsdR17 (rk-, mk+) phoAsupE44-thi-1 gyrA96relA1.

E. coli BL21-RP was used for recombinant protein expression. Genotype: FHUa2 [Ion] ompT gal (λ DE3) [dcm] ΔhsdS.

2.9.4 Bacterial Culture Materials

Luria-Bertani (LB) Broth was purchased from Thermo Fisher Scientific and made according to the manufacturer's instructions (25 g LB in 1 l dH_2O). LB solutions were autoclaved prior to use.

Terrific Broth (TB) for 10 litres: 120 g tryptone, 240 g yeast extract, 23.1 g KH_2PO_4, 125.4 g K_2HPO_4, 40 ml glycerol in dH_2O. TB solutions were autoclaved prior to use.

2.9.5 PCR Reaction

A touchdown PCR was conducted to amplify full length occludin, N-terminal and C-terminal sequences, Table 2.9. A touchdown PCR is designed to avoid the amplification of non-specific sequences by using a cycling program with a range of

primer annealing temperatures which encompasses the optimal annealing temperature, Table 2.10.

HerII PCR Reaction	
500 ng	c DNA Template
0.5 µM	Forward Primer
0.5 µM	Reverse Primer
1.6 µM	dNTP Mix (Bioline)
10 µl	5x HerII Reaction Buffer (Agilent)
5%	DMSO (Agilent)
1.0 µl	HerII Fusion DNA Polymerase (Agilent)
make 50 µl final volume	MQ H_2O

Table 2.9 PCR reaction for Herculase II Fusion DNA Polymerase

HerII PCR Program		
Heated Lid	110 °C	
Temperature Step	95 °C	2 mins
Touchdown		
Denaturing Temperature	95 °C	20 sec
Max. Annealing Temperature	65 °C	20 sec
Min. Annealing Temperature	50 °C	
Elongation Temperature	65 °C	2 mins
Cycles	15	
Start Cycle (35x)		
Temperature Step	95 °C	20 sec
Temperature Step	55 °C	20 sec
Temperature Step	68 °C	2 mins
End Cycle		
Temperature Step	68 °C	4 mins
Hold	10 °C	Infinite

Table 2.10: Touchdown PCR Program for Herculase II Fusion DNA Polymerase

2.9.6 Agarose Gel Electrophoresis

Agarose gel electrophoresis was used to separate and analyse PCR products. Agarose gels (2%) were made by using a microwave to dissolve 4 g agarose (Melford) in 200 ml TAE buffer (40 mM Tris, 20 mM acetic acid, 1 mM EDTA). Once dissolved, 4 µl of 10 mg/ml ethidium bromide (Invitrogen) was added to the solution. 10 µl 6x Laemmli buffer was added to each PCR sample. The samples were loaded with a GeneRuler Mix Ladder (bands ranging from 100-1000 bp) (Thermo Scientific) and run at 80-100 V for 40-60 minutes. DNA bands were imaged using a GENi (Syngene).

2.9.7 Gel Extraction

The DNA bands were visualised using an ultra-violet (UV) transilluminator and excised using a clean scalpel blade. The DNA was extracted from the gel piece and purified using the QIAquick Gel Extraction kit (QIAGEN) according to the manufacturer's instructions. Each excised DNA band was placed in a fresh 1.5 ml Eppendorf tube to which was added 900 µl QG buffer. The tubes were then incubated at 50 ^{o}C until the gel had dissolved after which 300 µl isopropanol was added and the solution transferred to a spin column and centrifuged for 1 minute at 17, 000 x g. The flow through was discarded and 500 µl added to the spin column which was again centrifuged for 1 minute at 17, 000 x g. The flow through was discarded and 750 µl PE buffer added to the spin column which was centrifuged for 1 minute at 17, 000 x g. The spin column was then transferred to a fresh 1.5 ml Eppendorf tube. 50 µl EB was added to the spin column and then left to stand for 3 minutes at room temperature after which it was centrifuged for 1 minute at 17, 000 x g.

2.9.8 PRC Product Restriction Digest

The purified DNA was digested with the same restriction enzymes used to cut the pET24b-GB1-6His plasmid. Restriction digest reaction: 50 µl DNA, 10 µl 10x Fast Digest buffer (Thermo Fisher Scientific), 5 µl *Nde*I restriction enzyme (10 U/µl) (Thermo Fisher Scientific), 5 µl *Xho*I restriction enzyme (10 U/µl) (Thermo Fisher Scientific), 30 µl ultrapure H_2O (final reaction volume 100 µl). The reactions were incubated O/N at 37 ^{o}C (heat block).

2.9.9 DNA Precipitation

Following restriction digestion, 100 µl chloroform was added to each DNA sample, vortexed for 1 minute and centrifuged at 17, 000 x g for 3 minutes at room temperature. The top phase was transferred to a fresh Eppendorf tube and, if necessary, made up to a final volume of 90 µl with ultrapure water after which 10 µl 3 M sodium acetate (NaAc) and 300 µl ethanol were added. The DNA samples were inverted 5x and incubated for 20 minutes at -20 ^{o}C, after which they were centrifuged at 17, 000 x g for 20 minutes at room temperature. The supernatant was removed and the DNA pellets were left to air dry.

2.9.10 Ligation into pET24b-GB1-6His Plasmid

The DNA pellets were resuspended in 16 µl ultrapure H_2O and transferred to 0.5 ml Eppendorfs tubes. Ligation reaction composition: 16 µl DNA, 1 µl pET24b-GB1-6His cut vector, 2 µl ligation buffer (Thermo Fisher Scientific), 5 U T4 DNA ligase (Thermo Fisher Scientific). The reactions were incubated O/N at 16 ^{o}C (PCR machine) and stored at -20 ^{o}C.

2.9.11 Transformation of pET24b-GB1-6His plasmid into DH5α

A heat shock method was used to induce plasmid uptake into the DH5α *E. coli* strain. 10 µl plasmid was incubated with 50 µl DH5α on ice for 10 minutes after which the samples were incubated at 37 ^{o}C (heat block) for 5 minutes and then placed on ice for a further 2 minutes. 950 µl LB was added and the culture incubated at 37 ^{o}C for 1 hour on a rotary shaker set to 220 rpm. The culture was centrifuged at 4, 700 x g for 1 minute at room temperature. Most of the supernatant was discarded leaving approximately 100 µl which was used to resuspend the bacterial pellet. The bacterial suspension was plated out onto LB agar plates with 30 µg/ml kanamycin (kanamycin stock conc. 50 mg/ml) which were inverted and incubated O/N at 37 ^{o}C to allow colony growth. Individual colonies (transformants) from each plate were inoculated in LB broth with kanamycin (1:1000) and incubated O/N at 37 ^{o}C on a rotary shaker set to 220 rpm.

2.9.12 Spin Miniprep & Transformant Screen by Restriction Digest

Spin minipreps were conducted on all inoculated colonies to establish the presence of the required insert in the bacteria prior to sequencing. All spin minipreps were conducted using the QIAprep spin miniprep kit (QIAGEN) according to the manufacturer's instructions. Fast digest reaction: 8 µl DNA, 1 µl 10x fast digest buffer, 0.5 µl *Nde*I, 0.5 µl *Xho*I. All reagents from Thermo Fisher Scientific. Samples were incubated at 37 ^{o}C (heat block) for 20 minutes and run on a 2% agarose gel for 40 minutes at 100 V.

2.9.13 Sanger Sequencing PCR

Sequencing reaction: 1 µg DNA (500 ng/µl), 1 µl primer, 2 µl 5x BigDye Terminator v3.1 Sequencing Buffer (Applied Biosystems), 1 µl BigDye Terminator v3.1 Ready Reaction Mix (Applied Biosystems), ultrapure H_2O to make 10 µl final volume, Table 2.11.

PCR Program		
Heated Lid	110 °C	
Start Cycle (45x)		
Temperature Step	95 °C	30 sec
Temperature Ramp	1 °C per second	
Temperature Step	50 °C	15 sec
Temperature Ramp	1 °C per second	
Temperature Step	60 °C	4 mins
End Cycle		
Hold	10 °C	Infinite

Table 2.11: PCR program for Sanger Sequencing

2.9.14 DNA Precipitation

90 µl 10x Master Mix (MM) (30 µl 3M sodium acetate, 245 µl ultrapure H_2O and 625 µl 100% ethanol) was added to each sample. Samples were briefly vortexed and incubated for 20 minutes at room temperature after which they were centrifuged at 17, 000 x g for 20 minutes at room temperature. Samples were washed with 150 µl 70% ethanol, vortexed briefly and centrifuged at 17, 000 x g for 10 minutes at room temperature. The supernatant was discarded and the DNA pellets air dried prior to being sent to Source BioScience for analysis.

2.9.15 Transformation of pET24b-GB1 plasmid into BL21-RP *E. coli*

A heat shock transformation was performed in which 50 µl BL21-RP was added to 2 µl DNA (500 ng/µl) in a 1.5 ml Eppendorf tube and incubated on ice for 7 minutes, after which samples were incubated at 37 °C (heat block) for 5 minutes then placed on ice for 2 minutes. 950 µl SOC medium was added to the cultures which were incubated at 37 °C for 1 hour on a rotary shaker set to 220 rpm and centrifuged at 4, 700 x g for 1 minute at room temperature. Most of the supernatant was discarded leaving approximately 100 µl which was used to resuspend the bacterial pellet. The bacterial suspension was plated out onto LB agar plates (30 µg/ml kanamycin) which were inverted and incubated O/N at 37 °C. A few colonies were scrapped together using a pipette tip which was ejected into a flask containing 50 ml TB, 50 µl kanamycin and 50 µl chloramphenicol. The flasks were incubated O/N at 37 °C on a rotary shaker set to 220 rpm. Glycerol stocks of the N-terminal, C-terminal and full length occludin bacterial cultures were made in which 500 µl of each culture was mixed with 500 µl 50% glycerol and stored at -80 °C.

2.9.16 Recombinant Protein Expression in BL21-RP *E. coli*

A 50 ml transformed BL21-RP culture was set up 24 hours prior to protein expression. Using a stripette, 1.5 ml of the 50 ml BL21-RP culture was added to 750 ml TB and 750 µl kanamycin in a baffled flask. The baffled flask was incubated at 37 ^{o}C on a rotary shaker (220 rpm). Bacterial growth was monitored by determining the culture's optical density using a spectrophotometer until the culture had reached OD_{600} 0.7 at which point 300 µl isopropyl β-D-1-thiogalactopyranoside (IPTG) was added and the flasks were incubated O/N at room temperature on a rotary shaker set to 210 rpm.

2.9.17 Protein Purification

The induced cultures were centrifuged at 4500 rpm for 15 minutes at 4 ^{o}C. A 0.25 g bacterial pellet was weighed out in a 1.5 ml Eppendorf tube and lysed in 1 ml lysis buffer (50 mM Tris, 1 M NaCl, 0.5% (v/v) triton X-100, PIC, pH 8.0). The pellets were sonicated 3x on ice in 30 second cycles (5 seconds sonicated, 25 seconds cooled) and the lysates centrifuged at 17, 000 x g for 7 minutes at 4 ^{o}C. The supernatant was added to 40 µl slurry TALON Metal Affinity Cobalt Beads (Clontech Laboratories) and incubated for 1 hour on a rotary wheel at 4 ^{o}C. Prior to the addition of supernatant, the beads were washed twice in 1 ml lysis buffer. The lysates were centrifuged at 0.5 x g for 1 minute and the supernatant discarded. The beads were washed once in 1 ml lysis buffer and twice in 1 ml wash buffer (50 mM Tris, 1 M NaCl, 5 mM Imidazole, pH 8.0). The beads were incubated for 12 minutes in 50 µl elution buffer (20 mM Tris, 500 mM NaCl, 200 mM Imidazole, pH 8.0) to elute the GB1-tagged protein. The beads were briefly vortexed every 2 minutes during the 12 minute incubation after which they were centrifuged at 0.5 x g for 1 minute and the supernatant removed and retained. SDS-polyacrylamide gel electrophoresis was used to confirm the size and purity of the recombinant proteins. 15 µl of each supernatant was added to 5 µl 4x Laemmli buffer and boiled at 95 ^{o}C for 5 minutes. The samples were loaded onto a 15% gel along with an SDS-PAGE Standards ladder (bands ranging from 6.5-200 kDa) (BioRad) and run at 150 V. The bands were visualised with Coomassie Blue.

Once it had been established that the recombinant proteins were the correct size the entire bacterial pellet was lysed in 25 ml lysis buffer. The pellets were then sonicated 6x on ice (30 seconds sonicated, 30 seconds cooled) after which the lysates were centrifuged at 4500 rpm for 20 minutes at 4 ^{o}C. 3 ml TALON Metal

Affinity Cobalt Bead slurry was placed into a column and washed once in 10 ml ultrapure H_2O and once in 10 ml lysis buffer. The bacterial lysate was run twice over the beads after which the beads were washed once in 10 ml lysis buffer and twice in 10 ml wash buffer. Proteins were eluted from the beads in 3 ml elution buffer. The protein concentration of the eluate was determined using a Bradford assay (as detailed in 2.5) and SDS-polyacrylamide gel electrophoresis (2.6) was again used to check the size and purity of the recombinant proteins. The eluate was aliquoted, flash frozen in liquid nitrogen and stored at -80 ^{o}C.

2.10 Immunocytochemistry of BL21-RP *E. coli*

The E.coli ICC protocol used in this project was developed from a previous study (Jose et al., 2005). 100 µl of bacterial culture was placed in each well of a 24 well tissue culture plate containing a 13 mm coverslip and incubated at 37 ^{o}C until dry. To fix the bacteria, 500 µl 4% PFA was added to each well and incubated for 20 minutes at room temperature. The coverslips were washed three times in PSB and incubated in blocking solution (3% (w/v) bovine serum albumin (BSA), 0.01% Tween 20 in PBS) for 5 minutes at room temperature. Anti-occludin rabbit polyclonal antibody (Thermo Fisher Scientific) diluted 1:50 in blocking solution was added to each well and the plate incubated on ice for 1 hour. The coverslips were washed three times in PBS and the plate incubated on ice in darkness for 1 hour in Alexa-Fluor® 488 goat anti-rabbit secondary antibody diluted 1:500 in blocking solution. The coverslips were again washed three times in PBS and mounted using fluorescent mounting medium (DAKO) onto glass slides. Images were taken using a Nikon microscope.

2.11 Pull-Down Protein Binding Assay

For each condition, 30 µl IgG bead slurry (GE Healthcare) was blocked in 2% BSA-wash buffer (150 mM NaCl, 25 mM TrisHCl, pH 8.0) O/N at 4 ^{o}C on a rotary wheel. Beads were washed 3 times in wash buffer and incubated with 20 µg GB1-OCLN_N or GB1-OCLN_C for 1 hour at 4 ^{o}C. A GB1-6His control was also included in each experiment. Prior to lysis, 1321N1 astrocytoma cells cultured in 10 cm dishes were treated with 5 mM $CaCl_2$ and 4 µM A23187 calcium ionophore (Sigma) and incubated at 37 ^{o}C for 15 minutes. The cells were then washed once in PBS and lysed on ice in 500 µl lysis buffer (150 mM NaCl, 25 mM TrisHCl, 1% (v/v) Triton X-100, 0.05% (w/v) SDS, 10 mM NaF, 1 mM $NaVO_4$, PIC, pH 8.0).

Note: During the optimisation of this protocol, pull-down protein binding assays were initially conducted using the following buffer compositions: wash buffer (150 mM NaCl, 50 mM HEPES, 1 mM DTT, pH 7.5) and lysis buffer (150 mM NaCl, 50 mM HEPES, 1 mM DTT, 0.5% (v/v) Triton X-100, 10% (v/v) glycerol, PIC, pH 7.5).

The lysates were incubated on ice for 30 minutes and passed through a 25 G needle 10x before being centrifuged at 17, 000 x g for 5 minutes, after which the supernatants were combined and the concentration determined by Bradford assay (as detailed in 2.5). The beads were washed once in wash buffer, twice in lysis buffer and transferred to 15 ml falcon tubes. The lysate was diluted to 1.5 mg/ml and divided equally between the beads with a small quantity retained for use as an input sample. The bead-lysate mixture was incubated O/N at 4 ^{o}C on a rotary wheel. The tubes were centrifuged at 0.5 x g for 2 minutes and the supernatant removed. The beads were washed twice in lysis buffer and three times in wash buffer. 60 µl 2x Laemmli buffer was added to the beads which were subsequently boiled at 95 ^{o}C for 5 minutes to elute any proteins. The eluates were analysed by SDS-polyacrylamide gel electrophoresis (as detailed in 2.6). Protein bands were visualised with either Instant*Blue* coomassie (Expedeon) or a SilverXpress® Silver Staining Kit (Thermo Fisher Scientific). This kit was used according to the manufacturer's instructions.

2.12 Mass Spectrometry

2.12.1 In-Gel Digest Sample Preparation

The gel was cut into pieces using a clean scalpel blade. These pieces were then transferred into individual fresh 1.5 ml LoBind Eppendorf tubes (Capitol Scientific). The excised gel pieces were incubated in 200 µl 200 mM Ammonium Bicarbonate (ABC) solution in 40% Acetonitrile (ACN) at 37 ^{o}C for 30 minutes to destain the gel after which the supernatant was discarded and this step repeated. The gel pieces were incubated in 100 µl acetonitrile (ACN) at 37 ^{o}C for 10 minutes to dehydrate the gel. The gel pieces were incubated in 100 µl reduction buffer (10 mM DTT in 50 mM ABC solution) at 56 ^{o}C for 30 minutes after which they were pulse centrifuged and the supernatant discarded. The gel pieces were incubated in 100 µl alkylation buffer (55 mM Iodoacetic acid (IAA) in 50 mM ABC solution) for 30 minutes at room temperature in the dark, washed twice in 200 µl 50 mM ABC solution and once in 200 µl 50 mM ABC solution in 50% ACN after which the pieces were pulse centrifuged and dried in 100 µl Acetonitrile (ACN) at 37 ^{o}C for 10 minutes. 20 µl

(equivalent to 0.4 µg trypsin) trypsin solution (20 µg/ml Trypsin (Sigma), 100 µl 1 mM HCl, 900 µl 40 mM ABC in 9% ACN) was added to the dehydrated bands and incubated for 5 minutes at 4 ^{o}C. Once the trypsin solution had soaked into the gel pieces, 50 µl 40 mM ABC in 9% ACN was added and they were incubated at 37 ^{o}C O/N. The gel pieces were pulse centrifuged and the supernatants transferred into fresh 1.5 ml LoBind Eppendorf tubes. 20 µl ACN was added to the gel pieces which were then vortexed and incubated at 37 ^{o}C for 15 minutes followed by 50 µl 5% formic acid (FA). The gel pieces were again briefly vortexed and incubated at 37 ^{o}C for 15 minutes. The supernatants were then removed and added to the previous transfer tubes. 50 µl 50% ACN in 5% FA was added to the gel pieces which were briefly vortexed and incubated at 37 ^{o}C for 30 minutes. The gel pieces were pulse centrifuged and the supernatants transferred. The gel pieces were then discarded and the supernatants dried in a vacuum concentrator. The samples were stored at -20 ^{o}C prior to mass spectrometry analysis.

2.12.2 ESI-MS Analysis

The peptides were resuspended in 12 µl 0.1% trifluoroacetic acid (TFA) and vortexed twice. The samples were then centrifuged at 17, 000 x g for 6 minutes after which 7µl was transferred to snap ring microvials (VWR) and loaded into an AmaZon speed (Brucker) ion trap mass spectrometer. The ESI-MS was conducted by a collaborator: Dr. Mark Dickman's research group in Chemical and Biological Engineering of the University of Sheffield.

Mascot generic files (MGFs) for the data were created using Mascot Distiller software and submitted to automated database searching using the Mascot search engine, a software package from Matrix Science. Proteins were identified using a significance threshold $p < 0.05$. Peptides with a Mascot score ≥ 50 and the number of significant queries > 1 were considered to be significant in this project.

2.13 Co-Immunoprecipitation

For each condition, 30 µl Protein G Sepharose bead slurry (GE Healthcare) was washed once in PBS and blocked in 2% BSA-PBS O/N at 4 ^{o}C on a rotary wheel. Cells, either HEK and 1321N1 astrocytoma cells (10x 10 cm dishes) or ScienCell primary human astrocytes (6x 175 cm^2 tissue culture flasks) were washed once in PBS and lysed in IP lysis buffer (50 mM HEPES, 150 mM NaCl, 1 mM EDTA, 1 mM DTT, 0.5% (v/v) Triton X-100, 10% (v/v) glycerol, PIC, pH 7.5) The lysates were collected using a cell scraper, passed 10x through a 25 G needle and centrifuged at

17, 000 x g at 4 °C for 5 minutes. The supernatants were combined and the concentration determined by Bradford assay (as detailed in 2.5). The supernatant was diluted in lysis buffer to a concentration ranging from 0.5-2.0 mg/ml and incubated with fresh Protein G Sepharose beads for 1 hour at 4 °C on a rotary wheel. This is known as a pre-clear and is designed to reduce non-specific-binding. The blocked beads were washed once in lysis buffer and incubated with the pre-cleared cell lysate and the relevant antibody, Table 2.12, for 1 hour at 4 °C on a rotary wheel.

Antibody	Species	Quantity	Supplier	Code
Flag M2	Mouse Monoclonal	5 µg	Sigma	F1804
DDX3X	Rabbit Polyclonal	1.5 µg	Atlas Antibodies	HPA001648
DDX3	Mouse Monoclonal	1.5 µg	Abcam	ab50703
Occludin	Rabbit Polyclonal	3 µg	Thermo Fisher Scientific	71-1500
Occludin	Mouse Monoclonal	5 µg	Novus Biologicals	H00004950-M01

Table 2.12: Co-immunoprecipitation antibodies. These are the antibodies which were used for immunoprecipitation and co-immunoprecipitation experiments. The flag M2 antibody was used as negative control.

The beads were centrifuged at 0.5 x g for 2 minutes at 4 °C and the supernatant removed. Samples of the supernatant, known as flow through, were retained as well as an input sample. The beads were washed 5x in IP lysis buffer. All residual buffer was removed and any proteins bound to the bead-antibody complex were eluted either by an acid or boil elution. For an acid elution, 50 µl 100 mM glycine pH 2.6 was added to the beads and incubated at room temperature for 15 minutes with gentle agitation. The beads were centrifuged at 0.5 x g for 1 minute and the supernatant removed and neutralised with 2.5 µl 1 M tris. For the boil elution, 50 µl 2x Laemmli buffer was added to the beads and boiled at 95 °C for 5-10 minutes after which the beads were centrifuged 0.5 x g for 1 minute and the eluate removed. Samples of the eluates along with input and flow through samples were analysed by SDS-polyacrylamide gel electrophoresis, 2.6 and western blotting, 2.7.

2.14 Statistical Analysis – Western blotting

Western blotting experiments subject to statistical analysis were run in triplicate from three independent experiments. Densitometric analysis was conducted using ImageJ and the data analysed using an unpaired t test with GraphPad Prism software (version 6.02). Data were plotted as mean immunoreactivity following normalisation to a loading control ± standard error of the mean (SEM). Differences were considered statistically significant when $p < 0.05$.

3. Characterisation of Tight Junction Protein Expression in Astrocytes

3.1 Introduction

Occludin and claudins are tight junction integral membrane proteins whose expression is predominantly associated with epithelial and endothelial cells. The localisation of these proteins in these cells is associated with the cell membrane and the cytoplasm (Furuse et al., 1998a; Furuse et al., 1993; Furuse et al., 1998b). ZO-1 is a tight junction cytoplasmic scaffolding protein which is also typically associated with epithelial and endothelial cells. This protein is cytoplasmic but localises close to the cell membrane (Stevenson et al., 1986). ZO-1 is also known to express nuclear localisation and exportation signals and localises to the nucleus in MDCK cells (González-Mariscal et al., 1999; González-Mariscal et al., 2006). These proteins are not exclusively expressed in epithelial/endothelial cells and have also been shown to be expressed in astrocytes.

Occludin has been shown to be highly expressed *in vitro* in undifferentiated murine astrocytes whilst differentiated astrocytes express lower levels of this protein (Bauer et al., 1999). Undifferentiated astrocytes in this study are defined as cells between passage 2-4 whilst differentiated astrocytes have a higher passage number (Bauer et al., 1999). Occludin is shown to be localised to the cell membrane in undifferentiated murine astrocytes and diffusely expressed throughout the cytoplasm in differentiated cells (Bauer et al., 1999). Astrocytic nuclear occludin expression has also been seen *in vivo* in the human frontal cortex (Romanitan et al., 2007). Astrocytes were also found to express claudin 5 *in vivo* in the same cohort (Romanitan et al., 2010).

Human foetal cortical astrocytes have also been shown to express occludin, ZO-1 and ZO-2 *in vitro* (Duffy et al., 2000). The expression of all three of these proteins is localised to the cell membrane in these cells (Duffy et al., 2000). ZO-1 also co-localises at the cell membrane with connexin 43 *in vitro* in murine cortical astrocytes (Duffy et al., 2004). *In vivo* experiments involving mice have also observed the co-localisation of ZO-1 with Cx30 and Cx43 in astrocytes (Penes et al., 2005).

This initial aim of this study was to characterise the expression of occludin, claudin 5 and ZO-1 in human primary astrocytes and 1321N1 astrocytoma cells. Another aim of this study was to define the cellular localisation of these three proteins in the temporal cortex and investigate whether the expression of these proteins is altered in MCI and AD cases compared with non-neurological controls.

3.2 Results

3.2.1 Astrocyte Culture Medium Comparison

There is considerable variation within the literature regarding the culture conditions for human astrocytes with various different media being used for tissue culture (Gibbons and Dragunow, 2010). It was considered worthwhile to determine the ideal culture conditions for ScienCell human primary astrocytes and consequently a media comparison was conducted between the ScienCell Astrocyte Medium and MEMα/F-10 medium.

Initial experiments sought to compare the expression of the intermediate filaments GFAP, vimentin and nestin in human primary astrocytes cultured in either medium by ICC and western blotting. Experiments comparing human primary astrocytes cultured in either ScienCell Astrocyte Medium or MEMα/F-10 medium were conducted using cells of the same passage number. The negative and isotype controls for these experiments are included in Figure 3.5 and Figure 3.7. No staining was observed in the negative controls or the mouse IgG isotypes control. Very weak non-specific background staining was seen in the rabbit IgG isotype control.

Figure 3.1 shows the expression of GFAP in human primary astrocytes cultured in either ScienCell Astrocyte Medium or MEMα/F-10 medium. ICC showed that GFAP expression was exclusively cytoplasmic. It is also clear from the ICC that, in either culture medium, only a few astrocytes in the total population were seen to express GFAP, Figure 3.1 A. This would suggest that the majority of human primary astrocytes do not express this protein.

An example western blot comparing GFAP expression in human primary astrocytes is shown in Figure 3.1 panel B. A 50 kDa GFAP protein band was observed in both sets of human primary astrocytes. These protein bands were fainter in the MEMα/F-10 medium compared with the ScienCell Medium suggesting that human primary astrocytes express higher levels of GFAP in ScienCell Astrocyte Medium. Three independent western blot experiments were conducted using three different astrocyte cultures to further explore GFAP expression. These blots were subject to densitometric analysis and the data analysed using an unpaired t test. The results were plotted as mean immunoreactivity following normalisation to a loading control ± standard error of the mean (SEM), Figure 3.1 panel C. Differences were considered statistically significant when $p < 0.05$. This analysis concluded,

however, that there was no significant difference in the level of GFAP expression between human primary astrocytes cultured in either ScienCell or MEMα/F-10 medium.

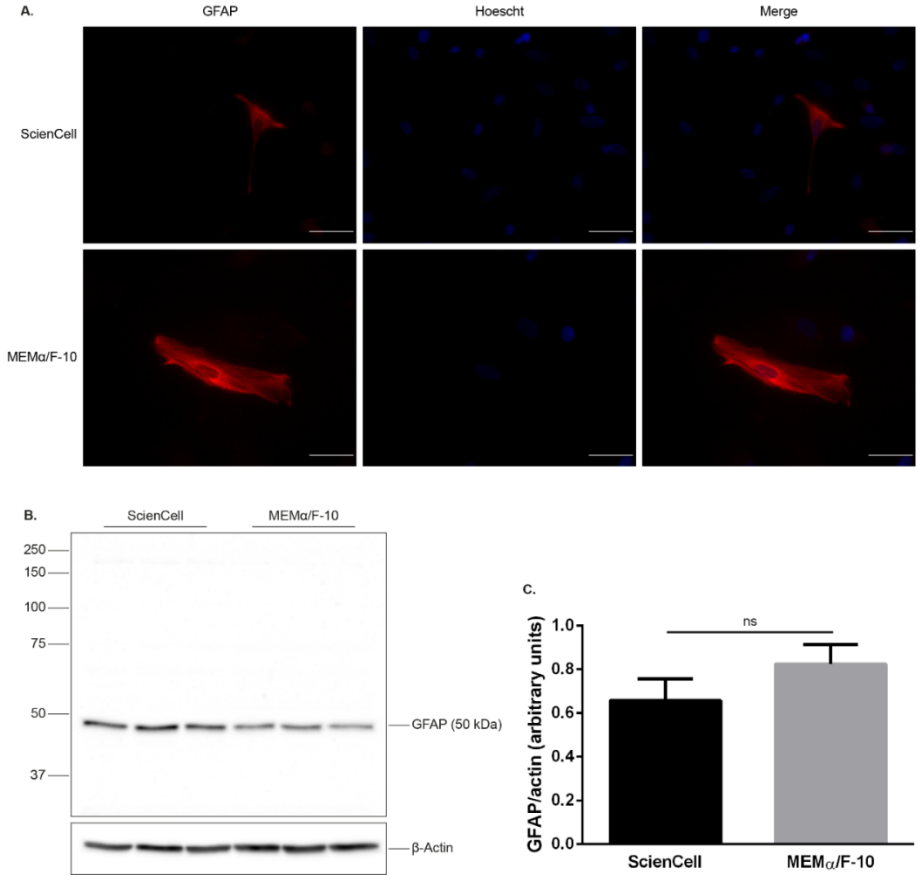

Figure 3.1: GFAP expression in human primary astrocytes cultured in two different media. A) Immunocytochemistry comparing the expression of GFAP in human primary astrocytes cultured in either ScienCell Astrocyte Medium or MEMα/F-10 medium. Scale bar 50 μm. B) Western blot comparing the expression of GFAP in human primary astrocytes. Molecular weight markers are indicated (kDa). GFAP predicted molecular weight 50 kDa. Loading control β-Actin. C) Bar chart showing GFAP immunoreactivity of astrocytes cultured in either ScienCell or MEMα/F-10 media following normalisation to β-Actin loading control. Values represent mean ± SEM n=3, ns means not significant where P > 0.05. P value = 0.2257.

Figure 3.2 shows the expression of vimentin in human primary astrocytes cultured in either ScienCell Astrocyte Medium or MEMα/F-10 medium. ICC showed that vimentin was expressed throughout the astrocyte population and was exclusively cytoplasmic, Figure 3.2 panel A. The ICC did not suggest that the level of vimentin expression in these cells was affected by the culture medium. This observation was confirmed by western blot as a 57 kDa vimentin protein band of the same intensity was observed in human primary astrocytes cultured in either medium, Figure 3.2 panel B.

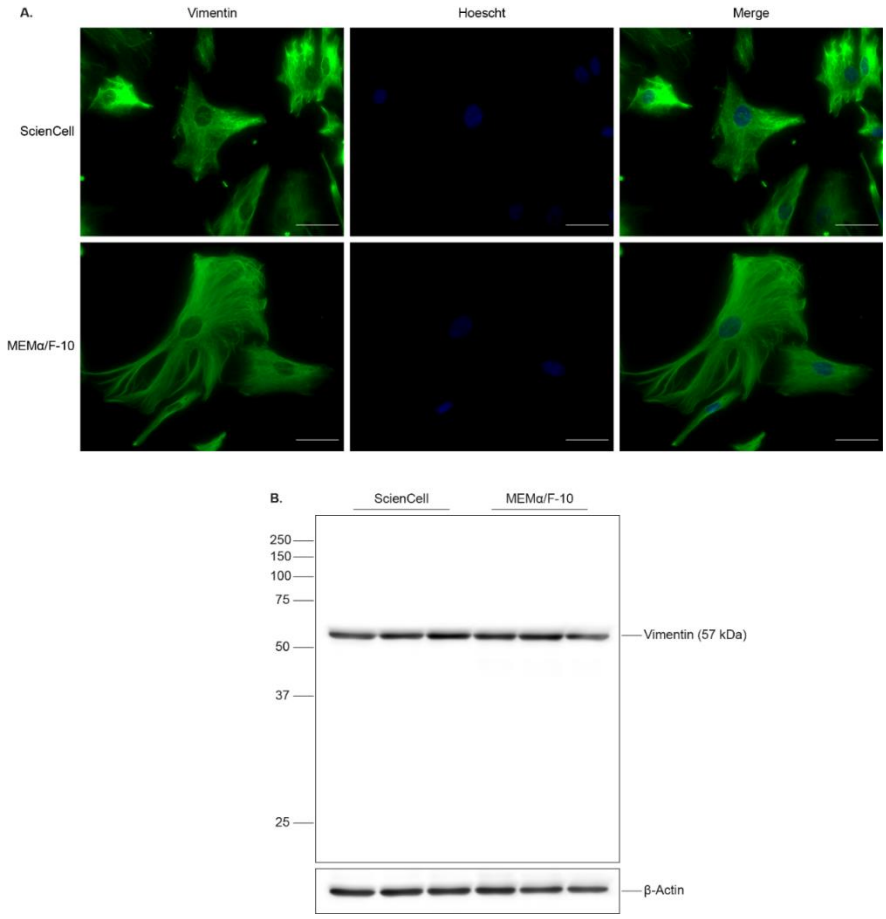

Figure 3.2: Vimentin expression in human primary astrocytes cultured in two different media. A) Immunocytochemistry comparing the expression of vimentin in human primary astrocytes cultured in either ScienCell Astrocyte Medium or MEMα/F-10 medium. Scale bar 50 μm. B) Western blot comparing the expression of vimentin in human primary astrocytes. Molecular weight markers are indicated (kDa). Vimentin predicted molecular weight 57 kDa. Loading control β-Actin.

Figure 3.3 shows the expression of nestin in human primary astrocytes cultured in either ScienCell Astrocyte Medium or MEMα/F-10 medium. ICC showed that nestin was expressed throughout the astrocyte population and was both nuclear and cytoplasmic, Figure 3.3 panel A. The ICC did not suggest that the level of nestin expression in these cells was affected by the culture medium. The predicted molecular weight for nestin is a single band of 177kDa, however, a 220-250 kDa doublet was observed in human primary astrocytes cultured in either medium, Figure 3.3 B. A 240 kDa nestin protein band is observed in the G6 human embryonic muscle cell line and is caused by protein glycosylation (Grigelioniene et al., 1996). A nestin doublet between 220-250 kDa is also observed in U373 and U251 human glioblastoma cell lines (Messam et al., 2000). The 220-250 kDa doublet observed in human primary astrocytes is therefore likely to be nestin protein that has been subjected to post-translational modification.

The intensity of this nestin doublet was the same for human primary astrocytes cultured in either ScienCell Astrocyte Medium or MEMα/F-10 medium. This confirms the ICC observations and demonstrates that nestin expression is unaffected by the culture medium.

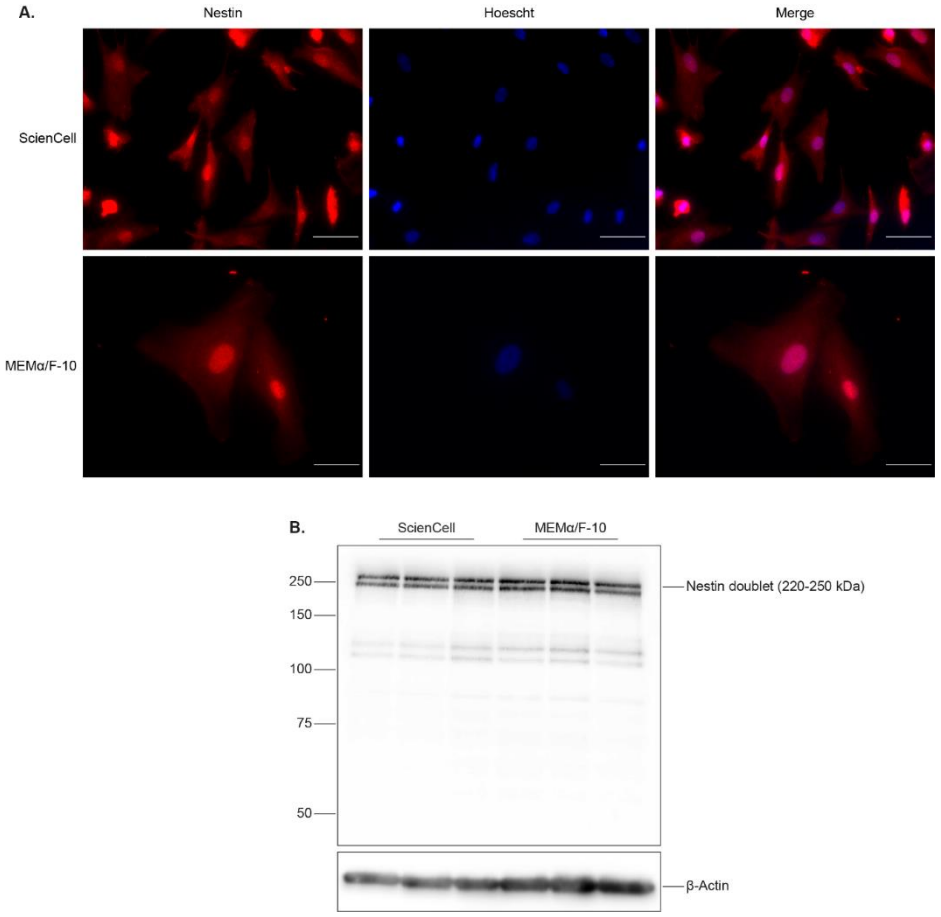

Figure 3.3: Nestin expression in human primary astrocytes cultured in two different media. A) Immunocytochemistry comparing the expression of nestin in human primary astrocytes cultured in either ScienCell Astrocyte Medium or MEMα/F-10 medium. Scale bar 50 μm. B) Western blot comparing the expression of nestin in human primary astrocytes. Molecular weight markers are indicated (kDa). Nestin predicted molecular weight 177 kDa. Loading control β-Actin.

3.2.2 Tight Junction Protein Expression in Human Primary Astrocytes

The expression of occludin, claudin 5 and ZO-1 in human primary astrocytes cultured in either ScienCell Astrocyte Medium or MEMα/F-10 was first investigated by immunocytochemistry. Experiments comparing human primary astrocytes cultured in either ScienCell Astrocyte Medium or MEMα/F-10 medium were conducted using cells of the same passage number.

Figure 3.4 shows immunocytochemistry staining for occludin, claudin 5 and ZO-1 in human primary astrocytes cultured in ScienCell Astrocyte Medium. The negative

and isotype controls for this experiment are shown in Figure 3.5. Figure 3.6 shows immunocytochemistry staining for occludin, claudin 5 and ZO-1 in human primary astrocytes cultured in MEMα/F-10 whilst the negative and isotype controls for this experiment are shown in Figure 3.7. No staining was observed in the negative controls or the mouse IgG isotypes control for human primary astrocytes cultured in either medium. Very weak non-specific background staining was seen in the rabbit IgG isotype control. The images presented in these figures are representative of the staining patterns exhibited by the whole cell population.

Human primary astrocytes cultured in either ScienCell Astrocyte Medium or MEMα/F-10 displayed clear punctate nuclear occludin staining and diffuse cytoplasmic staining. No membrane-associated occludin staining was observed in these cells. Occludin is a tight junction integral membrane protein, consequently the absence of membrane-associated staining in human primary astrocytes is surprising. Similarly, the nuclear localisation of this protein is unusual.

Diffuse claudin 5 staining was observed throughout the cytoplasm and nucleus of astrocytes cultured in either medium. No membrane-associated claudin 5 staining was observed in these cells. Claudin 5 is another tight junction integral membrane protein and again the absence of membrane-associated staining in human primary astrocytes is surprising. The apparent nuclear localisation of this protein is also unexpected.

Strong diffuse cytoplasmic and nuclear staining was observed for ZO-1 in human primary astrocytes cultured in either medium. ZO-1 is known to express both nuclear localisation and nuclear exportation signals and is known to be diffusely expressed throughout the cytoplasm and nucleus of MDCK cells (González-Mariscal et al., 1999; González-Mariscal et al., 2006). The nuclear localisation of ZO-1 in human primary astrocytes, is, therefore, not unusual for this protein.

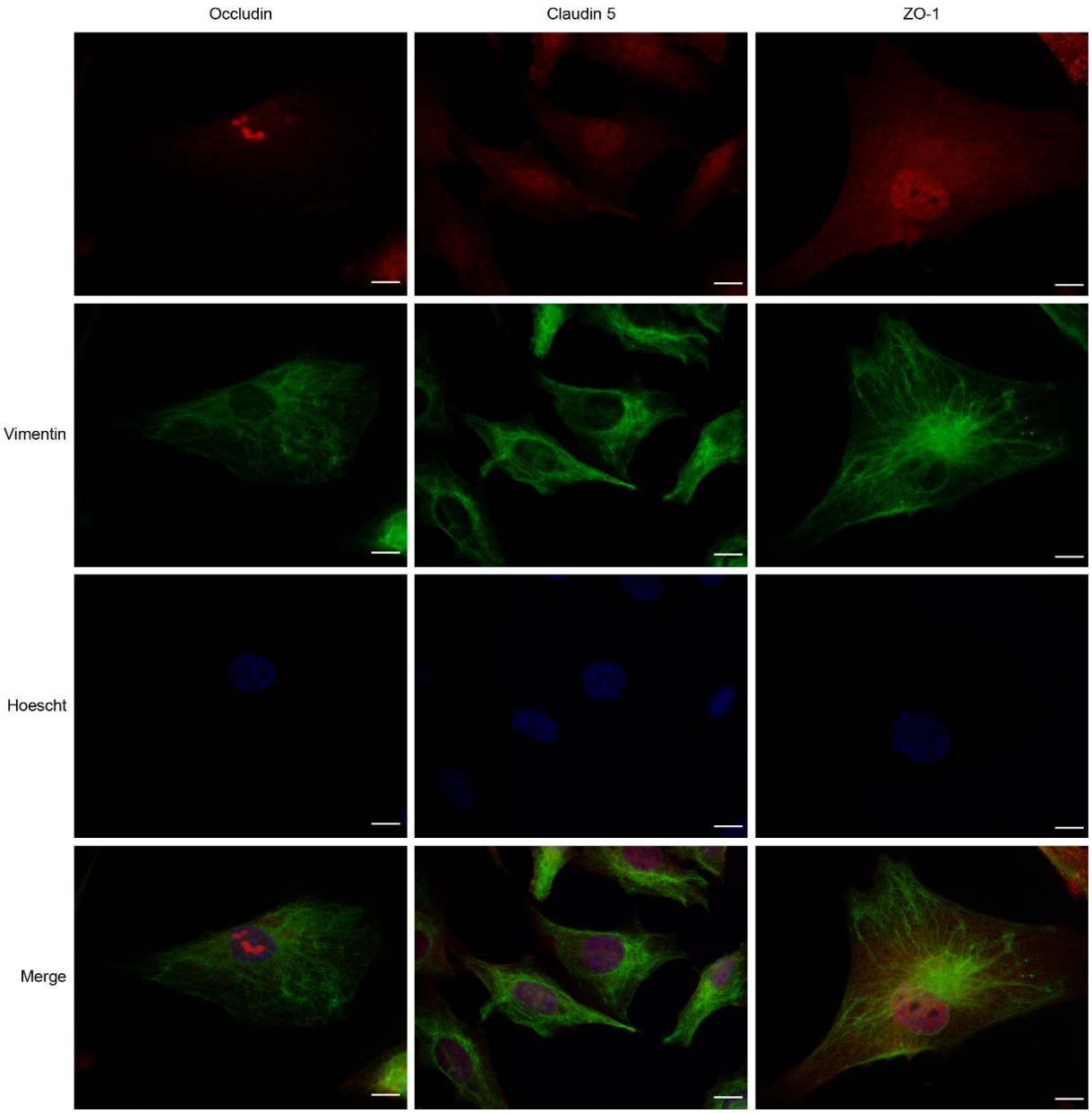

Figure 3.4: Immunocytochemistry characterising the expression of Occludin, Claudin 5 and ZO-1 in human primary astrocytes cultured in ScienCell Astrocyte Medium The human primary astrocytes used in this experiment were cultured in ScienCell Astrocyte Medium. Vimentin was used as a cell marker. The antibodies and dilutions used in this experiment: anti-vimentin mouse monoclonal (1:250), anti-occludin rabbit polyclonal antibody (1:50), anti-claudin 5 rabbit polyclonal antibody (1:50) and anti-ZO-1 rabbit polyclonal antibody (1:100). Scale bar 10 µm.

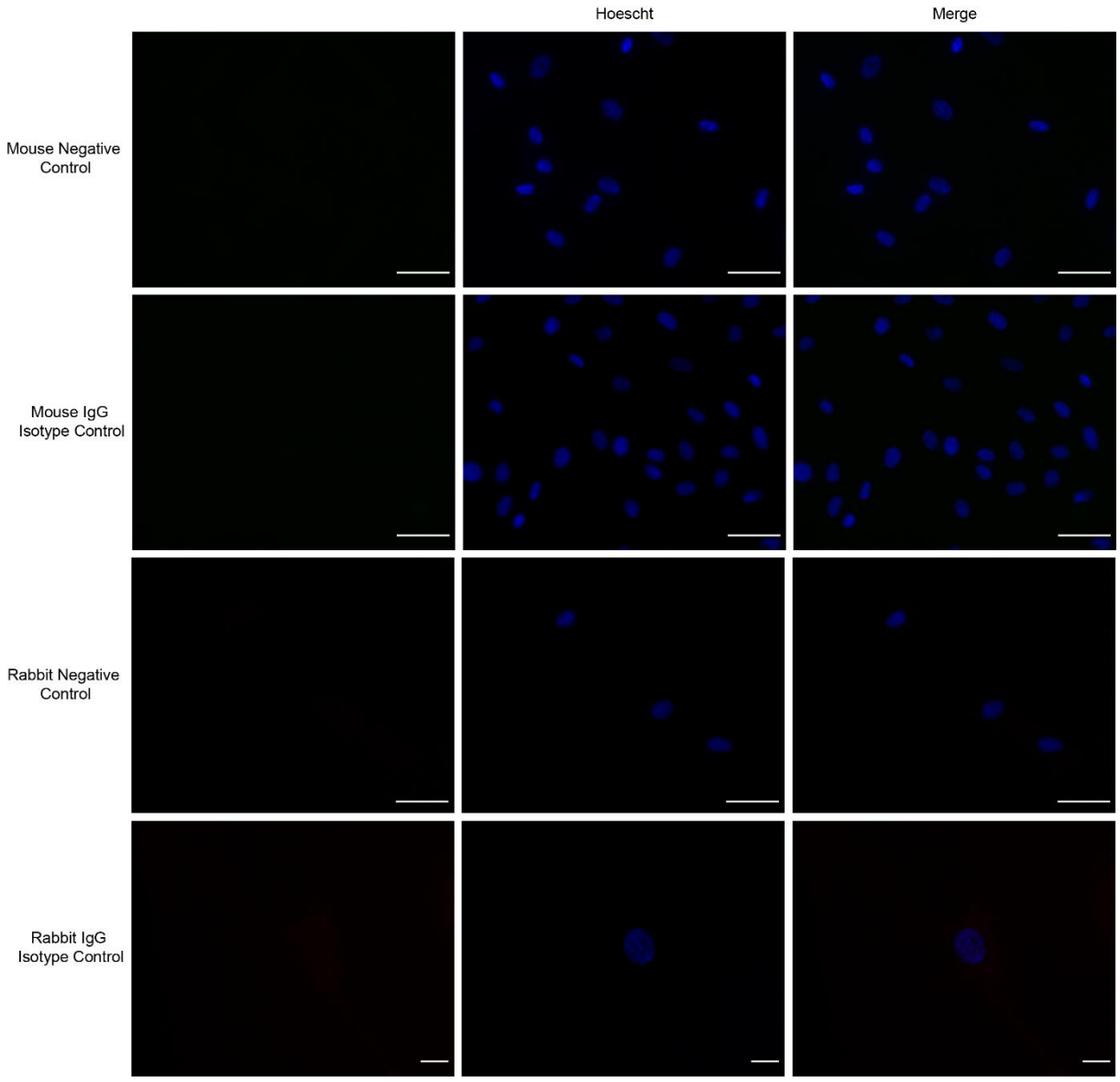

Figure 3.5: ICC Negative and Isotype controls for human primary astrocytes cultured in ScienCell Astrocyte Medium Negative and isotype controls were conducted for both mouse and rabbit antibodies. The negative control consisted of the omision of the primary antibody. The isotype control was conducted with either a mouse or rabbit IgG antibody (Vector Laboratories) used at the same concentration as the primary antibody. The human primary astrocytes used in this experiment were cultured in ScienCell Astrocyte Medium. Scale bar 50 μm except for rabbit IgG isotype control images for which scale bar 10 μm.

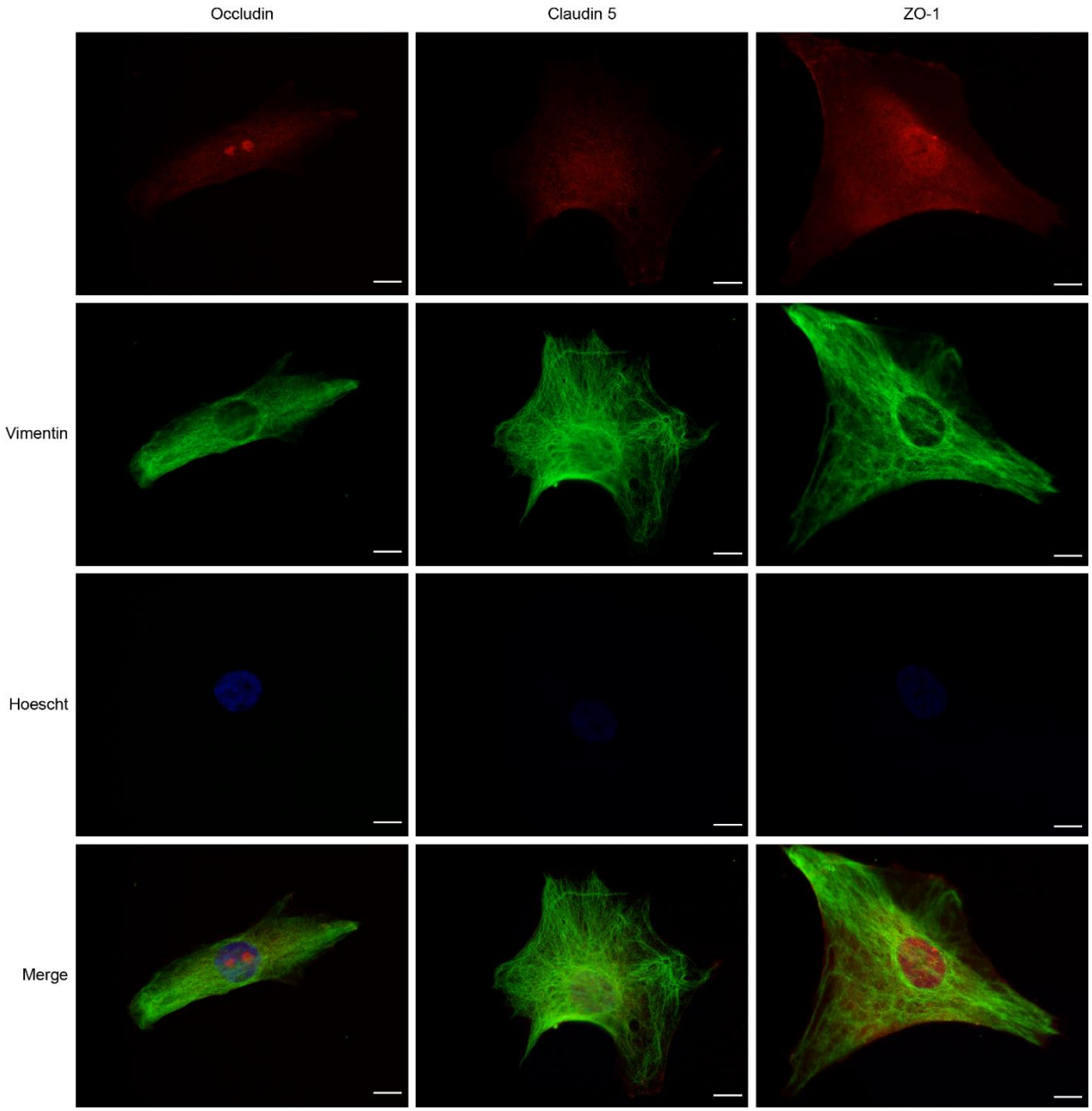

Figure 3.6: Immunocytochemistry investigating the expression of Occludin, Claudin 5 and ZO-1 in human prrimary astrocytes cultured in MEMα/F-10 medium The human primary astrocytes used in this experiment were cultured in MEMα/F-10 medium. Vimentin was used as a cell marker. The antibodies and dilutions used in this experiment: anti-vimentin mouse monoclonal (1:250), anti-occludin rabbit polyclonal antibody (1:50), anti-claudin 5 rabbit polyclonal antibody (1:50) and anti-ZO-1 rabbit polyclonal antibody (1:100). Scale bar 10 µm.

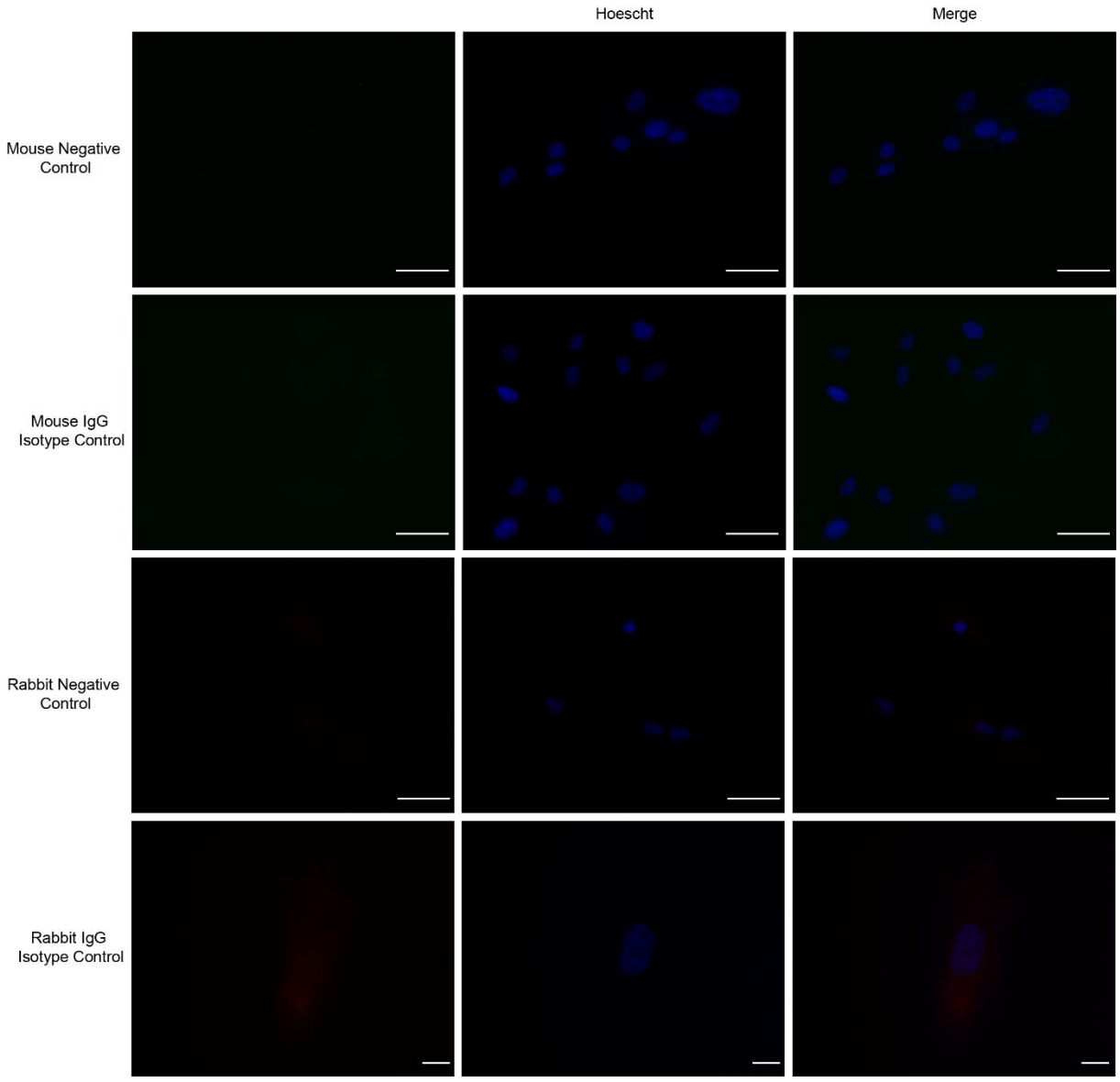

Figure 3.7: ICC Negative and Isotype controls for human primary astrocytes cultured in MEMα/F-10 medium Negative and isotype controls were conducted for both mouse and rabbit antibodies. The negative control consisted of the omision of the primary antibody. The isotype control was conducted with either a mouse or rabbit IgG antibody (Vector Laboratories) used at the same concentration as the primary antibody. The human primary astrocytes used in this experiment were cultured in MEMα/F-10 medium. Scale bar 50 µm except for rabbit IgG isotype control images for which scale bar 10 µm.

Other staining patterns for ZO-1 were also identified by ICC. A small population of human primary astrocytes cultured in ScienCell Astrocyte Medium displayed cytoplasmic ZO-1 aggregates which were localised close to the cell membrane, Figure 3.8. Proximate human primary astrocytes cultured in either medium also showed ZO-1 to be localised to intercellular strand-like structures, Figure 3.9.

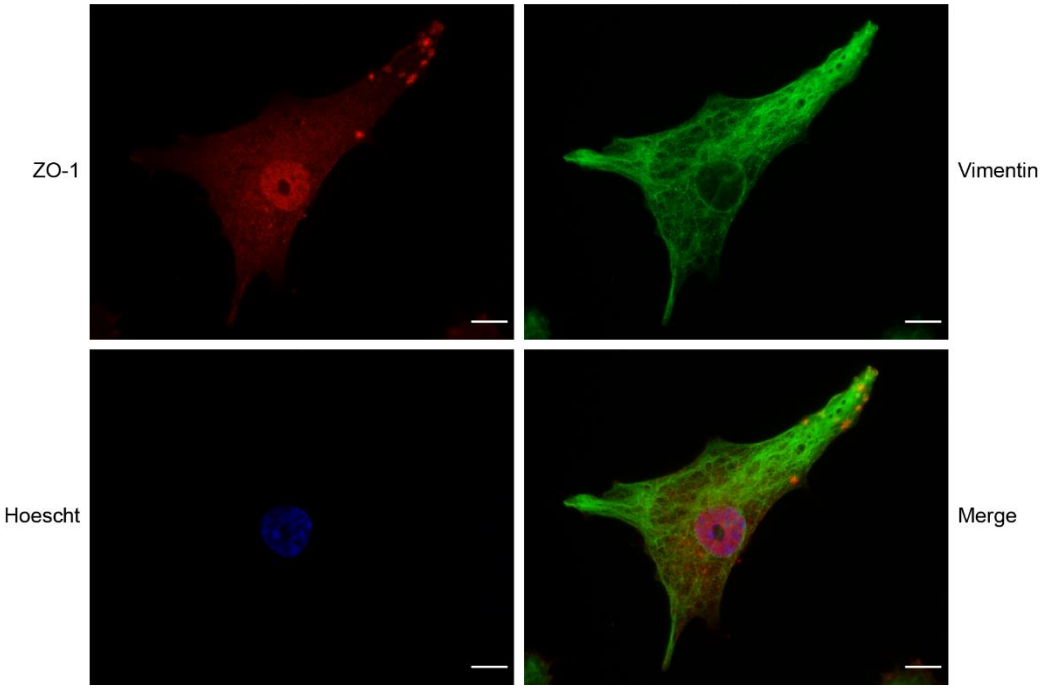

Figure 3.8: ZO-1 Aggregates in Human Primary Astrocytes ZO-1 cytoplasmic aggregate staining localised close to the cell membrane is occasionally seen in human primary astrocytes. This staining pattern was only observed in human primary astrocytes cultured in ScienCell Astrocyte Medium. Scale bar 10 µm.

The ZO-1 aggregates shown in Figure 3.8 resemble the staining pattern produced by connexin 43 in primary murine cortical astrocytes (Duffy et al., 2004). ZO-1 is known to bind to connexin 30 and connexin 43 in murine astrocytes, consequently this staining may suggest that ZO-1 interacts with gap junction connexin proteins in human primary astrocytes (Duffy et al., 2004; Penes et al., 2005).

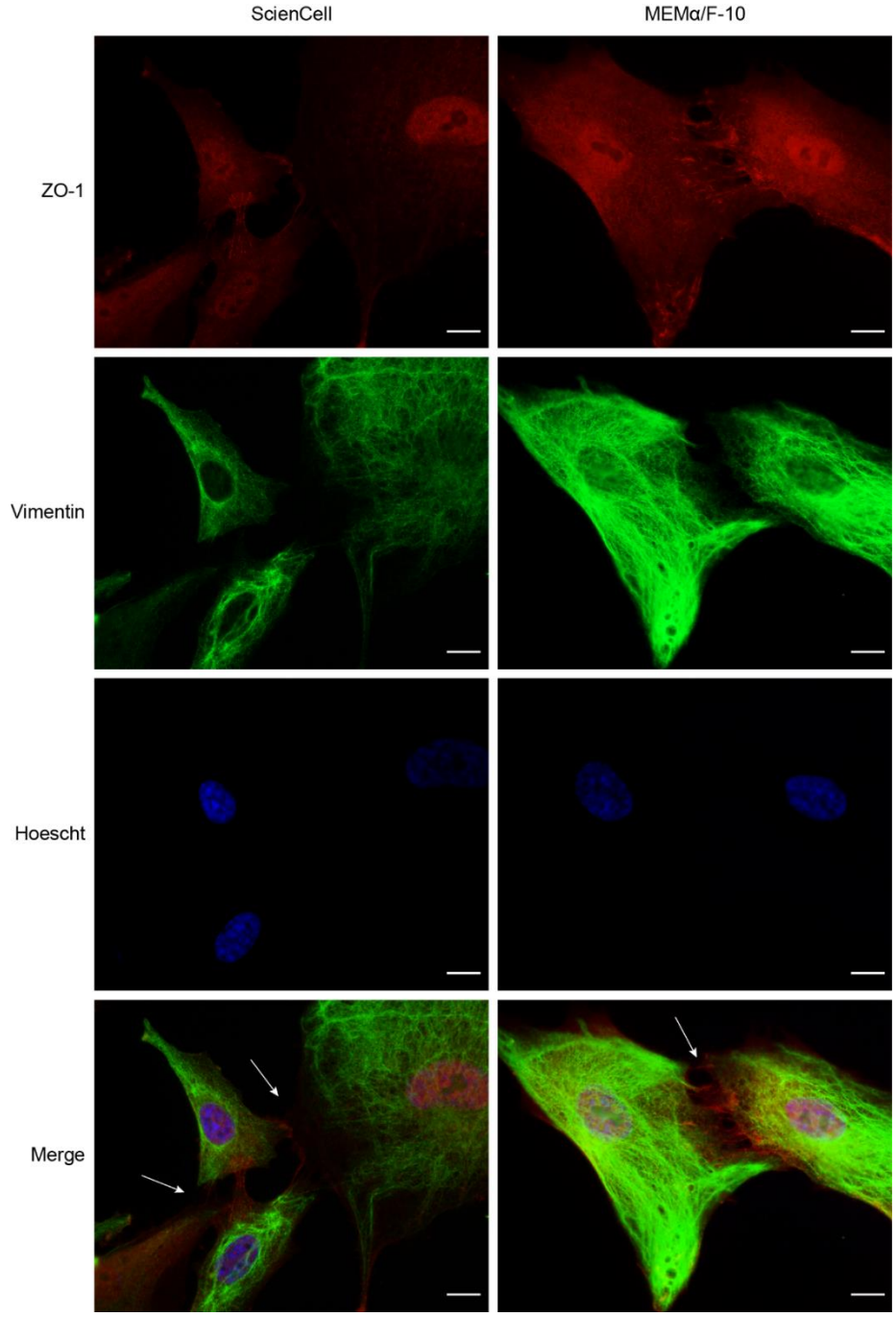

Figure 3.9: ZO-1 Intercellular Contacts in Human Primary Astrocytes ZO-1 localises to intercellular contacts formed between proximate human primary astrocytes cultured in either ScienCell Astrocyte Medium or MEMα/F-10 medium (see arrows). These contacts appear as thread or stand-like structures. Scale bar 10 µm.

The intercellular ZO-1 strands shown in Figure 3.9 are structurally similar to ZO-2 intercellular contacts made between vascular smooth muscle cells (VSMCs) (Tkachuk et al., 2011). The association of ZO-1 with intercellular contacts is not surprising given the function of this protein. It is, however, unclear with which proteins ZO-1 is associated in these intercellular structures.

The expression of occludin, claudin 5 and ZO-1 in human primary astrocytes was further investigated by western blotting. Experiments comparing human primary astrocytes cultured in either ScienCell Astrocyte Medium or MEMα/F-10 medium were conducted using cells of the same passage number. Occludin has a molecular weight of 59 kDa, however, occludin protein bands ranging between 62-82 kDa are observed in western blots due to protein phosphorylation (Sakakibara et al., 1997). Figure 3.10 shows a western blot characterising the expression of occludin in human primary astrocytes cultured in either ScienCell Astrocyte Medium or MEMα/F-10 medium. This experiment was conducted using the anti-occludin rabbit polyclonal antibody. The predicted molecular weight of occludin using this antibody is between 65-79 kDa.

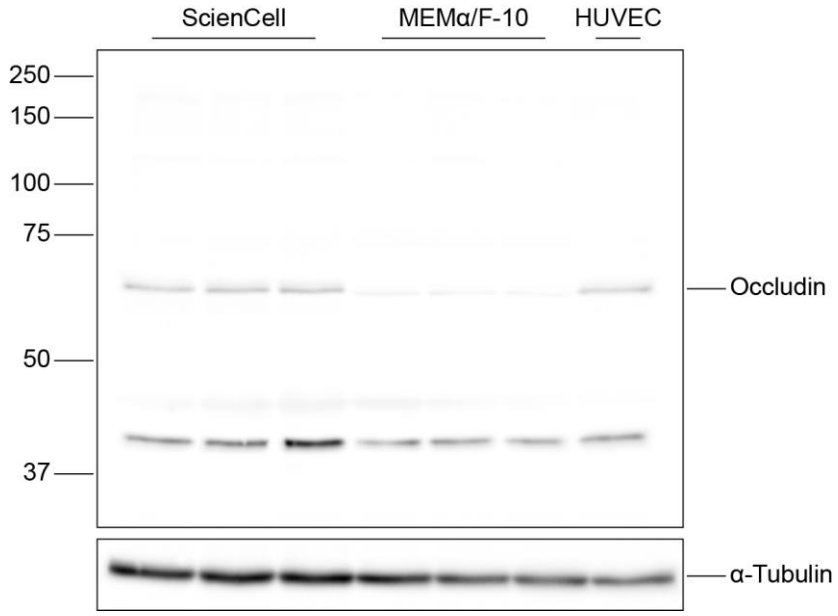

Figure 3.10: Western blot characterising Occludin expression in human primary astrocytes cultured in ScienCell Astrocyte Medium and MEMα/F-10 Medium This experiment was conducted using an anti-occludin rabbit polyclonal antibody (Thermo 71-1500). This blot includes a HUVEC positive control and an α-Tubulin loading control. Molecular weight markers are indicated (kDa).

A clear 65 kDa protein band at the predicted molecular weight for occludin was observed in human primary astrocytes cultured in ScienCell Astrocyte Medium and the HUVEC positive control. This supports the immunocytochemistry staining and confirms the expression of occludin in human primary astrocytes. The molecular weight of this band suggests that occludin is phosphorylated in these cells. A very faint 65 kDa band is present in astrocytes cultured in MEMα/F-10 medium. Although the ICC staining for occludin in either medium appears similar, the western blot suggests that this protein is not highly expressed in astrocytes cultured in

MEMα/F-10 medium. A 40 kDa protein band was also observed in every astrocyte sample as well as the HUVEC positive control. This band could be the product of proteolysis or non-specific binding.

The nuclear localisation of occludin which was identified by ICC was further investigated by subcellular fractionation. This experiment was conducted using human primary astrocytes cultured in ScienCell Astrocyte Medium as the cells appear to express higher levels of occludin when cultured in this medium. The cells were fractionated into cytoplasmic and nuclear lysates, Figure 3.11.

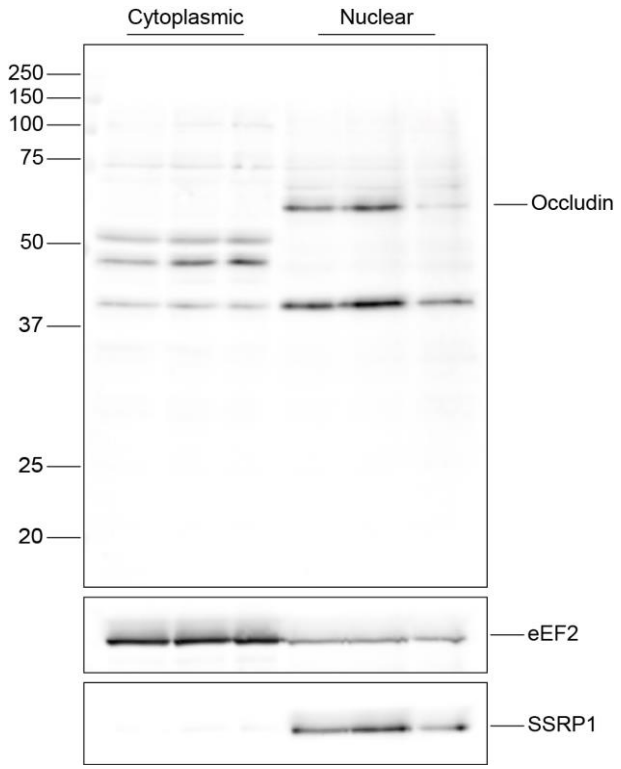

Figure 3.11: Subcellular Localisation of Occludin in Human Primary Astrocytes Western blot of fractionated cytoplasmic and nuclear lysates from human primary astrocytes cultured in ScienCell Astrocyte Medium. This experiment was conducted using an anti-occludin rabbit polyclonal antibody (Thermo 71-1500). The enrichment of cytoplasmic and nuclear fractions was determined using anti-eEF2 and anti-SSRP1 antibodies resectively. Molecular weight markers are indicated (kDa).

The nuclear fraction exhibited occludin protein bands ranging between 65-75 kDa. A faint 75 kDa protein band was observed in the cytoplasmic fraction as well as two lower molecular weight protein bands between 45-55 kDa which were not previously observed in the whole cell lysate western blot, Figure 3.10. These bands may be degradation products. This would again suggest that occludin is phosphorylated in human primary astrocytes. A strong 50 kDa protein band exclusive to the

cytoplasmic fraction was also observed. The 40 kDa protein bands previously identified in Figure 3.10 was present in both cytoplasmic and nuclear fractions.

Eukaryotic translation elongation factor 2 (eEF2) and structure specific recognition protein 1 (SSRP1) were used to determine the enrichment of the cytoplasmic and nuclear fractions. eEF2 is a cytoplasmic protein involved in protein translation whilst SSRP1 is a nuclear protein which is a component of the FACT (facilitates chromatin transcription) complex (Belotserkovskaya et al., 2004; Browne and Proud, 2002). An SSRP1 protein band was exclusive to the nuclear fraction and demonstrated that there was no nuclear contamination present in the cytoplasmic fraction. There were, however, faint eEF2 bands present in the nuclear fraction indicative of some cytoplasmic contamination.

Claudin 5 is a 23 kDa protein. The phosphorylation of claudin 5 is, however, known to produce higher molecular weight protein bands in western blotting experiments. 21 kDa, 25 kDa, 31 kDa, 42 kDa and 62 kDa protein bands were previously observed in claudin 5 western blots using primary porcine brain capillary endothelial cell lysates (Ishizaki et al., 2003). Phosphoamino acid analysis showed that the 25 kDa band was due to claudin 5 serine phosphorylation whilst the 31 kDa protein band is due to threonine phosphorylation (Ishizaki et al., 2003). It was speculated that the 42 and 62 kDa protein bands may be caused by claudin dimerisation, although this was not experimentally confirmed (Ishizaki et al., 2003). A 27 and 29 kDa claudin 5 doublet was also observed in Sprague-Dawley rat alveolar type II cells (Wang et al., 2003). The 27 kDa protein band was considered to be claudin 5 whilst the 29 kDa form was not subjected to any further investigation but was speculated to be a possible claudin 5 isoform or a product of post-translational modification (Wang et al., 2003).

Figure 3.12 shows western blots characterising the expression of claudin 5 in human primary astrocytes cultured in either ScienCell Astrocyte Medium or MEMα/F-10 medium. Panel A was produced with anti-claudin 5 rabbit monoclonal antibody (ab131259) whilst panel B was produced with anti-claudin 5 rabbit polyclonal antibody (ab15106).

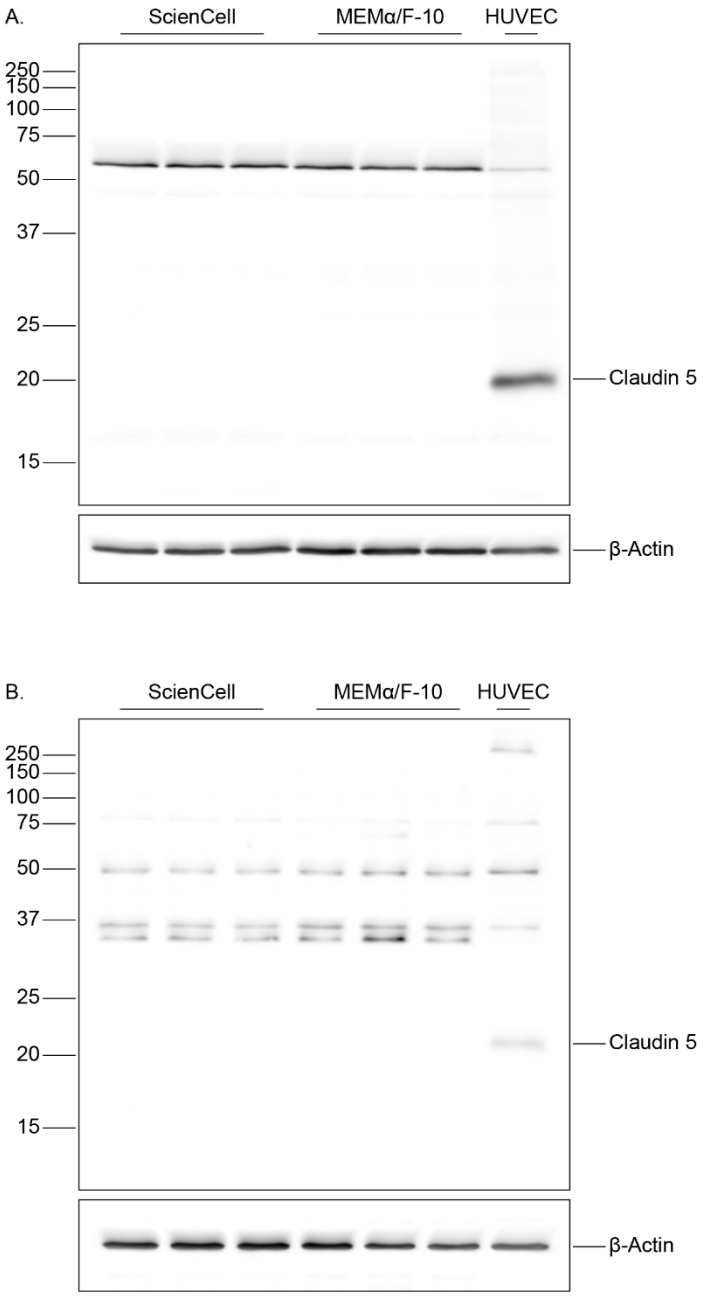

Figure 3.12: Western blots of claudin 5 expression in human primary astrocytes cultured in ScienCell Astrocyte Medium and MEMα/F-10 Medium
A) This experiment was conducted using an anti-claudin 5 rabbit monoclonal antibody (Abcam ab131259). B) This experiment was conducted using anti-claudin 5 rabbit polyclonal (Abcam ab15106). Both blots include a HUVEC positive control and a β-Actin loading control. Molecular weight markers are indicated (kDa).

A 23 kDa claudin 5 protein band was seen only in the HUVEC positive control in both western blots, suggesting that claudin 5 is not expressed in human primary astrocytes. This conclusion is, however, not supported by the immunocytochemistry staining which suggests that claudin 5 is diffusely expressed throughout the cytoplasm and nucleus of these cells.

The anti-claudin 5 rabbit polyclonal antibody (ab15106) was used in the ICC experiments and for the western blot shown in Figure 3.12 panel B. The company datasheet for this antibody acknowledges the presence of additional 35 kDa protein bands which are attributed to possible non-specific binding. Bands of around this molecular weight were observed in human primary astrocytes, Figure 3.12 panel B, and may be the result of non-specific binding.

These bands are, however, of a similar molecular weight to the 31 kDa threonine phosphorylated claudin 5 protein band seen in primary porcine brain capillary endothelial cells (Ishizaki et al., 2003). This might suggest that human primary astrocytes express phosphorylated claudin 5. Given the current evidence, however, and in the absence of further investigation, it seems more likely that the claudin 5 ICC staining is non-specific and that claudin 5 is not expressed in human primary astrocytes.

ZO-1 is a 195 kDa protein, however, higher molecular weight forms of this protein have been observed in western blots due to protein phosphorylation (Anderson et al., 1988; Howarth et al., 1994). Figure 3.13 shows a western blot characterising the expression of ZO-1 in human primary astrocytes cultured in either ScienCell Astrocyte Medium or MEMα/F-10 medium.

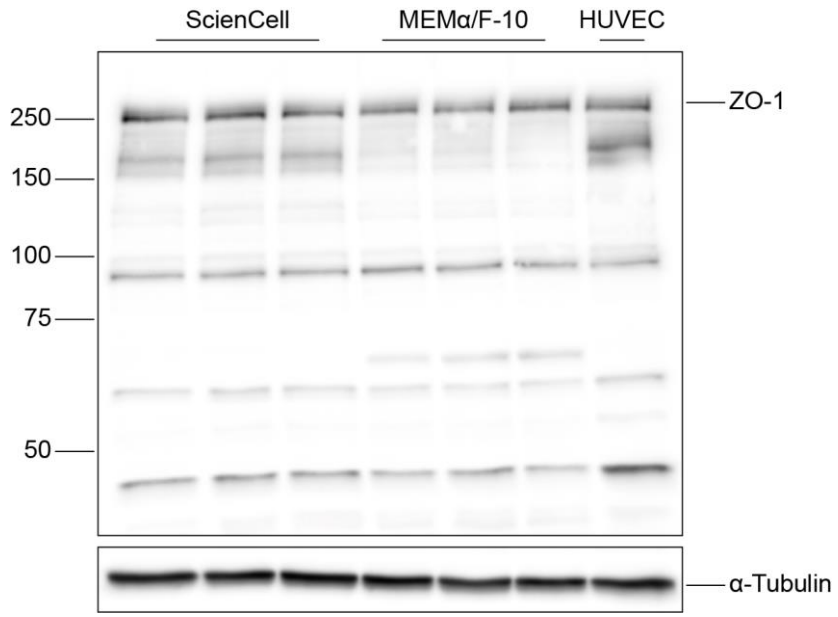

Figure 3.13: Western blot of ZO-1 expression in human primary astrocytes cultured in ScienCell Astrocyte Medium and MEMα/F-10 This experiment was conducted using an anti-ZO-1 rabbit polyclonal antibody (Thermo 40-2200) This blot includes a HUVEC positive control and an α-Tubulin loading control. Molecular weight markers are indicated (kDa).

A clear band of 250 kDa was observed in human primary astrocytes and the HUVEC positive control. This supports the immunocytochemistry staining and confirms the expression of ZO-1 in human primary astrocytes. The expression of this protein was not affected by the culture medium. Several lower molecular weight protein bands were observed in astrocyte and HUVEC protein samples. The antibody datasheet for the anti-ZO-1 rabbit polyclonal antibody used in this experiment acknowledges the presence of several lower molecular weight protein bands which are attributed to degradation products but may also be caused by shorter ZO-1 isoforms.

3.2.3 Tight Junction Protein Expression in 1321N1 Astrocytoma cells

The expression of occludin, claudin 5 and ZO-1 was also investigated in 1321N1 human astrocytoma through immunocytochemistry and western blotting techniques. Figure 3.14 shows immunocytochemistry staining for occludin, claudin 5 and ZO-1 in 1321N1 astrocytoma cells. The negative and isotype controls for this experiment are shown in Figure 3.15.

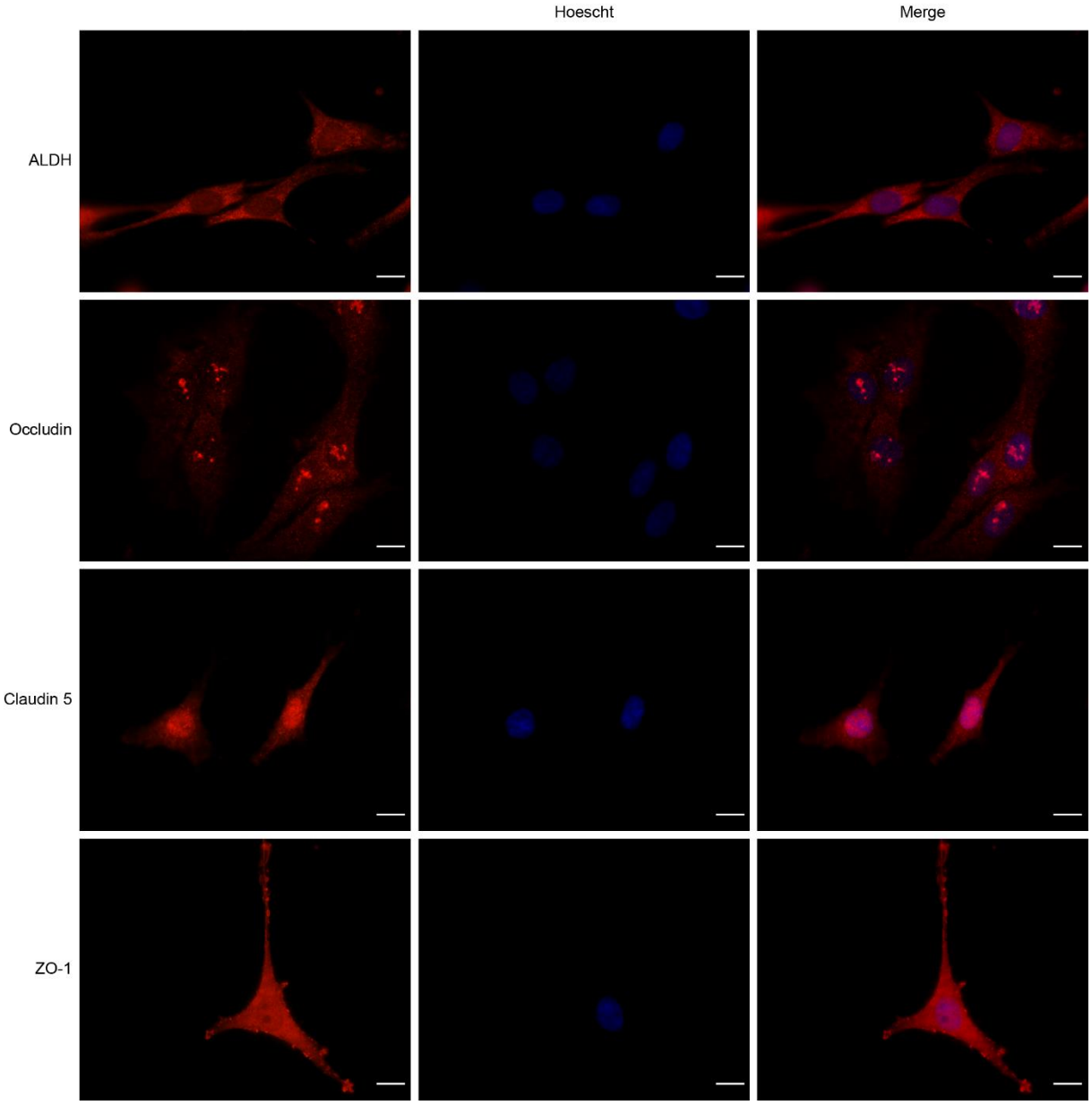

Figure 3.14: Immunocytochemistry characterising the expression of Occludin, Claudin 5 and ZO-1 in 1321N1 human astrocytoma cells Immunocytochemistry characterising the expression of occludin, claudin 5 and ZO-1 in the 1321N1 human astrocytoma cell line. ALDH1L1 was included as an astrocyte marker. The antibodies and dilutions used in this experiment: anti-ALDH1L1 rabbit polyclonal antibody (1:50), anti-occludin rabbit polyclonal antibody (1:50), anti-claudin 5 rabbit polyclonal antibody (1:50) and anti-ZO-1 rabbit polyclonal antibody (1:100). Scale bar 10 µm.

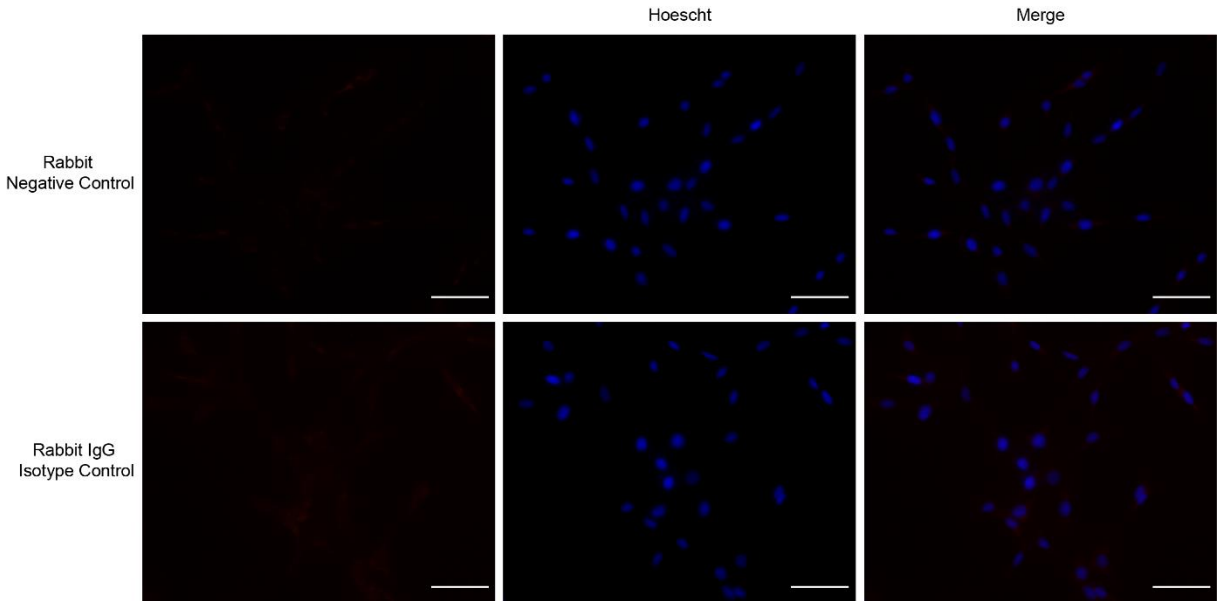

Figure 3.15: ICC Negative and Isotype controls for 1321N1 Astrocytoma Cells
Negative and isotype controls were conducted for rabbit antibodies. The negative control consisted of the omision of the primary antibody. The isotype control was conducted with a rabbit IgG antibody (Vector Laboratories) used at the same concentration as the primary antibody. Scale bar 50 µm.

1321N1 astrocytoma cells exhibited similar staining patterns for all three tight junction proteins to those previously seen in human primary astrocytes. Occludin again presented with distinct nuclear punctate staining and diffuse cytoplasmic staining. 1321N1 astrocytoma cells did not exhibit any membrane-associated occludin staining.

Claudin 5 was diffusely expressed throughout the cytoplasm and nucleus of 1321N1 astrocytoma cells and again no membrane-associated claudin 5 staining was observed in these cells whilst ZO-1 presented with strong nuclear and cytoplasmic staining. No staining was observed in the negative control and a very weak non-specific background staining was seen in the rabbit IgG isotype control. The expression of occludin, claudin 5 and ZO-1 in 1321N1 astrocytoma cells was further investigated by western blotting, Figure 3.16.

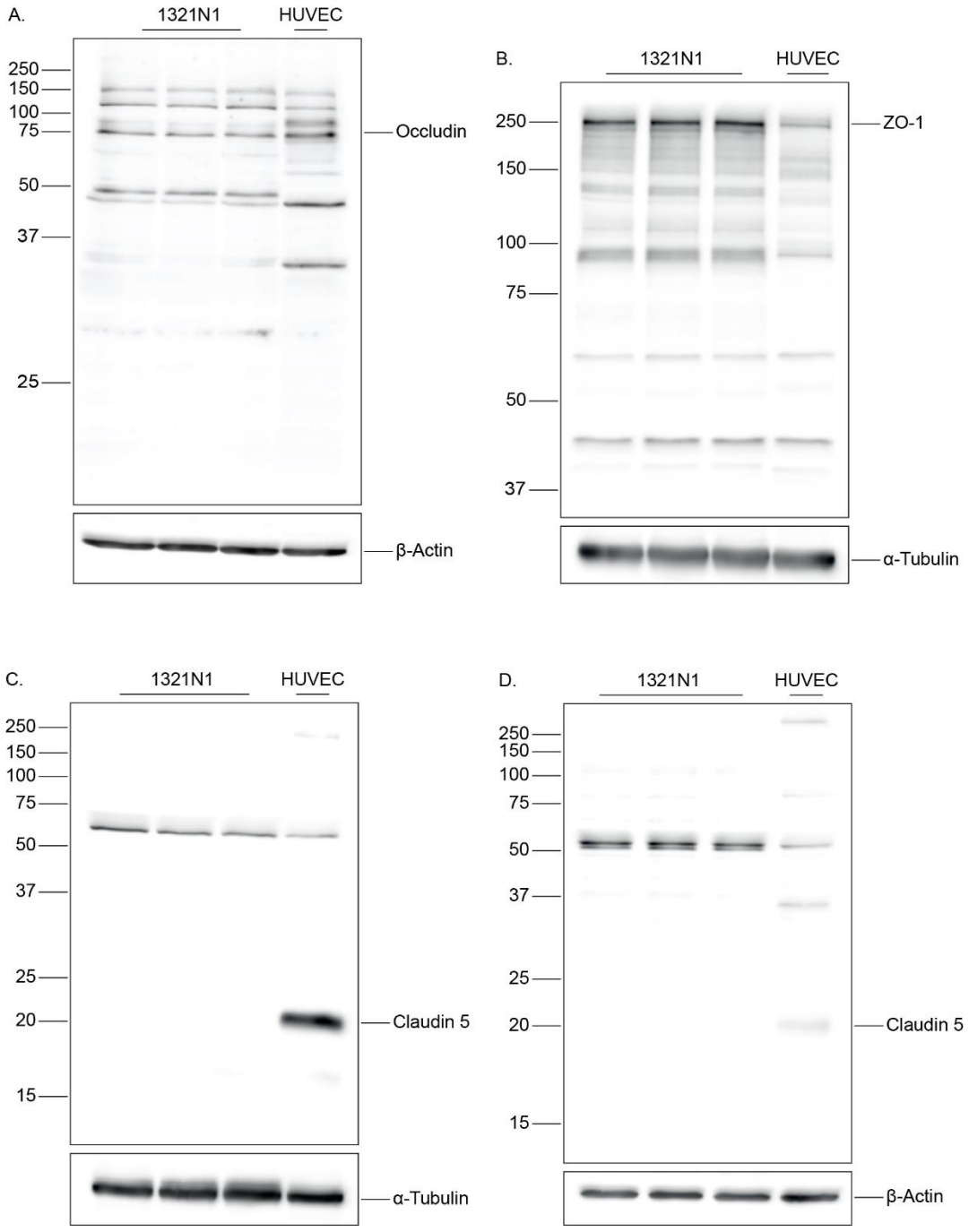

Figure 3.16: Western blots characterising the expression of Occludin, Claudin 5 and ZO-1 in 1321N1 astrocytoma cells A) Occludin western blot using anti-occludin rabbit polyclonal antibody. B) ZO-1 western blot using anti-ZO-1 rabbit polyclonal antibody. C) Claudin 5 blot using anti-claudin 5 rabbit monoclonal antibody (ab131259). D) Claudin 5 blot using anti-claudin 5 rabbit polyclonal antibody (ab15106). All blots include a HUVEC positive control and either an α-Tubulin or β-Actin loading control. Molecular weight markers are indicated (kDa).

Figure 3.16 panel A shows the western blot characterising the expression of occludin in 1321N1 astrocytoma cells. A 75 kDa occludin protein band was observed in 1321N1 astrocytoma cells and the HUVEC positive control. This

supports the immunocytochemistry staining and confirms the expression of occludin in 1321N1 astrocytoma cells. The molecular weight of this protein band suggests that occludin is phosphorylated in these cells. Higher molecular weight protein bands ranging from 100-150 kDa and a protein band just below 50 kDa were also observed in this blot. The presence of these bands may indicate that this antibody is not very specific and that these bands are the result of non-specific antibody binding, however, these bands may also be caused by occludin dimers or oligomers.

A study investigating occludin oligomerisation using protein extracts from rat cerebral microvessels showed western blots in which multiple high molecular weight protein bands above 100 kDa are present (McCaffrey et al., 2008). These experiments used the same anti-occludin rabbit polyclonal antibody as the one used in the current project. In this previous study, bands greater than 150 kDa were defined as occludin oligomers, whilst bands ranging from 100-120 kDa were considered to be occludin dimers (McCaffrey et al., 2008). The higher molecular weight bands in Figure 3.16 panel A may, therefore, be produced by occludin dimers.

Figure 3.16 panel C was produced with the anti-claudin 5 rabbit monoclonal antibody (ab131259) whilst panel D was produced with the anti-claudin 5 rabbit polyclonal antibody (ab15106). A 23 kDa claudin 5 protein band was only seen in the HUVEC positive controls of both blots whilst the 1321N1 astrocytoma cells exhibited a non-specific protein band around 50 kDa. These blots demonstrate that claudin 5 is not expressed in 1321N1 astrocytoma cells and suggest that the staining seen in Figure 3.14 is unlikely to be specific.

A clear band of 250 kDa was observed in 1321N1 astrocytoma cells and the HUVEC positive control, Figure 3.16 panel B. This supports the immunocytochemistry staining and confirms the expression of ZO-1 in these cells. Lower molecular weight bands were also observed in these cells and are likely to be caused by degradation products

3.2.4 Tight Junction Protein Expression in Human Tissue

Non-endothelial cell expression of occludin, claudin 5 and ZO-1 was investigated *in vivo* in the temporal cortex. Details of the tissue cohort used for these experiments are disclosed in Table 2.6 . This cohort consisted of 10 non-neurological control cases, 9 MCI cases and 10 AD cases.

3.2.4.1. Occludin Expression *in vivo*

Figure 3.17 shows the immunoreactive profile of occludin in the temporal cortex in non-neurological control, MCI and AD cases. The negative and isotype controls for this experiment are shown in Figure 3.18. Neither of the controls exhibited any positive immunoreactivity. Positive immunoreactivity associated with blood vessels was observed throughout the whole tissue cohort and in all cases. This observation is expected given that occludin in a tight junction protein and a component of the blood brain barrier.

Positive immunoreactivity was also observed in large pyramidal neurons localised to the cytoplasm and nucleus. Examples of this staining pattern were also seen throughout the entire cohort and in all cases. Positive nuclear immunoreactivity was also observed for occludin throughout the temporal cortex in all cases. It was not possible to determine the type of cells with which these positive nuclei were associated with single-labelling alone.

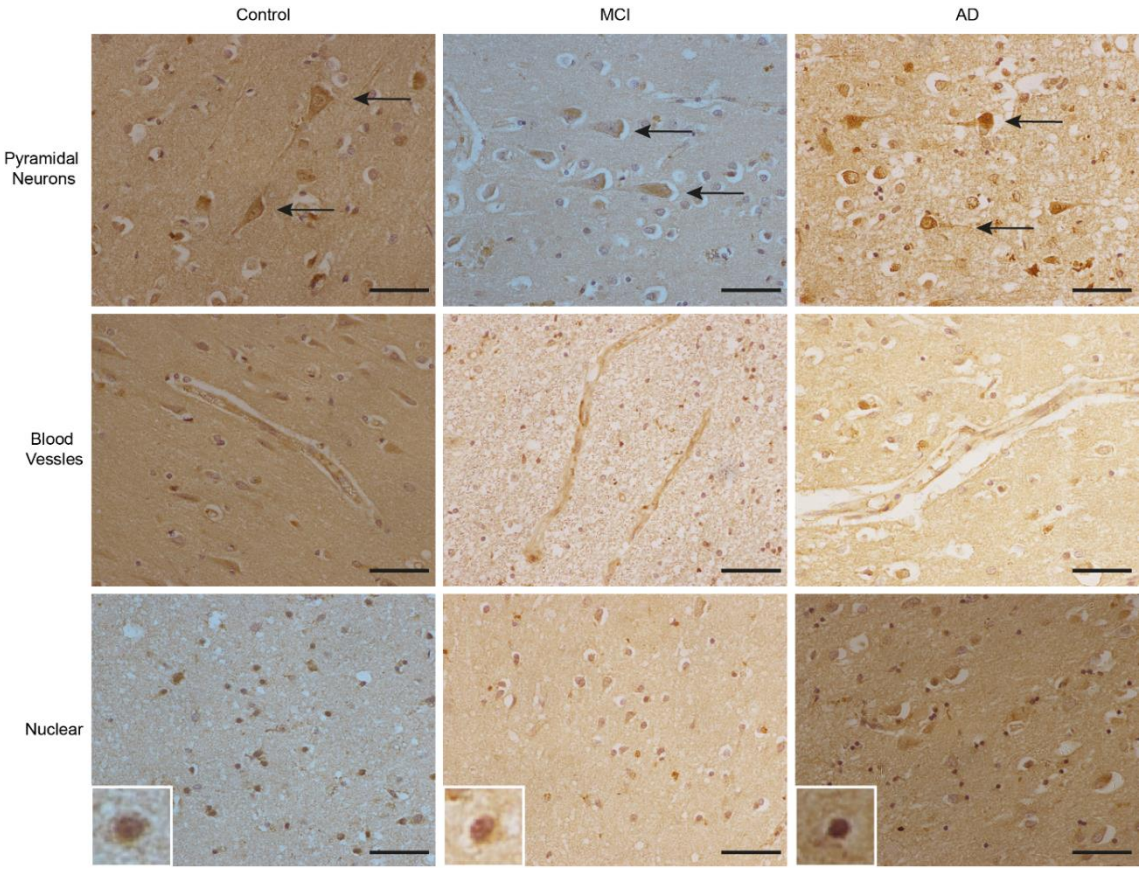

Figure 3.17: Occludin Expression in the Temporal Cortex Occludin expression in the human temporal cortex in non-neurological control, MCI and AD cases. The anti-occludin rabbit polyclonal antibody (1:100) was used for this experiment. Positive occludin immunorecativity was observed in pyramidal neurones, blood vessels and nuclei in the cortex of control, MCI and AD cases. Scale bar 50 µm.

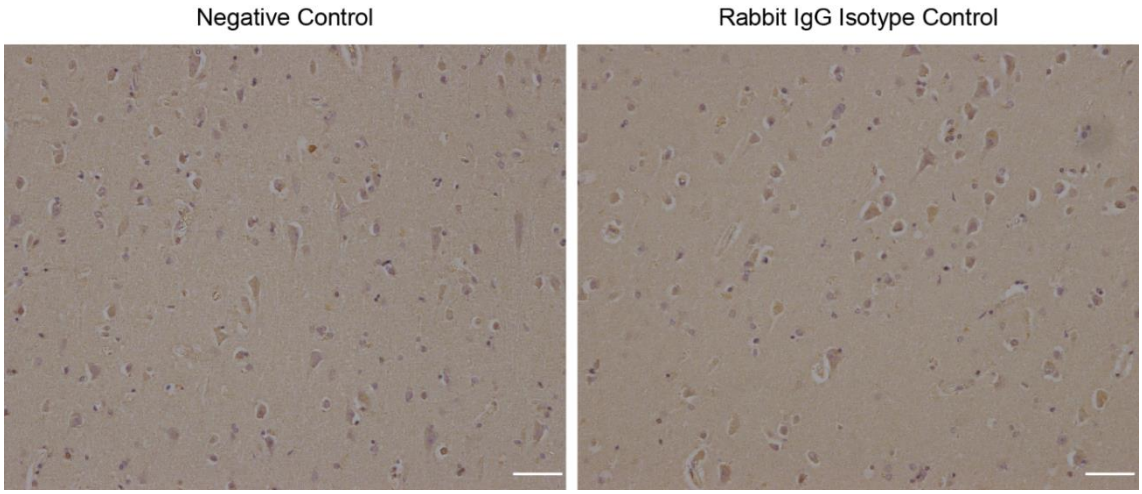

Figure 3.18: IHC Negative and Isotype Controls for Occludin The occludin IHC experiment used an anti-occludin rabbit polyclonal antibody. A negative and isotype control was conducted for this rabbit antibody. The negative control consisted of the omision of the primary antibody. The isotype control was conducted with a rabbit IgG antibody (Vector Laboratories) used at the same concentration as the primary antibody. Scale bar 50 µm.

Dual-labelling immunohistochemistry was conducted to establish if occludin immunoreactivity co-localised with the astrocytic marker GFAP, Figure 3.19. Occludin-positive nuclei were found to co-localise with GFAP-positive astrocytes, Figure 3.19 panel B. This demonstrates that occludin is expressed in the nucleus in human astrocytes *in vivo*. Not all cases demonstrated this pattern of co-localisation and not all GFAP-positive cells co-localised with occludin immunoreactivity, Figure 3.19 A.

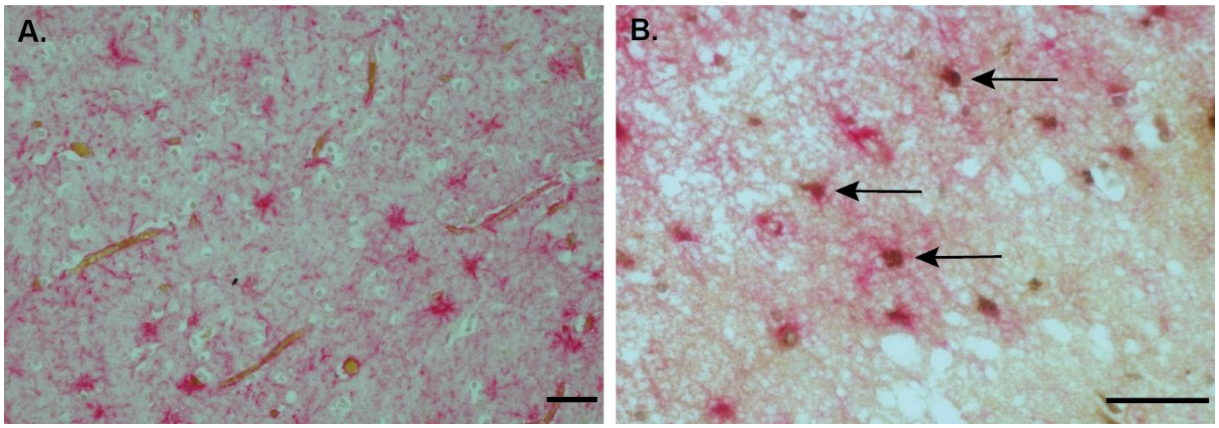

Figure 3.19: Astrocytic expression of Occludin *in vivo* A) A case in which dual-labelling shows no co-localisation of occludin (brown) with GFAP (red). Scale bar 50 µm. B) A case in which dual-labelling shows co-localisation of occludin (brown) with GFAP (red), as indicated by the arrows. Scale bar 50 µm.

3.2.4.2. ZO-1 Expression *in vivo*

Figure 3.20 shows the expression of ZO-1 in the temporal cortex in non-neurological controls, along with MCI and AD cases. The negative and isotype controls for this experiment are shown in Figure 3.21. Neither of the controls exhibited any positive immunoreactivity. This observation is again expected given that ZO-1 is a tight junction protein and a component of the blood brain barrier.

Positive immunoreactivity associated with blood vessels was observed throughout the whole tissue cohort and in all cases. Positive immunoreactivity was also observed in large pyramidal neurons localised to the cytoplasm and nucleus. Examples of this staining pattern were seen throughout the entire cohort and in all cases.

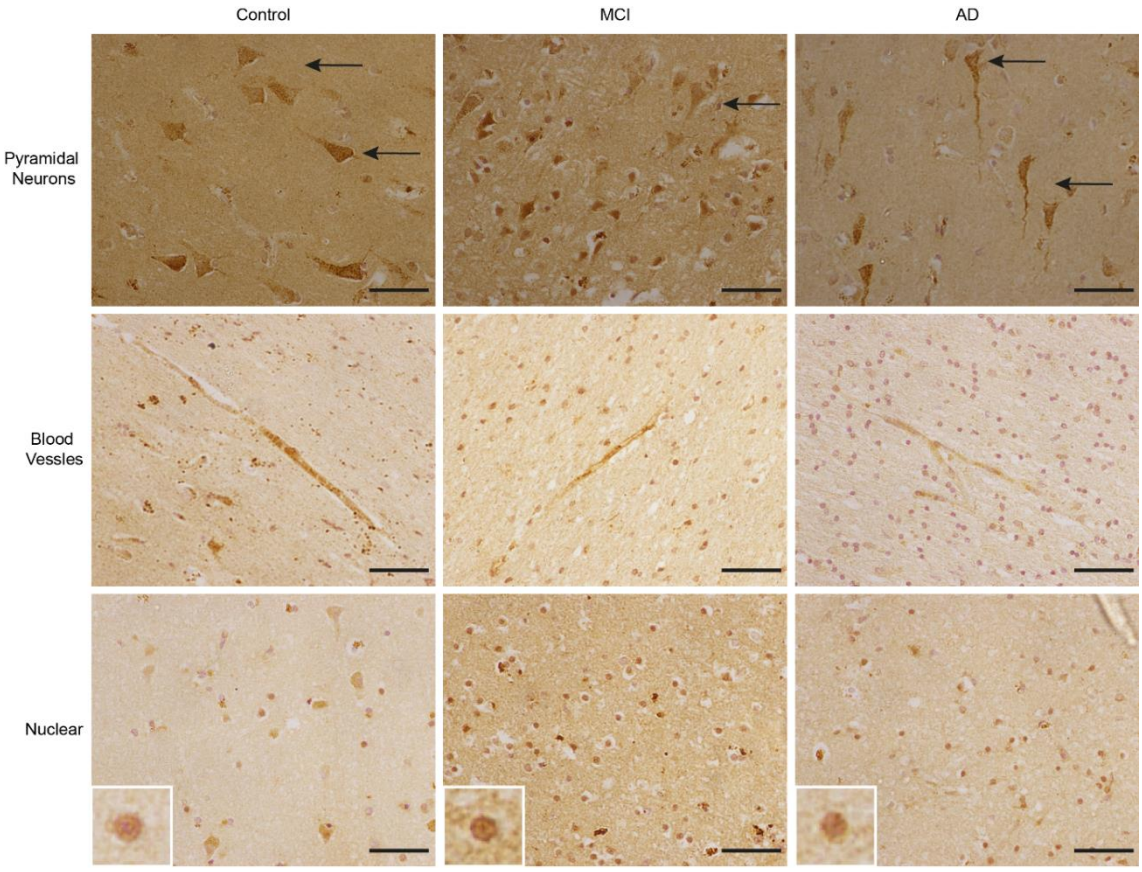

Figure 3.20: ZO-1 Expression in the Temporal Cortex ZO-1 expression in the human temporal cortex in non-neurological control, MCI and AD cases. The anti-ZO-1 rabbit polyclonal antibody (1:50) was used for this experiment. Positive ZO-1 immunorecativity was observed in pyramidal neurones, blood vessels and nuclei in the cortex of control, MCI and AD cases. Scale bar 50 µm.

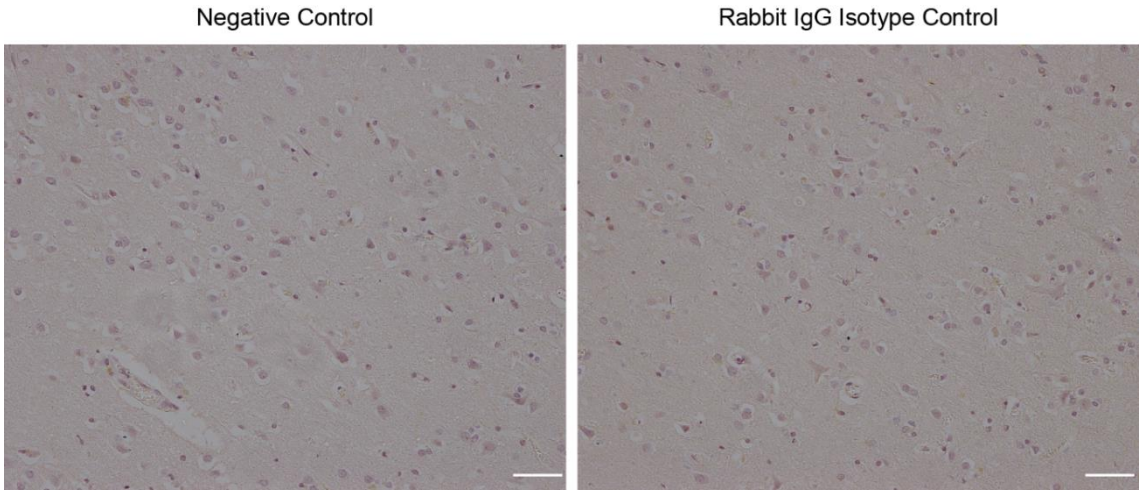

Figure 3.21: IHC Negative and Isotype Controls for ZO-1 The ZO-1 IHC experiment used an anti-ZO-1 rabbit polyclonal antibody. A negative and isotype control was conducted for this rabbit antibody. The negative control consisted of the omision of the primary antibody. The isotype control was conducted with a rabbit IgG antibody (Vector Laboratories) used at the same concentration as the primary antibody. Scale bar 50 µm.

3.2.4.3. Claudin 5 Expression *in vivo*

Figure 3.22 shows the expression of claudin 5 in the temporal cortex in non-neurological controls, MCI and AD cases. The negative and isotype controls for this experiment are shown in Figure 3.23. Neither of the controls exhibited any positive immunoreactivity. Claudin 5 immunoreactivity was associated exclusively with blood vessels. No apparent immunoreactivity was associated with pyramidal neurons.

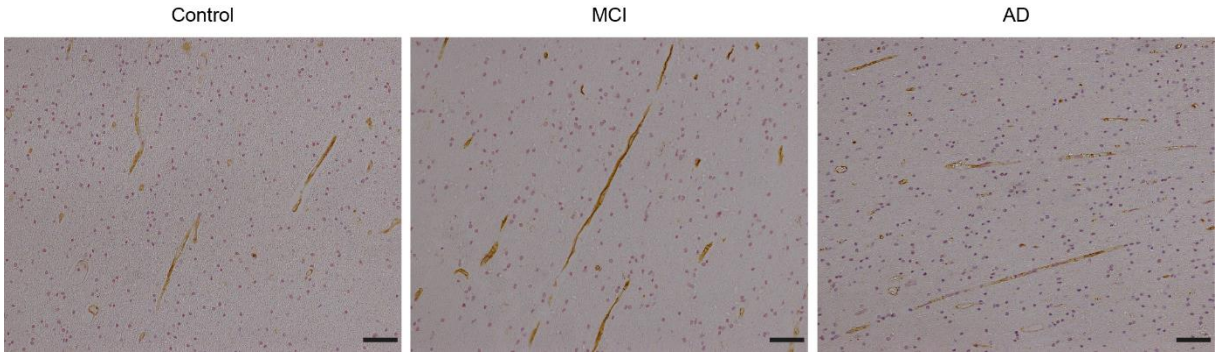

Figure 3.22: Claudin 5 Expression in the Temporal Cortex Claudin 5 expression in the human temporal cortex in non-neurological control, MCI and AD cases. The anti-claudin 5 mouse monoclonal antibody (1:50) was used for this experiment. Positive claudin 5 immunorecativity was exclusively associated with blood vessels in the temporal cortex of control, MCI and AD cases. Scale bar 50 µm.

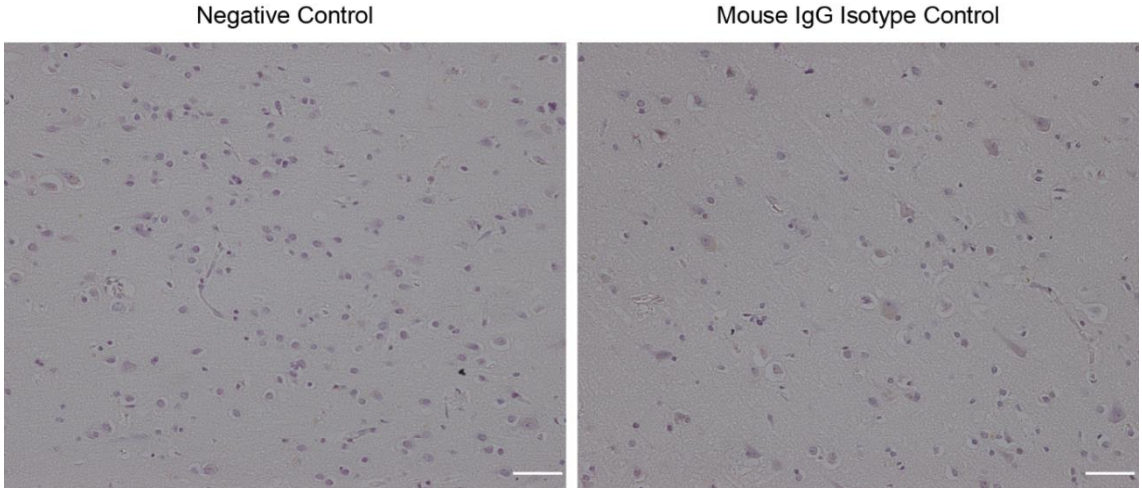

Figure 3.23: IHC Negative and Isotype Controls for Claudin 5 The claudin 5 IHC experiment used an anti-claudin 5 mouse monoclonal antibody. A negative and isotype control was conducted for this mouse antibody. The negative control consisted of the omision of the primary antibody. The isotype control was conducted with a mouse IgG antibody (Vector Laboratories) used at the same concentration as the primary antibody. Scale bar 50 µm.

3.2.5 Tight Junction Protein Expression in Neurons

The neuronal staining observed in the tissue cohort for occludin and ZO-1 was further explored *in vitro* using Lund human mesencephalic (LUHMES) cells. LUHMES are neuronal precursor cells which have been immortalised by transformation with a myc oncogene. These cells can be differentiated into post-mitotic neurons following the introduction of factors which inhibit the myc transgene (Lotharius et al., 2005; Schildknecht et al., 2009). LUHMES were cultured and provided by Irina Vasquez-Villasenor.

Immunocytochemistry experiments were conducted to investigate neuronal expression of occludin, claudin 5 and ZO-1 in differentiated LUHMES cells, Figure 3.24. The negative and isotype controls for this experiment are shown in Figure 3.25. Occludin was diffusely expressed in the cytoplasm of the neuronal cell body with distinct nuclear punctate staining. Claudin 5 and ZO-1 were diffusely expressed throughout the nucleus and cell body of the LUHMES. All three proteins also showed axonal staining. No staining is seen in either the omission of the primary antibody or the isotype control.

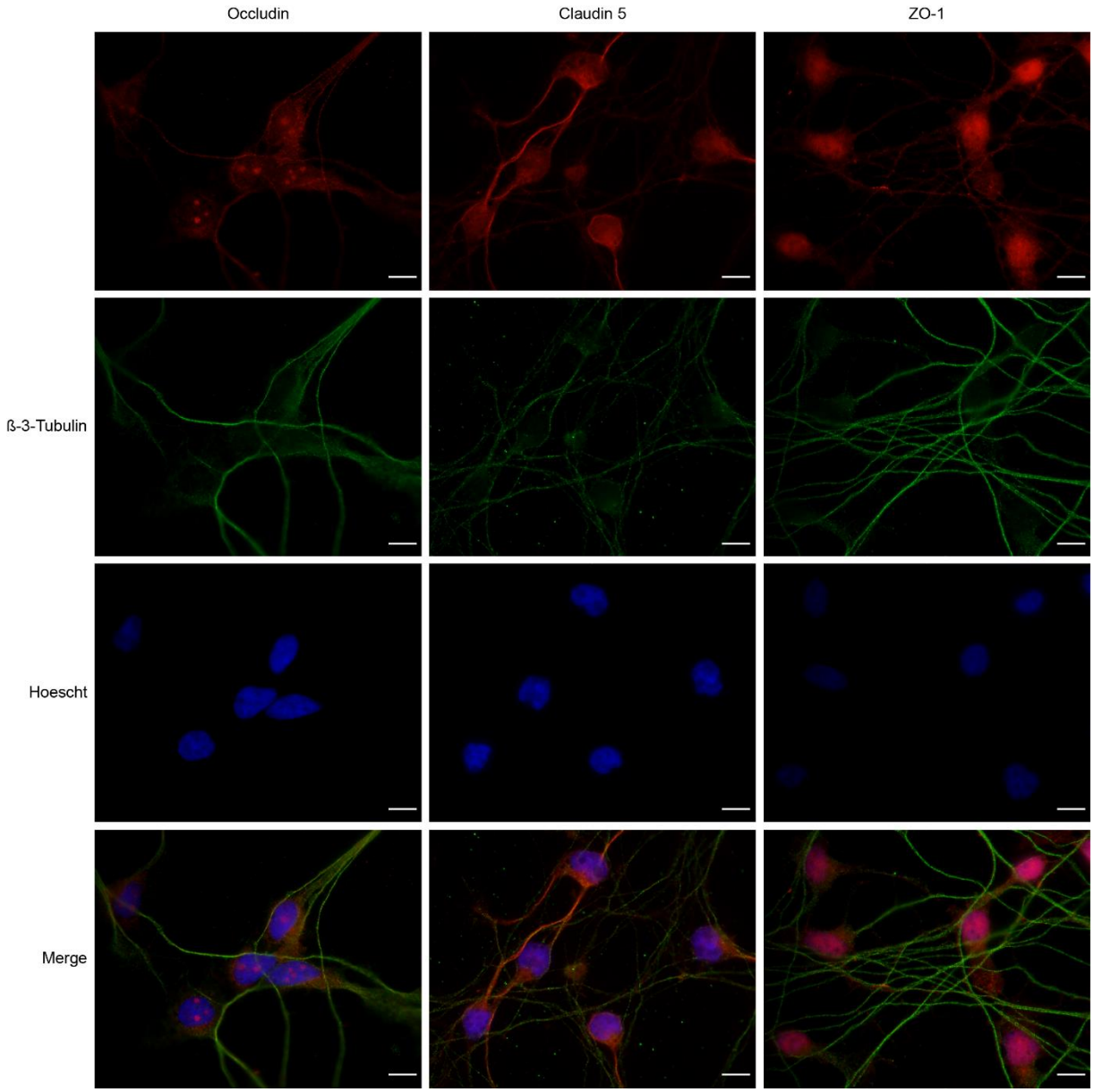

Figure 3.24: Immunocytochemistry characterising the expression of Occludin, Claudin 5 and ZO-1 in LUHMES Immunocytochemistry characterising the expression of occludin, claudin 5 and ZO-1 in LUHME cells. β-3-Tubulin was used as a cell marker. The antibodies and dilutions used in this experiment: anti- β-3-tubulin chicken polyclonal (1:1000), anti-occludin rabbit polyclonal antibody (1:50), anti-claudin 5 rabbit polyclonal antibody (1:50) and anti-ZO-1 rabbit polyclonal antibody (1:100). Scale bar 10 µm.

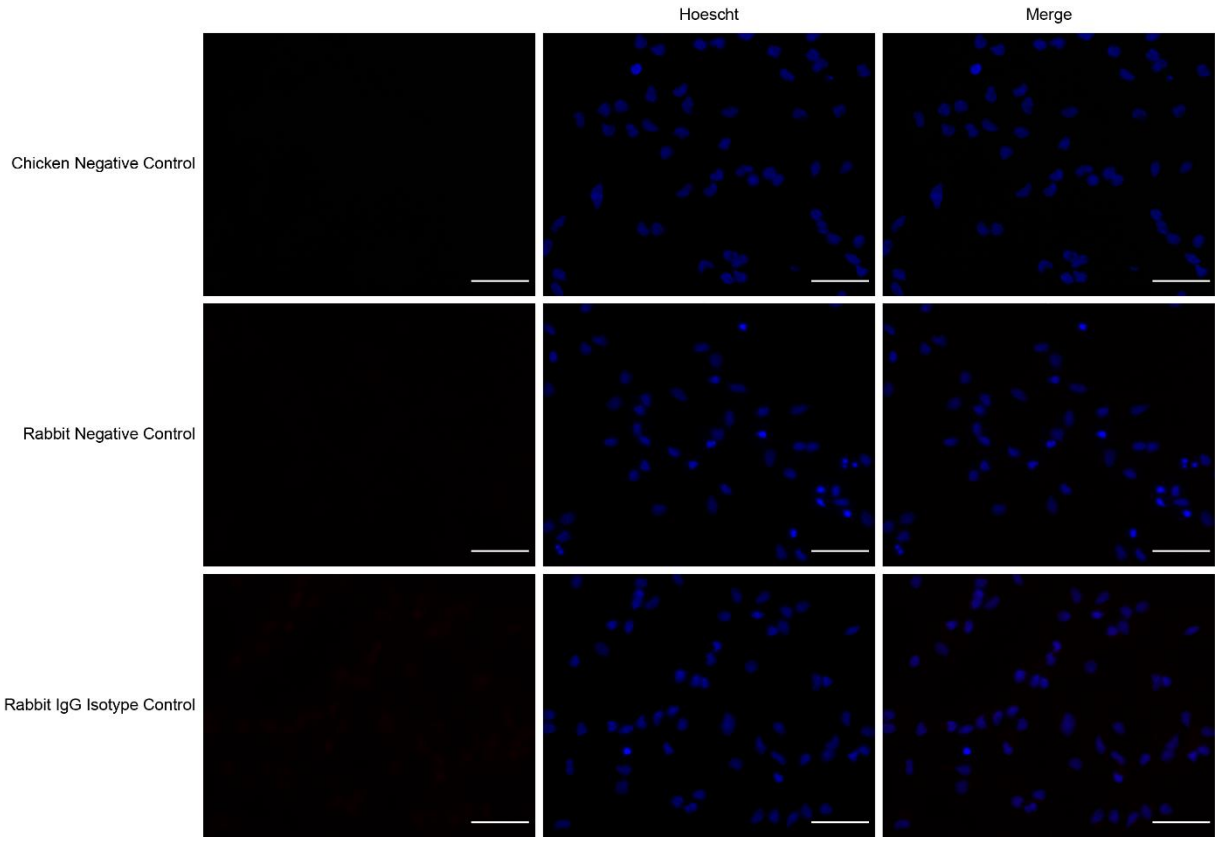

Figure 3.25: ICC Negative and Isotype controls for LUHMES Negative and isotype controls were conducted for rabbit antibodies and a neagtvie control was conducted for the chicken antibody. A chicken IgG isotype could not be conducted due to the inavailability of an chicken IgG antibody. The negative controls consisted of the omision of the primary antibody. The rabbit isotype control was conducted with a rabbit IgG antibody (Vector Laboratories) used at the same concentration as the primary antibody. Scale bar 50 µm.

3.3 Discussion

The initial aims of this study were to characterise the expression of occludin, claudin 5 and ZO-1 in human primary astrocytes and 1321N1 astrocytoma cells as well as to define the cellular localisation of these proteins in the temporal cortex and investigate whether the expression of these proteins is altered in MCI and AD cases compared with controls.

3.3.1 Astrocyte Culture Medium

The level of expression of both vimentin and nestin were the same in human primary astrocytes cultured in either ScienCell Astrocyte Medium MEMα/F-10 medium. The level of GFAP expressed by human primary astrocytes appears to fluctuate but overall there is statistically no significant difference in the expression of this protein between human primary astrocytes cultured in either ScienCell Astrocyte Medium or MEMα/F-10 medium.

The ICC for GFAP showed that only a small proportion of astrocytes in the population expressed this protein. Although GFAP is a commonly used astrocyte marker, not all human astrocytes are GFAP-positive (Sofroniew and Vinters, 2010). Currently there is no definitive marker capable of labelling all human astrocyte populations. GFAP is the major intermediate filament expressed in the adult human brain whilst vimentin is the major intermediate filament in the neonatal brain (Middeldorp and Hol, 2011). Studies vary regarding the age at which GFAP begins to be expressed in glia in the foetal brain and it appears that the expression of this protein also varies between brain areas (Middeldorp and Hol, 2011). The human primary astrocytes used in the current project are embryonic cells isolated from the cerebral cortex. This may account for the limited GFAP staining observed in these cells as, being embryonic, they may not have developed sufficiently for GFAP expression.

The expression of occludin in human primary astrocytes was affected by the culture medium as western blotting showed higher levels of this protein to be expressed in cells cultured in ScienCell Astrocyte Medium compared with MEMα/F-10 medium. ZO-1 expression does not appear to be affected by the cell culture medium. The difference in occludin expression may be attributable to the differences in media composition. ScienCell Astrocyte Medium contains 10 mM of L-glutamine whilst MEMα/F-10 medium only contains 1.5 mM. L-Glutamine is an amino acid which is essential for cell growth and has been identified, along with glucose, as an

important substrate for the progression of the cell proliferation cycle (Colombo et al., 2011). The amount of glucose is the same in both media but higher levels of glutamine may enhance the proliferation of astrocytes cultured in ScienCell Astrocyte Medium which in turn may have an effect upon the level of occludin expressed in these cells.

3.3.2 Occludin Expression in Astrocytes

The ICC and western blotting data demonstrate that occludin is expressed in both human primary astrocytes and in the 1321N1 astrocytoma cell line. The western blots would also suggest that occludin is phosphorylated in these cells. Occludin is a tight junction integral membrane which is predominantly associated with cell membrane in endothelial cells (Furuse et al., 1993; Kohaar et al., 2010). Neither human primary astrocytes nor 1321N1 astrocytoma cells, however, appeared to exhibit any membrane-associated occludin expression. Instead occludin presented with nuclear punctate staining in both human primary astrocytes and 1321N1 astrocytoma cells.

The astrocytic nuclear expression of occludin observed *in vitro* is supported by observations *in vivo* as occludin was seen to co-localise with GFAP-positive astrocytes in the temporal cortex. This project's *in vivo* findings confirm that the astrocytic occludin expression observed *in vitro* is not an artefact of cell culture and is a real physiological observation. Nuclear astrocytic occludin expression has been previously observed in a study investigating occludin expression in the frontal cortex and basal ganglia of control, VD and AD cases (Romanitan et al., 2007).

The mechanism by which occludin is able to translocate across the nuclear membrane is not known. The PSORTII program was used to analyse the occludin peptide sequence for possible nuclear localisation sequences, however, none were identified (Surapornsawasd et al., 2015). Similarly occludin is not known to express any nuclear export signals. The mechanism by which occludin is able to enter the nucleus therefore remains to be established. It is possible that occludin may be able to translocate between the cytoplasm and the nucleus by binding to proteins which themselves have NLS or NES signals.

Human primary astrocytes and 1321N1 astrocytoma cell occludin western blots also exhibited other bands. These bands may simply be due to nonspecific antibody binding, but some of them correspond to the molecular weights of known occludin isoforms. The datasheet for the anti-occludin rabbit polyclonal 71.1500 antibody

used for the ICC and western blotting experiments in this study does not disclose any information concerning occludin isoforms. The immunogen used to generate this antibody was a fusion protein containing the C-terminal membrane-distal domain of human occludin protein. Occludin isoform OCLN-ex3p-9pdel has completely lost the membrane-distal C-terminal domain (Kohaar et al., 2010), therefore the antibody used in this study will not detect this isoform. All other occludin isoforms express this domain, except for isoforms OCLN-ex7ext which lacks amino acids 476-522 causing the partial loss of the membrane distal C-terminal domain (Kohaar et al., 2010). The ability of this antibody to detect this occludin isoform is, therefore, uncertain.

The ICC images show cytoplasmic occludin localisation. There are also strong bands around 50 kDa in the cytoplasm and not in the nucleus in the fractionation blot. These bands could be attributable to occludin isoforms OCLN-ex4del or OCLN-ex7ext which are 52 and 54 kDa are respectively. In the case of OCLN-ex4del, amino acids 244-297 are missing resulting in the loss of the fourth transmembrane domain (Kohaar et al., 2010). The cellular localisation of occludin isoforms in transfected HeLa cells shows that OCLN-ex7ext predominantly localises at the cell membrane, whilst isoforms lacking either part or the entirety of the MARVEL domain tend to be localised in the cytoplasm (Kohaar et al., 2010). The astrocytic expression of OCLN-ex4del, therefore, appears more likely as the ICC does not show any membrane-associated occludin localisation in astrocytes. The localisation of occludin to both the cytoplasm and nucleus but not the cell membrane is perhaps indicative of a complete or partial loss of the MARVEL domain in astrocytic occludin.

Similar to human primary astrocytes, a band of around 50 kDa is also present in the 1321N1 astrocytoma cell line. This band is also present within the HUVEC positive control and may suggest the presence of either OCLN-ex4del or OCLN-ex7ext.

A 40 kDa band was also observed in the human primary astrocyte whole cell lysate blot as well as in the cytoplasmic and nuclear fractions of the fractionation blot. Occludin isoform OCLN-ex3del is 31 kDa and lacks amino acids 1-251 resulting in the complete loss of the MARVEL domain. It is possible that this isoform may be expressed in astrocytes. It is, however, possible that astrocytes express unique isoforms which have not yet been characterised.

3.3.3 Claudin 5 Expression in Astrocytes

The current project concludes that claudin 5 is not expressed in either human primary astrocytes of 1321N1 astrocytoma cells. The ICC suggests that claudin 5 is diffusely expressed throughout the cytoplasm and nucleus in both human primary astrocytes and the 1321N1 astrocytoma cells, however, the western blots do not corroborate this expression and would suggest that the ICC staining is non-specific. Although there are higher molecular weight bands present in some of the claudin 5 western blots which may be accounted for by post-translational modifications and the possible dimerisation of this protein, the current evidence would suggest that claudin 5 is not expressed in these cells.

This conclusion is supported by the current *in vivo* study and previous research in which claudin 5 expression is exclusively associated with endothelial cells (Simpson et al., 2010). Another study, however, contradicts this conclusion as claudin 5 has been shown to be expressed in both astrocytes and neurons in the frontal cortex of both AD and VD cases as well as non-neurological controls (Romanitan et al., 2010). This study found no significant increase in the ratio of astrocytes expressing claudin 5 between AD and VD cases compared with non-neurological controls (Romanitan et al., 2010). The study did not conduct any dual-labelling immunohistochemistry and the criteria by which astrocytic occludin-positive nuclei were distinguished from other cells in human tissue was not disclosed; consequently it is not certain if claudin 5 expression co-localises with astrocytes in this study (Romanitan et al., 2010).

3.3.4 ZO-1 Expression in Astrocytes

The ICC and western blotting data confirm that ZO-1 is expressed in both human primary astrocytes and 1321N1 astrocytoma cells. The diffuse nuclear staining of ZO-1 exhibited by these cells is similar to the staining pattern seen in MDCK cells for this protein (González-Mariscal et al., 1999). The nuclear expression of ZO-1 is confirmed by the *in vivo* study. The astrocytic expression of ZO-1 *in vivo* has been previously confirmed by dual-labelling immunohistochemistry which shows the co-localisation of ZO-1 with GFAP-positive astrocytes in human post-mortem tissue (Simpson et al., 2011).

A small population of human primary astrocytes cultured in ScienCell Astrocyte Medium also exhibited cytoplasmic ZO-1 aggregates which were localised close to the cell membrane. ZO-1 co-localises with connexin 43 aggregates in murine

cortical astrocytes which are structurally similar to the ZO-1 aggregates observed in the current study (Duffy et al., 2004). ZO-1 also co-localises with connexin 30 and connexin 43 in murine astrocytes in vivo (Penes et al., 2005). It is possible that ZO-1 similarly localises with gap junction protein in human primary astrocytes.

3.3.5 Tight Junction Protein expression in Neurons

The current study shows occludin and ZO-1 to be expressed in the cytoplasm and nucleus of pyramidal neurons *in vivo*. Occludin has previously been shown to be expressed in pyramidal neurons in human post-mortem tissue (Romanitan et al., 2007). ZO-1 is also expressed in neurons in mouse brain and co-localises with connexin 36 in these cells (Li et al., 2004).

The identification of occludin and ZO-1 expression in human pyramidal neurons *in vivo* was further explored *in vitro* using LUHME cells. Occludin exhibited the same punctate nuclear staining in these cells as that previously seen in astrocytes for this protein. Occludin was also expressed diffusely throughout the cytoplasm and also appeared to be expressed in the neuronal axons of LUHME cells.

ZO-1 exhibited a strong diffuse cytoplasmic and nuclear staining throughout LUHME cells. ZO-1 also appeared to be expressed in the neuronal axons. ZO-1 has previously been shown to be expressed in the dendrites of murine hippocampal neurons *in vitro* (Inagaki et al., 2003). This protein has also been shown to be diffusely expressed throughout the cell body, axon and dendrites of rat hippocampal neurons *in vitro* (Komaki et al., 2013).

The neuronal expression of claudin 5 remains uncertain. The *in vivo* study shows that claudin 5 expression is exclusively associated with endothelial cells, however, this observation is contradicted by previous research in which claudin 5 is shown to be expressed in both pyramidal neurons and astrocytes in the frontal cortex (Romanitan et al., 2010).

In vitro, claudin 5 appears to be expressed throughout the cytoplasm, nucleus and axons of LUHME cells. The reliability of this staining is, however, uncertain as the LUHMES ICC experiment was conducted using the same anti-claudin 5 rabbit polyclonal antibody (ab15106) which was previously used in the ICC experiments characterising the expression of claudin 5 in human primary astrocyte and 1321N1 astrocytoma cells. The staining produced by this antibody in both human primary astrocyte and 1321N1 astrocytoma cells was not supported by the western blots,

consequently it was concluded that the staining produced by the anti-claudin 5 rabbit polyclonal antibody (ab15106) was non-specific. The claudin 5 staining exhibited in the LUHME cells may, therefore, also be a result of non-specific antibody binding. Future research into the neuronal expression of tight junction proteins should include western blotting experiments. Given the current evidence, however, it must be concluded that the neuronal expression of claudin 5 remains unknown.

3.3.6 Tight Junction Protein Expression and Alzheimer's Disease

Another of this study's aims was to investigate whether there were any changes in tight junction protein expression in MCI and AD cases compared with controls. Previous research has shown that there is a significant increase in the ratio of neurons which express occludin in the frontal cortex and basal ganglia in AD and VD cases compared with controls (Romanitan et al., 2007). A qualitative analysis also concluded that there are more occludin positive astrocytes in AD and VD cases compared with non-neurological controls (Romanitan et al., 2007). The same cohort was also used to investigate the expression of claudin 2, claudin 5 and claudin 11 in the frontal cortex (Romanitan et al., 2010). This study found that there was a significant increase in the ratio of pyramidal neurons expressing all three claudins in AD and VD cases compared with controls whilst there was a significant increase in the ratio of astrocytes expressing claudin 2 and claudin 11, but not claudin 5, in AD and VD cases compared with controls (Romanitan et al., 2010).

Both of these studies suggest that the pathogenesis of two neurological diseases may be associated with an increase in tight junction protein expression in astrocytes and neurons. Neither of these studies, however, conducted any dual-labelling immunohistochemistry and the criteria by which astrocytic nuclei were distinguished from other cells in human tissue was not disclosed. The size of the cohort used in these studies was also very small.

The cohort used in the current project was larger than the ones used in previous research and it was hoped that a greater understating of tight junction protein expression in relation to AD pathogenesis might be obtained. The poor and often faint quality of the IHC staining obtained in this project meant, however, that the staining was too difficult to quantify and consequently this research objective could not be fulfilled.

In summary, the current study has shown the cytoplasmic and nuclear expression of occludin and ZO-1 in human primary astrocytes and 1321N1 astrocytoma cells. The astrocytic and nuclear expression of occludin is further supported by an *in vivo* study involving human post-mortem tissue. The *in vivo* study also shows occludin and ZO-1 to be expressed in pyramidal neurons, an observation which is corroborated by the expression of these two proteins in cultured human neurons. There is considerable contradictory evidence, both *in vitro* and *in vivo*, concerning the astrocytic and neuronal expression of claudin 5 however this study concludes that claudin 5 is not expressed in human astrocytes.

The nuclear expression of occludin was particularly interesting and function of this protein in astrocytes was the focus of further investigation. The subsequent aim of this project was to elucidate the function(s) of this protein in astrocytes through the identification of protein binding partners.

4. Recombinant Proteins & Pull-Down Assay Development

4.1 Introduction

In vitro characterisation of TJP expression demonstrated both cytoplasmic and nuclear expression of occludin and ZO-1 in human primary astrocytes and 1321N1 astrocytoma cells. The function(s) of these proteins in astrocytes, however, remains undetermined. The absence of membrane association suggests that these proteins do not form tight junction complexes in astrocytes. It is known that ZO proteins do not function solely as scaffolding proteins but localise to the nucleus and interact with many different nuclear proteins including transcription factors in MDCK cells (Betanzos et al., 2004; Huerta et al., 2007). The nuclear localisation of occludin indicates that this protein may have functional capabilities beyond the tight junction complex. The potential involvement of occludin in nuclear processes such as transcription is supported by the ELL homology in the membrane-distal domain of occludin's C-terminus (Li et al., 2005b).

Having demonstrated the astrocytic and nuclear expression of occludin *in vitro* and *in vivo*, the current study aimed to elucidate possible functions of occludin in astrocytes by identifying binding partners for this protein. Previous research has used either antibodies or tagged-proteins to develop co-immunoprecipitation or binding assays to identify binding partners for TJPs. Cx30 and Cx43 were found to co-immunoprecipitate with ZO-1 from homogenised mouse brain tissue in experiments utilising a ZO-1 antibody and protein A-coated agarose beads (Penes et al., 2005). Epsin-1, Esp15 and Hrs were found to co-immunoprecipitate with occludin from BREC lysates using an occludin antibody and protein G-sepharose beads (Murakami et al., 2009).

The region within the C-terminal domain of occludin which binds to ZO-1 was identified though a pull-down binding assay involving GST fusion proteins of wild type and mutant human occludin (aa371-522) (Li et al., 2005b). The interaction between occludin and dynamin was also established by co-transfecting FLAG-tagged occludin domains with GFP-tagged dynamin into 293T cells, a human kidney epithelial cell line. Immunoprecipitation experiments involving anti-FLAG M2 affinity resin demonstrated that some of the FLAG-occludin proteins precipitate GFP-dynamin. (Liu et al., 2010).

In the experiments outlined in Chapter 2, co-immunoprecipitation was trialled to identify novel binding partners of occludin in astrocytes. These experiments utilised two commercially available anti-occludin antibodies but neither were able to reliably

immunoprecipitate occludin from either human primary astrocyte or 1321N1 astrocytoma cell lysates. Consequently this line of investigation was terminated. The subsequent approach was to develop a pull-down protein binding assay using GB1-6His-tagged recombinant occludin proteins and IgG beads. GB1 is derived from protein G and binds with a high affinity to IgG. This allows for stringent washing during the pull-down protein binding assay experiment thus reducing the likelihood of non-specific protein binding. The presence of six histidines (6His) within this tag allows for the efficient purification of the tagged recombinant proteins.

Initially an IMAGE clone of the occludin cDNA sequence was purchased and primers were designed to PCR amplify full length occludin (OCLN 1-522) as well as the cytoplasmic N-terminal (OCLN 1-65) and C-terminal (OCLN 271-522) domains using a pET24b-GB1-6His plasmid and the DH5α *E. coli* strain. GB1-6His-tagged recombinant proteins for occludin aa1-522 (GB1-OCLN), occludin N-terminal domain aa1-65 (GB1-OCLN_N) and occludin C-terminal domain aa271-522 (GB1-OCLN_C) were subsequently generated by the BL21-RP *E. coli* strain. These proteins were then extracted and purified for use in the development of a pull-down protein binding assay in which any proteins which bound to the occludin constructs were eluted, subjected to SDS-polyacrylamide gel electrophoresis and identified by mass spectrometry analysis. This chapter highlights the detailed strategic approach through which the recombinant proteins were generated and outlines the optimisation of the pull-down protein binding assay protocol.

4.2 Results

4.2.1 Molecular Cloning of Occludin constructs

Figure 4.1 shows the successful PCR amplification of full length occludin (OCLN 1-522), N-terminal (OCLN 1-65) and C-terminal (OCLN 271-522) domain sequences. OCLN 1-65 is 195 bp, OCLN 1-522 is 1566 bp and OCLN 271-522 is 753 bp. The N-terminal band appears less intense because it is masked by the dye front produced by the 6x Laemmli buffer. These bands were excised and purified as described in 2.9.7.

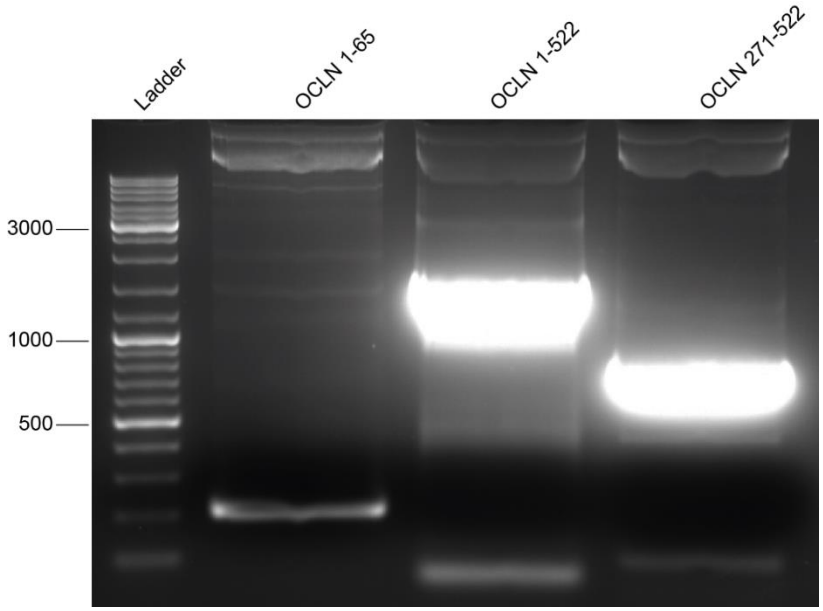

Figure 4.1: PCR for OCLN 1-65, OCLN 1-522 and OCLN 271-522 This agarose gel shows the successful amplification of the DNA sequences for the occludin N-terminal domain (OCLN 1-65), occludin full length (OCLN 1-522) and occludin C-terminal domain (OCLN 271-522). OCLN 1-65 is 195 bp, OCLN 1-522 is 1566 bp and OCLN 271-522 is 753 bp. Ladder markers in bp.

The three occludin DNA sequences were digested using *Nde*I and *Xho*I enzymes and ligated into the pET24b-GB1-6His vector followed by transformation into the DH5α *E. coli* strain. Transformants were inoculated and analysed through a spin miniprep and restriction digest to establish the presence of the correct insert. Figure 4.2 shows the restriction digestion of three OCLN 1-65 transformants. A 195 bp DNA band was present in all three transformants confirming the presence of the OCLN 1-65 insert. Each lane also contained a larger 5.5 kbp DNA band produced by the pET24b-GB1-6His plasmid. The DNA sequences of all three inserts were verified by Sanger sequencing prior to recombinant protein expression in the BL21-RP *E. coli* strain. The Sanger sequencing was conducted by Source Bioscience.

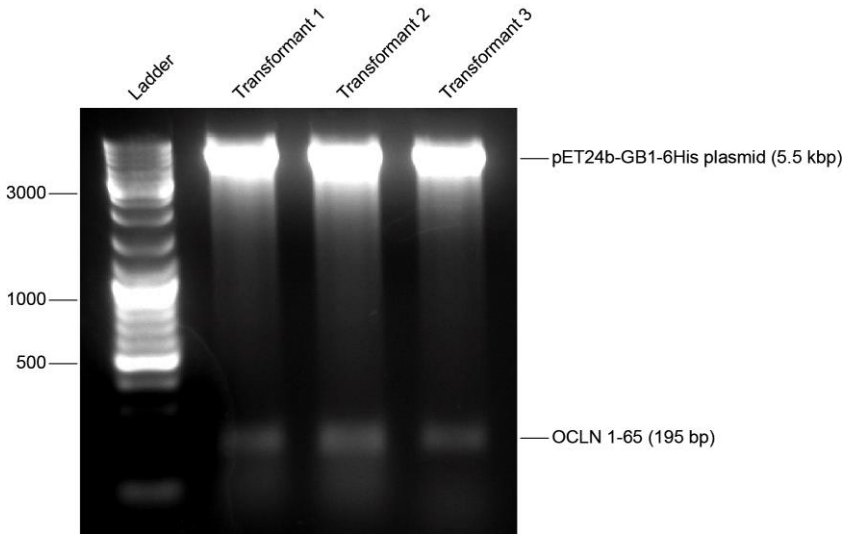

Figure 4.2: *Nde*I/*Xho*I restriction digest of bacterial transformants This agarose gel shows the restriction digest of three DH5α colonies after bacterial transformation with pET24b-GB1-6His-OCLN 1-65 using by *Nde*I/*Xho*I restriction enzymes. All three colonies have the correct insert for OCLN 1-65 with a band of 195 bp. The 5.5 kbp DNA band is the pET24b-GB1-6His vector. Ladder markers in bp.

4.2.2 Recombinant Protein Expression

The plasmids containing OCLN 1-65, OCLN 1-522 and OCLN 271-522 DNA sequences were transformed into the BL21-RP *E. coli* strain. This bacterial strain was used to express full length occludin (GB1-OCLN) occludin N-terminal domain (GB1-OCLN_N) and occludin C-terminal domain (GB1-OCLN_C) recombinant proteins. These proteins were purified from the bacteria and analysed by SDS-polyacrylamide gel electrophoresis.

GB1-OCLN_N and GB1-OCLN_C recombinant proteins were successfully purified from the bacteria, Figure 4.3 panel A. Occludin's N-terminal domain is 7.57 kDa and occludin's C-terminal domain is 29.39 kDa whilst the GB1-6His tag has a molecular weight of 10 kDa, consequently GB1-OCLN_N should produce a 17 kDa protein band whilst GB1-OCLN_C should produce a protein band around 40 kDa. Panel A shows that the GB1-OCLN_C recombinant protein produced a single protein band of around 45 kDa. The GB1-OCLN_N recombinant protein produced several protein bands the highest band of which is the correct molecular weight for GB1-OCLN_N (17 kDa) the lower protein bands are probably due to protein degradation.

Figure 4.3 panel B shows the purification of GB1-OCLN. It was anticipated that difficulties would be encountered in the purification of GB1-OCLN due to the size

and hydrophobicity of the occludin protein. Consequently, a sample of the bacterial pellet was also analysed in this experiment. The purified GB1-OCLN recombinant protein should weigh approximately 69 kDa. There were faint bands around this height in the purified sample. A strong band of this molecular weight was also present within the bacterial pellet which suggests that most of the GB1-OCLN recombinant protein is insoluble. The inclusion of a bacterial pellet from uninduced cells in this experiment, however, would have given a clearer indication of bacterial protein expression.

There were also many other bands present within the purified GB1-OCLN lane indicating that this protein is not stably expressed by the bacteria. These bands may be the product of protein degradation or could be the product of abortive translation as occludin is a large protein for *E. coli* expression.

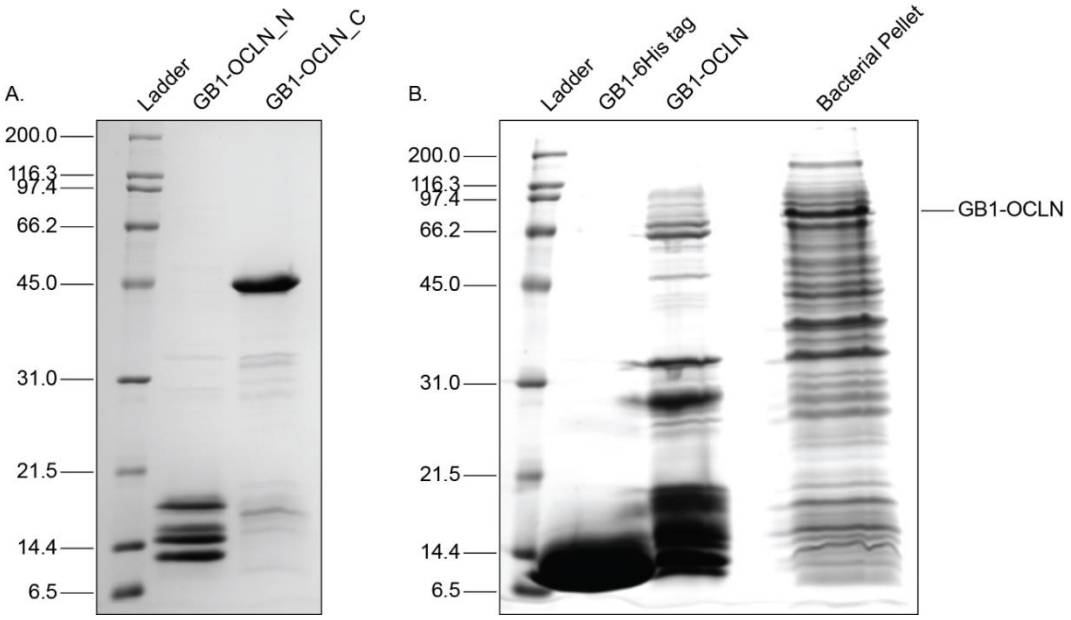

Figure 4.3: Purified recombinant proteins A) Purified GB1-OCLN_N and GB1-OCLN_C recombinant proteins which were expressed by BL21-RP *E. coli*. B) Purification of GB1-OCLN. This recombinant protein was insoluble and remained in the bacterial pellet. Molecular weight markers are indicated (kDa).

Western blots utilising antibodies with epitopes located in either the N- or C-terminal domain of occludin were also used to confirm the size and successful expression of GB1-OCLN_ N and GB1-OCLN_C recombinant proteins. A protein sample of GB1-OCLN_N was used to produce western blot which was probed with the anti-occludin rabbit monoclonal antibody (ab167161) Figure 4.4 panel A. The epitope for this antibody is located in in the N-terminal domain of occludin. A protein sample of GB1-OCLN_C was similarly used to produce western blot which was probed with

the anti-occludin rabbit polyclonal antibody (71.1500) Figure 4.4 panel B. The epitope for this antibody is located in the C-terminal domain of occludin.

The GB1-OCLN_N recombinant protein was recognised by its specific antibody and produced a protein band just above 15 kDa. There were also two lower molecular weight bands which are possibly due to protein degradation. Faint bands around 30 kDa were also visible. The GB1-OCLN_C recombinant protein was also recognised by its specific antibody and produced a protein band of approximately 45 kDa which corresponds with the size of the protein seen in Figure 4.3 panel A. Lower molecular weight bands were also present and are likely to be the result of protein degradation.

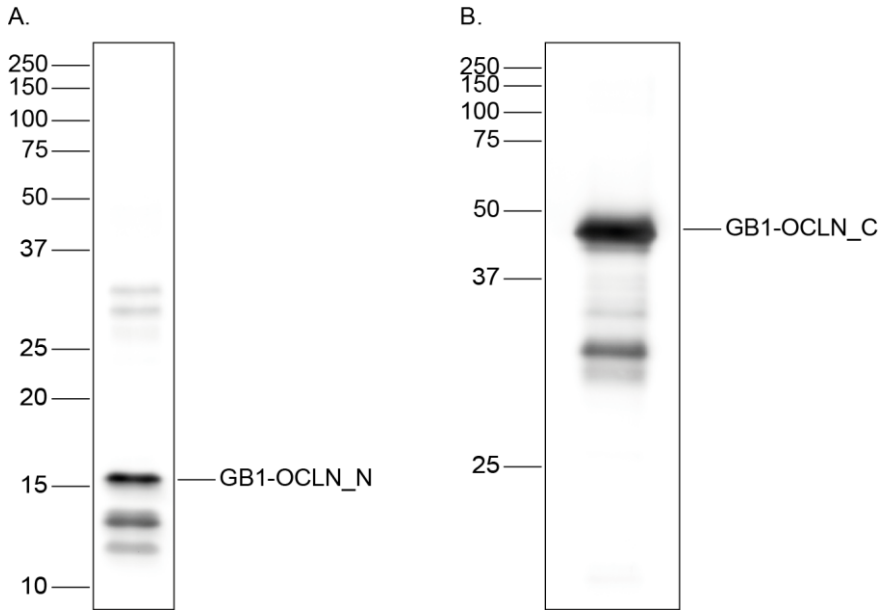

Figure 4.4: Western blots of GB1-OCLN_N and GB1-OCLN_C A) Western blot of GB1-OCLN_N probed with anti-occludin rabbit monoclonal antibody (ab167161). B) Western blot of GB1-OCLN_C probed with anti-occludin rabbit polyclonal antibody (71-1500). Molecular weight markers are indicated (kDa).

4.2.3 GB1-OCLN localisation in BL21-RP Bacteria

The difficulties encountered in purifying the GB1-OCLN recombinant protein suggest that this protein may be trapped in inclusion bodies in the bacteria. Inclusion bodies are dense insoluble protein aggregates located typically within the bacterial cytoplasm which are generated during high levels of heterologous protein expression (Singh and Panda, 2005). The aggregates are generated by the oligomerisation of partially folded or misfolded proteins although proteins containing disulphide bonds are particularly susceptible to aggregation because the reducing environment of the bacterial cytosol disrupts the formation of these bonds (Langley

et al., 1987; Singh and Panda, 2005). Protein hydrophobicity is another factor which contributes to inclusion body formation with highly hydrophobic proteins being more susceptible to aggregation (Singh and Panda, 2005). The hydrophobicity of occludin due to the MARVEL domain and the presence of a conserved disulphide bridge within ECL2 suggests that the GB1-OCLN protein may be vulnerable to aggregation and entrapment within inclusion bodies. It could also be hypothesised that, due to the hydrophobicity of occludin, the GB1-OCLN recombinant protein may localise to the bacterial cell envelope. An exploratory ICC experiment was trialled to investigate the localisation of the GB1-OCLN recombinant protein in these cells.

The method for this experiment is outlined in 2.10. Figure 4.5 shows a panel of ICC images for GB1-OCLN expression in BL21-RP *E. coli.* The rod-shaped appearance of the bacterial cells was clearly defined and a faint punctate staining extending out from the bacterial envelope reminiscent of bacterial flagella was also observed, Figure 4.6 panel C and D. The method used to stain bacteria was adapted from a previous study and the images shown in Figure 4.4 suggest that this method is successful (Jose et al., 2005). This experiment has limitations, however, as negative and isotype controls were not included. Any future experiments should include these controls to confirm that the bacterial staining is specific. Although these images suggest that GB1-OCLN protein is expressed in these cells, the localisation of this protein cannot be determined as the microscope used was insufficiently powerful to define either the bacterial cell envelope or identify inclusion bodies. Further exploration of GB1-OCLN bacterial protein expression should utilise a confocal microscope.

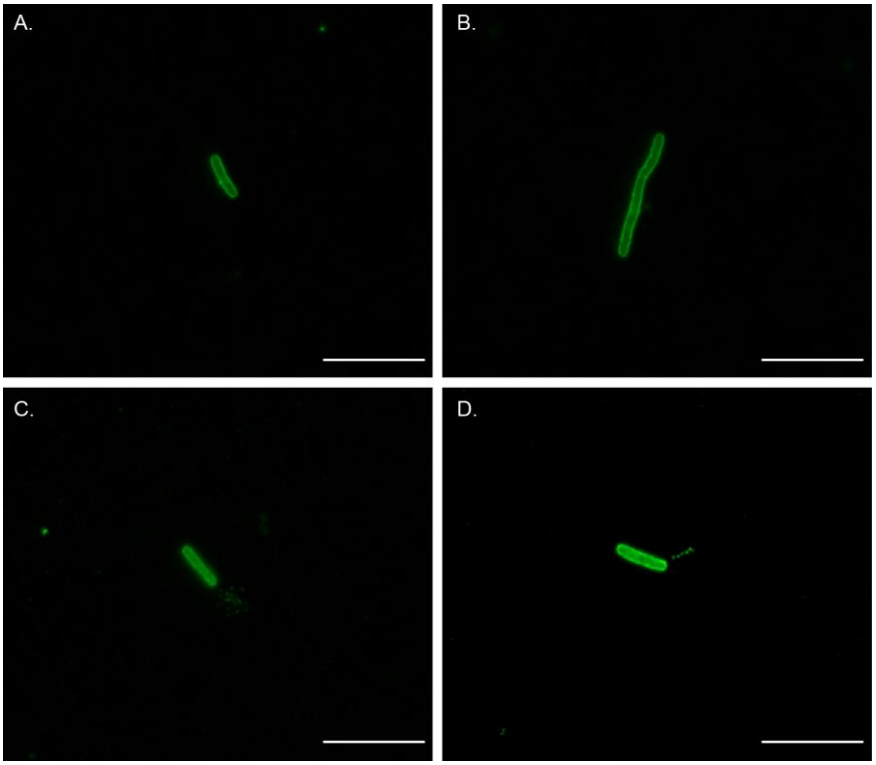

Figure 4.5: Immunocytochemistry of BL21-RP E.coli expressing GB1-OCLN
Panels A and B show possible localisation of GB1-OCLN protein in the bacterial envelope of BL21-RP *E. coli*. Panels C and D show punctate staining extending out from the bacterial envelope possibly indicating localisation of the GB1-OCLN protein with bacterial flagella. Scale bar 10 µm

4.2.4 Pull-down Assay Development

The successful purification of GB1-OCLN_N and GB1-OCLN_C recombinant proteins enabled the development of a pull-down protein binding assay to identify occludin protein binding partners in astrocytes. Every pull-down protein binding assay was conducted using 1321N1 astrocytoma cell lysates.

4.2.4.1. The effect of the presence or absence of EDTA or $CaCl_2$

The aim of this experiment was to determine whether protein binding to either GB1-OCLN_N or GB1-OCLN_C was affected in the presence or absence of EDTA or $CaCl_2$. Prior to 1321N1 lysis, either 1 mM EDTA or 1 mM $CaCl_2$ was added to the lysis buffer. The samples were analysed by SDS-polyacrylamide gel electrophoresis and the gel was initially stained with Instant*Blue* coomassie, Figure 4.6 A, followed by a silver stain, Figure 4.6 B.

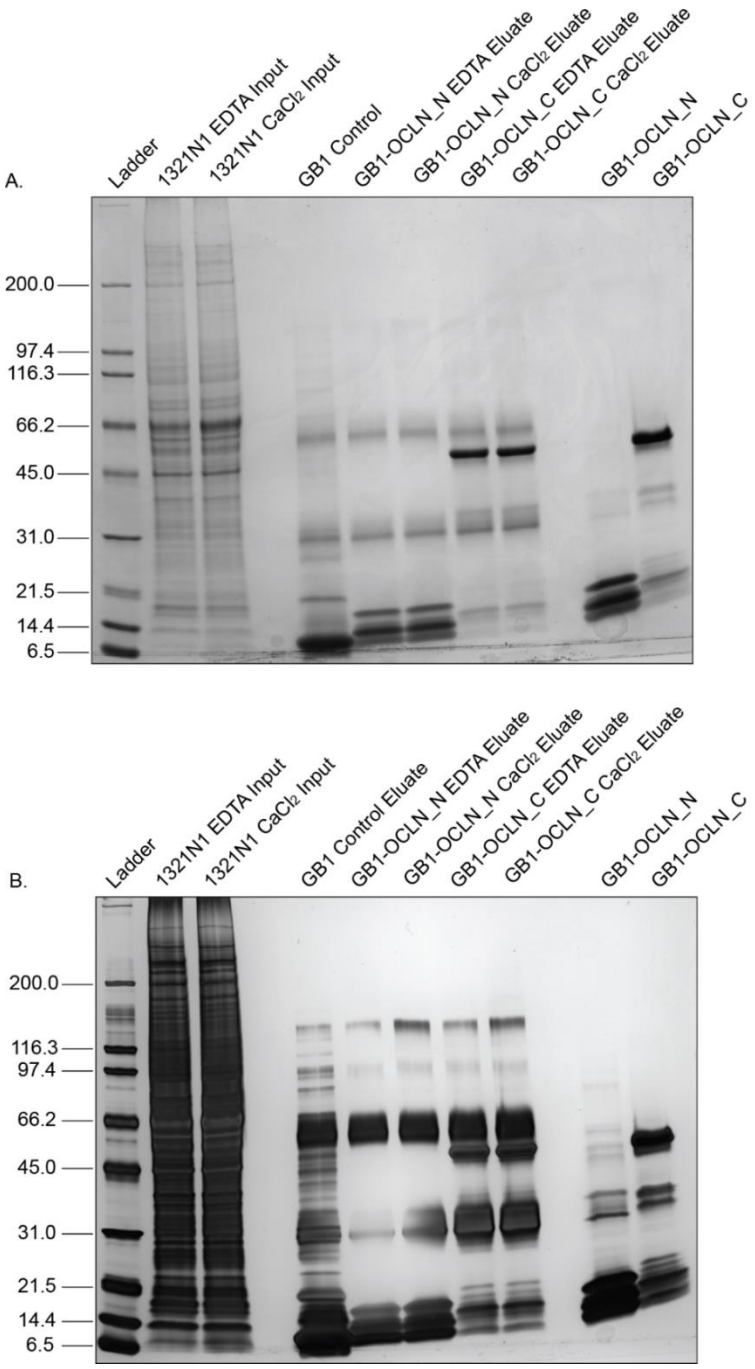

Figure 4.6: Pull-down assay using GB1-OCLN_N and GB1-OCLN_C in the presence or absence of EDTA or $CaCl_2$ This figure shows a pull-down assay gel in which either EDTA or $CaCl_2$ was added to the lysis buffer to determine the effect on the eluted proteins. The gel was initially stained with Instant*Blue* coomassie (A) and then a silver stain (B). This experiment was condicted using a 12% resolving gel with a 4% stacking gel. Molecular weight markers are indicated (kDa).

Figure 4.6 panel B shows that higher molecular weight protein bands located between the 66.2 and 116.6 kDa ladder markers were detected with the silver stain which were absent in the coomassie stained gel. The silver stain also detected more protein bands between the 14.4 and 21.5 kDa ladder markers compared with

the Instant*Blue* coomassie. This is due to the fact that the silver stain is a more sensitive method for protein detection. There were, however, no bands specific to either GB1-OCLN_N or GB1-OCLN_C compared with the GB1 control. This may suggest that the proteins observed in this experiment are not binding to occludin but are instead binding to the GB1-6His tag.

A comparison between the EDTA and $CaCl_2$ samples does not appear to show any differences when stained with Instant*Blue* coomassie, Figure 4.6 panel A. The 116 kDa band detected by the silver stain in panel B is more intense in $CaCl_2$ treated lysates for both GB1-OCLN_N and GB1-OCLN_C, which may suggest that calcium enhances protein binding to occludin. This band is, however, also present in the GB1 control, consequently another interpretation is that the 116 kDa protein binds to GB1 and that this interaction is enhanced in the presence of calcium. These experiments did not include a $CaCl_2$-treated GB1 control. In the absence of this control, it is not possible to determine whether calcium enhances protein binding specifically to occludin or non-specifically to the GB1 tag. Consequently, the effect of $CaCl_2$ on occludin protein binding remains ambiguous.

4.2.4.2. Buffer Composition Optimisation

Buffer compositions were trialled during the development of this assay to determine the optimal conditions for protein identification and detection. Figure 4.7 shows a silver stained gel produced from a pull down assay using different buffer compositions. 1321N1 astrocytoma cells were treated with 5 mM $CaCl_2$ and 4 µM A23187 prior to lysis.

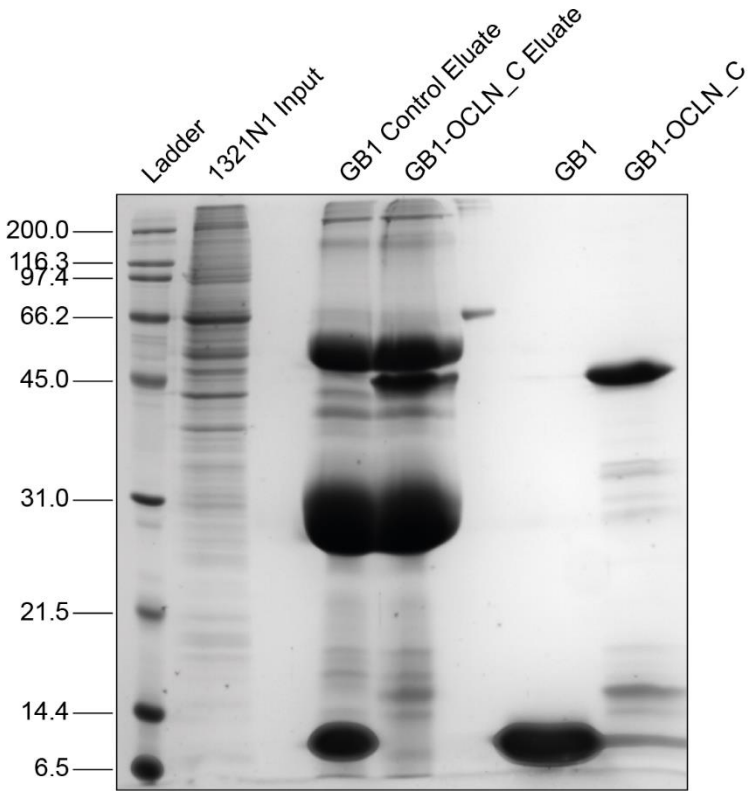

Figure 4.7: GB1-OCLN_C Pull-down assay This figure shows a silver stained gel produced from a pull-down assay utilising a different wash buffer and lysis buffer composition. The 1321N1 cells used in this experiment were treated with 5 mM $CaCl_2$ and 4 µM A23187 prior to lysis. This experiment was conducted using a 12% resolving gel with a 4% stacking gel. Molecular weight markers are indicated (kDa).

4.2.4.3. Mass Spectrometry Analysis – Gels

Figure 4.8 shows the two gels which were submitted for mass spectrometry analysis. Panel A shows the pull-down binding assay conducted using GB1-OCLN_C whilst panel B was conducted using GB1-OCLN_N. Both assays were run with a GB1-6His control which was also subjected to mass spectrometry analysis. The silver stain is not compatible with mass spectrometry analysis, consequently, although this stain was used during pull-down protein binding assay optimisation, the gels sent for mass spectrometry analysis were stained with Instant*Blue* coomassie.

Although there are no clear differences between either of the occludin-tagged eluates and the GB1-6His control, subtle difference beyond the detection of the Instant*Blue* coomassie may be present, consequently these gels were taken forward for exploratory mass spectrometry analysis to identify candidate occludin binding partners.

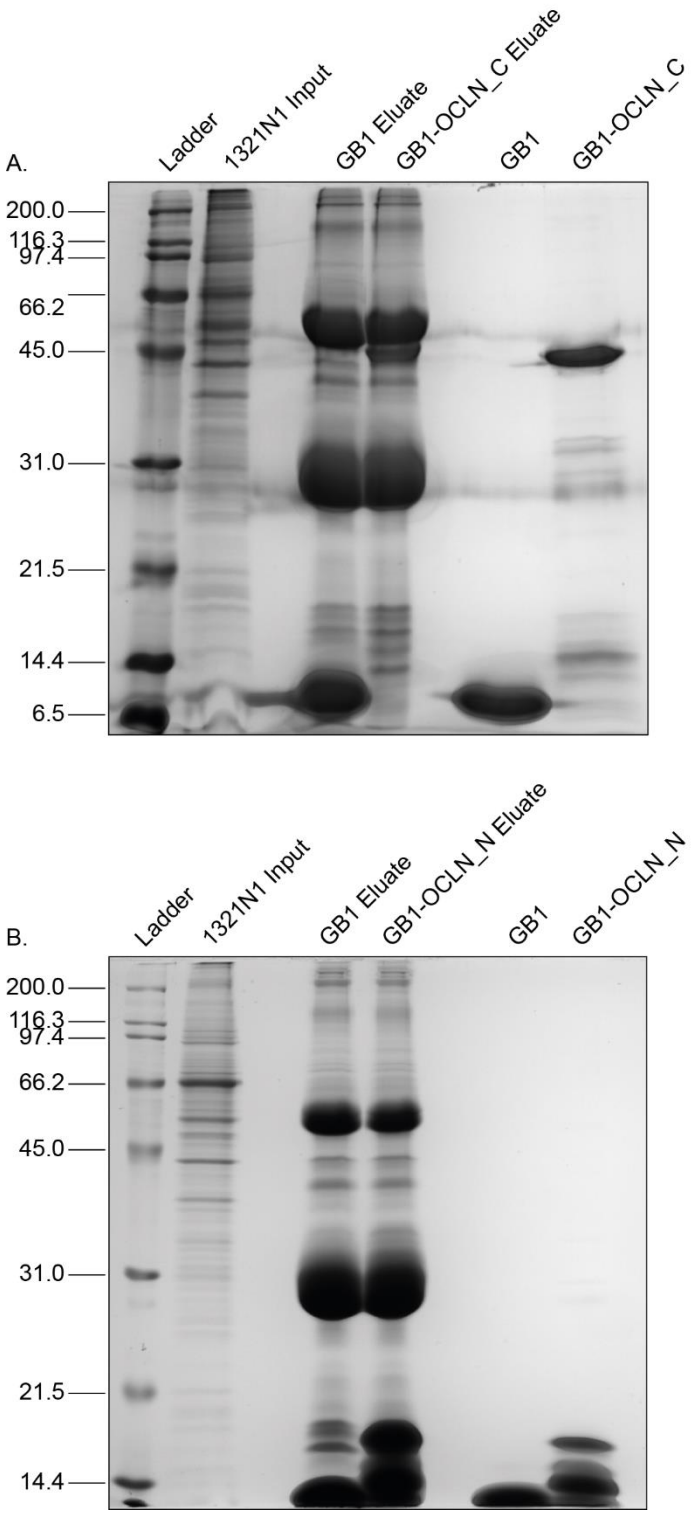

Figure 4.8: GB1-OCLN_C and GB1-OCLN_N pull-down protein binding assay gels sent for Mass Spectrometry Analysis A) GB1-OCLN_C pull-down protein binding assay gel. B) GB1-OCLN_N pull-down protein binding assay gel. Both gels were stained with Instant*Blue* coomassie. These experiments were conducted using a 12% resolving gels with a 4% stacking gel. Molecular weight markers are indicated (kDa).

4.3 Discussion

The data presented in this chapter outlines the detailed, strategic approach used to generate GB1-6His tagged recombinant occludin proteins and develop a pull-down protein binding assay designed to find putative occludin binding partners in astrocytes. The pull-down protein binding assays were conducted using 1321N1 astrocytoma cell lysates instead of human primary astrocytes due to time constraints and financial implications associated with difficulties in obtaining sufficient material from human primary astrocytes for the assay.

4.3.1 Pull-down Protein Binding Assay Optimisation

Calcium was incorporated into the pull-down protein binding assay optimisation experiments to explore the effect of this ion on protein binding. Calcium is fundamental to astrocytic function as it through calcium transients that astrocytes are able to functionally engage in the tripartite synapse and in neurovascular coupling signalling mechanisms.

Initially, 1321N1 astrocytoma cell lysates were treated either with EDTA and $CaCl_2$. EDTA is a chelator capable of sequestering metal ions including Ca^{2+} whilst $CaCl_2$ stimulates the cells. In this experiment more proteins were detected in the pull-down assay in the presence of $CaCl_2$ ions. This may suggest that calcium enhances protein binding to occludin, however, because this experiment did not include a $CaCl_2$-treated GB1 control the effect of $CaCl_2$ on occludin protein binding remains ambiguous. Despite this ambiguity, the pull-down assay protocol was adapted to incorporate a cellular incubation prior to lysis with $CaCl_2$ and A23187, an ionophore.

Ionophores are lipophilic complexing agents which are capable of reversibly binding ions and transporting them across membranes (Bakker et al., 1997). A23187 has been previously used in research exploring the physiological effects of Ca^{2+} ions. A23187 was utilised in research investigating the role of Ca^{2+} on the interaction between amyloid precursor protein (APP) and Homer3 in HEK293 cells (Kyratzi and Efthimiopoulos, 2014). This ionophore was also used in research involving primary rat cortical astrocytes and C6 rat glioma cells exploring the effect of Ca^{2+} on signalling mechanisms (Köller et al., 2001; Oya et al., 2013).

Research investigating mitochondrial function in primary rat cortical astrocytes has used 4-BrA23187, another calcium ionophore (Kahraman et al., 2011; Tan et al.,

2011). This ionophore, however, has a lower selectivity for Ca^{2+} ions and a higher selectivity for other divalent cations, Zn^{2+} and Mn^{2+}, compared with A23187 (Erdahl et al., 1996; Wang et al., 1998). Consequently, A23187 was considered to be the more suitable agent and was used in the pull-down assay to enhance astrocytic activation in response to $CaCl_2$.

The compositions of both the wash buffer and lysis buffer used in the pull-down assay were developed from a published protein binding assay protocol which was used in the identification of the ZO-1 binding surface in occludin (Li et al., 2005b). The lysis buffer used in the current study is compositionally identical to the published buffer except for the omission of 10 mM sodium pyrophosphate tetrabasic ($Na_4P_2O_7$). This compound was found to generate a white precipitate in the presence of $CaCl_2$ which masked the beads, making it impossible to complete the assay.

4.3.2 GB1-OCLN Purification

Difficulties were encountered in the purification of the GB1-OCLN recombinant protein from the BL21-RP *E. coli* stain. This may be due to the entrapment of this protein in inclusion bodies or the localisation of this protein to the bacterial envelope. An ICC experiment was trialled to investigate the localisation of this protein within the bacteria and provide an explanation for the extraction difficulties. The rod-like structure of *E. coli* bacteria was clearly defined in this experiment suggesting that this protein is expressed by the bacteria. The specificity of the staining observed in this experiment is not certain, however, in the absence of a negative and isotype control.

The purpose of this experiment was to determine the localisation of GB1-OCLN in the bacterial cells. It was not possible to establish the localisation of this protein, however, as the microscope used in this experiment was insufficiently powerful to define either the bacterial cell envelope or identify inclusion bodies. Further exploration of GB1-OCLN bacterial protein expression should utilise a confocal microscope.

The cell envelope of gram-negative bacteria such as *E. coli* is formed from two concentric membranes known as the inner and outer membranes (IM and OM), which are separated by a periplasmic space containing a peptidoglycan cell wall (Silhavy et al., 2010). The IM is formed from a phospholipid bilayer predominantly composed of phosphatidylethanolamine and phosphatidylglycerol (Raetz and

Dowhan, 1990). The inner leaflet of the OM is similarly composed of phospholipids the outer leaflet, however, is formed from glycolipids, predominantly lipopolysaccharide (LPS) (Raetz and Dowhan, 1990). The integral membrane proteins of these two membranes are structurally distinct as the transmembrane domains of IM proteins are composed of α-helices whilst the OM contains fewer proteins whose transmembrane regions are formed from β-barrel motifs (Weiner and Li, 2008).

Future experiments could focus on extracting the GB1-OCLN protein from the bacteria. A proteomics study investigating the protein composition of the *E. coli* cell envelope successfully solubilised many membrane proteins from the JM109 strain (Fountoulakis and Gasser, 2003). The application of the same methodology to the BL21-RP *E. coli* strain may succeed in the purification of the GB1-OCLN protein. OM proteins have also been extracted from *E. coli* using a twostep protocol involving anion exchange and size exclusion chromatography (Beis et al., 2006). The protein complexes from both the IM and OM of BL21-RP *E. coli* have also been analysed in another proteomics study (Stenberg et al., 2005). The methodology used in this study to isolate the two bacterial membranes and purify their respective proteins may also aid in the purification of GB1-OCLN and confirm the localisation of GB1-OCLN.

The recovery of a functionally active protein from inclusion bodies is an extensive process. Initially the inclusion bodies must be isolated and the proteins solubilised using strong protein denaturants, such as organic solutes, and a reducing agent after which the proteins are refolded in the presence of an oxidising agent and subsequently purified (Singh and Panda, 2005). The various methodologies used to extract proteins from inclusion bodies may also be of use in developing a protocol to successfully solubilise and purify GB1-OCLN (Palmer and Wingfield, 2012; Singh and Panda, 2005).

In summary, this chapter details the successful development of a pull-down protein binding assay utilising GB1-OCLN_N and GB1-OCLN_C recombinant proteins. Difficulties were encountered in purifying the GB1-OCLN recombinant protein from the BL21-RP *E. coli* strain for which the structure of the occludin protein is likely to be accountable. The gels produced from the GB1-OCLN_N and GB1-OCLN_C pull-down protein binding assays were subsequently subjected to mass spectrometry analysis to identify putative occludin binding partners in astrocytes.

5. Occludin Binding Partner Identification & Validation

5.1 Introduction

GB1-OCLN_N and GB1-OCLN_C recombinant proteins were successfully generated and utilised to develop a pull-down protein binding assay. The gels produced from this assay were submitted for mass spectrometry analysis in order to identify putative protein binding partners for occludin and consequently elucidate putative function(s) of this protein in astrocytes. The mass spectrometry was conducted by a collaborator: Dr. Mark Dickman's research group in Chemical and Biological Engineering of the University of Sheffield.

Mass spectrometry has previously been used to analyse the composition of the tight junction proteome by identifying proteins proximal to both occludin and claudin 4 in the tight junction complex (Fredriksson et al., 2015). This research fused myc-tagged biotin ligase (BL) to full length occludin and claudin 4 proteins. The BL was placed at either the N-terminal or the C-terminal domain of occludin and at the N-terminal domain of claudin 4. These constructs were transfected into MDCK II cells which were subsequently incubated with biotin. Any proteins proximate to the respective domains of occludin or claudin 4 were biotinylated by BL. The cells were then lysed and the biotinylated proteins purified on streptavidin resin. These proteins were then subjected to SDS-PAGE electrophoresis and identified through mass spectrometry analysis (Fredriksson et al., 2015). Aside from numerous proteins known be components of the tight junction complex, various signalling and trafficking proteins were also identified from this study, consequently expanding the known constituents of the tight junction proteasome (Fredriksson et al., 2015).

The current study has used a similar approach by utilising mass spectrometry analysis to identify proteins from astrocyte lysates which bind to either the N- or C-terminal domain of occludin. Validation was subsequently undertaken to verify the protein interactions identified from this study through co-immunoprecipitation. This chapter presents the proteins identified as putative binding partners for the occludin N- and C-terminal domains and shows the initial validation undertaken to confirm these interactions.

5.2 Results

Mascot was used to analyse and interpret the mass spectral data obtained from the AmaZon speed (Brucker) ion trap mass spectrometer for the GB1-OCLN_C and GB1-OCLN_N pull-down protein binding assays. Mascot compares the spectral data to a protein database and identifies peptide matches to specific proteins. Each protein identified from this analysis is assigned an overall protein score which reflects the combined scores of all the peptide spectra which were matched to this protein. The Mascot protein score, consequently, indicates the confidence of the match. The number of spectra or queries matched to a protein also determines the confidence of the result. A protein with a high score and multiple queries suggests a reliable and confident match. Peptides with a Mascot score ≥ 50 and the number of significant queries > 1 were considered to be significant in this project.

5.2.1 Mass Spectrometry Protein Binding Partners: C-terminal domain

This experiment included GB1-OCLN_C and GB1 control samples. Any matches which were identified in both GB1-OCLN_C and the GB1 control were discounted as being non-specific. Keratin is a contaminant and all matches for this protein were discarded. Table 5.1 shows the nine specific proteins identified as putative occludin C-terminal domain binding partners. Occludin was identified in this experiment as a protein binding partner with the highest protein score. Although occludin is known to dimerise and oligomerise, the very high protein score for occludin is attributable to the presence of GB1-OCLN_C in the samples submitted for mass spectrometry analysis.

The second highest match is 60S ribosomal protein. Ribosomal subunit proteins and histones are commonly identified in spectral analysis and generally considered to be unreliable matches due to their prevalence. The 60S ribosomal protein match was, therefore, not pursued further. Actin and ZO-1 were also identified in this experiment. Both of these proteins are known to bind to occludin's C-terminal domain (Li et al., 2005b; Wittchen et al., 1999). The identification of these binding partners validates the experimental methodology used in this project.

Accession	Name	Score	Mass (Da)	Description
OCLN_HUMAN	Occludin	1629	59505	An integral membrane protein of the TJC
RLA0_HUMAN	60S acidic ribosomal protein P0	202	34423	A structural component of the ribosome
ACTB_HUMAN	Actin, cytoplasmic 1	141	42052	A component of the cellular cytoskeleton
DDX3X_HUMAN	ATP-dependent RNA helicase DDX3X	87	73597	Involved in many stages of gene expression including transcription
PCBP1_HUMAN	Poly(rC)-binding protein 1	78	37987	Single-stranded nucleic acid binding protein
G3P_HUMAN	Glyceraldehyde-3-phosphate dehydrogenase	77	36201	Participates in nuclear events including transcription, RNA transport, DNA replication and apoptosis
LMNA_HUMAN	Prelamin-A/C	58	74380	A component of the nuclear lamina
HORN_HUMAN	Hornerin	56	283140	A component of the epidermal cornified cell envelope
ZO1_HUMAN	Tight junction protein ZO-1	56	195682	A cytoplasmic scaffolding protein of the TJC

Table 5.1: Putative C-terminal Domain Occludin Binding Partners These proteins were identified by mass spectrometry analysis from a gel produced by a pull-down protein binding assay using GB1-OCLN_C. None of these proteins was present in the GB1 control and are, therefore, specific to the occludin C-terminal domain. Known occludin binding partners are shown in red.

The interaction between occludin and ZO-1 was validated by western blot. Protein samples from two separate pull-down protein binding assay experiments utilising 1321N1 astrocytoma cell lysates were analysed by gel electrophoresis and the membrane probed with anti-ZO-1 antibody, Figure 5.1. A clear 250 kDa ZO-1 protein band was observed in the input and GB1-OCLN_C eluate but absent in the GB1 control for both sample sets. This confirms the specificity of the interaction between occludin and ZO-1.

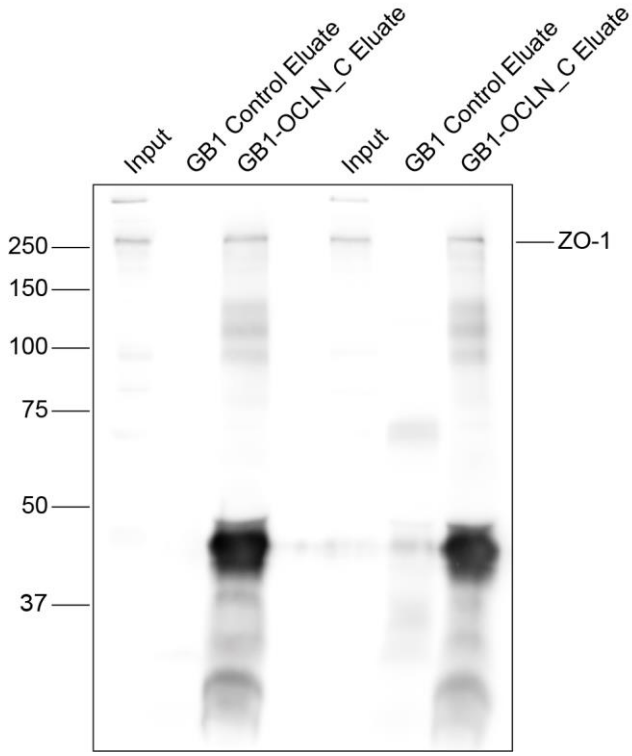

Figure 5.1: A Western Blot confirming the interaction between Occludin and ZO-1 This experiment was conducted using protein samples from two separate pull-down protein binding assays. The assays were both conducted using 1321N1 astrocytoma cell lysates. The membrane was probed with anti-ZO-1 antibody. A ZO-1 protein band is present in the input and GB1-OCLN_C eluate but absent in the GB1 control, confirming the interaction between occludin and ZO-1. Molecular weight markers are indicated (kDa).

After occludin, S60 ribosomal protein and actin, the protein with the highest score was DDX3X, DEAD-box helicase 3, X-linked. DDX3X is a nucleocytoplasmic ATP-dependent RNA helicase. This protein was selected for further investigation as a putative occludin binding partner due to the high Mascot score and the nucleocytoplasmic functions of this protein.

Initially, the expression of DDX3X in both human primary astrocytes and 1321N1 astrocytoma cells was characterised by immunocytochemistry, Figure 5.2. The human primary astrocytes used in this experiment were cultured in ScienCell Astrocyte Medium. A strong diffuse staining was observed throughout the cytoplasm in both human primary astrocytes and 1321N1 astrocytoma cells. Faint diffuse nuclear staining was also seen in these cells. The specificity of this staining was confirmed by a negative and isotype control in which no staining was observed.

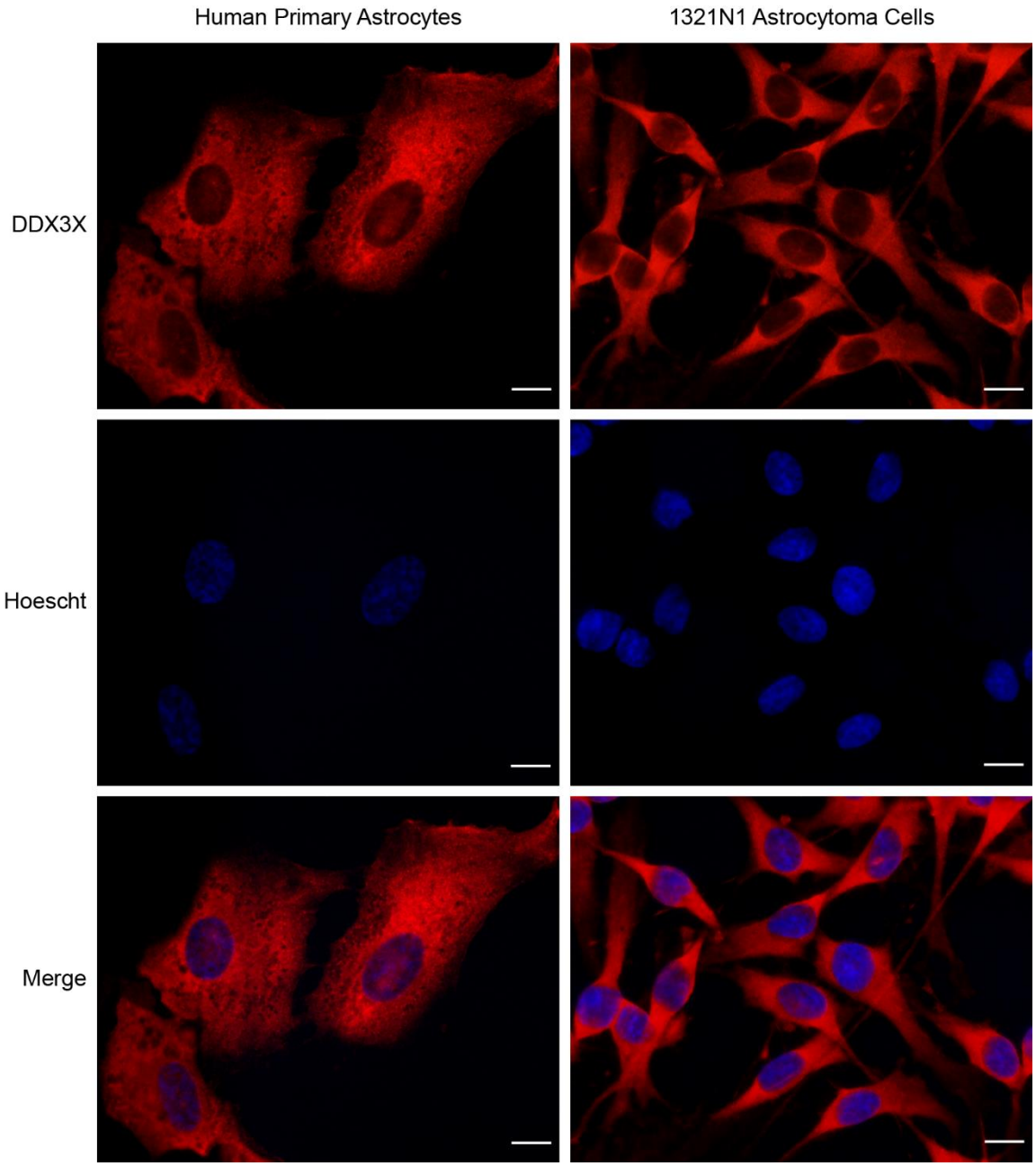

Figure 5.2: DDX3X Expression in Astrocytes The expression of DDX3X was characterised in human primary astrocytes and 1321N1 astrocytoma cells. The human primary astrocytes used for this experiment were cultured in ScienCell Astrocyte Medium. Scale bar 10 µm.

The putative interaction between occludin and DDX3X was initially investigated by western blot. Protein samples from a pull-down protein binding assay utilising 1321N1 astrocytoma cell lysates were analysed by gel electrophoresis and the membrane probed with anti-DDX3X antibody, Figure 5.3. A strong 73 kDa DDX3X protein band was observed in the input whilst a fainter 73 kDa protein band was seen in both the GB1-OCLN_C and GB1 control. This suggests that the interaction between occludin and DDX3X is non-specific.

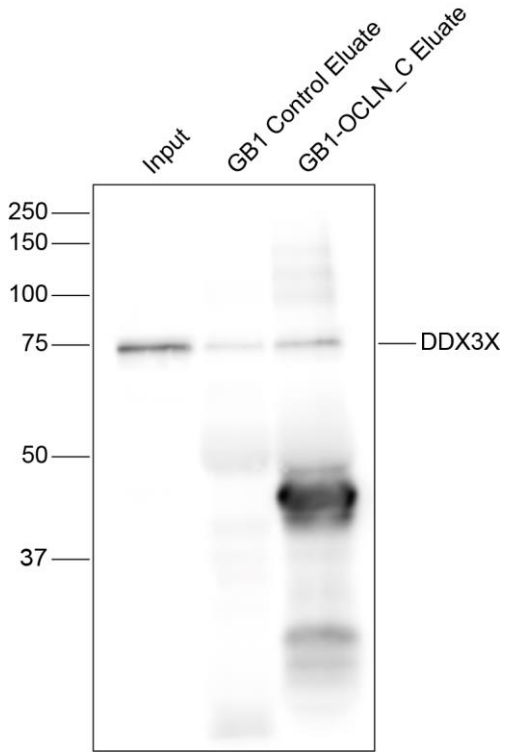

Figure 5.3: A Western Blot investigating the putative interaction between Occludin and DDX3X This experiment was conducted using protein samples from a pull-down protein binding assay. This assay was conducted using 1321N1 astrocytoma cell lysates. The membrane was probed with anti-DDX3X antibody. Molecular weight markers are indicated (kDa).

5.2.2 Co-Immunoprecipitation Validation

The putative interaction between occludin and DDX3X was investigated further by co-immunoprecipitation. Co-immunoprecipitation experiments were conducted using lysates from human primary astrocytes and 1321N1 astrocytoma cells to ensure that the putative interaction was not specific to the astrocytoma cell line. The human primary astrocytes used for these experiments were cultured in ScienCell Astrocyte Medium.

5.2.2.1. Trialling Occludin Antibodies for Immunoprecipitation

Initially, the capability of two commercially available anti-occludin antibodies to immunoprecipitate occludin protein was trialled using HEK 293 cell lysates, Figure 5.4. This experiment utilised an anti-occludin rabbit polyclonal antibody and an anti-occludin mouse monoclonal antibody. Proteins were eluted from the Protein G Sepharose beads initially with an acid elution and then a boil elution to determine which elution method was more efficient. A boil elution is more stringent than an acid elution, however, the boil elution can also elute antibody fragments. This

experiment included an anti-flag negative control. Input, flow through (FT) and eluate samples were included for every antibody used in this experiment. The membrane was probed with the anti-occludin rabbit polyclonal antibody.

A faint 65 kDa occludin protein band was observed in all input and FT samples. A strong 65 kDa occludin protein band was also seen in both the acid and boil elution samples for the anti-occludin rabbit polyclonal antibody demonstrating that this antibody is capable of immunoprecipitating occludin from HEK 293 cell lysates. Conversely no 65 kDa occludin band was present in either the acid or boil elution samples for the anti-occludin mouse monoclonal antibody indicating that this antibody is unable to immunoprecipitate occludin from HEK 293 cell lysates. The absence of the 65 kDa protein band from the anti-flag control eluates confirms the specificity of the anti-occludin rabbit polyclonal antibody occludin IP. The anti-occludin rabbit polyclonal antibody was subsequently selected for use in future IP and Co-IP experiments.

Appendix 7.1 shows examples of unsuccessful occludin IP experiments from 1321N1 astrocytoma cell lysates. In these experiments, occludin was detected in the inputs, however, the same banding pattern was present in both the negative control and occludin antibody and consequently the IP was not specific.

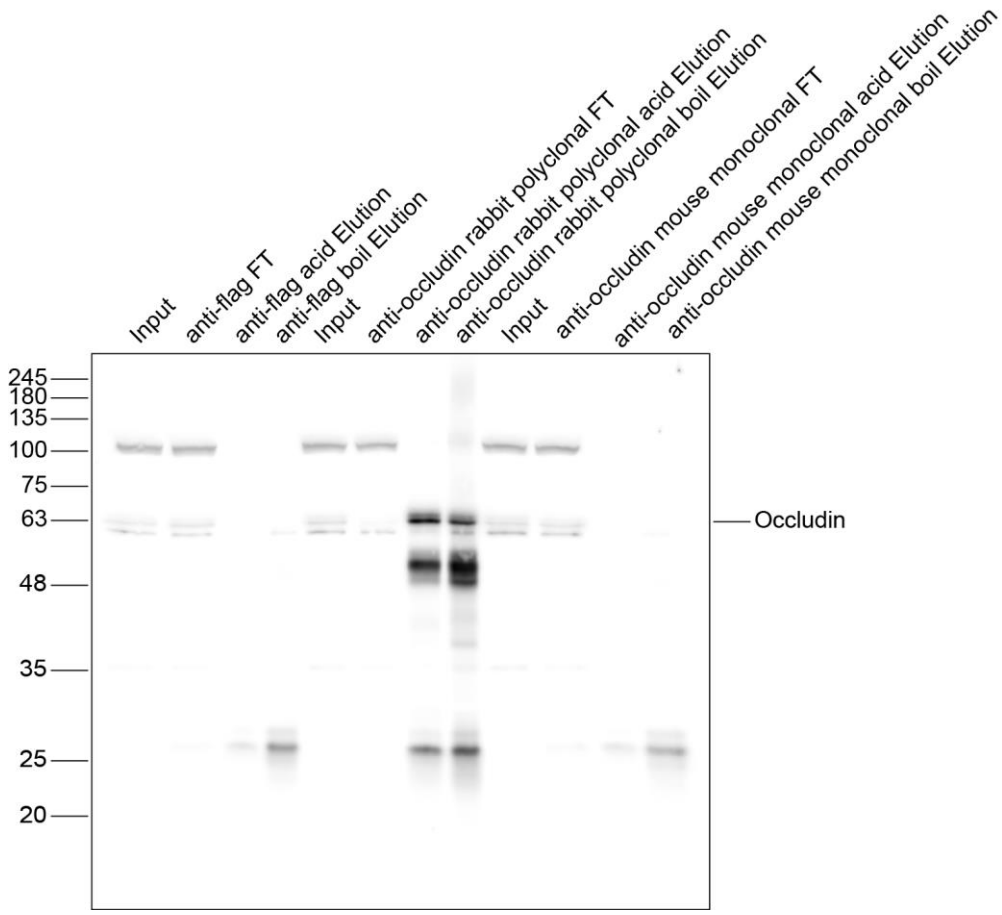

Figure 5.4: Occludin Immunoprecipitation from HEK 293 cells Occludin was successfully immunoprecipitated from HEK 293 cell lysates with the anti-occludin rabbit polyclonal antibody. The anti-occludin mouse monoclonal antibody was unable to immunoprecipitate occludin. An anti-flag antibody was included as a negative control. This experiment was conducted using a 12% resolving gel and a 4% stacking gel. The membrane was probed with anti-occludin rabbit polyclonal antibody (Thermo Fisher Scientific). A BLUeye Prestained Protein Ladder (bands ranging from 11-245 kDa) (Geneflow) was used for this western blot. Molecular weight markers are indicated (kDa).

5.2.2.2. Trialling DDX3X Antibodies for Immunoprecipitation

The capability of two commercially available anti-DDX3X antibodies to immunoprecipitate DDX3X and co-immunoprecipitate occludin was initially trialled using human primary astrocyte cell lysates, Figure 5.5. The human primary astrocytes used for this experiment were cultured in ScienCell Astrocyte Medium. This experiment utilised an anti-DDX3X rabbit polyclonal antibody and an anti-DDX3X mouse monoclonal antibody. The anti-occludin rabbit polyclonal antibody was also included in this experiment and an anti-flag antibody was used as a negative control. The protein samples produced from this experiment were run on two separate 12% gels. One gel was used to produce a blot which was probed with

anti-occludin rabbit polyclonal antibody, Figure 5.5 panel A. The other gel was used to produce a blot which was probed with anti-DDX3X mouse monoclonal antibody, Figure 5.5 panel B.

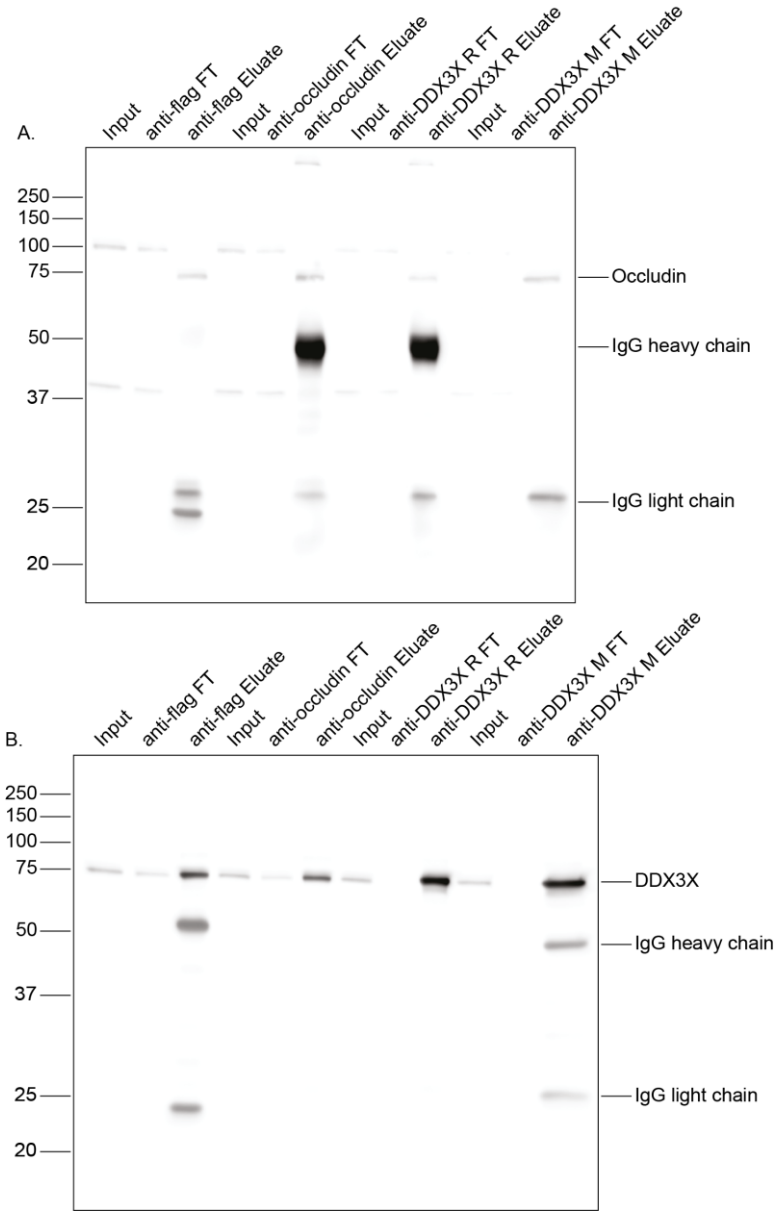

Figure 5.5: The Immunoprecipitation/Co-immunoprecipitation of Occludin and DDX3X from Human Primary Astrocytes Immunoprecipitation/co-immunoprecipitation of occludin and DDX3X from human primary astrocyte cell lysates. Human pritmary astrocytes were cultured in ScienCell Astrocyte Medium. This experiment utilised an anti-occludin rabbit polyclonal antibody, an anti-DDX3X rabbit polyclonal antibody and an anti-DDX3X mouse monoclonal antibody. An anti-flag negative control was also included in this experiment. 12% resolving gels with 4% stacking gels were used in this experiment. The two blots shown here were produced from separate gels. A) Blot probed with the anti-occludin rabbit polyclonal antibody. B) Blot probed with the anti-DDX3X mouse monoclonal antibody. Molecular weight markers are indicated (kDa).

In panel A, a 75 kDa protein band was observed in every elution sample including the anti-flag negative control. No corresponding protein band of this height was observed in any of the input samples, consequently, although the molecular weight of this band corresponds to occludin the absence of this protein in the input samples means that the identity of the band in the eluate samples is not certain. It cannot, therefore, be determined from this experiment whether the anti-occludin rabbit polyclonal antibody is able to immunoprecipitate occludin from human primary astrocyte protein lysates. Similarly it cannot be determined from this experiment if either of the anti-DDX3X antibodies are able to co-immunoprecipitate occludin from these cells.

In panel B, a faint 73 kDa DDX3X protein band was observed in all input samples. This protein band was also present in the anti-flag and anti-occludin FT samples but not in either of the anti-DDX3X FT samples. The anti-flag control displayed a clear 73 kDa DDX3X protein band in the eluate suggesting that this protein binds non-specifically to either GB1 or the Protein G Sepharose beads. A more intense 73 kDa protein band was observed, however, in both the anti-DDX3X eluates suggesting that DDX3X is enriched in these samples compared with the anti-flag control. This enrichment is supported by the absence of a 73 kDa DDX3X protein band in either of the anti-DDX3X antibody FT samples and would suggest that both the rabbit polyclonal and mouse monoclonal DDX3X antibodies are capable of immunoprecipitating this protein from human primary astrocytes. This enrichment would also suggest that the protein band in the anti-flag control eluate represents background binding to the Protein G Sepharose beads. A 73 kDa protein band was seen in the anti-occludin eluate, however, this band is of a similar intensity to the one exhibited in the anti-flag control consequently this band is also likely to the product of non-specific background binding and not an indication that the anti-occludin antibody is capable of co-immunoprecipitating DDX3X.

Some of the eluates in both of these blots also exhibited a 50 kDa protein band and a 23 kDa protein band which were produced by the antibody IgG heavy and light chains respectively. A 50 kDa heavy chain band was seen in the anti-occludin rabbit polyclonal eluate and the anti-DDX3X rabbit polyclonal eluate in panel A. This band was observed in these two eluates because this blot was probed with an antibody which was raised in the same species (rabbit). Similarly, a 50 kDa IgG heavy chain band and a 23 kDa IgG light chain band were observed in the anti-flag and anti-DDX3X mouse monoclonal eluates in panel B because this blot was probed with an antibody the anti-DDX3X mouse monoclonal antibody.

5.2.2.3. Non-specific Binding

The presence of a 73 kDa DDX3X protein band in the anti-flag eluate suggests that this protein binds non-specifically to the beads. This non-specific binding was investigated further in an experiment in which the cell lysate was incubated with just blocked Protein G Sepharose beads and no antibody. This was known as the no antibody control. This experiment was conducted using 1321N1 astrocytoma cell lysates and also included an anti-flag control, a DDX3X co-IP using anti-occludin rabbit polyclonal antibody and a DDX3X IP using anti-DDX3X mouse monoclonal antibody, Figure 5.6.

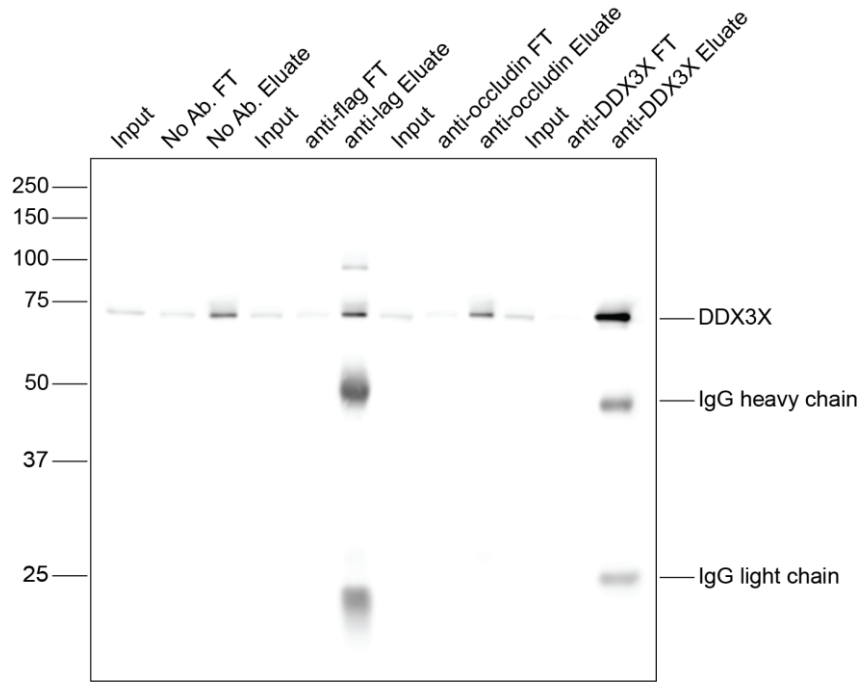

Figure 5.6: DDX3X Immunoprecipitation and Co-immunoprecipitation from 1321N1 Astrocytoma cells. DDX3X immunoprecipitation and co-immunoprecipitation from 1321N1 astrocytoma cell protein lysates. This experiment was conducted using an anti-occludin rabbit polyclonal antibody and an anti-DDX3X mouse monoclonal antibody. A no antibody control consisting of blocked protein G Sepharose beads as well as an anti-flag negative control were also included in this experiment. The blot was probed with anti-DDX3X mouse monoclonal antibody. A 12% resolving gel with 4% stacking gel was used in this experiment. Molecular weight markers are indicated (kDa).

A faint 73 kDa DDX3X protein band was observed in all inputs. This protein band was also present in the no antibody, anti-flag and anti-occludin eluates and was enriched in the anti-DDX3X eluate. This experiment reflects the results shown in Figure 5.5 panel B as DDX3X again appears to be enriched by the anti-DDX3X antibody. The presence of a 73 kDa protein band in both the no antibody and anti-flag controls suggests that there is non-specific background protein binding to the

Protein G Sepharose beads. The 73 kDa protein band present in the anti-occludin eluate is of a similar intensity to the protein band exhibited in both control eluates which suggests that it is the product of non-specific binding rather than a co-IP. A 50 kDa IgG heavy chain protein band and a 23 kDa IgG light chain protein band were observed in the anti-flag and anti-DDX3X eluates.

5.2.2.4. The Effect of Calcium Treatment

The effect of calcium on DDX3X immunoprecipitation was also investigated by pre-treating human primary astrocytes cultured in ScienCell Astrocyte Medium with 5 mM $CaCl_2$ and 4 µM A23187 for 15 mins at 37°C prior to lysing the cells. This experiment was conducted using the anti-DDX3X mouse monoclonal antibody and an anti-flag negative control, Figure 5.7.

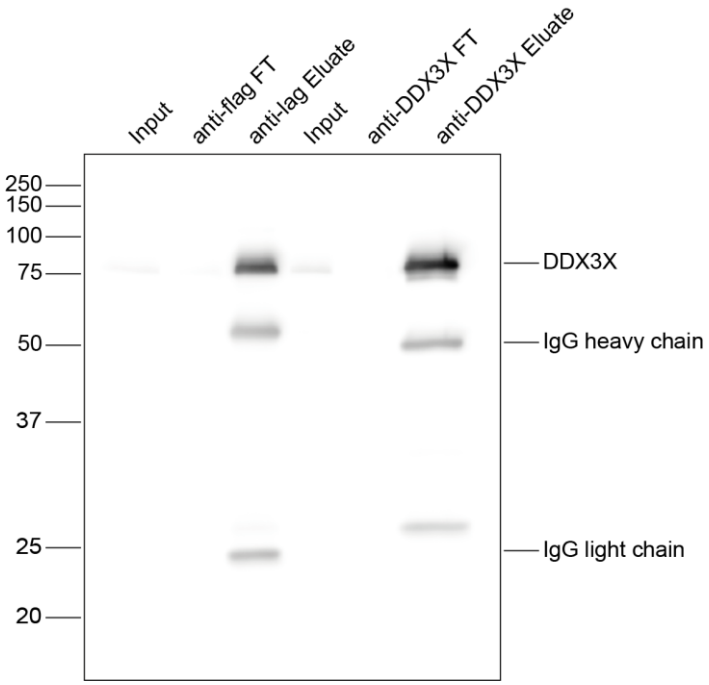

Figure 5.7: DDX3X Immunoprecipitation from Human Primary Astrocytes pre-treated with Calcium DDX3X immunoprecipitation from human primary astrocytes pre-treated with 5 mM $CaCl_2$ and 4 µM A23187 calcium ionophore. The human primary astrocytes used for this experiment were cultured in ScienCell Astrocyte Medium. This experiment was conducted using a 12% resolving gel and a 4% stacking gel. The blot was probed with anti-DDX3X mouse monoclonal antibody. Molecular weight markers are indicated (kDa).

A faint 73 kDa DDX3X protein band was observed in both inputs. This band was again present in the anti-flag eluate and enriched in the anti-DDX3X eluate. The calcium pre-treatment does not appear to alter the protein binding pattern. A 50

kDa IgG heavy chain protein band and a 23 kDa light chain protein band were observed in both antibody eluates.

5.2.3 Mass Spectrometry Protein Binding Partners: N-Terminal Domain

Any matches which were identified in GB1-OCLN_N and the GB1 control were discounted as being non-specific. Keratin is a contaminant and all matches for this protein were discarded. Table 5.2 shows the forty-one specific proteins identified as putative occludin N-terminal domain binding partners. This list includes Itch and Nedd4-2 both of which have previously been shown to interact with occludin at the PPPY motif located in the N-terminal domain of this protein (Raikwar et al., 2010; Traweger et al., 2002). Again, the identification of known occludin binding partners validates the experimental methodology used in this project. This list of putative binding partners contains many histones and ribosomal proteins. These proteins are commonly identified in mass spectral analysis and were consequently regarded as unreliable matches.

Accession	Name	Score	Mass (Da)	Description
MYH10_HUMAN	Myosin-10	685	229827	Involved in cytokinesis
H2B1K_HUMAN	Histone H2B type 1-K	1347	13882	Component of the nucleosome
H4_HUMAN	Histone H4	613	11360	Component of the nucleosome
H32_HUMAN	Histone H3.2	468	15436	Component of the nucleosome
DHX9_HUMAN	ATP-dependent RNA helicase A	396	142181	Unwinds duplex DNA and RNA
HNRPC_HUMAN	Heterogeneous nuclear ribonucleoproteins C1/C2	295	33707	Binds to pre-mRNA and is involved in the formation of hnRNP particles
PPIB_HUMAN	Peptidyl-prolyl cis-trans isomerase B	247	23785	Facilitates protein folding
SFPQ_HUMAN	Splicing factor, proline- and glutamine-rich	190	76216	Binds DNA and RNA and is involved in several nuclear processes
NONO_HUMAN	Non-POU domain-containing octamer-binding protein	88	54311	Binds DNA and RNA and is involved in several nuclear processes
ITCH_HUMAN	E3 ubiquitin-protein ligase Itchy homolog	186	103593	An E3 ubiquitin protein ligase

TOP2A_HUMAN	DNA topoisomerase 2-alpha	185	175017	Enzyme which catalyses the breakage and reannealing of DNA
TOP2B_HUMAN	DNA topoisomerase 2-beta	145	184122	Enzyme which catalyses the breakage and reannealing of DNA
SMCA5_HUMAN	SWI/SNF-related matrix-associated actin-dependent regulator of chromatin subfamily A member 5	181	122513	ATP-dependent helicase involved in the remodelling of nucleosomes
HNRPU_HUMAN	Heterogeneous nuclear ribonucleoprotein U	152	91269	Binds to RNA and is specific to the nucleus
ROA3_HUMAN	Heterogeneous nuclear ribonucleoprotein A3	140	39799	RNA-binding protein possibly involved in mRNA nuclear export
ML12A_HUMAN	Myosin regulatory light chain 12A	134	19839	Involved in cytokinesis
ROA2_HUMAN	Heterogeneous nuclear ribonucleoproteins A2/B1	133	37464	RNA-binding protein possibly involved in mRNA nuclear export
U520_HUMAN	U5 small nuclear ribonucleoprotein 200 kDa helicase	131	246006	RNA helicase
NOP56_HUMAN	Nucleolar protein 56	119	66408	Involved in ribosomal subunit biogenesis
HNRPL_HUMAN	Heterogeneous nuclear ribonucleoprotein L	114	64720	Splicing factor
H14_HUMAN	Histone H1.4	112	21852	Histone
NPM_HUMAN	Nucleophosmin	112	32726	Multifunctional protein involved in ribosome biogenesis and transport
RS14_HUMAN	40S ribosomal protein S14	96	16434	Component of the ribosome
NOP58_HUMAN	Nucleolar protein 58	95	60054	Involved in ribosomal subunit biogenesis
PSIP1_HUMAN	PC4 and SFRS1-interacting protein	95	60181	Transcriptional coactivator
DCD_HUMAN	Dermcidin	92	11391	An anti-microbial peptide
NEDD4_HUMAN	E3 ubiquitin-protein ligase NEDD4	83	150276	An E3 ubiquitin protein ligase
RBMX_HUMAN	RNA-binding motif protein, X chromosome	81	42306	RNA-binding protein
DDX21_HUMAN	Nucleolar RNA helicase 2	79	87804	RNA helicase

ARPC4_HUMAN	Actin-related protein 2/3 complex subunit 4	72	19768	An actin-binding component which is involved in actin polymerisation
RL40_HUMAN	Ubiquitin-60S ribosomal protein L40	72	15004	Component of the ribosome
U5S1_HUMAN	116 kDa U5 small nuclear ribonucleoprotein component	70	110336	A component required for pre-RNA splicing
RS6_HUMAN	40S ribosomal protein S6	68	28834	Ribosomal Protein
DHX15_HUMAN	Putative pre-mRNA-splicing factor ATP-dependent RNA helicase DHX15	66	91673	A factor involved in pre-mRNA processing
H2AY_HUMAN	Core histone macro-H2A.1	66	39764	Histone
RS25_HUMAN	40S ribosomal protein S25	65	13791	Ribosomal Protein
ILF2_HUMAN	Interleukin enhancer-binding factor 2	63	43263	Appears to interact with ILF3 and may regulate IL2 gene transcription
HNRPD_HUMAN	Heterogeneous nuclear ribonucleoprotein D0	59	38581	RNA-binding protein
NCBP1_HUMAN	Nuclear cap-binding protein subunit 1	56	92864	A component in complexes involved in RNA processing
ELAV1_HUMAN	ELAV-like protein 1	55	36240	RNA-binding protein
RS18_HUMAN	40S ribosomal protein S18	50	17708	Ribosomal Protein

Table 5.2: Putative N-terminal Domain Occludin Binding Partners. Proteins identified by mass spectrometry analysis from a gel produced by a pull-down protein binding assay conducted using GB1-OCLN_N. None of these proteins was present in the GB1 control and are, therefore, specifically interact with the occludin N-terminal domain. Known occludin binding partners are shown in red.

5.3 Discussion

Mass spectrometry analysis was utilised to identify the putative occludin binding partners which were obtained through pull-down protein binding assays. Nine proteins were identified as putative occludin C-terminal domain binding partners from the GB1-OCLN_C pull-down assay whilst 41 proteins were identified from the GB1-OCLN_N assay. The occludin binding partners identified in this study include proteins which have previously been shown to bind to occludin. Both ZO-1 and actin, which were identified in the GB1-OCLN_C pull-down protein binding assay, are known to interact with occludin at the C-terminal domain (Li et al., 2005b; Wittchen et al., 1999). Similarly the E3 ubiquitin ligases Itch and Nedd4-2, which have previously been shown to interact with occludin at the N-terminal domain, were identified as occludin binding partners in the GB1-OCLN_N pull-down protein binding assay (Raikwar et al., 2010; Traweger et al., 2002). The identification of these known occludin binding partners from the respective pull-down assay validates the experimental methodology used in this research.

A key limitation of these experiments is that, due to time constraints, only one set of pull-down protein binding assays were subjected to mass spectrometry analysis. Ideally these experiments should have been run in triplicate with the protein matches common to all three data sets considered to be putative binding partners and taken forward for validation.

5.3.1 DDX3X – Structure and Function

DEAD-box helicase 3, X-linked (DDX3X) is a protein identified in the current study as a putative occludin binding partner interacting at the C-terminal domain of this protein. Due to a high MASCOT score, and the various nucleocytoplasmic functions of this protein, DDX3X became the initial focus for validation.

DDX3X is a 662 amino acid, 73 kDa nucleocytoplasmic ATP-dependent RNA helicase. Helicases are classified by six superfamilies (SFs) of which eukaryotic helicases belong to SF1 and SF2 (Jankowsky, 2011). Eukaryotic helicases are structurally defined by a highly conserved helicase core consisting of two domains connected by a flexible linker. DEAD box helicases belong to SF2 and are characterised by the Asp-Glu-Ala-Asp (DEAD) motif which is one of twelve motifs located within the helicase core of these proteins (Fairman-Williams et al., 2010; Linder et al., 1989).

Most DEAD-box helicases also have an N- and C-terminal domain which flank the helicase core (Fairman-Williams et al., 2010). The function of these terminal accessory domains remains to be fully established, although it is possible that they enable DEAD-box helicases to interact with other proteins or enhance RNA binding (Fairman-Williams et al., 2010). The N-terminal domain of DDX3X contains an NES which binds to chromosomal maintenance 1 (CRM1), also known as exportin-1 (XPO1), a nuclear export protein (Yedavalli et al., 2004). The C-terminal domain includes a region rich in arginine and serine residues (aa 582-632). This region is known as the RS-like domain as it resembles the RS domain present in splicing factors such as serine/arginine-rich splicing factors 1 and 2 (SRSF1 and SRSF2) (Owsianka and Patel, 1999).

DEAD-box helicases have a diverse range of cellular functions. These proteins bind to RNA and ATP through motifs located in the helicase core domain and catalyse the unwinding of duplex RNA (Putnam and Jankowsky, 2013). RNA is subject to various metabolic processes including transcription, RNA splicing, RNA transport and translation. These processes are mediated by numerous proteins which bind to RNA and form ribonucleoprotein complexes (RNPs) in which many DEAD-box helicases are functional components (Jankowsky, 2011; Marintchev, 2013). Some DEAD-box helicases are able to clamp to RNA and act as a nucleation centre at which other proteins assemble to generate larger RNP complexes (Putnam and Jankowsky, 2013). A notable example is DDX48, also known as eukaryotic initiation factor 4A-III (eIF4A-III), which is a component of the exon junction complex (EJC) (Shibuya et al., 2004). The EJC binds at the junction of two spliced exons during pre-mRNA splicing and is functionally involved in RNA metabolic processes including RNA localisation and translation (Lee et al., 2009).

mRNA is exported from the nucleus in a complex known as the messenger ribonucleoprotein (mRNP) complex. DDX3X directly interacts with another nuclear export protein and component of the mRNP complex known as tip-associated protein (TAP) which functions as a heterodimer with NFT2-related export protein 1, also known as p15 (Guzik et al., 2001; Lai et al., 2008). The interaction between DDX3X and TAP is mediated by the C-terminal domain (aa 536-661) of the DDX3X protein (Lai et al., 2008). DDX3X also directly interacts with mRNA (Lai et al., 2008). These interactions associate DDX3X with the process of mRNA export, however, the extent to which DDX3X is functionally involved in the exportation mechanism remains to be established.

There is also evidence to suggest that DDX3X is involved in translation initiation. The eukaryotic initiation factor 4F (eIF4F) complex is a heterotrimeric protein complex which acts to recruit the 5' cap of mRNA to the 40S small ribosomal subunit (Hinnebusch, 2014). The eIF4F complex instigates translation initiation and facilitates the recruitment of other factors to form the 43S pre-initiation complex which is responsible for ribosomal scanning to identify the initiation codon in the mRNA transcript (Hinnebusch, 2014).

The eIF4F complex is composed of eIF4A-I, eIF4E and eIF4G. eIF4A-I is a DEAD-box RNA helicase which binds to mRNA and unwinds double-stranded RNA secondary structures which form in the 5' untranslated region (5'-UTR) of mRNA, a region directly upstream from the initiation codon (Hinnebusch, 2014). eIF4E binds to the RNA 5' cap and eIF4G functions as a protein scaffold due to its multiple binding domains. These domains enable eIF4G to bind other protein components involved in the translation mechanism including the poly(A)-binding protein (PABP), a protein which binds to the poly(A) tail located at the 3' end of mRNA (Hinnebusch, 2014).

DDX3X interacts directly with eIF4G and PABP within the eIF4F complex and has also been shown to bind to the 5'-UTR and destabilise secondary structures (Soto-Rifo et al., 2012). DDX3X is not an essential transcription factor, however, this protein does facilitate translation initiation as it promotes the interaction between the eIF4F complex and mRNA transcripts which have complex secondary structures (Soto-Rifo et al., 2012). DDX3X also appears to be involved in the functional assembly of 80S ribosomes (Geissler et al., 2012).

DDX3X is also implicated in the pathogenesis of viruses. Hepatitis C virus (HCV) is an enveloped, positive sense, single-stranded RNA virus of the *Flaviviridae* family (Dubuisson and Cosset, 2014). HCV requires DDX3X for viral replication as DDX3X knockdown in human hepatoma Huh 7-derived cells infected with HCV results in a reduction in viral RNA replication (Ariumi et al., 2007; Dubuisson and Cosset, 2014). The functional role of this protein in viral replication, however, remains to be determined (Ariumi et al., 2007).

The viral RNA genome encodes a single polyprotein which is cleaved by both host and viral proteases to generate ten viral proteins which can be subdivided into structural and non-structural proteins (Penin et al., 2004). The structural viral proteins consist of a core protein and two glycoproteins known as E1 and E2 (Penin et al., 2004). The core protein forms a structure which contains the viral genome

known as the nucleocapsid. The nucleocapsid is coated by a lipid membrane known as the viral envelope within which the two glycoproteins are situated (Penin et al., 2004).

DDX3X interacts directly with the HCV core protein (Mamiya and Worman, 1999; Owsianka and Patel, 1999). This interaction occurs between residues 1-59 located in the N-terminal of the core protein and residues 553-622 in the DDX3X C-terminal domain (Owsianka and Patel, 1999). The involvement of DDX3X in HCV replication may, however, be independent of this interaction. HuH-7 cells transfected with either a wildtype or core mutant HCV strain, in which the mutation prevents the core interacting with DDX3X, show similar levels of viral RNA replication (Angus et al., 2010). A similar reduction in the level of intracellular viral RNA also occurs in HuH-7 cells infected with either mutant or wildtype subsequent to DDX3X knockdown. This demonstrates that DDX3X is required for HCV replication but suggests that the mechanism by which DDX3X facilitates this process is independent of the interaction between this protein and the viral core protein (Angus et al., 2010).

Human immunodeficiency virus-1 (HIV-1) is an enveloped, positive sense, single-stranded RNA lentivirus which also utilises DDX3X in its replication cycle. Rev is a HIV-1 viral protein involved in the exportation of unspliced and partially spliced viral transcripts from the host nucleus (Malim et al., 1989). Rev localises to the host nucleus through an arginine-rich NLS which enables the viral Rev protein to bind directly to the host nuclear import receptor, importin-β (Henderson and Percipalle, 1997; Truant and Cullen, 1999). The Rev NLS overlaps with the RNA-binding domain of this protein, consequently the NLS domain is obscured when this protein binds to a region in unspliced and partially spliced viral transcripts known as the Rev response element (REE) (Henderson and Percipalle, 1997; Kjems et al., 1991; Malim et al., 1989). The exportation of Rev from the nucleus is mediated by the host protein CRM1 which Rev is able to recruit through a NES (Askjaer et al., 1998).

DDX3X may act as a Rev cofactor facilitating viral mRNA export as an endogenous knockdown of DDX3X in human peripheral blood mononuclear cells (PBMCs) inhibits HIV-1 replication (Yedavalli et al., 2004). DDX3X has also been implicated in facilitating HIV-1 mRNA translation mediated by interactions with a 5'-UTR structure in the viral mRNA known as the trans-activating response element (TAR) and Trans-activator of transcription (Tat), another viral protein (Lai et al., 2013).

5.3.2 Validation of the Interaction between Occludin and DDX3X

In HeLa cells DDX3X is predominantly localised to the nucleus exhibiting a speckled staining pattern which excludes nucleoli, and weak cytoplasmic staining (Owsianka and Patel, 1999). In the current study, ICC demonstrates cytoplasmic and nuclear expression of DDX3X in both human primary astrocytes and 1321N1 astrocytoma cells. The localisation of this protein in astrocytes is predominantly cytoplasmic. The HeLa cell images were obtained using confocal microscopy, consequently the DDX3X speckled nuclear staining is clearly visible. Confocal microscopy would be required to determine if DDX3X exhibits the same staining pattern in astrocytic nuclei. Dual-staining astrocytes for occludin and DDX3X to investigate co-localisation was not possible as the only available antibodies which successfully stained the cells for either of these proteins were raised in the same species.

An initial experiment designed to validate the putative interaction between DDX3X and occludin involved a western blot using pull-down protein binding assay protein. This experiment failed to confirm the putative interaction between these two proteins as a DDX3X protein band was present not only in GB1-OCLN_C but also in the GB1 control which suggests that DDX3X binds non-specifically to GB1. The putative interaction between occludin and DDX3X was investigated further by co-immunoprecipitation.

Occludin was successfully immunoprecipitated from HEK 293 cells, however, this IP was not replicable with either 1321N1 astrocytoma cells or human primary astrocytes. The principal issue encountered with the occludin IP from astrocytes was that the negative control eluate displayed the same banding pattern as the occludin antibody eluate. This occurred in both anti-flag and anti-myc negative controls.

It was concluded from the immunoprecipitation experiments for DDX3X that this protein binds non-specifically to the Protein G sepharose beads, producing a level of background binding which was present in all negative controls. The clear enrichment of the DDX3X protein band in IP experiments with anti-DDX3X antibodies, however, suggests that the IP does work. Unfortunately the DDX3X protein band present in the co-IP with anti-occludin antibody is probably due to the background protein binding consequently the putative interaction between occludin and DDX3X could not be validated.

As neither occludin nor DDX3X could be immunoprecipitated from astrocytic cell lysates with any specificity, the interaction between these two proteins could not be verified using the current methodology and, due to time constraints, neither could this method be further optimised nor any other experimental avenues explored through which this interaction might be verified.

Although the initial attempts to validate the interaction between occludin and DDX3X were unsuccessful, the validation process is only in its inception and further research is required before definitive conclusions can be drawn regarding occludin and the binding partner candidates identified in this study. It would, therefore, be premature to conclude that occludin does not interact with DDX3X based on the validation difficulties encountered in this study

5.3.3 Occludin Nuclear Translocation

It can be hypothesised from the subcellular localisation of occludin in astrocytes that this protein may be functionally involved in nuclear processes. The proteins identified in this study as putative occludin binding partners support this hypothesis as many of them are involved in different RNA metabolic processes. Some of the proteins identified from this study are nucleocytoplasmic proteins which are implicated in the nuclear exportation of mRNP complexes. The mechanism by which occludin is able to translocate between the cytoplasm and nucleus is yet to be established as this protein does not appear to contain a NLS or NES. An insight into this mechanism may be provided by conducting further research into the nucleocytoplasmic proteins identified as putative occludin binding partners in the current study.

CRM1 and the TAP-p15 heterodimer are both nuclear export proteins which facilitate the exportation of proteins and mRNA from the nucleus through the NPC. The mechanism by which CRM1 is imported into the nucleus remains to be established, whilst the N-terminal domain of TAP contains a NLS which enables the TAP-p15 heterodimer to bind to a nuclear import protein known as transportin (Bachi et al., 2000; Katahira et al., 1999). Neither CRM1 nor TAP-15 were identified from the mass spectrometry analysis as binding to occludin, however both of these proteins are known to interact with DDX3X (Lai et al., 2008; Yedavalli et al., 2004). It is possible that DDX3X may act as an adaptor protein connecting occludin with nuclear transport proteins which would enable occludin to translocate between the cytoplasm and nucleus. The interaction between occludin and DDX3X may also

suggest that occludin might be a component of the mRNP complex, although this would undoubtedly require further investigation.

Several heterogeneous nuclear ribonucleoproteins (hnRNPs) were also identified as putative occludin N-terminal domain binding partners. 19 hnRNP genes have currently been identified, of which there are numerous isoforms, however, the total number of proteins within the hnRNP family remains to be determined as putative hnRNPs have not yet been characterised (Carpenter et al., 2006). hnRNPs are functionally defined by the presence of RNA-binding motifs such as RNA recognition motifs (RRMs), hnRNP K homology domains (KHs) or arginine/glycine-rich box (RGG) (Krecic and Swanson, 1999). These proteins interact with pre-mRNAs and function as components of RNP complexes facilitating RNA metabolic processes including mRNA export (Dreyfuss et al., 2002).

hnRNP A2/B1 is one of the hnRNPs identified in this study as a putative occludin binding partner. hnRNP A2 (38 kDa) and hnRNP B1 (36kDa) are two isoforms encoded by the HNRNPA2B1 gene which are produced through alternative splicing (Kozu et al., 1995). Two other isoforms, A2b and B1b, have been identified in mice and rats (Hatfield et al., 2002; Kamma et al., 1999). hnRNP A2/B1 is part of a hnRNP A/B subfamily which structurally consists of two tandem N-terminal RRMs with a C-terminal glycine-rich domain (GRD) (Burd et al., 1989). A 38-residue motif known as the M9 motif located in the GRD acts as a dual nucleocytoplasmic transport signal which mediates both the nuclear import and export of hnRNP A2/B1 (Bogerd et al., 1999; Matthew Michael et al., 1995; Piñol-Roma, 1997; Pollard et al., 1996).

hnRNP A3 was also identified in the current study. This protein has a similar amino acid sequence to hnRNP A1 and displays a domain similar to the M9 motif suggesting that this protein is also capable of translocation between the nucleus and the cytoplasm (Ma et al., 2002). The M9 motif acts as a dual nuclear transport signal mediating both nuclear import and export, consequently the translocation of occludin between the nucleus and cytoplasm of astrocytes may be mediated by hnRNP A2/B1 or hnRNP A3.

5.3.4 Occludin and Viral Pathogenesis

The cellular entry of HCV particles is mediated by attachment factors and receptors located on the cell surface of hepatocytes which enables the clathrin-mediated endocytosis of the virus into these cells (Dubuisson and Cosset, 2014). Occludin

has been identified as one of the factors required for HCV entry (Liu et al., 2009; Ploss et al., 2009). Occludin is not the only tight junction protein which acts as a HCV attachment factor as claudin-1 is also involved in mediating viral entry (Evans et al., 2007). Occludin knockdown reduces the viral infection in two cell lines which are naturally permissive to HCV, Hep3B and Huh-7.5 cells (Ploss et al., 2009). The HCV-resistant renal carcinoma cell line 786-O expresses high levels of other entry factors but low levels of occludin and the overexpression of occludin in these cells enhances HCV infection (Ploss et al., 2009).

Endogenous occludin co-immunoprecipitates HCV E2 protein in infected hepatoma cells suggesting that the interaction between occludin and HCV is mediated by the E2 viral protein (Liu et al., 2009). This interaction occurs at the second occludin extracellular loop and is dependent upon dynamin II, a GTPase involved in endocytosis (Liu et al., 2010). The interaction between occludin and dynamin II is abrogated in the absence of the ECL2 indicating that this domain is necessary for the interaction between these two proteins (Liu et al., 2010). HCV entry is inhibited in Huh7 cells which have been treated with the dynamin inhibitor dynasore; similarly dynamin II knockdown in Huh7.5.1 cells decreases the level of HCV infection demonstrating that HCV entry occurs by a dynamin-dependent mechanism (Liu et al., 2010; Liu et al., 2009). The interaction between occludin and dynamin II, however, presents with a logistical difficulty as dynamin II is a cytoplasmic protein whilst the occludin ECL2 is located in the extracellular domain. It is possible that the interaction between occludin and dynamin II is mediated by another currently unidentified protein.

Both occludin and DDX3X are implicated in different stages of HCV pathogenesis. Occludin is involved in the entry of this virus into cells whilst DDX3X is involved in viral replication (Ariumi et al., 2007; Liu et al., 2010; Liu et al., 2009). An interaction between DDX3X and occludin, if verified, may suggest that occludin not only facilitates viral entry but also functions as an adaptor protein facilitating the interaction between HCV particles and a host protein known to be required for viral replication.

In summary the mass spectrometry analysis identified putative occludin binding partners which interact with either the N-terminal or C-terminal domain of this protein. DDX3X was one of the proteins identified as binding to the occludin C-terminal domain and was the initial focus for validation. Co-immunoprecipitation experiments were conducted in an attempt to confirm this interaction, however,

optimisation difficulties were encountered and consequently the interaction between occludin and DDX3X was not verified using this method and unfortunately, due to time constraints, further validation studies could not be pursued.

The binding partners identified in this study have various functions many of which relate to RNA binding, RNA splicing, mRNA transport and translation initiation. Although it was not possible to fully investigate and verify these proteins as occludin binding partners, the identification of these proteins does implicate occludin in many cellular processes beyond forming the tight junction complex. The findings from this study, therefore, provide a platform upon which future research can be constructed to further investigate the functional role(s) of occludin.

6. Discussion and Future Work

6.1 Astrocytic Tight Junction Protein Expression

The initial aim of this project was to characterise the expression of occludin, claudin 5 and ZO-1 in human primary astrocytes and 1321N1 astrocytoma cells and to define the cellular localisation of these proteins in the temporal cortex. This project has succeeded in demonstrating that both occludin and ZO-1 are expressed in the cytoplasm and nucleus of human primary astrocytes and 1321N1 astrocytoma cells. The astrocytic nuclear expression of occludin is also confirmed *in vivo* by the co-localisation of occludin immunoreactivity with GFAP-positive astrocytes in human post-mortem tissue from the temporal cortex. The *in vivo* study confirms the nuclear expression of ZO-1 and the astrocytic expression of ZO-1 is supported in a previous study which shows the co-localisation of ZO-1 immunoreactivity with GFAP-positive astrocytes in human post-mortem tissue (Simpson et al., 2011).

This project concludes that claudin 5 is not expressed in either human primary astrocytes or 1321N1 astrocytoma cells. The current *in vivo* study supports this conclusion as claudin 5 expression was found to be exclusively associated with endothelial cells. The same observations have also been made in previous research in which the expression of claudin 5 is shown to be exclusively associated with endothelial cells in human tissue (Simpson et al., 2010).

The conclusion that claudin 5 is not expressed in astrocytes is, however, contradicted by another study which shows this protein to be expressed in human astrocytes, oligodendrocytes and pyramidal neurons *in vivo* (Romanitan et al., 2010). This previous study, however, did not include any dual-labelling, consequently the co-localisation of claudin 5 with astrocytes is not certain. Based on the evidence from the current project, claudin 5 does not appear to be expressed in astrocytes.

Future research could investigate the astrocytic expression of other claudin proteins. Claudin 2 and claudin 11 have also been shown to be expressed in human astrocytes *in vivo* (Simpson et al., 2010). Again, no dual-labelling was conducted in this study for either of these claudin proteins so this could be addressed in future research to confirm the astrocytic expression of these two claudin proteins *in vivo*. The expression of either of these claudin proteins could also be investigated *in vitro* in human primary astrocytes and 1321N1 astrocytoma cells through ICC and western blotting.

6.2 Astrocytic & Neuronal Tight Junction Protein Expression and Alzheimer's Disease

Changes in the astrocytic and neuronal expression of tight junction proteins has been implicated in the pathogenesis of neurodegenerative diseases. A previous *in vivo* study using a human tissue cohort concluded that there is a significant increase in the expression of occludin in pyramidal neurons in AD and VD cases compared with controls (Romanitan et al., 2007). The same cohort was used to investigate changes in the expression of claudin 2, claudin 5 and claudin 11 (Romanitan et al., 2010). All three of these claudin proteins were found to be expressed in astrocytes and pyramidal neurons. This study found that there was a significant increase in the ratio of pyramidal neurons expressing all three claudins in AD and VD cases compared with controls whilst there was a significant increase in the ratio of astrocytes expressing claudin 2 and claudin 11, but not claudin 5, in AD and VD cases compared with controls (Romanitan et al., 2010). These studies suggest that an increase in tight junction protein expression is associated with AD and VD.

Conversely, however, a significant reduction in astrocytic transcripts which encode for TJPs is associated with increasing Alzheimer-type pathology (Simpson et al., 2011). Another aim of this study was to investigate possible changes in the expression of occludin, claudin 5 and ZO-1 in MCI and AD cases compared with control. The staining identified in this study was sufficient to characterise the cellular localisation of these proteins *in vivo*, however, it was not possible to quantify and analyse. Consequently the possible role of these tight junction proteins in AD pathology was not addressed in this project.

Although there is evidence to suggest that astrocytic tight junction protein expression is altered in AD, it is not known how these proteins may be functionally involved in the pathogenesis of this disease or even if these changes are causally linked to AD progression. It is undeniable that future research is required into the role of tight junction proteins in AD, however, until the functional role(s) of these proteins in astrocytes are fully understood, their possible involvement in disease will remain unclear.

6.3 The Function of Tight Junction Proteins in Astrocytes

The function(s) of occludin in astrocytes was investigated by the identification of putative protein binding partners using a pull-down protein binding assay and mass spectrometry analysis. Subsequent validation of the proteins identified in this study

was limited due to time constraints and unfortunately these interactions remain unconfirmed in a physiological context.

The candidates identified in this study as putative occludin binding partners have a variety of different functions, many of which pertain to RNA metabolic processes, including RNA binding, RNA splicing, mRNA transport and translation initiation. The possibility that occludin interacts with these proteins is an exciting prospect as it implicates occludin in cellular processes with which this protein has not previously been associated and supports the hypothesis that occludin is functionally involved in processes beyond the tight junction complex.

The putative binding partners identified in this study may also offer an insight into the currently unresolved issue of the mechanism by which occludin is able to translocate into the nucleus. Occludin is considered to be a membrane-associated protein, however, in astrocytes this protein appears to be nucleocytoplasmic. Occludin is not known to contain any nuclear localisation or nuclear export signals, the absence of which would suggest that this protein is unable to directly interact with nuclear transport proteins. It can be hypothesised, therefore, that the translocation of occludin across the nuclear envelope may be mediated by proteins which are themselves capable of interacting with nuclear transport proteins.

This hypothesis is supported by some of the proteins identified as putative occludin binding partners in this study. DDX3X and hnRNP A2/B1 are both nucleocytoplasmic proteins which are known to interact with nuclear transport proteins. Consequently the association of occludin with these proteins may provide an explanation for how occludin translocates between the cytoplasm and nucleus in astrocytes.

Future research should initially repeat the pull-down protein binding assay and mass spectrometry analysis in triplicate for both GB1-OCLN_C and GB1-OCLN_N. Any matches common to all three data sets should be subject to validation with priority given to any nucleocytoplasmic putative binding partners to try and understand the mechanism by which occludin translocates across the nuclear envelope.

This project attempted to validate the putative interaction between occludin and DDX3X through endogenous co-immunoprecipitation experiments. As difficulties were encountered with these experiments, it may be worth conducting co-immunoprecipitation experiments with human primary astrocytes or 1321N1 astrocytoma cells transfected with occludin to investigate putative binding partner

interactions in future research. As some of the putative occludin binding partners identified in this project are able to bind directly to DNA or RNA, it would also be interesting to investigate whether occludin is also capable of interacting with either of these molecules. This could be achieved by conducting DNA- and RNA-binding assays for occludin.

Future research could also investigate whether full length or processed forms of occludin are localised to the nucleus. There are several examples of integral membrane proteins which are involved in cell signalling pathways subsequent to proteolytic cleavage. Consequently the possibility that occludin may be cleaved into fragments which are functionally involved in cell signalling mechanisms is worth pursuing.

Notch proteins are a family of cell surface receptor integral membrane proteins which are structurally composed of a large extracellular domain, a single transmembrane domain and an intracellular domain (Fortini, 2002). The proteolytic cleavage of notch liberates the intracellular domain which translocates to the nucleus and regulates gene expression through interactions with transcription factors (Fortini, 2002). The release of the notch intracellular domain is mediated by γ- secretase, a multi-subunit intramembrane proteolytic complex which is also implicated in the proteolytic processing of amyloid precursor protein (APP) (Fortini, 2002). APP is another cell surface transmembrane protein the cleavage of which by γ- secretase produces β-amyloid, the principle component of amyloid plaques, one of the neuropathological hallmarks of AD (Fortini, 2002).

Intercellular barriers are not formed solely by tight junctions but also by adherens junctions (AJs). Adherens junctions are also multiprotein complexes which are architecturally similar to tight junctions as they are composed of transmembrane proteins, known as cadherins, and cytoplasmic proteins, known as catenins (Meng and Takeichi, 2009). Catenins function similarly to tight junction cytoplasmic scaffolding proteins as they connect the membrane-associated cadherins with the actin cytoskeleton (Meng and Takeichi, 2009).

Classical cadherins are a family of cadherin proteins which structurally consist of an extracellular domain, a single transmembrane domain and a cytoplasmic domain (Shapiro and Weis, 2009). The extracellular domain is composed of five repeat subdomains known as extracellular cadherin (EC) domains with three calcium-binding site located at each interdomain region (Shapiro and Weis, 2009). The

extracellular domain mediates the calcium-dependent trans-oligomerisation of classical cadherin proteins (Shapiro and Weis, 2009).

Epithelial cadherin (E-cadherin) and neural cadherin (N-cadherin) are members of the classical cadherin family. The extracellular domain of E-cadherin is cleaved by matrix metalloproteases (MPPs) to produce E-cadherin N-terminal fragment 1 (E-cad/NTF1) and E-cadherin C-terminal fragment 1 (E-cad/CTF1) (Marambaud et al., 2002). E-cad/CTF1 consists of the E-cadherin transmembrane and cytoplasmic domains and remains associated with the cell membrane. E-cad/CTF1 is cleaved by γ-secretase to produce the cytoplasmic E-cadherin C-terminal fragment 2 (E-cad/CTF2) which has been shown to translocate to the nucleus in HEK 293 and MDCK cells (Ferber et al., 2008; Marambaud et al., 2002). The nuclear localisation of E-cad/CTF2 is enhanced by p120, a catenin protein (Ferber et al., 2008). The interaction with p120 enables E-cad/CTF2 to bind to DNA and also form a complex with the transcriptional repressor Kaiso which acts to suppress Kaiso as it prevents this transcription factor from binding to DNA (Ferber et al., 2008).

N-cadherin is also cleaved by γ-secretase to produce the cytoplasmic N-cadherin C-terminal fragment 1 (N-cad/CTF1) which binds to the CREB-binding protein (CBP) in the cytoplasm (Marambaud et al., 2003). CBP is a coactivator for the cyclic AMP response element binding protein (CREB) transcription factor. The interaction between N-cad/CTF1 and CBP promotes the degradation of this coactivator and the down-regulation of CREB-dependent transcription (Marambaud et al., 2003).

It would be worthwhile investigating whether occludin is cleaved in astrocytes. Occludin is known to be cleaved by MPPs resulting in a disruption of the intercellular barrier, however, the fragments produced by MPPs do not translocate to the nucleus (Casas et al., 2010; Nava et al., 2013). A possible interaction between occludin and γ-secretase could be explored given that this enzyme complex is involved in the proteolytic cleavage of other integral membrane proteins, although γ-secretase is considered to exclusively cleave single transmembrane proteins and occludin has a four-transmembrane MARVEL domain (Tolia and De Strooper, 2009). Calpains and caspases are also known to cleave integral membrane proteins so the relationship between occludin and these enzymes could also be explored.

Given that p120 catenin is implicated in the translocation of the E-cadherin fragment E-cad/CTF2 to the nucleus and enhances the interaction of this fragment with transcription factors, it might be possible that some tight junction cytoplasmic

scaffolding proteins might perform a similar function for occludin. ZO proteins are known to possess nuclear localisation and export signals and both ZO-1 and ZO-2 localise to the nucleus of MDCK cells (González-Mariscal et al., 1999; González-Mariscal et al., 2006; Islas et al., 2002). This study has also shown ZO-1 to localise to the nucleus of astrocytes. ZO-2 is also known to interact with the transcription factors Jun, Fos and C/EBP, as well as the pre-mRNA splicing protein SC-35 (Betanzos et al., 2004; Islas et al., 2002). The astrocytic expression of ZO-2 and the possible involvement of this protein in occludin nuclear translocation might be an interesting avenue to pursue in future research.

Initially, the expression of ZO-2 in astrocytes could be determined through ICC and western blotting. The possible co-localisation of occludin and ZO-2 in the nucleus of astrocytes could also be investigated by ICC. The subcellular localisation of E-cad/CTF2 was established by transfecting HEK 293 and MDCK cells with HA-tagged E-cad/CTF2 and immunostaining with an anti-HA antibody (Ferber et al., 2008). A similar approach could be used to determine the localisation of full length occludin and potential cleaved fragments such as occludin N- and C-terminal domains in astrocytes.

6.4 Neuronal TJP expression

The *in vivo* study also showed the cytoplasmic and nuclear expression of both occludin and ZO-1 in pyramidal neurons. The neuronal expression of occludin, claudin 5 and ZO-1 was subsequently investigated in human neuronal cells, LUHMES, by ICC. This *in vitro* study showed both occludin and ZO-1 to be expressed in the cytoplasm, nucleus and axons of LUHME cells, confirming the *in vivo* study.

The expression of tight junction proteins in neurons raises the same functional questions as the expression of these proteins in astrocytes, therefore, the same methodological approach utilised in this study could be applied to investigate the function of occludin in neurons. The pull-down protein binding assay developed in this study could be conducted using neuronal cell lysates and mass spectrometry analysis could again be utilised to identify putative protein binding partners for occludin in neurons. It would be particularly interesting to compare the putative occludin binding partner candidates identified from both astrocytes and neurons.

6.5 Concluding Remarks

This thesis has shown that tight junction proteins are expressed in non-epithelial cells and that these proteins possess functions beyond the tight junction complex. This study has succeeded in identifying putative occludin binding partners in astrocytes and although these findings have not been validated they provide a platform upon which future research into the function(s) of tight junction proteins in non-epithelial cells can be constructed.

7. Appendix

7.1 Occludin Immunoprecipitation

This section discloses a few examples of unsuccessful experiments to IP occludin from 1321N1 astrocytoma cells using the anti-occludin rabbit polyclonal antibody (Invitrogen) which had previously worked with HEK cells. Buffer composition for these experiments: 20 mM Tris-HCl, 150 mM NaCl, 1 mM EDTA, 1 mM DTT, 1% (v/v) Triton X-100, 0.5% (w/v) sodium deoxycholate, PIC, pH 7.5. 2 mg/ml of cell lysate and a boil elution was utilised in these experiments.

Figure 7.1 shows an occludin IP from 1321N1 astrocytoma cells in which a Rabbit IgG (vector laboratories) was used as a negative control. 12 µg of both antibodies was used in this IP. The negative control and occludin eluates are identical showing that the IP is not specific. Figure 7.2 shows an occludin IP from 1321N1 astrocytoma cells in which an anti-myc antibody (Abcam) was used as a negative control. 10 µg of both antibodies was used in this IP. The negative control and occludin eluates are again identical showing that the IP is not specific.

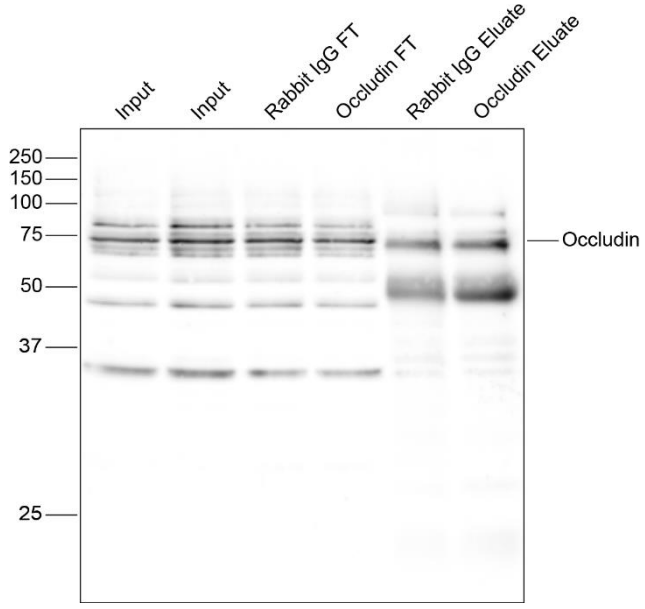

Figure 7.1: Occludin Immunoprecipitation from 1321N1 Astrocytoma Cells An occludin IP from 1321N1 astrocytoma cells using the anti-occludin rabbit polyclonal antibody. A rabbit IgG antibody was used as a negative control. The blot was probed with anti-occludin mouse monoclonal antibody.

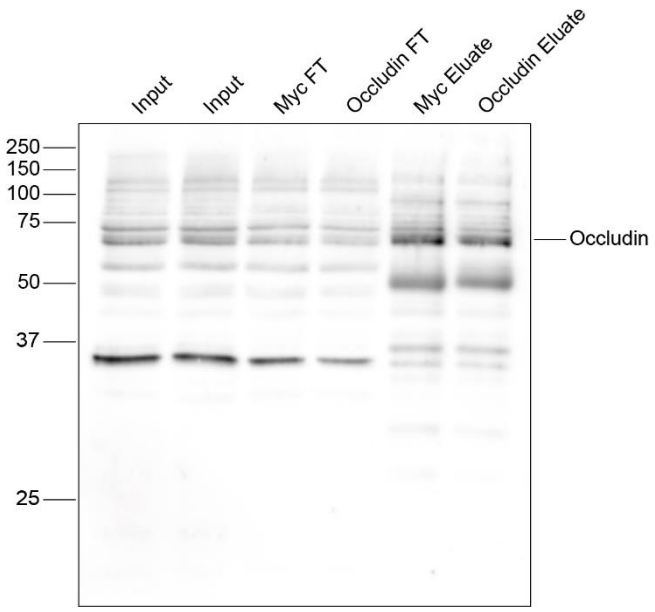

Figure 7.2: Occludin Immunoprecipitation from 1321N1 Astrocytoma Cells An occludin IP from 1321N1 astrocytoma cells using the anti-occludin rabbit polyclonal antibody. An anti-myc antibody was used as a negative control. The blot was probed with anti-occludin mouse monoclonal antibody.

8. References

Akoyev, V., and Takemoto, D.J. (2007). ZO-1 is required for protein kinase C gamma-driven disassembly of connexin 43. Cellular Signalling *19*, 958-967.

Alberto, P.-A., and Alfonso, A. (2013). Astrocyte-Neuron Interaction at Tripartite Synapses. Current Drug Targets *14*, 1220-1224.

Allen, N.J. (2014). Astrocyte Regulation of Synaptic Behavior. Annual Review of Cell and Developmental Biology *30*, 439-463.

Ambrosi, C., Gassmann, O., Pranskevich, J.N., Boassa, D., Smock, A., Wang, J., Dahl, G., Steinem, C., and Sosinsky, G.E. (2010). Pannexin1 and Pannexin2 Channels Show Quaternary Similarities to Connexons and Different Oligomerization Numbers from Each Other. Journal of Biological Chemistry *285*, 24420-24431.

Anderson, J.M., Stevenson, B.R., Jesaitis, L.A., Goodenough, D.A., and Mooseker, M.S. (1988). Characterization of ZO-1, a protein component of the tight junction from mouse liver and Madin-Darby canine kidney cells. The Journal of Cell Biology *106*, 1141-1149.

Ando-Akatsuka, Y., Saitou, M., Hirase, T., Kishi, M., Sakakibara, A., Itoh, M., Yonemura, S., Furuse, M., and Tsukita, S. (1996). Interspecies diversity of the occludin sequence: cDNA cloning of human, mouse, dog, and rat-kangaroo homologues. The Journal of Cell Biology *133*, 43-47.

Angelow, S., and Yu, A.S.L. (2009a). Cysteine Mutagenesis to Study the Structure of Claudin-2 Paracellular Pores. Annals of the New York Academy of Sciences *1165*, 143-147.

Angelow, S., and Yu, A.S.L. (2009b). Structure-Function Studies of Claudin Extracellular Domains by Cysteine-scanning Mutagenesis. Journal of Biological Chemistry *284*, 29205-29217.

Angus, A.G.N., Dalrymple, D., Boulant, S., McGivern, D.R., Clayton, R.F., Scott, M.J., Adair, R., Graham, S., Owsianka, A.M., Targett-Adams, P.*, et al.* (2010). Requirement of cellular DDX3 for hepatitis C virus replication is unrelated to its interaction with the viral core protein. The Journal of General Virology *91*, 122-132.

Araque, A., Li, N., Doyle, R.T., and Haydon, P.G. (2000). SNARE Protein-Dependent Glutamate Release from Astrocytes. The Journal of Neuroscience *20*, 666-673.

Araque, A., Parpura, V., Sanzgiri, R.P., and Haydon, P.G. (1999). Tripartite synapses: glia, the unacknowledged partner. Trends in Neurosciences *22*, 208-215.

Ariumi, Y., Kuroki, M., Abe, K.-i., Dansako, H., Ikeda, M., Wakita, T., and Kato, N. (2007). DDX3 DEAD-Box RNA Helicase Is Required for Hepatitis C Virus RNA Replication. Journal of Virology *81*, 13922-13926.

Askjaer, P., Jensen, T.H., Nilsson, J., Englmeier, L., and Kjems, J. (1998). The Specificity of the CRM1-Rev nuclear export signal interaction is mediated by RanGTP. The Journal of biological chemistry *273*, 33414-33422.

Bachi, A., Braun, I.C., Rodrigues, J.P., Panté, N., Ribbeck, K., von Kobbe, C., Kutay, U., Wilm, M., Görlich, D., Carmo-Fonseca, M.*, et al.* (2000). The C-terminal domain of TAP interacts with the nuclear pore complex and promotes export of specific CTE-bearing RNA substrates. RNA *6*, 136-158.

Bakker, E., Bühlmann, P., and Pretsch, E. (1997). Carrier-Based Ion-Selective Electrodes and Bulk Optodes. 1. General Characteristics. Chemical Reviews *97*, 3083-3132.

Balda, M.S., Garrett, M.D., and Matter, K. (2003). The ZO-1–associated Y-box factor ZONAB regulates epithelial cell proliferation and cell density. The Journal of Cell Biology *160*, 423-432.

Balda, M.S., and Matter, K. (2000). The tight junction protein ZO-1 and an interacting transcription factor regulate ErbB-2 expression. EMBO J *19*.

Bauer, H., Stelzhammer, W., Fuchs, R., Weiger, T.M., Danninger, C., Probst, G., and Krizbai, I.A. (1999). Astrocytes and Neurons Express the Tight Junction-Specific Protein Occludin in Vitro. Experimental Cell Research *250*, 434-438.

Beis, K., Whitfield, C., Booth, I., and Naismith, J.H. (2006). Two-step purification of outer membrane proteins. International Journal of Biological Macromolecules *39*, 10-14.

Bellmann, C., Schreivogel, S., Günther, R., Dabrowski, S., Schümann, M., Wolburg, H., and Blasig, I.E. (2014). Highly Conserved Cysteines Are Involved in the Oligomerization of Occludin—Redox Dependency of the Second Extracellular Loop. Antioxidants & Redox Signaling *20*, 855-867.

Belotserkovskaya, R., Saunders, A., Lis, J.T., and Reinberg, D. (2004). Transcription through chromatin: understanding a complex FACT. Biochimica et Biophysica Acta (BBA) - Gene Structure and Expression *1677*, 87-99.

Betanzos, A., Huerta, M., Lopez-Bayghen, E., Azuara, E., Amerena, J., and González-Mariscal, L. (2004). The tight junction protein ZO-2 associates with Jun, Fos and C/EBP transcription factors in epithelial cells. Experimental Cell Research *292*, 51-66.

Bezzi, P., Gundersen, V., Jos?uis, G., Seifert, G., Christian, S.e., Pilati, E., and Volterra, A. (2004). Astrocytes contain a vesicular compartment that is competent for regulated exocytosis of glutamate. Nature Neuroscience *7*, 613-620.

Biber, K., Laurie, D.J., Berthele, A., Sommer, B., Tölle, T.R., Gebicke-Härter, P.-J., Van Calker, D., and Boddeke, H.W.G.M. (1999). Expression and Signaling of Group I Metabotropic Glutamate Receptors in Astrocytes and Microglia. Journal of Neurochemistry *72*, 1671-1680.

Birukova, A.A., Zagranichnaya, T., Fu, P., Alekseeva, E., Chen, W., Jacobson, J.R., and Birukov, K.G. (2007). Prostaglandins PGE2 and PGI2 promote endothelial barrier enhancement via PKA- and Epac1/Rap1-dependent Rac activation. Experimental Cell Research *313*, 2504-2520.

Bogerd, H.P., Benson, R.E., Truant, R., Herold, A., Phingbodhipakkiya, M., and Cullen, B.R. (1999). Definition of a Consensus Transportin-specific Nucleocytoplasmic Transport Signal. The Journal of biological chemistry *274*, 9771-9777.

Bradley, S.J., and Challiss, R.A.J. (2012). G protein-coupled receptor signalling in astrocytes in health and disease: A focus on metabotropic glutamate receptors. Biochemical Pharmacology *84*, 249-259.

Browne, G.J., and Proud, C.G. (2002). Regulation of peptide-chain elongation in mammalian cells. European Journal of Biochemistry *269*, 5360-5368.

Burd, C.G., Swanson, M.S., Görlach, M., and Dreyfuss, G. (1989). Primary structures of the heterogeneous nuclear ribonucleoprotein A2, B1, and C2 proteins: a diversity of RNA binding proteins is generated by small peptide inserts. Proceedings of the National Academy of Sciences of the United States of America *86*, 9788-9792.

Butt, A.M., Feng, D., Nasrullah, I., Tahir, S., Idrees, M., Tong, Y., and Lu, J. (2012a). Computational identification of interplay between phosphorylation and O-β-glycosylation of human occludin as potential mechanism to impair hepatitis C virus entry. Infection, Genetics and Evolution *12*, 1235-1245.

Butt, A.M., Khan, I.B., Hussain, M., Idress, M., Lu, J., and Tong, Y. (2012b). Role of post translational modifications and novel crosstalk between

phosphorylation and O-beta-GlcNAc modifications in human claudin-1, -3 and -4. Molecular Biology Reports *39*, 1359-1369.

Carpenter, B., MacKay, C., Alnabulsi, A., MacKay, M., Telfer, C., Melvin, W.T., and Murray, G.I. (2006). The roles of heterogeneous nuclear ribonucleoproteins in tumour development and progression. Biochimica et Biophysica Acta (BBA) - Reviews on Cancer *1765*, 85-100.

Casas, E., Barron, C., Francis, S.A., McCormack, J.M., McCarthy, K.M., Schneeberger, E.E., and Lynch, R.D. (2010). Cholesterol efflux stimulates metalloproteinase-mediated cleavage of occludin and release of extracellular membrane particles containing its C-terminal fragments. Experimental Cell Research *316*, 353-365.

Chiba, H., Osanai, M., Murata, M., Kojima, T., and Sawada, N. (2008). Transmembrane proteins of tight junctions. Biochimica et Biophysica Acta (BBA) - Biomembranes *1778*, 588-600.

Chow, B.W., and Gu, C. (2015). The Molecular Constituents of the Blood-Brain Barrier. Trends in Neurosciences *38*, 598-608.

Christie, M., Chang, C.-W., Róna, G., Smith, K.M., Stewart, A.G., Takeda, A.A.S., Fontes, M.R.M., Stewart, M., Vértessy, B.G., Forwood, J.K.*, et al.* (2015). Structural Biology and Regulation of Protein Import into the Nucleus. Journal of Molecular Biology.

Colegio, O.R., Van Itallie, C.M., McCrea, H.J., Rahner, C., and Anderson, J.M. (2002). Claudins create charge-selective channels in the paracellular pathway between epithelial cells. American Journal of Physiology - Cell Physiology *283*, C142-C147.

Colombo, S.L., Palacios-Callender, M., Frakich, N., Carcamo, S., Kovacs, I., Tudzarova, S., and Moncada, S. (2011). Molecular basis for the differential use of glucose and glutamine in cell proliferation as revealed by synchronized HeLa cells. Proceedings of the National Academy of Sciences *108*, 21069-21074.

Conti, F., Minelli, A., and Melone, M. (2004). GABA transporters in the mammalian cerebral cortex: localization, development and pathological implications. Brain Research Reviews *45*, 196-212.

Daugherty, B.L., Ward, C., Smith, T., Ritzenthaler, J.D., and Koval, M. (2007). Regulation of heterotypic claudin compatibility. The Journal of biological chemistry *282*, 30005-30013.

De Bock, M., Decrock, E., Wang, N., Bol, M., Vinken, M., Bultynck, G., and Leybaert, L. (2014). The dual face of connexin-based astroglial Ca2 +

communication: A key player in brain physiology and a prime target in pathology. Biochimica et Biophysica Acta (BBA) - Molecular Cell Research *1843*, 2211-2232.

De Bock, M., Van Haver, V., Vandenbroucke, R.E., Decrock, E., Wang, N., and Leybaert, L. (2016). Into rather unexplored terrain—transcellular transport across the blood–brain barrier. Glia *64*, 1097-1123.

Decrock, E., Bock, M., Wang, N., Bultynck, G., Giaume, C., Naus, C.C., Green, C.R., and Leybaert, L. (2015). Connexin and pannexin signaling pathways, an architectural blueprint for CNS physiology and pathology? Cellular and Molecular Life Sciences *72*, 2823-2851.

Dermietzel, R., Hertberg, E., Kessler, J., and Spray, D. (1991). Gap junctions between cultured astrocytes: immunocytochemical, molecular, and electrophysiological analysis. The Journal of Neuroscience *11*, 1421-1432.

Dreyfuss, G., Kim, V.N., and Kataoka, N. (2002). Messenger-RNA-binding proteins and the messages they carry. Nat Rev Mol Cell Biol *3*, 195-205.

Dubuisson, J., and Cosset, F.-L. (2014). Virology and cell biology of the hepatitis C virus life cycle – An update. Journal of Hepatology *61*, S3-S13.

Duffy, H.S., Ashton, A.W., O'Donnell, P., Coombs, W., Taffet, S.M., Delmar, M., and Spray, D.C. (2004). Regulation of Connexin43 Protein Complexes by Intracellular Acidification. Circulation Research *94*, 215-222.

Duffy, H.S., John, G.R., Lee, S.C., Brosnan, C.F., and Spray, D.C. (2000). Reciprocal Regulation of the Junctional Proteins Claudin-1 and Connexin43 by Interleukin-1 beta in Primary Human Fetal Astrocytes. The Journal of Neuroscience *20*, 1-6.

Elias, B.C., Suzuki, T., Seth, A., Giorgianni, F., Kale, G., Shen, L., Turner, J.R., Naren, A., Desiderio, D.M., and Rao, R. (2009). Phosphorylation of Tyr-398 and Tyr-402 in Occludin Prevents Its Interaction with ZO-1 and Destabilizes Its Assembly at the Tight Junctions. Journal of Biological Chemistry *284*, 1559-1569.

Erdahl, W.L., Chapman, C.J., Wang, E., Taylor, R.W., and Pfeiffer, D.R. (1996). Ionophore 4-BrA23187 Transports Zn2+ and Mn2+ with High Selectivity Over Ca2+ Biochemistry *35*, 13817-13825.

Evans, M.J., von Hahn, T., Tscherne, D.M., Syder, A.J., Panis, M., Wolk, B., Hatziioannou, T., McKeating, J.A., Bieniasz, P.D., and Rice, C.M. (2007). Claudin-1 is a hepatitis C virus co-receptor required for a late step in entry. Nature *446*, 801-805.

Ezan, P., André, P., Cisternino, S., Saubaméa, B., Boulay, A.-C., Doutremer, S., Thomas, M.-A., Quenech'du, N., Giaume, C., and Cohen-Salmon, M. (2012). Deletion of Astroglial Connexins Weakens the Blood–Brain Barrier. Journal of Cerebral Blood Flow & Metabolism *32*, 1457-1467.

Fairman-Williams, M.E., Guenther, U.-P., and Jankowsky, E. (2010). SF1 and SF2 helicases: family matters. Current Opinion in Structural Biology *20*, 313-324.

Fanning, A.S., Jameson, B.J., Jesaitis, L.A., and Anderson, J.M. (1998). The Tight Junction Protein ZO-1 Establishes a Link between the Transmembrane Protein Occludin and the Actin Cytoskeleton. Journal of Biological Chemistry *273*, 29745-29753.

Fanning, A.S., Little, B.P., Rahner, C., Utepbergenov, D., Walther, Z., and Anderson, J.M. (2007). The Unique-5 and -6 Motifs of ZO-1 Regulate Tight Junction Strand Localization and Scaffolding Properties. Molecular Biology of the Cell *18*, 721-731.

Fanning, A.S., Ma, T.Y., and Anderson, J.M. (2002). Isolation and functional characterization of the actin-binding region in the tight junction protein ZO-1. The FASEB Journal.

Feller, S.M., Ren, R., Hanafusa, H., and Baltimore, D. (1994). SH2 and SH3 domains as molecular adhesives: the interactions of Crk and Abl. Trends in Biochemical Sciences *19*, 453-458.

Ferber, E.C., Kajita, M., Wadlow, A., Tobiansky, L., Niessen, C., Ariga, H., Daniel, J., and Fujita, Y. (2008). A Role for the Cleaved Cytoplasmic Domain of E-cadherin in the Nucleus. The Journal of biological chemistry *283*, 12691-12700.

Filosa, J.A., Bonev, A.D., Straub, S.V., Meredith, A.L., Wilkerson, M.K., Aldrich, R.W., and Nelson, M.T. (2006). Local potassium signaling couples neuronal activity to vasodilation in the brain. Nature Neuroscience *9*, 1397-1403.

Filosa, J.A., Morrison, H.W., Iddings, J.A., Du, W., and Kim, K.J. (2016). Beyond neurovascular coupling, role of astrocytes in the regulation of vascular tone. Neuroscience *323*, 96-109.

Fortini, M.E. (2002). [gamma]-Secretase-mediated proteolysis in cell-surface-receptor signalling. Nat Rev Mol Cell Biol *3*, 673-684.

Foskett, J.K., White, C., Cheung, K.-H., and Mak, D.-O.D. (2007). Inositol Trisphosphate Receptor Ca2+ Release Channels. Physiological Reviews *87*, 593-658.

Fountoulakis, M., and Gasser, R. (2003). Proteomic analysis of the cell envelope fraction of Escherichia coli. Amino Acids *24*, 19-41.

Fredriksson, K., Van Itallie, C.M., Aponte, A., Gucek, M., Tietgens, A.J., and Anderson, J.M. (2015). Proteomic Analysis of Proteins Surrounding Occludin and Claudin-4 Reveals Their Proximity to Signaling and Trafficking Networks. PLoS ONE *10*, e0117074.

Fujibe, M., Chiba, H., Kojima, T., Soma, T., Wada, T., Yamashita, T., and Sawada, N. (2004). Thr203 of claudin-1, a putative phosphorylation site for MAP kinase, is required to promote the barrier function of tight junctions. Experimental Cell Research *295*, 36-47.

Furuse, M., Fujita, K., Hiiragi, T., Fujimoto, K., and Tsukita, S. (1998a). Claudin-1 and -2: novel integral membrane proteins localizing at tight junctions with no sequence similarity to occludin. J Cell Biol *141*.

Furuse, M., Hirase, T., Itoh, M., Nagafuchi, A., Yonemura, S., and Tsukita, S. (1993). Occludin: a novel integral membrane protein localizing at tight junctions. The Journal of Cell Biology *123*, 1777-1788.

Furuse, M., Itoh, M., Hirase, T., Nagafuchi, A., Yonemura, S., Tsukita, S., and Tsukita, S. (1994). Direct association of occludin with ZO-1 and its possible involvement in the localization of occludin at tight junctions. The Journal of Cell Biology *127*, 1617-1626.

Furuse, M., Sasaki, H., Fujimoto, K., and Tsukita, S. (1998b). A single gene product, claudin-1 or -2, reconstitutes tight junction strands and recruits occludin in fibroblasts. J Cell Biol *143*.

Furuse, M., Sasaki, H., and Tsukita, S. (1999). Manner of Interaction of Heterogeneous Claudin Species within and between Tight Junction Strands. The Journal of Cell Biology *147*, 891-903.

Garrido-urbani, S., Bradfield, P.F., and Imhof, B.A. (2014). Tight junction dynamics: the role of junctional adhesion molecules (JAMs). Cell and Tissue Research *355*, 701-715.

Gee, K.R., Brown, K.A., Chen, W.N.U., Bishop-Stewart, J., Gray, D., and Johnson, I. (2000). Chemical and physiological characterization of fluo-4 Ca2+-indicator dyes. Cell Calcium *27*, 97-106.

Geissler, R., Golbik, R.P., and Behrens, S.-E. (2012). The DEAD-box helicase DDX3 supports the assembly of functional 80S ribosomes. Nucleic Acids Research *40*, 4998-5011.

Giaume, C., Leybaert, L., Naus, C., C, and Sáez, J.-C. (2013). Connexin and pannexin hemichannels in brain glial cells: properties, pharmacology and roles. Frontiers in Pharmacology *4*.

Gibbons, H.M., and Dragunow, M. (2010). Adult human brain cell culture for neuroscience research. The International Journal of Biochemistry & Cell Biology *42*, 844-856.

Giepmans, B.N.G., and Moolenaar, W.H. (1998). The gap junction protein connexin43 interacts with the second PDZ domain of the zona occludens-1 protein. Current Biology *8*, 931-934.

Gilleron, J., Fiorini, C., Carette, D., Avondet, C., Falk, M.M., Segretain, D., and Pointis, G. (2008). Molecular reorganization of Cx43, Zo-1 and Src complexes during the endocytosis of gap junction plaques in response to a non-genomic carcinogen. Journal of Cell Science *121*, 4069-4078.

González-Mariscal, L., Betanzos, A., and Ávila-Flores, A. (2000). MAGUK proteins: structure and role in the tight junction. Seminars in Cell & Developmental Biology *11*, 315-324.

González-Mariscal, L., Islas, S., Contreras, R.G., Garcı, amp, x, a-Villegas, M.R., Betanzos, A., Vega, J., Diaz-Quiñónez, A.*, et al.* (1999). Molecular Characterization of the Tight Junction Protein ZO-1 in MDCK Cells. Experimental Cell Research *248*, 97-109.

González-Mariscal, L., Ponce, A., Alarcón, L., and Jaramillo, B.E. (2006). The tight junction protein ZO-2 has several functional nuclear export signals. Experimental Cell Research *312*, 3323-3335.

Gordon, G.R.J., Choi, H.B., Ellis-Davies, G.C.R., and MacVicar, B.A. (2008). Brain metabolic state dictates the polarity of astrocyte control over the cerebrovasculature. Nature *456*, 745-749.

Grigelioniene, G., Blennow, M., Torok, C., Fried, G., Dahlin, I., Lendahl, U., and Lagercrantz, H. (1996). Cerebrospinal Fluid of Newborn Infants Contains a Deglycosylated Form of the Intermediate Filament Nestin. Pediatr Res *40*, 809-814.

Grynkiewicz, G., Poenie, M., and Tsien, R.Y. (1985). A new generation of Ca2+ indicators with greatly improved fluorescence properties. Journal of Biological Chemistry *260*, 3440-3450.

Guillemot, L., Paschoud, S., Pulimeno, P., Foglia, A., and Citi, S. (2008). The cytoplasmic plaque of tight junctions: A scaffolding and signalling center. Biochimica et Biophysica Acta (BBA) - Biomembranes *1778*, 601-613.

Günzel, D., and Yu, A.S.L. (2013). Claudins and the Modulation of Tight Junction Permeability. Physiological Reviews *93*, 525-569.

Guzik, B.W., Levesque, L., Prasad, S., Bor, Y.-C., Black, B.E., Paschal, B.M., Rekosh, D., and Hammarskjöld, M.-L. (2001). NXT1 (p15) Is a Crucial Cellular Cofactor in TAP-Dependent Export of Intron-Containing RNA in Mammalian Cells. Molecular and Cellular Biology *21*, 2545-2554.

Haltiwanger, R.S., Busby, S., Grove, K., Li, S., Mason, D., Medina, L., Moloney, D., Philipsberg, G., and Scartozzi, R. (1997). O-Glycosylation of Nuclear and Cytoplasmic Proteins: Regulation Analogous to Phosphorylation? Biochemical and Biophysical Research Communications *231*, 237-242.

Haseloff, R.F., Dithmer, S., Winkler, L., Wolburg, H., and Blasig, I.E. (2015). Transmembrane proteins of the tight junctions at the blood–brain barrier: Structural and functional aspects. Seminars in Cell & Developmental Biology *38*, 16-25.

Haskins, J., Gu, L., Wittchen, E.S., Hibbard, J., and Stevenson, B.R. (1998). ZO-3, a Novel Member of the MAGUK Protein Family Found at the Tight Junction, Interacts with ZO-1 and Occludin. The Journal of Cell Biology *141*, 199-208.

Hatfield, J.T., Rothnagel, J.A., and Smith, R. (2002). Characterization of the mouse hnRNP A2/B1/B0 gene and identification of processed pseudogenes. Gene *295*, 33-42.

Haustein, M.D., Kracun, S., Lu, X.-H., Shih, T., Jackson-Weaver, O., Tong, X., Xu, J., Yang, X.W., O'Dell, T.J., Marvin, J.S.*, et al.* (2014). Conditions and constraints for astrocyte calcium signaling in the hippocampal mossy fiber pathway. Neuron *82*, 413-429.

Henderson, B.R., and Percipalle, P. (1997). Interactions between HIV rev and nuclear import and export factors: the rev nuclear localisation signal mediates specific binding to human importin-β1. Journal of Molecular Biology *274*, 693-707.

Hinnebusch, A.G. (2014). The Scanning Mechanism of Eukaryotic Translation Initiation. Annual Review of Biochemistry *83*, 779-812.

Holtzclaw, L.A., Pandhit, S., Bare, D.J., Mignery, G.A., and Russell, J.T. (2002). Astrocytes in adult rat brain express type 2 inositol 1,4,5-trisphosphate receptors. Glia *39*, 69-84.

Hou, J., Renigunta, A., Konrad, M., Gomes, A.S., Schneeberger, E.E., Paul, D.L., Waldegger, S., and Goodenough, D.A. (2008). Claudin-16 and claudin-

19 interact and form a cation-selective tight junction complex. The Journal of Clinical Investigation *118*, 619-628.

Hou, J., Renigunta, A., Yang, J., and Waldegger, S. (2010). Claudin-4 forms paracellular chloride channel in the kidney and requires claudin-8 for tight junction localization. Proceedings of the National Academy of Sciences of the United States of America *107*, 18010-18015.

Howarth, A.G., Hughes, M.R., and Stevenson, B.R. (1992). Detection of the tight junction-associated protein ZO-1 in astrocytes and other nonepithelial cell types. American Journal of Physiology - Cell Physiology *262*, C461-C469.

Howarth, A.G., Singer, K.L., and Stevenson, B.R. (1994). Analysis of the distribution and phosphorylation state of ZO-1 in MDCK and nonepithelial cells. The Journal of Membrane Biology *137*, 261-270.

Hu, X., Yuan, Y., Wang, D., and Su, Z. (2016). Heterogeneous astrocytes: Active players in CNS. Brain Research Bulletin *125*, 1-18.

Huerta, M., Muñoz, R., Tapia, R., Soto-Reyes, E., Ramírez, L., Recillas-Targa, F., González-Mariscal, L., and López-Bayghen, E. (2007). Cyclin D1 Is Transcriptionally Down-Regulated by ZO-2 via an E Box and the Transcription Factor c-Myc. Molecular Biology of the Cell *18*, 4826-4836.

Hunter, A.W., Barker, R.J., Zhu, C., and Gourdie, R.G. (2005). Zonula Occludens-1 Alters Connexin43 Gap Junction Size and Organization by Influencing Channel Accretion. Molecular Biology of the Cell *16*, 5686-5698.

Huo, L., Wen, W., Wang, R., Kam, C., Xia, J., Feng, W., and Zhang, M. (2011). Cdc42-dependent formation of the ZO-1/MRCKβ complex at the leading edge controls cell migration. The EMBO Journal *30*, 665-678.

Ikenouchi, J., Furuse, M., Furuse, K., Sasaki, H., and Tsukita, S. (2005). Tricellulin constitutes a novel barrier at tricellular contacts of epithelial cells. J Cell Biol *171*.

Inagaki, M., Irie, K., Deguchi-Tawarada, M., Ikeda, W., Ohtsuka, T., Takeuchi, M., and Takai, Y. (2003). Nectin-dependent localization of ZO-1 at puncta adhaerentia junctions between the mossy fiber terminals and the dendrites of the pyramidal cells in the CA3 area of adult mouse hippocampus. The Journal of Comparative Neurology *460*, 514-524.

Ishizaki, T., Chiba, H., Kojima, T., Fujibe, M., Soma, T., Miyajima, H., Nagasawa, K., Wada, I., and Sawada, N. (2003). Cyclic AMP induces phosphorylation of claudin-5 immunoprecipitates and expression of claudin-5

gene in blood–brain-barrier endothelial cells via protein kinase A-dependent and -independent pathways. Experimental Cell Research *290*, 275-288.

Islas, S., Vega, J., Ponce, L., and González-Mariscal, L. (2002). Nuclear Localization of the Tight Junction Protein ZO-2 in Epithelial Cells. Experimental Cell Research *274*, 138-148.

Itoh, M., Furuse, M., Morita, K., Kubota, K., Saitou, M., and Tsukita, S. (1999). Direct Binding of Three Tight Junction-Associated Maguks, Zo-1, Zo-2, and Zo-3, with the Cooh Termini of Claudins. The Journal of Cell Biology *147*, 1351-1363.

Jankowsky, E. (2011). RNA helicases at work: binding and rearranging. Trends in Biochemical Sciences *36*, 19-29.

Jaramillo, B.E., Ponce, A., Moreno, J., Betanzos, A., Huerta, M., Lopez-Bayghen, E., and Gonzalez-Mariscal, L. (2004). Characterization of the tight junction protein ZO-2 localized at the nucleus of epithelial cells. Experimental Cell Research *297*, 247-258.

Jeftinija, S.D., Jeftinija, K.V., and Stefanovic, G. (1997). Cultured astrocytes express proteins involved in vesicular glutamate release. Brain Research *750*, 41-47.

Jesaitis, L., and Goodenough, D. (1994). Molecular characterization and tissue distribution of ZO-2, a tight junction protein homologous to ZO-1 and the Drosophila discs-large tumor suppressor protein. The Journal of Cell Biology *124*, 949-961.

Jiang, S., Yuan, H., Duan, L., Cao, R., Gao, B., Xiong, Y.-F., and Rao, Z.-R. (2011). Glutamate release through connexin 43 by cultured astrocytes in a stimulated hypertonicity model. Brain Research *1392*, 8-15.

Jose, J., Betscheider, D., and Zangen, D. (2005). Bacterial surface display library screening by target enzyme labeling: Identification of new human cathepsin G inhibitors. Analytical Biochemistry *346*, 258-267.

Kahraman, S., Bambrick, L.L., and Fiskum, G. (2011). Effects of FK506 and cyclosporin a on calcium ionophore-induced mitochondrial depolarization and cytosolic calcium in astrocytes and neurons. Journal of Neuroscience Research *89*, 1973-1978.

Kamma, H., Horiguchi, H., Wan, L., Matsui, M., Fujiwara, M., Fujimoto, M., Yazawa, T., and Dreyfuss, G. (1999). Molecular Characterization of the hnRNP A2/B1 Proteins: Tissue-Specific Expression and Novel Isoforms. Experimental Cell Research *246*, 399-411.

Kanemaru, K., Sekiya, H., Xu, M., Satoh, K., Kitajima, N., Yoshida, K., Okubo, Y., Sasaki, T., Moritoh, S., Hasuwa, H.*, et al.* (2014). In Vivo Visualization of Subtle, Transient, and Local Activity of Astrocytes Using an Ultrasensitive Ca2+ Indicator. Cell Reports *8*, 311-318.

Kang, J., Kang, N., Lovatt, D., Torres, A., Zhao, Z., Lin, J., and Nedergaard, M. (2008). Connexin 43 Hemichannels Are Permeable to ATP. The Journal of Neuroscience *28*, 4702-4711.

Kao, J.P., Harootunian, A.T., and Tsien, R.Y. (1989). Photochemically generated cytosolic calcium pulses and their detection by fluo-3. Journal of Biological Chemistry *264*, 8179-8184.

Katahira, J., Sträßer, K., Podtelejnikov, A., Mann, M., Jung, J.U., and Hurt, E. (1999). The Mex67p-mediated nuclear mRNA export pathway is conserved from yeast to human. The EMBO Journal *18*, 2593-2609.

Kausalya, P.J., Reichert, M., and Hunziker, W. (2001). Connexin45 directly binds to ZO-1 and localizes to the tight junction region in epithelial MDCK cells. FEBS Letters *505*, 92-96.

KAY, B.K., WILLIAMSON, M.P., and SUDOL, M. (2000). The importance of being proline: the interaction of proline-rich motifs in signaling proteins with their cognate domains. The FASEB Journal *14*, 231-241.

Kelly, W.G., Dahmus, M.E., and Hart, G.W. (1993). RNA polymerase II is a glycoprotein. Modification of the COOH-terminal domain by O-GlcNAc. Journal of Biological Chemistry *268*, 10416-10424.

Kjems, J., Brown, M., Chang, D.D., and Sharp, P.A. (1991). Structural analysis of the interaction between the human immunodeficiency virus Rev protein and the Rev response element. Proceedings of the National Academy of Sciences of the United States of America *88*, 683-687.

Kohaar, I., Ploss, A., Korol, E., Mu, K., Schoggins, J.W., O'Brien, T.R., Rice, C.M., and Prokunina-Olsson, L. (2010). Splicing Diversity of the Human OCLN Gene and Its Biological Significance for Hepatitis C Virus Entry. Journal of Virology *84*, 6987-6994.

Köller, H., Trimborn, M., von Giesen, H.-J., Schroeter, M., and Arendt, G. (2001). TNFα reduces glutamate induced intracellular Ca2+ increase in cultured cortical astrocytes. Brain Research *893*, 237-243.

Komaki, R., Togashi, H., and Takai, Y. (2013). Regulation of Dendritic Filopodial Interactions by ZO-1 and Implications for Dendrite Morphogenesis. PLoS ONE *8*, e76201.

Kozu, T., Henrich, B., and Schäfer, K.P. (1995). Structure and expression of the gene (HNRPA2B1) encoding the human hnRNP protein A2/B1. Genomics *25*, 365-371.

Krause, G., Protze, J., and Piontek, J. (2015). Assembly and function of claudins: Structure–function relationships based on homology models and crystal structures. Seminars in Cell & Developmental Biology *42*, 3-12.

Krause, G., Winkler, L., Mueller, S.L., Haseloff, R.F., Piontek, J., and Blasig, I.E. (2008). Structure and function of claudins. Biochimica et Biophysica Acta (BBA) - Biomembranes *1778*, 631-645.

Krecic, A.M., and Swanson, M.S. (1999). hnRNP complexes: composition, structure, and function. Current Opinion in Cell Biology *11*, 363-371.

Kreft, M., Stenovec, M., Rupnik, M., Grilc, S., Kržan, M., Potokar, M., Pangršič, T., Haydon, P.G., and Zorec, R. (2004). Properties of Ca2+-dependent exocytosis in cultured astrocytes. Glia *46*, 437-445.

Krug, S.M., Günzel, D., Conrad, M.P., Rosenthal, R., Fromm, A., Amasheh, S., Schulzke, J.D., and Fromm, M. (2012). Claudin-17 forms tight junction channels with distinct anion selectivity. Cellular and Molecular Life Sciences *69*, 2765-2778.

Kyratzi, E., and Efthimiopoulos, S. (2014). Calcium regulates the interaction of amyloid precursor protein with Homer3 protein. Neurobiology of Aging *35*, 2053-2063.

Lai, M.-C., Lee, Y.-H.W., and Tarn, W.-Y. (2008). The DEAD-Box RNA Helicase DDX3 Associates with Export Messenger Ribonucleoproteins as well asTip-associated Protein and Participates in Translational Control. Molecular Biology of the Cell *19*, 3847-3858.

Lai, M.-C., Wang, S.-W., Cheng, L., Tarn, W.-Y., Tsai, S.-J., and Sun, H.S. (2013). Human DDX3 Interacts with the HIV-1 Tat Protein to Facilitate Viral mRNA Translation. PLoS ONE *8*, e68665.

Lalo, U., Pankratov, Y., Parpura, V., and Verkhratsky, A. (2011). Ionotropic receptors in neuronal–astroglial signalling: What is the role of “excitable” molecules in non-excitable cells. Biochimica et Biophysica Acta (BBA) - Molecular Cell Research *1813*, 992-1002.

Langley, K.E., Berg, T.F., Strickland, T.W., Fenton, D.M., Boone, T.C., and Wypych, J. (1987). Recombinant-DNA-derived bovine growth hormone from Escherichia coli. European Journal of Biochemistry *163*, 313-321.

Lee, A., and Pow, D.V. (2010). Astrocytes: Glutamate transport and alternate splicing of transporters. The International Journal of Biochemistry & Cell Biology *42*, 1901-1906.

Lee, H.C., Choe, J., Chi, S.-G., and Kim, Y.K. (2009). Exon junction complex enhances translation of spliced mRNAs at multiple steps. Biochemical and Biophysical Research Communications *384*, 334-340.

Lee, M., Schwab, C., and McGeer, P.L. (2011). Astrocytes are GABAergic cells that modulate microglial activity. Glia *59*, 152-165.

Li, J., Zhuo, M., Pei, L., Rajagopal, M., and Yu, A.S.L. (2014). Comprehensive Cysteine-scanning Mutagenesis Reveals Claudin-2 Pore-lining Residues with Different Intrapore Locations. Journal of Biological Chemistry *289*, 6475-6484.

Li, J., Zhuo, M., Pei, L., and Yu, A.S.L. (2013). Conserved Aromatic Residue Confers Cation Selectivity in Claudin-2 and Claudin-10b. Journal of Biological Chemistry *288*, 22790-22797.

Li, X., Olson, C., Lu, S., Kamasawa, N., Yasumura, T., Rash, J.E., and Nagy, J.I. (2004). Neuronal connexin36 association with zonula occludens-1 protein (ZO-1) in mouse brain and interaction with the first PDZ domain of ZO-1. European Journal of Neuroscience *19*, 2132-2146.

Li, X., Zima, A.V., Sheikh, F., Blatter, L.A., and Chen, J. (2005a). Endothelin-1-Induced Arrhythmogenic Ca2+ Signaling Is Abolished in Atrial Myocytes of Inositol-1,4,5-Trisphosphate(IP3)-Receptor Type 2-Deficient Mice. Circulation Research *96*, 1274-1281.

Li, Y., Fanning, A.S., Anderson, J.M., and Lavie, A. (2005b). Structure of the Conserved Cytoplasmic C-terminal Domain of Occludin: Identification of the ZO-1 Binding Surface. Journal of Molecular Biology *352*, 151-164.

Liebner, S., Fischmann, A., Rascher, G., Duffner, F., Grote, E.-H., Kalbacher, H., and Wolburg, H. (2000). Claudin-1 and claudin-5 expression and tight junction morphology are altered in blood vessels of human glioblastoma multiforme. Acta Neuropathologica *100*, 323-331.

Linder, P., Lasko, P.F., Ashburner, M., Leroy, P., Nielsen, P.J., Nishi, K., Schnier, J., and Slonimski, P.P. (1989). Birth of the D-E-A-D box. Nature *337*, 121-122.

Liu, S., Kuo, W., Yang, W., Liu, W., Gibson, G.A., Dorko, K., Watkins, S.C., Strom, S.C., and Wang, T. (2010). The second extracellular loop dictates Occludin-mediated HCV entry. Virology *407*, 160-170.

Liu, S., Yang, W., Shen, L., Turner, J.R., Coyne, C.B., and Wang, T. (2009). Tight Junction Proteins Claudin-1 and Occludin Control Hepatitis C Virus Entry and Are Downregulated during Infection To Prevent Superinfection. Journal of Virology *83*, 2011-2014.

Lotharius, J., Falsig, J., van Beek, J., Payne, S., Dringen, R., Brundin, P., and Leist, M. (2005). Progressive Degeneration of Human Mesencephalic Neuron-Derived Cells Triggered by Dopamine-Dependent Oxidative Stress Is Dependent on the Mixed-Lineage Kinase Pathway. The Journal of Neuroscience *25*, 6329-6342.

Lynch, R.D., Francis, S.A., McCarthy, K.M., Casas, E., Thiele, C., and Schneeberger, E.E. (2007). Cholesterol depletion alters detergent-specific solubility profiles of selected tight junction proteins and the phosphorylation of occludin. Experimental Cell Research *313*, 2597-2610.

Ma, A., Moran-Jones, K., Shan, J., Munro, T., Snee, M., Hoek, K., and Smith, R. (2002). Heterogeneous Nuclear Ribonucleoprotein A3, a novel RNA Trafficking Response Element-binding Protein. The Journal of biological chemistry *277*, 18010-18020.

Malim, M.H., Hauber, J., Le, S.-Y., Maizel, J.V., and Cullen, B.R. (1989). The HIV-1 rev trans-activator acts through a structured target sequence to activate nuclear export of unspliced viral mRNA. Nature *338*, 254-257.

Mamiya, N., and Worman, H. (1999). Hepatitis C virus core protein binds to a DEAD box RNA helicase. J Biol Chem *274*, 15751-15756.

Mandel, I., Paperna, T., Volkowich, A., Merhav, M., Glass-Marmor, L., and Miller, A. (2012). The ubiquitin–proteasome pathway regulates claudin 5 degradation. Journal of Cellular Biochemistry *113*, 2415-2423.

Mankertz, J., Stefan Waller, J., Hillenbrand, B., Tavalali, S., Florian, P., Schöneberg, T., Fromm, M., and Dieter Schulzke, J. (2002). Gene expression of the tight junction protein occludin includes differential splicing and alternative promoter usage. Biochemical and Biophysical Research Communications *298*, 657-666.

Marambaud, P., Shioi, J., Serban, G., Georgakopoulos, A., Sarner, S., Nagy, V., Baki, L., Wen, P., Efthimiopoulos, S., Shao, Z.*, et al.* (2002). A presenilin-1/γ-secretase cleavage releases the E-cadherin intracellular domain and regulates disassembly of adherens junctions. The EMBO Journal *21*, 1948-1956.

Marambaud, P., Wen, P.H., Dutt, A., Shioi, J., Takashima, A., Siman, R., and Robakis, N.K. (2003). A CBP Binding Transcriptional Repressor Produced by

the PS1/epsilon-Cleavage of N-Cadherin Is Inhibited by PS1 FAD Mutations. Cell *114*, 635-645.

Marintchev, A. (2013). Roles of helicases in translation initiation: A mechanistic view. Biochimica et Biophysica Acta (BBA) - Gene Regulatory Mechanisms *1829*, 799-809.

Mark, K.S., and Davis, T.P. (2002). Cerebral microvascular changes in permeability and tight junctions induced by hypoxia-reoxygenation. American Journal of Physiology - Heart and Circulatory Physiology *282*, H1485-H1494.

Martineau, M., Shi, T., Puyal, J., Knolhoff, A.M., Dulong, J., Gasnier, B., Klingauf, J., Sweedler, J.V., Jahn, R., and Mothet, J.-P. (2013). Storage and Uptake of d-Serine into Astrocytic Synaptic-Like Vesicles Specify Gliotransmission. The Journal of Neuroscience *33*, 3413-3423.

Matter, K., and Balda, M.S. (1998). Biogenesis of tight junctions: the C-terminal domain of occludin mediates basolateral targeting. Journal of Cell Science *111*, 511-519.

Matthew Michael, W., Choi, M., and Dreyfuss, G. (1995). A nuclear export signal in hnRNP A1: A signal-mediated, temperature-dependent nuclear protein export pathway. Cell *83*, 415-422.

McCaffrey, G., Seelbach, M.J., Staatz, W.D., Nametz, N., Quigley, C., Campos, C.R., Brooks, T.A., and Davis, T.P. (2008). Occludin oligomeric assembly at tight junctions of the blood-brain barrier is disrupted by peripheral inflammatory hyperalgesia. Journal of Neurochemistry *106*, 2395-2409.

McCarthy, K.M., Skare, I.B., Stankewich, M.C., Furuse, M., Tsukita, S., Rogers, R.A., Lynch, R.D., and Schneeberger, E.E. (1996). Occludin is a functional component of the tight junction. J Cell Sci *109*.

McGee, A.W., and Bredt, D.S. (1999). Identification of an Intramolecular Interaction between the SH3 and Guanylate Kinase Domains of PSD-95. Journal of Biological Chemistry *274*, 17431-17436.

Meier, S.D., Kafitz, K.W., and Rose, C.R. (2008). Developmental profile and mechanisms of GABA-induced calcium signaling in hippocampal astrocytes. Glia *56*, 1127-1137.

Meng, W., and Takeichi, M. (2009). Adherens Junction: Molecular Architecture and Regulation. Cold Spring Harbor Perspectives in Biology *1*, a002899.

Messam, C.A., Hou, J., and Major, E.O. (2000). Coexpression of Nestin in Neural and Glial Cells in the Developing Human CNS Defined by a Human-Specific Anti-nestin Antibody. Experimental Neurology *161*, 585-596.

Metea, M.R., Kofuji, P., and Newman, E.A. (2007). Neurovascular Coupling Is Not Mediated by Potassium Siphoning from Glial Cells. The Journal of Neuroscience *27*, 2468-2471.

Metea, M.R., and Newman, E.A. (2006). Glial Cells Dilate and Constrict Blood Vessels: A Mechanism of Neurovascular Coupling. The Journal of Neuroscience *26*, 2862-2870.

Middeldorp, J., and Hol, E.M. (2011). GFAP in health and disease. Progress in Neurobiology *93*, 421-443.

Mineta, K., Yamamoto, Y., Yamazaki, Y., Tanaka, H., Tada, Y., Saito, K., Tamura, A., Igarashi, M., Endo, T., Takeuchi, K.*, et al.* (2011). Predicted expansion of the claudin multigene family. FEBS Letters *585*, 606-612.

Mishra, A., Hamid, A., and Newman, E.A. (2011). Oxygen modulation of neurovascular coupling in the retina. Proceedings of the National Academy of Sciences *108*, 17827-17831.

Montana, V., Malarkey, E.B., Verderio, C., Matteoli, M., and Parpura, V. (2006). Vesicular transmitter release from astrocytes. Glia *54*, 700-715.

Montana, V., Ni, Y., Sunjara, V., Hua, X., and Parpura, V. (2004). Vesicular Glutamate Transporter-Dependent Glutamate Release from Astrocytes. The Journal of Neuroscience *24*, 2633-2642.

Mothet, J.-P., Pollegioni, L., Ouanounou, G., Martineau, M., Fossier, P., and Baux, G. (2005). Glutamate receptor activation triggers a calcium-dependent and SNARE protein-dependent release of the gliotransmitter D-serine. Proceedings of the National Academy of Sciences of the United States of America *102*, 5606-5611.

Mulligan, S.J., and MacVicar, B.A. (2004). Calcium transients in astrocyte endfeet cause cerebrovascular constrictions. Nature *431*, 195-199.

Murakami, T., Felinski, E.A., and Antonetti, D.A. (2009). Occludin Phosphorylation and Ubiquitination Regulate Tight Junction Trafficking and Vascular Endothelial Growth Factor-induced Permeability. Journal of Biological Chemistry *284*, 21036-21046.

Nagy, J.I., Patel, D., Ochalski, P.A.Y., and Stelmack, G.L. (1999). Connexin30 in rodent, cat and human brain: selective expression in gray

matter astrocytes, co-localization with connexin43 at gap junctions and late developmental appearance. Neuroscience *88*, 447-468.

Nakai, J., Ohkura, M., and Imoto, K. (2001). A high signal-to-noise Ca2+ probe composed of a single green fluorescent protein. Nat Biotech *19*, 137-141.

Nava, P., Kamekura, R., and Nusrat, A. (2013). Cleavage of transmembrane junction proteins and their role in regulating epithelial homeostasis. Tissue Barriers *1*, e24783.

Nelson, A.R., Sweeney, M.D., Sagare, A.P., and Zlokovic, B.V. (2016). Neurovascular dysfunction and neurodegeneration in dementia and Alzheimer's disease. Biochimica et Biophysica Acta (BBA) - Molecular Basis of Disease *1862*, 887-900.

Neuhaus, W., Wirth, M., Plattner, V.E., Germann, B., Gabor, F., and Noe, C.R. (2008). Expression of Claudin-1, Claudin-3 and Claudin-5 in human blood–brain barrier mimicking cell line ECV304 is inducible by glioma-conditioned media. Neuroscience Letters *446*, 59-64.

Nitta, T., Hata, M., Gotoh, S., Seo, Y., Sasaki, H., Hashimoto, N., Furuse, M., and Tsukita, S. (2003). Size-selective loosening of the blood-brain barrier in claudin-5–deficient mice. The Journal of Cell Biology *161*, 653-660.

Nunbhakdi-Craig, V., Machleidt, T., Ogris, E., Bellotto, D., White, C.L., and Sontag, E. (2002). Protein phosphatase 2A associates with and regulates atypical PKC and the epithelial tight junction complex. The Journal of Cell Biology *158*, 967-978.

Owsianka, A.M., and Patel, A.H. (1999). Hepatitis C Virus Core Protein Interacts with a Human DEAD Box Protein DDX3. Virology *257*, 330-340.

Oya, M., Kitaguchi, T., Yanagihara, Y., Numano, R., Kakeyama, M., Ikematsu, K., and Tsuboi, T. (2013). Vesicular nucleotide transporter is involved in ATP storage of secretory lysosomes in astrocytes. Biochemical and Biophysical Research Communications *438*, 145-151.

Palmer, I., and Wingfield, P.T. (2012). Preparation and Extraction of Insoluble (Inclusion-Body) Proteins from Escherichia coli. Current protocols in protein science / editorial board, John E Coligan [et al] *0 6*, 10.1002/0471140864.ps0471140603s0471140870.

Paulson, O.B., and Newman, E.A. (1987). Does the Release of Potassium from Astrocyte Endfeet Regulate Cerebral Blood Flow? Science (New York, NY) *237*, 896-898.

Penes, M.C., Li, X., and Nagy, J.I. (2005). Expression of zonula occludens-1 (ZO-1) and the transcription factor ZO-1-associated nucleic acid-binding protein (ZONAB)–MsY3 in glial cells and colocalization at oligodendrocyte and astrocyte gap junctions in mouse brain. European Journal of Neuroscience *22*, 404-418.

Penin, F., Dubuisson, J., Rey, F.A., Moradpour, D., and Pawlotsky, J.-M. (2004). Structural biology of hepatitis C virus. Hepatology *39*, 5-19.

Penuela, S., Gehi, R., and Laird, D.W. (2013). The biochemistry and function of pannexin channels. Biochimica et Biophysica Acta (BBA) - Biomembranes *1828*, 15-22.

Pérez Koldenkova, V., and Nagai, T. (2013). Genetically encoded Ca2 + indicators: Properties and evaluation. Biochimica et Biophysica Acta (BBA) - Molecular Cell Research *1833*, 1787-1797.

Petravicz, J., Boyt, K.M., and McCarthy, K.D. (2014). Astrocyte IP3R2-dependent Ca(2+) signaling is not a major modulator of neuronal pathways governing behavior. Frontiers in Behavioral Neuroscience *8*, 384.

Petravicz, J., Fiacco, T.A., and McCarthy, K.D. (2008). Loss of IP3 Receptor-Dependent Ca2+ Increases in Hippocampal Astrocytes Does Not Affect Baseline CA1 Pyramidal Neuron Synaptic Activity. The Journal of Neuroscience *28*, 4967-4973.

Petrelli, F., and Bezzi, P. (2016). Novel insights into gliotransmitters. Current Opinion in Pharmacology *26*, 138-145.

Pickart, C.M., and Fushman, D. (2004). Polyubiquitin chains: polymeric protein signals. Current Opinion in Chemical Biology *8*, 610-616.

Piehl, C., Piontek, J., Cording, J., Wolburg, H., and Blasig, I.E. (2010). Participation of the second extracellular loop of claudin-5 in paracellular tightening against ions, small and large molecules. Cellular and Molecular Life Sciences *67*, 2131-2140.

Piñol-Roma, S.n. (1997). HnRNP proteins and the nuclear export of mRNA. Seminars in Cell & Developmental Biology *8*, 57-63.

Ploss, A., Evans, M.J., Gaysinskaya, V.A., Panis, M., You, H., de Jong, Y.P., and Rice, C.M. (2009). Human occludin is a hepatitis C virus entry factor required for infection of mouse cells. Nature *457*, 882-886.

Pollard, V.W., Michael, W.M., Nakielny, S., Siomi, M.C., Wang, F., and Dreyfuss, G. (1996). A Novel Receptor-Mediated Nuclear Protein Import Pathway. Cell *86*, 985-994.

Price, D.L., Ludwig, J.W., Mi, H., Schwarz, T.L., and Ellisman, M.H. (2002). Distribution of rSlo Ca2+-activated K+ channels in rat astrocyte perivascular endfeet. Brain Research *956*, 183-193.

Putnam, A.A., and Jankowsky, E. (2013). DEAD-box helicases as integrators of RNA, nucleotide and protein binding. Biochimica et Biophysica Acta (BBA) - Gene Regulatory Mechanisms *1829*, 884-893.

Raetz, C.R., and Dowhan, W. (1990). Biosynthesis and function of phospholipids in Escherichia coli. Journal of Biological Chemistry *265*, 1235-1238.

Raikwar, N.S., Vandewalle, A., and Thomas, C.P. (2010). Nedd4–2 interacts with occludin to inhibit tight junction formation and enhance paracellular conductance in collecting duct epithelia. American Journal of Physiology - Renal Physiology *299*, F436-F444.

Reeves, A., Shigetomi, E., and Khakh, B.S. (2011). Bulk loading of calcium indicator dyes to study astrocyte physiology: key limitations and improvements using morphological maps. The Journal of neuroscience : the official journal of the Society for Neuroscience *31*, 9353-9358.

Romanitan, M.O., Popescu, B.O., Spulber, Ş., Băjenaru, O., Popescu, L.i.M., Winblad, B., and Bogdanovic, N. (2010). Altered expression of claudin family proteins in Alzheimer's disease and vascular dementia brains. Journal of Cellular and Molecular Medicine *14*, 1088-1100.

Romanitan, M.O., Popescu, B.O., Winblad, B., Bajenaru, O.A., and Bogdanovic, N. (2007). Occludin is overexpressed in Alzheimer's disease and vascular dementia. Journal of Cellular and Molecular Medicine *11*, 569-579.

Rubin, L.L., Hall, D.E., Porter, S., Barbu, K., Cannon, C., Horner, H.C., Janatpour, M., Liaw, C.W., Manning, K., and Morales, J. (1991). A cell culture model of the blood-brain barrier. The Journal of Cell Biology *115*, 1725-1735.

Sahu, G., Sukumaran, S., and Bera, A.K. (2014). Pannexins form gap junctions with electrophysiological and pharmacological properties distinct from connexins. Scientific Reports *4*, 4955.

Saitou, M., Fujimoto, K., Doi, Y., Itoh, M., Fujimoto, T., Furuse, M., Takano, H., Noda, T., and Tsukita, S. (1998). Occludin-deficient Embryonic Stem Cells Can Differentiate into Polarized Epithelial Cells Bearing Tight Junctions. The Journal of Cell Biology *141*, 397-408.

Saitou, M., Furuse, M., Sasaki, H., Schulzke, J.D., Fromm, M., Takano, H., Noda, T., and Tsukita, S. (2000). Complex phenotype of mice lacking occludin, a component of tight junction strands. Mol Biol Cell *11*.

Sakakibara, A., Furuse, M., Saitou, M., Ando-Akatsuka, Y., and Tsukita, S. (1997). Possible Involvement of Phosphorylation of Occludin in Tight Junction Formation. The Journal of Cell Biology *137*, 1393-1401.

Sánchez-Pulido, L., Martín-Belmonte, F., Valencia, A., and Alonso, M.A. (2002). MARVEL: a conserved domain involved in membrane apposition events. Trends in Biochemical Sciences *27*, 599-601.

Schildknecht, S., Pöltl, D., Nagel, D.M., Matt, F., Scholz, D., Lotharius, J., Schmieg, N., Salvo-Vargas, A., and Leist, M. (2009). Requirement of a dopaminergic neuronal phenotype for toxicity of low concentrations of 1-methyl-4-phenylpyridinium to human cells. Toxicology and Applied Pharmacology *241*, 23-35.

Shapiro, L., and Weis, W.I. (2009). Structure and Biochemistry of Cadherins and Catenins. Cold Spring Harbor Perspectives in Biology *1*, a003053.

Shibuya, T., Tange, T.O., Sonenberg, N., and Moore, M.J. (2004). eIF4AIII binds spliced mRNA in the exon junction complex and is essential for nonsense-mediated decay. Nat Struct Mol Biol *11*, 346-351.

Shigetomi, E., Kracun, S., Sofroniew, M.V., and Khakh, B.S. (2010). A genetically targeted optical sensor to monitor calcium signals in astrocyte processes. Nat Neurosci *13*, 759-766.

Shigetomi, E., Patel, S., and Khakh, B.S. (2016). Probing the Complexities of Astrocyte Calcium Signaling. Trends in Cell Biology *26*, 300-312.

Shigetomi, E., Tong, X., Kwan, K.Y., Corey, D.P., and Khakh, B.S. (2012). TRPA1 channels regulate astrocyte resting calcium and inhibitory synapse efficacy through GAT-3. Nat Neurosci *15*, 70-80.

Shin, H., Hsueh, Y.-P., Yang, F.-C., Kim, E., and Sheng, M. (2000). An Intramolecular Interaction between Src Homology 3 Domain and Guanylate Kinase-Like Domain Required for Channel Clustering by Postsynaptic Density-95/SAP90. The Journal of Neuroscience *20*, 3580-3587.

Silhavy, T.J., Kahne, D., and Walker, S. (2010). The Bacterial Cell Envelope. Cold Spring Harbor Perspectives in Biology *2*.

Simpson, J.E., Ince, P.G., Shaw, P.J., Heath, P.R., Raman, R., Garwood, C.J., Gelsthorpe, C., Baxter, L., Forster, G., Matthews, F.E.*, et al.* (2011). Microarray analysis of the astrocyte transcriptome in the aging brain:

relationship to Alzheimer's pathology and APOE genotype. Neurobiology of Aging *32*, 1795-1807.

Simpson, J.E., Wharton, S.B., Cooper, J., Gelsthorpe, C., Baxter, L., Forster, G., Shaw, P.J., Savva, G., Matthews, F.E., Brayne, C.*, et al.* (2010). Alterations of the blood–brain barrier in cerebral white matter lesions in the ageing brain. Neuroscience Letters *486*, 246-251.

Singh, S.M., and Panda, A.K. (2005). Solubilization and refolding of bacterial inclusion body proteins. Journal of Bioscience and Bioengineering *99*, 303-310.

Sloan, K.E., Gleizes, P.-E., and Bohnsack, M.T. (2015). Nucleocytoplasmic Transport of RNAs and RNA–Protein Complexes. Journal of Molecular Biology.

Smith, P.K., Krohn, R.I., Hermanson, G.T., Mallia, A.K., Gartner, F.H., Provenzano, M.D., Fujimoto, E.K., Goeke, N.M., Olson, B.J., and Klenk, D.C. (1985). Measurement of protein using bicinchoninic acid. Analytical Biochemistry *150*, 76-85.

Sofroniew, M.V., and Vinters, H.V. (2010). Astrocytes: biology and pathology. Acta Neuropathologica *119*, 7-35.

Soghomonian, J.-J., and Martin, D.L. (1998). Two isoforms of glutamate decarboxylase: why? Trends in Pharmacological Sciences *19*, 500-505.

Söhl, G., and Willecke, K. (2003). An Update on Connexin Genes and their Nomenclature in Mouse and Man. Cell Communication & Adhesion *10*, 173-180.

Soma, T., Chiba, H., Kato-Mori, Y., Wada, T., Yamashita, T., Kojima, T., and Sawada, N. (2004). Thr207 of claudin-5 is involved in size-selective loosening of the endothelial barrier by cyclic AMP. Experimental Cell Research *300*, 202-212.

Song, X., Zhao, Y., Narcisse, L., Duffy, H., Kress, Y., Lee, S., and Brosnan, C.F. (2005). Canonical transient receptor potential channel 4 (TRPC4) co-localizes with the scaffolding protein ZO-1 in human fetal astrocytes in culture. Glia *49*, 418-429.

Soto-Rifo, R., Rubilar, P.S., Limousin, T., de Breyne, S., Décimo, D., and Ohlmann, T. (2012). DEAD-box protein DDX3 associates with eIF4F to promote translation of selected mRNAs. The EMBO Journal *31*, 3745-3756.

Spindler, V., Schlegel, N., and Waschke, J. (2010). Role of GTPases in control of microvascular permeability. Cardiovascular Research *87*, 243-253.

Srinivasan, R., Huang, B.S., Venugopal, S., Johnston, A.D., Chai, H., Zeng, H., Golshani, P., and Khakh, B.S. (2015). Ca2+ signaling in astrocytes from Ip3r2-/- mice in brain slices and during startle responses in vivo. Nat Neurosci *18*, 708-717.

Steed, E., Rodrigues, N.T., Balda, M.S., and Matter, K. (2009). Identification of MarvelD3 as a tight junction-associated transmembrane protein of the occludin family. BMC Cell Biology *10*, 1-14.

Stenberg, F., Chovanec, P., Maslen, S.L., Robinson, C.V., Ilag, L.L., von Heijne, G., and Daley, D.O. (2005). Protein Complexes of the Escherichia coli Cell Envelope. Journal of Biological Chemistry *280*, 34409-34419.

Stevenson, B.R., Siliciano, J.D., Mooseker, M.S., and Goodenough, D.A. (1986). Identification of ZO-1: a high molecular weight polypeptide associated with the tight junction (zonula occludens) in a variety of epithelia. The Journal of Cell Biology *103*, 755-766.

Stout, C.E., Costantin, J.L., Naus, C.C.G., and Charles, A.C. (2002). Intercellular Calcium Signaling in Astrocytes via ATP Release through Connexin Hemichannels. Journal of Biological Chemistry *277*, 10482-10488.

Stout, R.F., Snapp, E.L., and Spray, D.C. (2015). Connexin Type and Fluorescent Protein Fusion Tag Determine Structural Stability of Gap Junction Plaques. Journal of Biological Chemistry *290*, 23497-23514.

Subramanian, V.S., Marchant, J.S., Ye, D., Ma, T.Y., and Said, H.M. (2007). Tight junction targeting and intracellular trafficking of occludin in polarized epithelial cells. American Journal of Physiology - Cell Physiology *293*, C1717-C1726.

Sundstrom, J.M., Tash, B.R., Murakami, T., Flanagan, J.M., Bewley, M.C., Stanley, B.A., Gonsar, K.B., and Antonetti, D.A. (2009). Identification and Analysis of Occludin Phosphosites: A Combined Mass Spectrometry and Bioinformatics Approach. Journal of Proteome Research *8*, 808-817.

Surapornsawasd, T., Ogawa, T., and Moriyama, K. (2015). Identification of nuclear localization signals within the human BCOR protein. FEBS Letters *589*, 3313-3320.

Suzuki, H., Nishizawa, T., Tani, K., Yamazaki, Y., Tamura, A., Ishitani, R., Dohmae, N., Tsukita, S., Nureki, O., and Fujiyoshi, Y. (2014). Crystal Structure of a Claudin Provides Insight into the Architecture of Tight Junctions. Science *344*, 304-307.

Swatek, K.N., and Komander, D. (2016). Ubiquitin modifications. Cell Res *26*, 399-422.

Takahashi, S., Iwamoto, N., Sasaki, H., Ohashi, M., Oda, Y., Tsukita, S., and Furuse, M. (2009). The E3 ubiquitin ligase LNX1p80 promotes the removal of claudins from tight junctions in MDCK cells. Journal of Cell Science *122*, 985-994.

Takano, T., Tian, G.-F., Peng, W., Lou, N., Libionka, W., Han, X., and Nedergaard, M. (2006). Astrocyte-mediated control of cerebral blood flow. Nat Neurosci *9*, 260-267.

Tan, A.R., Cai, A.Y., Deheshi, S., and Rintoul, G.L. (2011). Elevated intracellular calcium causes distinct mitochondrial remodelling and calcineurin-dependent fission in astrocytes. Cell Calcium *49*, 108-114.

Tkachuk, N., Tkachuk, S., Patecki, M., Kusch, A., Korenbaum, E., Haller, H., and Dumler, I. (2011). The tight junction protein ZO-2 and Janus kinase 1 mediate intercellular communications in vascular smooth muscle cells. Biochemical and Biophysical Research Communications *410*, 531-536.

Tolia, A., and De Strooper, B. (2009). Structure and function of γ-secretase. Seminars in Cell & Developmental Biology *20*, 211-218.

Tong, X., Shigetomi, E., Looger, L.L., and Khakh, B.S. (2013). Genetically Encoded Calcium Indicators and Astrocyte Calcium Microdomains. The Neuroscientist *19*, 274-291.

Torres, A., Wang, F., Xu, Q., Fujita, T., Dobrowolski, R., Willecke, K., Takano, T., and Nedergaard, M. (2012). Extracellular Ca2+ Acts as a Mediator of Communication from Neurons to Glia. Science signaling *5*, ra8-ra8.

Toyofuku, T., Yabuki, M., Otsu, K., Kuzuya, T., Hori, M., and Tada, M. (1998). Direct Association of the Gap Junction Protein Connexin-43 with ZO-1 in Cardiac Myocytes. Journal of Biological Chemistry *273*, 12725-12731.

Traweger, A., Fang, D., Liu, Y.-C., Stelzhammer, W., Krizbai, I.A., Fresser, F., Bauer, H.-C., and Bauer, H. (2002). The Tight Junction-specific Protein Occludin Is a Functional Target of the E3 Ubiquitin-protein Ligase Itch. Journal of Biological Chemistry *277*, 10201-10208.

Traweger, A., Fuchs, R., Krizbai, I.A., Weiger, T.M., Bauer, H.-C., and Bauer, H. (2003). The Tight Junction Protein ZO-2 Localizes to the Nucleus and Interacts with the Heterogeneous Nuclear Ribonucleoprotein Scaffold Attachment Factor-B. Journal of Biological Chemistry *278*, 2692-2700.

Truant, R., and Cullen, B.R. (1999). The Arginine-Rich Domains Present in Human Immunodeficiency Virus Type 1 Tat and Rev Function as Direct

Importin β-Dependent Nuclear Localization Signals. Molecular and Cellular Biology *19*, 1210-1217.

Utepbergenov, D.I., Fanning, A.S., and Anderson, J.M. (2006). Dimerization of the Scaffolding Protein ZO-1 through the Second PDZ Domain. Journal of Biological Chemistry *281*, 24671-24677.

Van Itallie, C., Rahner, C., and Anderson, J.M. (2001). Regulated expression of claudin-4 decreases paracellular conductance through a selective decrease in sodium permeability. Journal of Clinical Investigation *107*, 1319-1327.

Van Itallie, C.M., and Anderson, J.M. (2006). Claudins and epithelial paracellular transport. Annu Rev Physiol *68*.

Van Itallie, C.M., and Anderson, J.M. (2014). Architecture of tight junctions and principles of molecular composition. Seminars in Cell & Developmental Biology *36*, 157-165.

Van Itallie, C.M., Fanning, A.S., and Anderson, J.M. (2003). Reversal of charge selectivity in cation or anion-selective epithelial lines by expression of different claudins. American Journal of Physiology - Renal Physiology *285*, F1078-F1084.

Van Itallie, C.M., Gambling, T.M., Carson, J.L., and Anderson, J.M. (2005). Palmitoylation of claudins is required for efficient tight-junction localization. Journal of Cell Science *118*, 1427-1436.

Van Itallie, C.M., Rogan, S., Yu, A., Vidal, L.S., Holmes, J., and Anderson, J.M. (2006). Two splice variants of claudin-10 in the kidney create paracellular pores with different ion selectivities. American Journal of Physiology - Renal Physiology *291*, F1288-F1299.

Van Itallie, C.M., Tietgens, A.J., LoGrande, K., Aponte, A., Gucek, M., and Anderson, J.M. (2012). Phosphorylation of claudin-2 on serine 208 promotes membrane retention and reduces trafficking to lysosomes. Journal of Cell Science *125*, 4902-4912.

Viggars, A.P., Wharton, S.B., Simpson, J.E., Matthews, F.E., Brayne, C., Savva, G.M., Garwood, C., Drew, D., Shaw, P.J., and Ince, P.G. (2011). Alterations in the blood brain barrier in ageing cerebral cortex in relationship to Alzheimer-type pathology: A study in the MRC-CFAS population neuropathology cohort. Neuroscience Letters *505*, 25-30.

Wang, E., Taylor, R.W., and Pfeiffer, D.R. (1998). Mechanism and Specificity of Lanthanide Series Cation Transport by Ionophores A23187, 4-BrA23187, and Ionomycin. Biophysical Journal *75*, 1244-1254.

Wang, F., Daugherty, B., Keise, L.L., Wei, Z., Foley, J.P., Savani, R.C., and Koval, M. (2003). Heterogeneity of Claudin Expression by Alveolar Epithelial Cells. American Journal of Respiratory Cell and Molecular Biology *29*, 62-70.

Webster, B.M., and Lusk, C.P. (2016). Border Safety: Quality Control at the Nuclear Envelope. Trends in Cell Biology *26*, 29-39.

Weiner, J.H., and Li, L. (2008). Proteome of the Escherichia coli envelope and technological challenges in membrane proteome analysis. Biochimica et Biophysica Acta (BBA) - Biomembranes *1778*, 1698-1713.

Wells, L., Vosseller, K., and Hart, G.W. (2001). Glycosylation of Nucleocytoplasmic Proteins: Signal Transduction and O-GlcNAc. Science *291*, 2376-2378.

Wilhelm, A., Volknandt, W., Langer, D., Nolte, C., Kettenmann, H., and Zimmermann, H. (2004). Localization of SNARE proteins and secretory organelle proteins in astrocytes in vitro and in situ. Neuroscience Research *48*, 249-257.

Wittchen, E.S., Haskins, J., and Stevenson, B.R. (1999). Protein Interactions at the Tight Junction: ACTIN HAS MULTIPLE BINDING PARTNERS, AND ZO-1 FORMS INDEPENDENT COMPLEXES WITH ZO-2 AND ZO-3. Journal of Biological Chemistry *274*, 35179-35185.

Wolburg, H., Wolburg-buchholz, K., Kraus, J., Rascher-eggstein, G., Liebner, S., Hamm, S., Duffner, F., Grote, E.-h., Risau, W., and Engelhardt, B. (2003). Localization of claudin-3 in tight junctions of the blood-brain barrier is selectively lost during experimental autoimmune encephalomyelitis and human glioblastoma multiforme. Acta Neuropathologica *105*, 586-592.

Wong, V. (1997). Phosphorylation of occludin correlates with occludin localization and function at the tight junction. American Journal of Physiology - Cell Physiology *273*, C1859-C1867.

Yaffe, Y., Shepshelovitch, J., Nevo-Yassaf, I., Yeheskel, A., Shmerling, H., Kwiatek, J.M., Gaus, K., Pasmanik-Chor, M., and Hirschberg, K. (2012). The MARVEL transmembrane motif of occludin mediates oligomerization and targeting to the basolateral surface in epithelia. Journal of Cell Science *125*, 3545-3556.

Ye, Z.-C., Wyeth, M.S., Baltan-Tekkok, S., and Ransom, B.R. (2003). Functional Hemichannels in Astrocytes: A Novel Mechanism of Glutamate Release. The Journal of Neuroscience *23*, 3588-3596.

Yedavalli, V.S.R.K., Neuveut, C., Chi, Y.-h., Kleiman, L., and Jeang, K.-T. (2004). Requirement of DDX3 DEAD Box RNA Helicase for HIV-1 Rev-RRE Export Function. Cell *119*, 381-392.

Zhang, Q., Pangršič, T., Kreft, M., Kržan, M., Li, N., Sul, J.-Y., Halassa, M., Van Bockstaele, E., Zorec, R., and Haydon, P.G. (2004). Fusion-related Release of Glutamate from Astrocytes. Journal of Biological Chemistry *279*, 12724-12733.

Zhang, Y., Chen, K., Sloan, S.A., Bennett, M.L., Scholze, A.R., O'Keeffe, S., Phatnani, H.P., Guarnieri, P., Caneda, C., Ruderisch, N.*, et al.* (2014). An RNA-Sequencing Transcriptome and Splicing Database of Glia, Neurons, and Vascular Cells of the Cerebral Cortex. The Journal of Neuroscience *34*, 11929-11947.

Zlokovic, B.V. (2011). Neurovascular pathways to neurodegeneration in Alzheimer's disease and other disorders. Nature reviews Neuroscience *12*, 723-738.

Zonta, M., Angulo, M.C., Gobbo, S., Rosengarten, B., Hossmann, K.-A., Pozzan, T., and Carmignoto, G. (2003). Neuron-to-astrocyte signaling is central to the dynamic control of brain microcirculation. Nat Neurosci *6*, 43-50.

Zorec, R., Verkhratsky, A., Rodríguez, J.J., and Parpura, V. (2015). Astrocytic vesicles and gliotransmitters: Slowness of vesicular release and synaptobrevin2-laden vesicle nanoarchitecture. Neuroscience.